SUPPLEMENT 3.I

STRUCTURAL EVALUATION FOR THE HI-STORM 100U SYSTEM

3.I.0 OVERVIEW

In this supplement, the structural adequacy of the HI-STORM 100U Vertical Ventilated Module (VVM) is evaluated pursuant to the guidelines of NUREG-1536. The organization of technical information in this supplement mirrors the format and content of Chapter 3 except that it only contains material directly pertinent to the HI-STORM 100U VVM.

The HI-STORM 100U VVM serves as the storage space for the loaded MPC and consists of the CEC (the Container Shell, the Divider Shell and MPC Guides, and a welded Bottom Plate), and a lid consisting of plain concrete encased in structural steel arranged to provide appropriate inlet and outlet air passages (the Closure Lid). These individual components are collectively referred to as VVM Components. Interfacing SSCs that surround and support the VVM, as well as proximate structures, collectively referred to as ISFSI Structures, are explained in Supplement 2.I. Section 1.I.2 contains a complete description of the VVM Components and the ISFSI Structures (accompanied by appropriate figures) and their respective functions within the HI-STORM 100U ISFSI. The essential design details of both the VVM Components and the ISFSI Structures are set down in the licensing drawing in Supplement 1.I. The design basis loadings for the facility are provided in Supplement 2.I. The applicable codes, standards, and practices governing the structural analysis of the HI-STORM 100U module as well as the design criteria, are also presented in Supplement 2.I. Throughout this supplement, in the context of the VVM components, the term "*safety factor*" is defined as the *ratio of the allowable stress (load) or displacement for the applicable load combination to the maximum computed stress (load) or displacement.*

For the ISFSI Structures made of reinforced concrete, the safety factor is defined as the ratio of the ultimate moment (or shear) capacity to the actual maximum moment (or shear) developed under the factored load combination.

MPC structural integrity has been evaluated in Chapter 3. In this supplement, the integrity of the MPC, due to its rattling motion inside the VVM storage cavity during a seismic event (a new loading condition in the underground storage configuration) is considered.

3.I.1 STRUCTURAL DESIGN

3.I.1.1 Discussion

The HI-STORM 100U system consists of three principal components: the Multi-Purpose Canister (MPC), the HI-STORM 100U storage module, herein denoted as the Vertical Ventilated Module (VVM) (includes the Cavity Enclosure Container (CEC) and the Closure Lid), and the HI-TRAC transfer cask. This supplement to Chapter 3 presents the structural evaluation of a VVM for the

applicable load cases summarized in Supplement 2.I (Table 2.I.5). In Section 3.I.4, the safety factors for each load case for the VVM Components are quantified. In addition, the safety evaluation of the ISFSI Structures is carried out using the factored load combinations from ACI-318 (2005) (see Table 2.I.11). Summary tables of bounding safety factors are provided for governing load combination for the ISFSI Structures. A licensing drawing for the HI-STORM 100U VVM is provided in Section 1.I.5. Table 2.I.1 provides a listing of the applicable regulations, codes and standards for the VVM Components and the ISFSI structures. The design of the VVM components and the ISFSI Structures is fully articulated in the licensing drawing and Table 2.I.2. The applicable Design Basis Earthquake is defined by the free field spectra shown in Figure 2.I.4.

3.I.1.2 Design Criteria

Design (and acceptance) criteria for the HI-STORM 100U VVM Components and the ISFSI structures are summarized in Tables 2.I.1 and 2.I.6.

3.I.1.3 Loads

Individual loads, applicable to the HI-STORM 100U System, are defined in Sections 2.I.4, 2.I.5, and 2.I.6, and load cases applicable to the VVM Components are summarized in Table 2.I.5. Table 2.I.11 contains load combinations applicable to the ISFSI Structures (reinforced concrete structures) in the HI-STORM 100U ISFSI.

3.I.1.4 Allowables

Allowable stresses for carbon steel and Alloy X used in the structural components of the HI-STORM 100U and the stored MPC are provided in Sections 3.1 and 3.3. The relevant data from those sections is reproduced here, as Tables 3.I.3 (a)-(d) to make the supplement self-contained.

3.I.1.5 Brittle Fracture

Brittle fracture considerations for HI-STORM 100U are bounded by HI-STORM 100 and 100S because of the VVM's underground configuration, and the use of the same material types and thicknesses as in the aboveground overpacks.

3.I.1.6 Fatigue

The HI-STORM 100U system is not subject to significant long-term cyclic loads. Therefore, failure due to fatigue is not a concern for the HI-STORM 100U system.

3.I.1.7 Buckling

The CEC Container Shell is the only component of the VVM subject to axial compression. However, since the shell is backed by a substrate, welded to a Bottom Plate at its base, and surrounded by the

ISFSI Pad at the top, instability is not considered credible. The Divider Shell does not experience any axial compressive stress that might induce buckling.

3.I.2 WEIGHTS AND CENTERS OF GRAVITY

Table 3.I.1 provides bounding weights of the individual HI-STORM 100U components.

The locations of the calculated centers of gravity (C.G's) are presented in Table 3.I.2 and are computed using the bounding weights. All centers of gravity are located on the VVM centerline.

Bounding weight values for the CEC and the Closure Lid include an overage on the weight generated by the CAD drawing package.

3.I.3 MECHANICAL PROPERTIES OF MATERIALS

Tables 2.I.3 and 2.I.8 list applicable codes, materials of construction, and ITS designations for all functional parts in the HI-STORM 100U system except for the MPC and its internals, which remain unchanged (listed in Table 2.2.6).

3.I.3.1 VVM Steel Properties

Applicable material property and allowable stress tables in Chapter 3 for the VVM are reproduced in Tables 3.I.3 (a)-(c) for convenience.

3.I.3.2 Unreinforced Concrete

The primary function of the unreinforced concrete in the HI-STORM 100U VVM Closure Lid is shielding. Unreinforced concrete is not considered as a primary load-bearing (structural) member. However, its ability to withstand compressive, bearing and penetrant loads under the design basis and various service conditions is analyzed. The allowable bearing strength of plain concrete for normal loading conditions is calculated in accordance with ACI 318 (2005) [2.I.5]. Table 3.I.4 provides a bearing limit consistent with the concrete compressive strength in the same table. The procedure specified in ASTM C-39 is utilized to verify that the assumed compressive strength will be realized in the actual in-situ pours. Unless specifically called out in Table 3.I.4, Appendix 1.D provides requirements on unreinforced concrete.

3.I.3.3 Reinforced Concrete

Reinforced concrete is used in the construction of the ISFSI Structures, namely, the retaining wall, the TSP, the VIP, and the SFP. All reinforced concrete in the HI-STORM 100U ISFSI will conform to stress criteria of ACI-318 (2005).

3.I.4 GENERAL STANDARDS FOR CASKS

In this section, new or additional material applicable to the HI-STORM 100U system is included. Section 3.4 contains all required information associated with the MPCs and with the HI-TRAC transfer cask and is not repeated here. Results reported in this supplement section are generally applicable only to the HI-STORM 100U VVM.

3.I.4.1 Chemical and Galvanic Reactions

In order to provide reasonable assurance that the VVM will meet its intended Design Life of 40 years (the License Life is 20 years) and perform its intended safety function(s), chemical and galvanic reactions and other potentially degrading mechanisms must be accounted for in its design and construction.

The HI-STORM 100U VVM is a buried structure and as such chemical and galvanic reactions and other potentially degrading factors are, in some respects, more challenging than for aboveground models. Although the CEC is not a part of the MPC containment boundary, it should not corrode to the extent where localized in-leakage of water occurs or where gross general corrosion prevents the component from performing its primary safety function. In the following, considerations in the VVM's design and construction consistent with the applicable guidance provided in ISG-15 [3.I.3] are summarized.

All VVM components are galvanically compatible. Except for the CEC exterior surfaces, all steel surfaces of the VVM are lined and coated with the same surface preservative that is used in the aboveground HI-STORM overpacks. (The surface preservative used to protect HI-STORM 100S steel surfaces is a proven zinc rich inorganic/metallic material that protects galvanically and has self healing characteristics for added assurance). All exposed surfaces interior to the VVM, as stated in Supplement 1.I, are accessible for the reapplication of surface preservative, if necessary.

The steel Divider Shell requires insulation to perform its primary thermal function. The insulation selected shall be suitable for high temperature and high humidity operation and shall be foil faced, jacketed or otherwise made water resistant to ensure the required thermal resistance is maintained in accordance with Supplement 4.I. The high zinc content in the coating of the Divider Shell provides protection for both the Divider Shell and the jacketing or foil from any potential galvanic corrosion concerns. With respect to radiation resistance, the insulation blanket does not contain any organic binders. The damage threshold for ceramics is known to be approximately $1x10^{10}$ Rads. Chloride corrosion is not a concern since chloride leachables are limited and sufficiently low and the Divider Shell is not made from stainless steel [3.I.20]. Stress corrosion cracking of the foil or jacketing, whether made from stainless steel or other material is not an applicable corrosion mechanism due to minimal stresses derived from self-weight. The foil or jacketing and attachment hardware shall either have sufficient corrosion resistance (e.g. stainless steel, aluminum or galvanized steel) or shall be protected with a suitable surface preservative. The insulation is adequately secured to prevent significant blockage of the ventilation passages in case of failure of a single attachment (strap, clamp,

bolt or other attachment hardware). The following table provides the acceptance criteria for the selection of insulation material for the Divider Shell and ranks them in order of importance.

Acceptance Criteria for the Selection of the Insulation Material	
Rank	**Criteria**
1	Adequate thermal resistance
2	Adequate high temperature resistance
3	Adequate humidity resistance
4	Adequate radiation resistance
5	Adequate resistance to the ambient environment
6	Sufficiently low chloride leachables
7	Adequate integrity and resistance to degradation and corrosion during long-term storage

Kaowool® ceramic fiber insulation [3.I.20] is selected as one that satisfies the acceptance criteria to the maximum degree. The Kaowool® insulation material provides excellent resistance to chemical attack and is not degraded by oil or water. Alternatively, a Holtec approved equivalent that meets the acceptance criteria set forth in the table above may be used.

The CEC Container Shell, which is exposed to the substrate, requires additional pre-emptive measures to prevent corrosion, if the substrate is of aggressive chemistry. This subsection provides a description of corrosion mitigation measures required to be implemented to protect the HI-STORM 100 VVM. Because the guiding principle in the HI-STORM Systems is to target a service life of 100 years so as to guarantee a design life of 40 years, these corrosion prevention measures are in addition to the preemptively incorporated standard corrosion allowance of 1/8-inch applied to the subterranean parts of the CEC in direct contact with the surrounding substrate. Calculation of the required CEC Container Shell and Bottom Plate thicknesses on a site-specific basis may indicate the availability of an additional corrosion reserve.

Soil Corrosivity and Corrosion Mitigation Measures for the Exterior of the CEC

Corrosion mitigation of the exterior of the CEC warrants special consideration for the following reasons: (i) inaccessibility of the exterior coated surface after installation (ii) potential for a highly aggressive (i.e., corrosive) soil environment at certain sites, and (iii) potential for a high radiation field. Since the buried configuration will not allow for the reapplication of surface preservative, corrosion mitigation measures shall be determined after careful evaluation of the soil's corrosivity at the user's ISFSI site.

To evaluate soil corrosivity, a "10 point" soil-test evaluation procedure, in accordance with the guidelines of Appendix A of ANSI/AWWA C105/A21 [3.I.4], will be utilized. The classical soil evaluation criteria in the aforementioned standard focuses on parameters such as: 1) resistivity, 2) pH, 3) redox (oxidation-reduction) potential, 4) sulfides, 5) moisture content, 6) potential for stray

current, and 7) experience with existing installations in the area. Using the procedure outlined in ref. [3.I.4], the ISFSI soil environment corrosivity is categorized as either "mild" for a soil test evaluation resulting in 9 points or less or "aggressive" for a soil test evaluation resulting in 10 points or greater. The following table details the corrosion mitigation measures that shall be implemented based on soil environment corrosivity:

Implementation of Corrosion Mitigation Measures			
Soil Environment Corrosivity	**Corrosion Mitigation Measures**		
	Coating (see note i)	Concrete Encasement (see note ii)	Cathodic Protection (see note iii)
Mild	Required	Choice of either concrete encasement or cathodic protection; or both	
Aggressive	Required	Optional	Required
Notes: i. An acceptable exterior surface preservative (coating) applied on the CEC. ii. Concrete encasement of the CEC external surfaces to establish a high pH buffer around the metal mass. iii. A suitably engineered impressed current cathodic protection system (ICCPS)			

The corrosion mitigation measures tabulated above are further detailed in the following subsections:

i. Coating

In addition to the corrosion allowance, the CEC shall be coated with a radiation resistant surface preservative designed for below-grade and/or immersion service. Inorganic and/or metallic coatings are sufficiently radiation resistant for this application; therefore, radiation testing is not required [3.I.5]. Organic coatings such as epoxy, however, must have proven radiation resistance [3.I.5] or must be tested without failure to at least 10^7 Rad. Radiation resistance to lower radiation levels is acceptable on a site-specific basis. Radiation testing shall be performed in accordance with ASTM D 4082 [3.I.6] or equivalent. The coating should be conservatively treated as a Service Level II coating as described in Reg. Guide 1.54 [3.I.7]. As such, the coating shall be subjected to appropriate quality assurance in accordance with the applicable guidance provided by ASTM D 3843-00 [3.I.8]. The coating should preferably be shop applied in accordance with manufacturer's instructions and, if appropriate, applicable guidance from ANSI C 210-03 [3.I.9]. The Keeler & Long polyamide-epoxy coating, according to the manufacturer's product data sheet [3.I.10], is pre-tested to radiation levels up to $1x10^9$ Rads without failure. The following table provides the acceptance criteria for the selection of coatings for the exterior surfaces of the CEC and ranks them in order of importance.

Acceptance Criteria for the Selection of Coatings	
Rank	**Criteria**
1	suitable for immersion and/or below grade service

Acceptance Criteria for the Selection of Coatings	
Rank	**Criteria**
2a	compatible with the ICCPS (if used) • adequate dielectric strength • adequate resistance to cathodic disbondment
2b	compatible with concrete encasement (if used) • adequate resistance to high alkalinity
3	adequate radiation resistance
4	adequate adhesion to steel
5	adequate bendability/ductility/cracking resistance/abrasion resistance
6	adequate strength to resist handling abuse and substrate stress

The Keeler & Long polyamide-epoxy coating is selected as one that satisfies the acceptance criteria to the maximum degree. Alternatively, a Holtec approved equivalent that meets the acceptance criteria set forth in the table above may be used.

ii. Concrete Encasement

The CEC concrete encasement shall provide a minimum of 5 inches of cover to provide a pH buffering effect for additional corrosion mitigation. The above concrete cover thickness has been conservatively determined for a 100-year service life in a strongly aggressive environment based on the concrete corrosion/degradation data provided in the literature [3.I.12, Table 5.3] (1.2 mm/yr surface depth failure rate). The required 5 inch minimum thickness is more conservative than that recommended in ACI Codes, such as ACI 318 [3.3.2], which call for up to 3 inches of concrete cover over steel reinforcement in aggressive environments. Considering that the concrete encasement is restricted to mild soil environments (unless used in conjunction with cathodic protection) and has a non-structural role, the 5 inch concrete encasement thickness is considered more than sufficient to provide reasonable assurance that a 40 year service life can be achieved. The lowest part of the CEC sits in a recessed region of the Support Foundation with an annular gap normally filled with substrate. If present, the CEC concrete encasement slurry will fill this annular gap during construction.

The function of the concrete encasement is for corrosion mitigation only; however, cracks larger than hairline cracks may significantly reduce its effectiveness. To control size and population of cracks, concrete reinforcement is included. The following reinforcement methods may be applied:

a. Fiber reinforcement: Fiber reinforcement may be of several materials, including steel, glass and plastic (polypropylene). The selection of the fiber reinforcement material shall be such that adequate resistance to radiation and high alkalinity is maintained. If using steel fibers, adequate damage protection of the CEC coating shall be ensured during concrete placement per written procedures. Steel fiber shall be implemented using written procedures and the

applicable guidance from ACI 544.3R [3.I.25] or a similar consensus code or standard. Fiber reinforcement materials other than steel shall be implemented using written procedures, manufacturer recommendations and applicable guidance from ACI, ASCE and/or ASTM. One such document is ASTM C1116-03 [3.I.26].

b. Steel wire reinforcement: Steel wire reinforcement shall be implemented in accordance with written procedures and the guidance from ACI 318 [3.3.2] or more recent version. For corrosion protection, the steel wire reinforcement shall have a concrete cover of approximately 2 to 3 inches from the interfacing substrate.

Regardless of reinforcement method, the material selected shall be corrosion resistant or otherwise appropriately coated (e.g. epoxy coated steel wire) for corrosion resistance.

The concrete encasement shall be installed in accordance with Holtec approved procedures following applicable guidance from the ACI code (e.g. ACI 318 [3.3.2]), as appropriate, for commercial concrete. Installation procedures shall address mix designs (incorporating Portland cement), testing, mixing, placement, and reinforcement, with the aim to enhance concrete durability and minimize voids and micro-cracks.

iii. Impressed Current Cathodic Protection System (ICCPS)

For a particular ISFSI site, the user may choose to either extend an existing ICCPS to protect the installed ISFSI, or to establish an autonomous ICCPS. The initial startup of the ICCPS must occur within one year after installation of the VVM to ensure timely corrosion mitigation. In addition, the ICCPS should be maintained operable at all times after initial startup except for system shutdowns due to power outages, repair or preventive maintenance and testing, or system modifications. Because there are a multitude of ISFSI variables that will bear upon the design of the ICCPS for a particular site, the essential criteria for its performance and operational characteristics are set down in this FSAR, which the detailed design work for each ISFSI site must follow.

Design Criteria for the Impressed Current Cathodic Protection System
a. The cathodic protection system shall be capable of maintaining the CEC at a minimum (cathodic) potential as required by NACE Standard RP0285-2002 [3.I.21].
b. The ICCPS shall include provisions to infer its proper operation and effectiveness on a periodic basis.
c. The system shall be designed to mitigate corrosion of the CEC for its design life.
d. The cathodic protection system design, installation, operation, testing, and maintenance shall follow the applicable guidelines of: - 49CFR195 Subpart H "Corrosion Control", Oct. 1, 2004 edition [3.I.13] - NACE Standard RP0285-2002 "Corrosion Control of Underground Storage Tank Systems by Cathodic Protection" [3.I.21]

The following standards and/or publications may also be utilized for additional guidance in the design, installation, operation, testing, and maintenance of the ICCPS as needed (in case of conflict, the guidelines of item d above shall prevail):

- API RP1632, "Cathodic Protection of Underground Petroleum Storage Tanks and Piping Systems" [3.I.22]
- NACE RP0169-96, "Control of External Corrosion on Underground or Submerged Piping Systems" [3.I.23]
- 49CFR192 Subpart I, "Requirements for Corrosion Control", Oct. 1, 2004 edition [3.I.24]
- Other standards or publications referenced by any of the above three standards and publications.

Records of system operating data necessary to adequately track the operable status of the ICCPS shall be maintained in accordance with the user's quality assurance program.

Finally, the surface preservative used to coat the CEC must meet the requirements described in (i) above but must also be compatible with cathodic protection and resistant to the alkaline conditions created by cathodic protection and/or concrete encasement. Organic coatings, such as the Keeler & Long coating selected for (i) above, are inherently compatible with both cathodic protection [3.I.11] and concrete [3.I.10].

3.I.4.2 Positive Closure

There are no quick-connect/disconnect ports in the confinement boundary of the HI-STORM 100U system. Because the only access to the MPC is through the VVM Closure Lid, which weighs well over 10 tons, inadvertent opening of the VVM cavity is not feasible.

3.I.4.3 Lifting Devices

As required by Reg. Guide 3.61, lifting operations applicable to the VVM lid are analyzed. Because of the nature of the HI-STORM 100U system, lid placement or removal may occur with a loaded MPC inside the VVM cavity; these are the sole operations requiring analysis in accordance with Reg. Guide 3.61 and are examined in this supplement.

As discussed in Subsection 3.4.3, the lifting component itself (the four lift lugs) must meet the primary stress limits prescribed by ANSI N14.6-1993; the welds in the load path, near the lifting holes, are required to meet the condition that stresses remain below yield under three times the lifted load (per Reg. Guide 3.61). Further, for additional conservatism, away from the lifting location, the ASME Code limit for the Level A service condition applies.

The lifting analysis results summarized below include a 15% inertia amplifier.

HI-STORM 100U VVM Closure Lid Lifting Analysis (Load Case 05 in Table 2.I.5)

The four lifting lugs are analyzed to ANSI N14.6 stress limits using simple strength of materials calculations. Each of four lugs is considered as a cantilever beam attached to the lid and carries 25% of the lid weight. The bending moment and shear force at the root of the cantilever (where it is attached to the lid) is computed and the maximum stress is compared with the minimum of the yield strength/6 or the ultimate strength/10. As required, increasing the lid weight by 15% includes inertia effects. Using the calculated bending moment and shear force at the root of the lug, the structural evaluation of the weld attaching the lug to the lid is performed and compared with the requirements of Regulatory Guide 3.61. The results from these two calculations demonstrate that the required safety factors are substantially greater than 1.0 (exceeding the requirements of ANSI N14.6 and Reg. Guide 3.61, respectively). The details of the calculations are presented in the calculation package supporting this submittal [3.I.27]. Lifting slings that attach to the lugs shall be sized to meet the safety factors set forth in ANSI B30.3.

To evaluate the global state of stress in the lid body, a finite element model of the lid, which includes contact interfaces between steel and concrete, is constructed to evaluate the state of stress under lifting conditions. Figure 3.I.1 shows the constructed ANSYS finite element model. The lifted scenario is simulated by fixing the four lifting locations at the lift lug sling attachment location, and applying an appropriate weight density to match the lifted weight. The results are evaluated for satisfaction of normal condition (ASME Level A) limits at the appropriate locations.

The table below summarizes key results obtained from the lifting analyses for the HI-STORM 100U VVM Closure Lid for a bounding set of input design loads.

HI-STORM 100U VVM Lid Lifting Analyses (Load Case 05 in Table 2.I.5)			
Item	Calculated Value	Allowable	Safety Factor
Bending of Lift Lugs (kip)(ANSI N14.6)	4.000	5.275	1.32 (see Note 1)
Shear in Lift Lugs (kip)(ANSI N14.6)	1.609	3.165	1.97 (see Note 1)
Load in Welds Near Lifting Lugs (kip) (Reg. Guide 3.61)	5.657	6.33	1.12 (see Note 2)
Primary Stress in Lid (ksi)(ASME Level A Limit)	< 10	26.25	> 2.63
Note 1: Computed safety factors represent the margin over that required by ANSI N14.6-1993 (0.1 x ultimate load). Note 2: Computed safety factor is based on 60% of yield strength for base metal and represents margin over limit set by Reg. Guide 3.61.			

It is concluded that all structural integrity requirements are met during a lift of the HI-STORM 100U VVM Closure Lid. All factors of safety, using applicable criteria from the ASME Code Section III, Subsection NF for Class 3 plate and shell supports, from USNRC Regulatory Guide 3.61, and from ANSI N14.6, are greater than 1.0.

3.I.4.4 Heat

i. Summary of Pressures and Temperatures

Tables 2.I.1 and 2.I.2 present applicable design inputs for the HI-STORM 100U VVM. No new inputs are required for the HI-TRAC and the MPC.

ii. Differential Thermal Expansion

All clearances between the MPC and the HI-STORM 100U VVM are equal to or larger than the corresponding clearances in the aboveground HI-STORM 100 systems (see Section 4.4). Therefore, no interferences between the MPC and the VVM will occur due to thermal expansion of the loaded MPC. The Divider Shell is insulated on one surface and is exposed to heated air on the other shell surface. Therefore an analysis to demonstrate that free axial thermal expansion of the Divider Shell will not close the initial gap between the top end of the Divider Shell and the base of the Closure Lid is provided. The Divider Shell is considered as a heated member, subject to an average temperature increase over its entire length. The actual axial absolute temperature profile can be integrated over the length of the Divider Shell to define the average absolute temperature. Once the average absolute temperature is known, the free thermal growth is computed and compared with the provided gap between the Divider Shell and the Closure Lid.

The average temperature rise above ambient is bounded by DT (ambient is 80°F per Table 2.I.1, and average metal temperature over the length of the Divider Shell is from Table 4.I.3, footnote):

$DT = (300°F - 80°F) = 220°F$

From Table 3.I.3 (a), a bounding coefficient of thermal expansion, appropriate to DT, is:

$\alpha = 6.27 \times 10^{-6}$ in./in.-°F

The nominal length of the divider shell is:

L = 221.5625"

Therefore, the free thermal expansion, based on the nominal length is $\alpha \times L \times DT$, and is computed and compared against the nominal gap provided (as shown in the licensing drawing).

Key Result from Free Thermal Growth Analysis of Divider Shell

Item	Bounding Value	Allowable Value*	Safety Factor
Thermal Growth (inch)	< 0.4	0.5	>1.25 (against contact)
*This is the nominal gap provided between the top end of the Divider Shell and the Closure Lid Surface (see Dwg. 4501, sheet 4 in Subsection 1.I.5).			

iii. Stress Calculations – VVM Components

a. HI-STORM 100U VVM Stresses Under Transporter Loading and Substrate Overburden (Load Case 07 in Table 2.I.5)

During HI-STORM 100U system loading, a HI-TRAC transfer cask with a fully loaded MPC is placed over a HI-STORM 100U VVM using a specially designed transporter and a lifting device meeting "single-failure proof" requirements, as applicable. The transfer cask is connected to the CEC using an ancillary mating device (see Figure 3.I.4). Although a handling accident is not credible, the CEC must possess the capacity to support any transporter loads imposed at and below the substrate surface during the short time when the transporter is positioned over a VVM cavity and carrying the weight of the loaded HI-TRAC (i.e., before the HI-TRAC is placed on the mating device). This loading condition leads to a maximum sub-surface lateral pressure on the CEC shell which may potentially cause its ovalization. This configuration also includes the loaded transporter traveling over a previously loaded VVM on its way to an empty CEC.

Table 3.I.1 gives the essential data on the representative transporter including its loaded weight and its track length and width (i.e., size of the load patch (Figure 3.I.5)). The average normal pressure, at the transporter track and TSP interface is computed by dividing the weight of the loaded transporter by the total area of the two load patches.

To determine the stress and displacement field in the CEC due to the combined action of the loaded transporter and the soil overburden, a 3-D ANSYS model of a VVM (see Figure 3.I.2) is prepared. The finite element model has the following attributes:

- The soil is modeled as an elastic continuum with properties specified in Tables 2.I.2 and 3.I.5. The VVM Interface Pad (VIP), which is separated from the Top Surface Pad (TSP) by a construction joint, is unaffected by the deflection of the TSP under the transporter weight. The VIP essentially is a dead weight on the soil column below and is appropriately incorporated in the model. To appropriately model the VIP within the confines of a linearly elastic construct, it is represented by a material with a very low Young's Modulus, but the correct weight density. This modeling assumption provides the appropriate weight on the substrate from the VIP but provides no additional strength to the TSP or to the CEC.

- The minimum CEC pitch from the licensing drawing is used.

- The TSP, shown in the licensing drawings, is represented by its appropriate elastic properties (Table 3.I.4).

- The soil mass surrounding the ISFSI is assumed to be constrained from expansion across the planes of symmetry (so as to maximize the Poisson compression load on the CEC). The bottom of the soil continuum extends to the SFP.

- The CEC shell is assumed to have its nominal un-corroded thickness; the stress and strain results are subsequently adjusted to reflect the postulated corrosion allowance (see Table 2.I.1).

- To linearize the problem, the soil is assumed to be bonded to all interfacing surfaces.

Table 3.I.10 provides the input data used in the analysis.

The results of the stress analysis are pictorially shown in Figure 3.I.11, where stress intensity in the CEC is plotted. As can be seen from the figure, the maximum primary stress intensity value is 1,390 psi based on the nominal shell thickness of 1 in. Accounting for the corrosion allowance in the CEC shell, the maximum stress intensity (essentially bending in nature) is appropriately adjusted to 1,816 psi ((1 in/0.875 in)^2 x 1390 psi). When compared with the Level A stress limit from ASME code Section III, Subsection NF (per Table 2.I.5), the maximum computed stress intensity provides a factor of safety:

$$SF = \frac{allowable}{actual} = \frac{26.25}{1.82} = 14.4$$

Because the stresses in the CEC shell remain elastic, no reduction in the diametrical opening of the CEC due to plastic deformation is indicated. Therefore, the retrievability of the MPC is assured.

b. HI-STORM 100U Lid Integrity Evaluation for Normal plus Explosion Loads, CEC Container Shell Evaluation Under Bounding Vertical Load (Load Case 02 in Table 2.I.5), and Design Basis Fire (Load Case 06 in Table 2.I.5)

The VVM Closure Lid rests on the CEC and resists vertical loads, arising from dead weight, and from induced loadings from explosions, from seismic accelerations, and from tornado missile impact. In this subsection, the analysis considers only the normal loading condition plus the steady pressure bounding the explosion pressure (see Table 2.I.1). The finite element model shown in Figure 3.I.1 is used to obtain this solution; the Closure Lid vertical support is now all around and is provided by the CEC Container Shell Flange (instead of by the lift lugs). The stresses from the solution are compared, per the criteria in Table 2.I.5, with allowable stress values for plate and shell structures as provided in ASME Section III Code, Subsection NF. The allowable stress intensity is per Table 3.I.3 (c) for Level D conditions at a bounding temperature of 350 °F.

The vertical load on the Container Shell ring flange, which can be computed from equilibrium, does not bound the vertical load under normal conditions when the Closure Lid is removed and replaced by a loaded HI-TRAC plus a Mating Device. The bounding vertical load during the transfer operation is an input for the evaluation of the Container Shell for this load case using Strength of Materials methodology. Key results from the analysis of the Closure Lid under the normal loading condition plus the steady pressure, and the follow-on analysis of the corroded Container Shell under the bounding vertical load (during the MPC transfer operation) are summarized in the following table:

Stress Analysis of the Closure Lid and CEC Container Shell Under Bounding Vertical Load During Normal Operations (Load Case 02 in Table 2.I.5)			
Item	Bounding Value from calculations	Allowable Limit	Safety Factor
Maximum Primary Principal Stress Anywhere in Lid (ksi)	< 12.0	59.65(Level D Stress Intensity Limit) 26.25 (Level A Stress Limit)	> 4.97* > 2.19*
CEC Container Ring Flange Weld (kips)	< 300	3,018	> 10.06
Compression Stress in CEC Container Shell Under Bounding Vertical Load (ksi)	< 1.425**	17.5	> 12.28
* The results from the analysis are presented in terms of principal stresses for simplicity. Safety factors are determined by comparison with the Level D stress intensity limits (Table 3.I.3(c)), or with Level A stress limits (Table 3.I.3 (b)). Regardless of the measure used, the safety factors are large. ** The bounding compressive stress is based on a fully corroded shell thickness and also conservatively includes the full weight of the CEC in addition to the bounding load at the top.			

From the above results, it is concluded that there is minimum structural demand on the HI-STORM 100U Closure Lid and CEC Container Shell during normal operation (even if the explosion pressure is conservatively considered as a normal condition).

With respect to the fire event (Load Case 06 in Table 2.I.5), where the Closure Lid steel temperature rises to the limit set in Table 2.I.5, it is noted from Tables 3.I.3 (a) and (b) that the Level A stress limit is reduced to 0.68 of the room temperature value, the yield strength is reduced to 0.66 of its room temperature value, and the ultimate strength is reduced to 0.92 of its room temperature value. From the stress values obtained in the lid (even with the explosion 10 psi surface pressure load included), it is evident that a total collapse of the lid due to reduction of the ultimate strength is not credible.

Seismic loading on the VVM is considered in Subsection 3.I.4.7 (Load Case 04 in Table 2.I.5). Subsection 3.I.4.8 considers tornado missile impact (Load Case 03 in Table 2.I.5).

iv. Stress Calculations – ISFSI Structures

The 100U ISFSI consists of plate-type reinforced concrete structures whose minimum section strength properties are defined by Table 2.I.2 and the licensing drawings. The ISFSI is supported by the subgrade underneath the SFP, which may include pilings, if required, to meet the effective stress wave velocity in Table 2.I.2. The loadings on the ISFSI are:

a. Dead load of the VVM and the concomitant effect of settlement over the Design Life of the system. (D in Table 2.I.11). The method to incorporate the effect of long-term settlement of the subgrade underneath the SFP (may also be referred to as the undergrade), described in Subsection 2.I.2, is used. This method essentially consists of using the deflection properties of the different layers to define equivalent elastic properties of the subgrade underneath the SFP. In the finite element analysis of the SFP, the degraded elastic properties of the subgrade underneath the SFP are utilized to account for the effect of long-term settlement. The long-term settlement of the subgrade underneath the TSP and VIP is also considered in a similar manner.

   The Dead load on the SFP from the weight of the loaded VVM's nearly equals the weight of the earth removed. Therefore, the long-term settlement of the SFP is expected to be quite small. Likewise, the dead load on the TSP and the VIP is relatively small (from self-weight of the pads).

   The retaining wall under excavated condition (see Subsection 2.I.2) supports the soil overburden pressure (classified herein as Dead load).

b. Live load from the loaded transporter acts directly on the TSP (see Figure 3.I.4 and 3.I.5). This load also adds to the overall load on the SFP (L in Table 2.I.11). The load from the transporter is the sole live load applicable to the ISFSI structures. For structural qualification, the loaded transporter (live load) is assumed to be situated over the centrally located cavity.

c. Seismic load is computed using the methodology presented in Subsection 3.I.4.7. This load, denoted as E in Table 2.I.11, is the aggregate of the peak dynamic load exerted on the ISFSI less the dead weight. For conservatism, the load E is applied as a static load in the stress analysis of ISFSI structures even though it is impulsive in nature.

Paragraph 3.I.4.7.3 contains details on the stress analysis of the ISFSI structures to demonstrate ACI code compliance.

3.I.4.5 Cold

Due to its subterranean configuration, the structural components of the VVM are relatively protected from extremes in the ambient temperature in comparison to the HI-STORM 100 or 100S overpacks. Therefore, no new analyses are identified for the HI-STORM 100U system.

3.I.4.6 Flood

The buried configuration of the HI-STORM 100U system renders it immune from sliding under the action of a design basis flood. No new analyses are needed for an actual extreme environmental event.

Although the condition does not necessarily arise due to a flood, a limiting uplift scenario where the VVM CEC is in place and the surrounding substrate produces a buoyant force by unspecified means is considered. For this condition (Load Case 01 in Table 2.I.5), the limiting uplift condition determines the minimum weight that needs to be in place to prevent uplift during construction. This could be in the form of a temporary cover. The upward directed buoyant force exerted on the CEC cavity is computed assuming a weight density of water and compared with the dead weight of the CEC. Under the postulated condition, the net uplift load (Buoyant Force – Weight of CEC) can be calculated. The required temporary weight that is needed to produce a net downward force is calculated in [3.I.27] and specified in Table 2.I.5.

For the case of a loaded VVM with the Closure Lid in place, or for an empty CEC with the Closure Lid in-place, the buoyant force is less than the vertical download, so there is no uplift.

Should the full buoyant force develop from any means, a lateral pressure load is imposed on the CEC bottom plate. Conservatively assuming an empty VVM, the full buoyant force provides a pressure causing bending of the CEC Bottom Plate, which is partially restrained against rotation by the CEC shells (note that in a loaded VVM, the MPC also helps to support the Bottom Plate of the CEC as its weight causes the central shim to act as a support for the Bottom Plate of the CEC). The stress intensity resulting from CEC Bottom Plate bending is compared to the Level D allowable stress intensity. Using the solutions for maximum stress in a clamped and simply supported plate, and averaging the results from the two solutions to approximately account for the rotational restraint provided by the CEC Container Shell, gives the following bounding safety factor for stress in the

bottom plate under the postulated buoyancy loading:

Allowable Stress = 66,875 psi (Table 3.I.3(c) @ 125 °F per Table 2.I.5). Safety Factor is calculated to be greater than 4.0.

3.I.4.7 Seismic Event - HI-STORM 100U (Load Case 04 in Table 2.I.5)

The HI-STORM 100U system, plus its contents, may be subject to the Design Basis Earthquake (DBE) defined by the response spectra in Figure 2.I.4. As mentioned in supplement 2.I and further explained in this subsection, the DBE has been defined for the 100U ISFSI to insure that the operative spectra (Figure 2.I.4) essentially envelope the corresponding site DBE spectra at virtually all US sites. Because the VVM is buried in the substrate, tipover of the VVM is not credible. The entire VVM can move laterally with the surrounding and supporting substrate.

Under the action of lateral seismic loads, the CEC Container Shell globally acts as a beam-like structure supported on a foundation driven by the site seismic accelerations. During a seismic event, the lateral loading on the CEC consists of:

i) Inertia force from CEC self-weight
ii) Inertia forces from the Closure Lid self-weight
iii) Inertia forces from the self weight of the VIP
iv) Interface forces from the rattling of the MPC within its confines of the CEC and the rattling of the contents inside the MPC
v) Interface forces from the subgrade and from the SFP

The CEC Container Shell develops longitudinal stresses as it bends like a beam to resist the input seismic loads. In addition, the CEC Container Shell tends to ovalize under the loads. Both effects are captured in the seismic analysis.

The Design Basis Seismic Model (DBSM) used to perform the safety analysis of the 100U ISFSI under the Design Basis Earthquake (DBE) defined by Figure 2.I.4 is described in the following.

3.I.4.7.1 Design Basis Seismic Analysis Model

Parametric studies were performed to support the initial certification of the HI-STORM 100U VVM. These studies defined the Design Basis Seismic Model. In particular, a non-linear dynamic model on LS-DYNA was found to produce much greater response and internal stresses than a linear analysis on SASSI. Further, a 5x5 VVM array model was standardized for dynamic analysis purposes. Accordingly, LS-DYNA is used for all required dynamic analysis of the VVM array. The DBSM consists of three discrete models, namely:

1. A VVM Array Model used to characterize the interaction of the ISFSI with the surrounding soil continuum. This is performed using a 5x5 VVM array (see Figure 3.I.3-B).

2. A VVM Array Model for the optional 100U design where retaining walls are in place (see Figure 3.I.3-C). The lateral subgrade beyond the retaining wall is assumed to be removed all the way down to the bottom of the SFP, which conservatively represents an excavation configuration.

3. A single VVM model with a detailed simulation of the internal parts of the VVM to obtain an accurate characterization of the stress/displacement field (see Figure 3.I.3-D).

The seismic analysis consists of three discrete steps, namely:

A. Soil-structure model development.
B. Use of the VVM Array Model to determine the bounding dynamic loads applied to the ISFSI Structures.
C. Use of the Single VVM Model to compute stresses in the VVM Components.

A. Soil–Structure Model Development

i. Based on the lower bound shear wave velocity profile of US nuclear power plants (Figure 2.I.6), a two-step earthquake response analysis using the computer code SHAKE2000 and LS-DYNA is performed to establish a bounding seismic loading condition for the 100U underground fuel storage system. The Design Basis Earthquake for the HI-STORM 100U system thus obtained is defined by the seismic response spectra at both the ground surface and the ISFSI foundation surface elevations as shown in Figure 2.I.4. The input seismic acceleration time history used in the first step (SHAKE) analysis is derived from the Regulatory Guide 1.60 seismic response spectrum and designated as the rock outcrop motion. The input acceleration time history is scaled to yield ground surface ZPAs (at the top of grade elevation) specified in Table 2.I.2. The 1-D SHAKE analysis model consists of 21 native soil layers of the 100U ISFSI site with a total thickness of 101 ft; the top of the 6^{th} soil layer is aligned with the bottom of the SFP. The total soil depth of the SSI Model is about five times the height of the underground ISFSI (Due to the limitation of the linear code, a further increase of the soil depth in the SHAKE model leads to questionable seismic response results in the case of a strong seismic motion and weak soil properties). The averaged strain compatible shear wave velocity is 450 ft/s for the soil layers above the SFP and is 485 ft/s for the layers below the SFP, which has been set as the lower-bound soil design data in Table 2.I.2 for a candidate 100U ISFSI site. The finite element soil model in the second step (LS-DYNA seismic response analysis) uses the average strain-compatible wave velocities obtained from the SHAKE analysis to represent the soil layers above and below the SFP elevation. The acceleration time history at the soil column bottom surface, also obtained from the SHAKE analysis in the first step, is used as the input seismic motion for the LS-DYNA seismic response analysis. The response spectrum plots shown in Figure 2.I.4 are the results of the LS-DYNA seismic response analysis.

Figure 3.I.3-A shows the LS-DYNA soil model for the seismic response analysis. Note that the lateral dimension of the ISFSI soil model is significantly greater than that of the ISFSI. The periphery nodes of the soil model space at the same elevation are constrained to move together to simulate the seismic response of the semi-infinite space of soil. According to the numerical study on various lateral boundary conditions of the finite element soil model [2.I.10], this lateral boundary condition, also known as a "slave boundary condition", is appropriate to predict the soil response in a seismic event. The same soil model and input seismic motion used in the LS-DYNA seismic response analysis will be used for the LS-DYNA soil-structure interaction analysis for the 100U ISFSI loaded with VVMs. The boundaries of the soil model are sufficiently away from the ISFSI pads to ensure that structural response of the ISFSI will not be significantly affected.

ii. The spectra in Figure 2.I.4 define the seismic input against which the spectra at a candidate ISFSI site should be compared to determine whether the generic analysis in this FSAR is bounding or additional site specific analysis set down per sub-section 2.I.6 are required.

iii. Consistent with the sketch in Figure 2.I.5, the 100U soil-structure LS-DYNA model consists of loaded VVMs, concrete pads, and soil spaces with properties as defined in Tables 2.I.2 and 3.I.4. The ISFSI model is developed based on a 5×5 VVM configuration, which has previously been approved under LAR 1014-6 and is considered to be appropriate for capturing the effect of the ISFSI size on the structural analysis results. Depending on the purpose of the analysis, the 100U soil-structure model may include 5x5 fully loaded VVMs or just one loaded VVM. Similarly, a loaded Vertical Cask Transporter (VCT) may be considered in the model to obtain the bounding load applied to the TSP and to demonstrate the seismic stability of the loaded VCT. For the optional ISFSI design including a retaining wall, the soil-structure model is developed based on the governing configuration where the subgrade outside the retaining wall is excavated all the way to the depth of the SFP elevation. Therefore, a total of three 100U soil-structure LS-DYNA models (see Figures 3.I.3-B to 3.I.3-D) are developed to perform the design basis earthquake analysis.

iv. The corrosion of the CEC is considered by using a reduced thickness (i.e., 1/8" thinner than the nominal thickness) in the soil-structure LS-DYNA models.

v. Proper element size and time step controls in the dynamic model are implemented following the guidance in references [3.I.28] and [3.I.29].

B. VVM Array Model

The object of the VVM Array model is to obtain conservative values of the loads on the ISFSI structures under the Design Basis Earthquake (Figure 2.I.4). The VVM Array model has the following essential attributes:

i. The MPC is represented by a solid rigid cylinder of mass equal to its total mass. This means that all internal masses will move in unison and the inertia forces of the MPC are maximized, which will conservatively result in greater impact loads applied to MPC guides and the CEC base plate.
ii. The Divider Shell and the CEC shell are modeled as elastic shells but the Closure Lid and the Lid Ring are simulated as rigid bodies. Note that the combination of elastic shells and rigid lid ring used in the finite element model has little effect on the load path between the Divider Shell and the CEC flange during the seismic event.
iii. The ISFSI pads (i.e., TSP, SFP, etc.) are simulated as a flexible plate-type structure, as is the retaining wall, if used. The retaining wall is added to the finite element model in the optional ISFSI design case (see Table 3.I.6).
iv. The SFP is fully loaded with a 5×5 VVM array.
v. A loaded VCT is assumed to be located at the center of the fully populated ISFSI except for the case with retaining walls. The VCT, along with the carried transfer cask, is modeled as a freestanding rigid body.
vi. The elastic material model is used for all ISFSI concrete structures except for the TSP, which is characterized by an inelastic concrete model to account for energy dissipation in the concrete due to the impact loading from the loaded VCT. For the case where cracking of the concrete needs to be considered, the Young's Modulus of the SFP is reduced to 50% of its nominal value per the guidance in Section 3.4 of [3.I.29].

C. Single VVM Model

The Single VVM model is used to perform the safety evaluation of the VVM components and the stored MPC under the Design Basis Earthquake. The applicable acceptance criteria are provided in Table 2.I.6. To conservatively evaluate the structural integrity of the VVM components, the Young's Modulus for the SFP is assumed to be equal to 50% of its nominal value. This is prompted by the results of VVM Array Model runs (see Table 3.I.7), which indicate that the VVM Components experience amplified responses if the reduced modulus is used for the SFP.

The Single VVM model complies with the provisions set forth in the following:

i. The SFP is loaded with only one VVM at the edge of the SFP. A loaded VCT, modeled as a freestanding rigid body, is conservatively assumed to be located above the center of the loaded VVM.
ii. The Cavity Enclosure Container (CEC) is discretized by an appropriate finite element grid to simulate its Container Shell and Bottom Plate, the Divider Shell, and the MPC guides in an explicit manner. The true stress-strain relationship of the material is used to obtain the realistic deformation of these structural members.
iii. The MPC shell, baseplate, and top lid are modeled using sufficient element discretization so that the peak primary stresses of the MPC components under the seismic loading condition can be captured for structural evaluation.
iv. The fuel basket is modeled with thin shell finite elements arrayed to simulate inter-cell

connectivity in an explicit manner.

v. Nominal small gaps between the fuel basket and the MPC are explicitly modeled, as is the nominal gap between the MPC and the CEC at the upper and lower MPC guide locations.

vi. Each fuel assembly is represented by an equivalent homogeneous, isotropic prismatic beam of an equivalent elastic modulus whose fundamental lateral natural frequency accords with that of the actual fuel assembly. A bounding fuel assembly weight is used and the fuel basket is assumed to be fully populated with fuel assemblies.

vii. The seismic responses of MPC structural components are simulated using the elastic material model so that the stress results can be directly compared with the corresponding ASME NB stress limits.

3.I.4.7.2 Qualification of VVM Components

The CEC Components and parts of the MPC subject to significant loadings during the DBE event are:

a. CEC shell and Divider Shell (subject to ovalization)
b. MPC shell (bending of the shell as a beam, resulting in axial membrane stress in the shell)
c. MPC top and bottom guides
d. Lateral loading on the fuel basket panels.
e. Localized strain in the MPC shell (due to impact of the MPC with the MPC guides attached to the Divider Shell)

The safety analysis of each component under the DBE event is summarized below:

a. CEC shell and Divider Shell: Maximum radial deformation of the two shells is tracked for the single VVM simulation scenario in Table 3.I.6. The ratio of the original ovalization to the actual ovalization gives the safety factor:

$$Safety\ Factor = \frac{Permissible\ radial\ displacement}{Maximum\ computed\ radial\ displacement\ from\ Figure\ 3.I.23}$$
$$= \frac{2.5"}{0.1325"} = 18.86$$

b. Primary stress in the MPC shell: The maximum stress intensity in the MPC shell is computed under the single VVM simulation scenario. The allowable stress intensity for this case corresponds to the Level D condition. The safety factor is computed as:

$$Safety\ Factor = \frac{Level\ D\ allowable\ Stress\ Intensity\ from\ Table\ 3.I.3(d)}{Maximum\ computed\ primary\ Stress\ Intensity\ from\ Figure\ 3.I.24}$$

$$= \frac{42{,}000 psi}{12{,}860 psi} = 3.26$$

c. Top and Bottom MPC Guides: The maximum lateral load bearing capacity of the top and bottom plate guides is computed in Supplement 4 of Reference [3.I.27]. The maximum dynamic impact loads from the single VVM model can be extracted from the impact load time history results shown in Figure 3.I.25. The safety factor is calculated as:

$$Safety\ Factor = \frac{MPC\ Guides\ Lateral\ Load\ Bearing\ Capacity}{Maximum\ MPC\ to\ MPC\ Guides\ Contact\ Force}$$

$$= \frac{4.41 \times 10^5 lb}{108{,}826 lb} = 4.05$$

For the tubular MPC top guide design, the MPC impact analysis documented in Supplement 11 of Reference [3.I.27] demonstrates that the tube guide would not experience any global plastic deformation under the Design Basis Earthquake condition. This means that there is no risk of progressive flattening of the guide tubes from repetitive impacts during the seismic event.

d. Loading on the Fuel Basket panel: The fuel basket panels are qualified to withstand 45 g's of lateral acceleration (during the non-mechanistic tip-over event). The maximum fuel g-load predicted by the LS-DYNA simulation is 2.5 g's as shown in Figure 3.I.26. The factor of safety, therefore, will be equal to the ratio of the two. Hence,

$$Safety\ Factor = \frac{45}{2.5} = 18$$

e. Maximum Local Strain in the Confinement Boundary in the Impact Region:

The small clearance between the MPC and the MPC guides can lead to a high localized strain in the region of the shell where the impact from rattling of the canister under a seismic event occurs. The extent of local strain from impact is minimized by locating the MPC guide in the vertical direction such that the mid-height of the impact footprint is aligned with the bottom surface of the closure lid. Thus the location of impact is removed from the lid-to-shell weld junction. It is necessary to insure that the maximum value of the local (true) strain in the shell (confinement boundary) region of impact is well below the failure strain. For this purpose, the recommendation in [3.I.31] is used. The methodology for computing the local strain is presented in the following and applied to the seismic problem analyzed in this subsection.

A finite element model of the MPC suitable for implementation in LS-DYNA is prepared with special emphasis on the top region of the canister where a very fine grid is

employed. All elements have elasto-plastic and large strain capability. The solid elements in the lid and the lid-to-shell weld are of type 2 (fully integrated) and those in the shell are type 16 (fully integrated). The integration across the shell wall employs the maximum number of points available in LS-DYNA (10 points). A mesh sensitivity study has been performed using a finer grid size for the MPC shell to verify that the results are converged.

The MPC contents, namely the fuel basket and the SNF, are modeled exactly as set forth in the DBSM in the foregoing (articles (iii.), (iv.), and (v.) in Subsection 3.I.4.7.1 C Single VVM Model). To define a conservative scenario of MPC/MPC guide impact, the velocity time history of the top of the MPC is surveyed from the dynamic analysis of the VVM using the DBSM. The maximum velocity thus obtained is assumed to exist as the initial condition in the LS-DYNA simulation. This assumption is most conservative because it assumes that the cyclic motion transmitted by the earthquake does not detract from the canister's momentum before impact occurs (observations show that the canister slows down by the earthquake's cyclic energy input, thus significantly lessening the severity of the impact). In addition, the MPC guide is fixed at its base, which conservatively ignores the deformation of the divider shell and therefore maximizes the impact. The finite element model is shown in Figure 3.I.12. To implement the above model, the search for the maximum velocity in the dynamic solution yielded less than 24.7 in/sec as shown in Figure 3.I.27. Applying an initial velocity of 26.0 in/sec as the initial condition to the above model provided the strain field shown in Figure 3.I.13 for the tubular guide design. The impact between the MPC and the MPC top guides results in an MPC shell maximum plastic (true) strain of less than 1.52×10^{-2} in/in for the tubular guide design and 3.1×10^{-2} in/in for the optional plate guide design (see Calculation 11 of [3.I.27]), respectively, which are only a small fraction of the acceptable value (0.1) per [3.I.31]. Therefore the integrity of the confinement boundary is assured.

3.I.4.7.3 Strength Qualification of the ISFSI Structure

Under the Design Basis Earthquake (Figure 2.I.4), the loads exerted on the Support Foundation Pad and the Top Surface Pad (as illustrated in Figure 3.I.4) are obtained from the LS-DYNA SSI simulations listed in Table 3.I.6. Table 3.I.7 lists the peak ISFSI interface loads obtained from various LS-DYNA runs listed in Table 3.I.6. In order to incorporate an additional margin of safety in the ISFSI structural analysis, the structural evaluation of ISFSI components uses input loads (see Table 3.I.8) that bound the peak ISFSI interface loads from the LS-DYNA SSI simulations in Table 3.I.7. The use of the bounding loads is in keeping with a similarly bounding value of settlement specified for the strength analysis of the SFP and the TSP (see Table 2.I.2).

The SFP and TSP shall meet the minimum structural requirements set down in Table 2.I.2 and the licensing drawings. The SFP and TSP are required to satisfy ACI-318 (2005) strength limits under all applicable load combinations (Table 2.I.11).

Likewise, the retaining wall, if used, shall meet the minimum concrete and rebar requirements provided in Table 2.I.2 and the licensing drawings. The site specific design may utilize a thicker and more heavily reinforced wall, if necessary, at user's option.

Table 3.I.8 provides the loading data used in the strength analysis of the ISFSI structures. The following discrete analyses are required:

(i) Compute the long-term settlement of the undergrade supporting the SFP assuming all VVM locations are loaded for the entire Design Life: Determine the "effective" elastic modulus of the subgrade under the SFP to simulate the effect of differential settlement in the structural analyses model. As discussed in Section 2.I.4, the long-term settlement of the undergrade from the loaded VVMs and the dead weight of the SFP is very small because the combined equivalent density of the loaded VVM's and the SFP is nearly equal to the density of the excavated subgrade.

(ii) Compute the long-term settlement of the subgrade under the TSP/VIP relative to the SFP from subgrade weight in addition to the dead weight of the TSP and VIP. Determine the "effective" elastic modulus of the subgrade between the TSP/VIP and the SFP to simulate the effect of long term differential settlement in the structural analyses model. As discussed in Section 2.I.4, the long-term settlement of the well conditioned subgrade under the TSP is appreciably small because of the small long-term loadings acting on the TSP.

(iii) Prepare a finite element model of the pads in ANSYS and determine the stress field under the factored Dead and Live loads with the settlement based "degraded" elastic moduli for the soil regions directly beneath the TSP and SFP (Spaces A and C in Figure 2.I.5). For the lateral subgrade adjacent to the HI-STORM 100U ISFSI (Spaces B and D in Figure 2.I.5), the dynamic (strain compatible) elastic moduli from Table 3.I.4 are conservatively used as input to maximize the flexural moments due to differential settlement.

(iv) Compute the stress field in the pads under factored seismic loads using dynamic elastic modulus corresponding to the minimum shear wave velocity of the subgrade specified in Table 2.I.2.

(v) Use the bounding loads listed in Table 3.I.8 to compute the stress fields in the pads (SFP and TSP) from the DBE.

(vi) Combine the factored loads and determine the total stress resultants. Compare with the respective section strengths to establish the factors of safety for the SFP and TSP.

(vii) Compute the bearing stress (or load) on the subgrade under the TSP using the combined factored loads from the transporter and the TSP/VIP and compare with the corresponding allowable limit to establish the safety factor for the subgrade under the TSP.

A comprehensive summary of the analyses and the associated margins of safety are discussed below:

The structural evaluation of the HI-STORM 100U ISFSI is performed using the commercial computer code ANSYS [3.I.33]. The constituents of the ISFSI namely the Support Foundation Pad (SFP), the subgrade under the SFP (the undergrade), the Top Surface Pad (TSP) and the subgrade lateral to the CEC under the TSP are all modeled using linear elastic SOLID45 elements. The VVM

interface pad (VIP), which carries no load except for its self-weight, is conservatively omitted in the model. The lateral subgrade adjacent to the HI-STORM 100U ISFSI (Spaces B and D in Figure 2.I.5) is included in the FE model and extends laterally a distance that exceeds the overall depth of the FE model considered for structural analysis. The element mesh is intentionally kept fine in the areas of load application on the SFP and the TSP. For convenience of load application, the footprint of the CEC base on the SFP is carefully articulated in the finite element model. The substrate under the SFP is terminated at approximately 101 ft below the TSP, which is consistent with the Design Basis Seismic Model discussed in Subsection 3.I.4.7.1. The "base" model (Simulation Model I) considers that all the storage locations in ISFSI are populated and experience identical peak vertical seismic loading from Table 3.I.8, which bounds the peak result obtained from the LS-DYNA SSI solution as discussed previously. Because of the symmetric geometry and loading, a quarter symmetric finite element model is sufficient to represent the fully loaded ISFSI. Figure 3.I.14 shows the finite element model of HI-STORM 100U ISFSI. For a non-symmetric model as in case of Simulation Model II, a full FE model of the HI-STORM 100U ISFSI as shown in Figure 3.I.15 is used. The "degraded" elastic moduli of the subgrade under the SFP and the subgrade between the TSP and SFP is appropriately computed to account for the long-term differential settlement effects as described in Subsection 2.I.4. The long-term settlement and the "effective" subgrade elastic moduli are derived using the governing soil characteristics following guidelines from [2.I.6]. Table 3.I.5 lists the bounding subgrade characteristics and the concomitant elastic moduli effective under dynamic loading. To address different loading patterns on the ISFSI and for completeness, additional partially loaded ISFSI configurations are considered in the evaluations. The partial loaded configurations include a two row loaded ISFSI (two rows of VVM locations adjacent to the symmetry line are loaded), a single row loaded ISFSI (the middle row of VVM locations is loaded) and a single VVM loaded ISFSI (a single VVM location centered near the periphery of the ISFSI is loaded). Figures 3.I.19, 3.I.20 and 3.I.21 illustrate the partial loading configurations for the ISFSI. These loading configurations are hereinafter referred to as Simulation Models II, III, and IV, respectively. Note that the terms "Loading Configuration" and "Simulation Model" are intermittently referred throughout the calculation. For Simulation Models I through IV, the optional retaining walls are not included in the finite element model.

The effects of the retaining wall are evaluated in a fifth Simulation Model (Simulation Model V), which is shown in Figure 3.I.16. In this model, the lateral subgrade surrounding the retaining walls is completely removed to bound any future excavation activities associated with the construction of a new underground ISFSI, and for consistency with the LS-DYNA SSI simulation model (see Figure 3.I.3-C). For Simulation Model V, the middle row of VVM locations is loaded similar to Simulation Model III (see Figure 3.I.22) which excludes the transporter load as discussed previously.

To simulate the material continuity at the extreme boundary surfaces of the model, translations are constrained at the lateral face of the subgrade. The extreme bottom surface of the model is fixed representing the bedrock (or competent soil) elevation.

The following individual load steps are considered in the analysis:

1. Bounding load transmitted by the VVM, as determined from the LS-DYNA SSI analysis and summarized in Table 3.I.8, is applied as an effective pressure on the footprints of the CEC base at all VVM locations.
2. The load from the transporter is applied as a normal pressure (see Figures 3.I.17, 3.I.19 3.I.20 and 3.I.21) over the transporter load patch on the TSP. For Simulation Model V, the transporter load is not applied to the TSP since no VVM loading/unloading operations are expected to occur during excavation activities associated with the construction on a new underground ISFSI.
3. The dead weight from VIP is applied as normal pressures on the substrate elements directly beneath the VIP.
4. In-plane tensile loads on the SFP and TSP from the retaining wall are applied as lateral pressures on the SFP and TSP boundaries for Simulation Model V.
5. To simulate the self weight of the modeled portion of the ISFSI, a 1g gravity load is applied. The densities of the various constituents are appropriately input in the model to accurately reflect the individual component weights.

It must be noted that the structural analysis of the ISFSI conservatively considers the peak dynamic loads from the LS-DYNA SSI analysis. However, it shall be permitted to use equivalent static loads obtained by removing high frequency components that would not contribute to the structural response using appropriate filters.

Since the peak loads from the LS-DYNA SSI analyses are substantially larger in comparison to the dead and live loads, the load combination LC-3 from Table 2.I.11 governs for the ISFSI structural evaluation. However, the analyses are carried out for load combinations LC-2 and LC-3, and the corresponding results substantiate that the load combination LC-3 is governing.

Figures 3.I.18a through 3.I.22c depict the maximum in-plane stresses in the ISFSI concrete structures (viz. SFP and TSP) for the governing load combination LC-3 for all the ISFSI configurations analyzed. The in-plane axial and bending stress on the SFP and the TSP elements are post-processed to compute the equivalent moments. The induced moments are compared to the respective moment capacities to determine the corresponding factor of safety. Table 3.I.10 summarizes the results for the SFP and the TSP respectively for all ISFSI configurations analyzed.

The minimum flexure safety factor is produced by Simulation Model IV, and it is associated with the TSP. In the Simulation Models I, II, III and IV, the peak load from the LS-DYNA SSI analysis acting on one transporter track (bearing on the TSP) is conservatively applied as a static load on both transporter tracks simultaneously, thereby significantly overestimating the load on the TSP. As mentioned previously, the peak dynamic loads obtained from the LS-DYNA SSI analyses from a DBE event are of impulsive nature. Use of the peak loads for static structural evaluations of the ISFSI is evidently conservative. Furthermore, no credit is taken for the Dynamic Increase Factor of 25% for flexure and 10% for shear permitted by [3.I.32] in the strength qualification of reinforced concrete.

The Table 3.I.11 summarizes the punching shear safety factor for the SFP and TSP. The minimum punching shear safety factor is associated with the TSP under the transporter seismic load, and it is well above 1.0.

The peak transporter load on the TSP from the LS-DYNA SSI analyses plus the load from the TSP are used to compute the maximum bearing stress in the substrate surface under the TSP. According to ACI-360 [2.I.8], the bearing stress can be calculated by uniformly distributing the load over the entire bearing area of the pad. For conservatism, the bearing stress calculation for the 100U sub-grade is performed using a bearing area significantly less than that of the smallest TSP (i.e., the TSP of one-VVM ISFSI). The maximum bearing stress in the sub-grade (Table 3.I.12) is smaller than the presumptive bearing stress limit, resulting in minimum safety factor above 2.0 imposed by the ACI code [2.I.8].

The evaluation of the CEC shell under the loads from the transporter load in addition to the subgrade overburden is presented in Subsection 3.I.4.4.

Finally, the structural integrity of the retaining wall is evaluated for the Design Basis Earthquake loading condition; the structural demand to the wall under normal operational conditions is small and therefore not structurally governing. Since the retaining wall is connected with the TSP and SFP through a shear key at the top and dowels at the bottom (see licensing drawing in Section 1.I.5), it can be treated as a simply supported plate (along its top and bottom edges) in the structural analysis. Therefore, the wall essentially experiences bending stress in the DBE event due to lateral soil pressure. The maximum bending moment of the retaining wall, which can be determined based on Figure 3.5-1 of Reference [3.I.28] or based on the retaining wall stress results obtained from the LS-DYNA SSI analysis for Case 3 in Table 3.I.6 (both approaches yield approximately the same result), is shown in Table 3.I.10 to be well below the bending capacity of the wall. The shear connections at the top and bottom of the retaining wall have also been evaluated for the loads induced during a Design Basis Earthquake. The results of the strength evaluation are provided in Table 3.I.13.

3.I.4.8 Tornado Missile Evaluation

3.I.4.8.1 HI-STORM 100U Lid Integrity Evaluation for Tornado Missile Strike (Load Case 03 in Table 2.I.5)

Design basis tornado missiles are specified in Table 2.2.5. The Closure Lid is the only above ground component of the VVM; therefore, missile impact analyses focus on this component. Large and intermediate tornado missiles are assumed to strike the center top surface of the lid at the design basis speed (see Table 2.2.5). For both missile analyses, a finite element model of the Closure Lid is employed (using dimensions from licensing drawings and applicable material properties), and includes contact between concrete and steel (see Figure 3.I.1). LS-DYNA is used to perform dynamic simulations of the impacts to demonstrate that neither missile completely penetrates the composite structure. The ANSYS model shown in Figure 3.I.1 is simplified to develop an input file for the LS-DYNA simulation. Elastic-Plastic Material 24 is used for the steel and Material 72 is used for the

concrete. For a conservative result, engineering stress relations for the lid steel work are used with an assumed ultimate strain of 21% (per ASME Code, Sec. II, Part A). As LS-DYNA expects that true stress-strain data is input, the use of true stress-strain data, to obtain a more realistic result, is permitted (if appropriate justification is provided for the true stress-strain relation). The solution obtained using engineering stress strain data is clearly conservative in that material failure is set at the engineering ultimate strain limit rather than reflecting the true strain at failure, which will be considerably larger. A strain rate effect is incorporated by increasing the yield and ultimate strengths by a maximum of 50% (depending on the rate) as suggested by data for SA-36 steel [3.I.19]. This is the same strain rate increase used in the evaluations to assess the performance of the aboveground HI-STORM when impacted by a jet fighter aircraft [3.I.16]. A time history normal pressure loading is applied over the metal annular region around the outlet opening to simulate the large missile, and the global deformation damage to the lid is assessed. The formula from "Topical Report – Design of Structures for Missile Impact", BC-TOP-9A, Rev. 2, 9/74 [3.I.17] is used to establish appropriate pressure-time data. For the speed and mass associated with the large missile, the impact force-time curve has the form

$$F(t) = 0.625 \text{ sec/ft} \times 184.8 \text{ ft/sec} \times 4000 \text{ lb} \times \sin(20t) = 462{,}000 \text{ lb} \times \sin(20t) \text{ for } t < 0.0785 \text{ sec.}$$
$$= 0 \text{ for } t >= 0.0785 \text{ sec.}$$

This representation of the large missile impact load is appropriate as recent full-scale impact testing of a modern passenger vehicle demonstrates. Figure 3.I.6 shows the force-time history from the full-scale test of a full-size Ford passenger vehicle [3.I.18]. The test was performed at an impact speed of 35 mph and the vehicle had approximately the same weight as the design basis large deformable missile. Since the force is directly proportional to the pre-impact momentum, an estimate of the peak force at 126 mph for the vehicle is obtained by a simple ratio of the impact velocities and missile mass. Estimating the peak value from the plot produces a resulting peak force of 496,000 lb, which is the same order of magnitude as the peak value predicted from the Bechtel Topical Report, although the shape and duration of the curve is different. The results from the analysis using the load-time function from the Bechtel formula show no significant lid damage from the large missile strike on the lid because of the concrete backing. Inspection of the result concludes that the deformed shape after the event does not preclude lid removal, the lid remains in-place, and the MPC has not been impacted. The maximum lid vertical deflection during the strike is less than 0.1 inch and there are a few local regions of permanent effective plastic strain. The details of this calculation are found in [3.I.27]. The large missile impact is not the bounding strike because of the large area of impact and significant energy loss that occurs when the vehicle is crushed upon impact; the rigid, intermediate missile imparts more local and global damage to the Closure Lid.

The impact of the intermediate missile is conservatively simulated as a rigid 8" diameter cylindrical steel bar weighing 275 lb. (per Table 2.2.5), traveling at 126 mph and striking the Closure Lid at the most vulnerable location, which is through the top vent opening. The strike can be either at the center of the inner shield dome or slightly off-center so as to miss the central steel connecting bar. In order to strike the MPC top lid, the intermediate missile must penetrate the steel weldment and encased concrete (see licensing drawings in Section 1.I.5). Figures 3.I.7 and 3.I.8 show the intermediate

impact scenarios considered. Figures 3.I.9 and 3.I.10 show the lid state at the time of maximum bottom plate vertical displacement. For both cases, no dislodgement of the lid is indicated and plastic strains occur only in the immediate vicinity of the strike. A summary of results that bound the computed results for the two intermediate missile strikes is presented in Table 3.I.9.

Next, consider that the intermediate or large missile is traveling horizontally and strikes the side of the Closure Lid. A large missile strike at this location with a horizontal orientation is most likely not credible because of the low profile of the lid. The large missile would rotate as it broke up, resulting only in a glancing blow to the lid. However, an evaluation of the Closure Lid flange ring in either missile side strike is needed to ensure that the Closure Lid will not be driven sideways under the impact and separate from the CEC. A key structural element is the weld connecting the Closure Lid restraint ring to the Closure Lid. The capacity of the welds in the load path that resist the lateral impact load is:

Closure Lid Weld Capacity = 8,381,000 lb.

This capacity is computed assuming a limiting weld stress of 60% of the ultimate tensile strength of the base material. In any of the evaluated missile strikes from above, the peak impact load (filtered at 350 Hz (see similar filtering in the HI-STAR 100 transport license)) does not exceed 1,200,000 lb. Interface loads from top impacts are expected to bound impact loads from side impacts because of the geometry involved; therefore, the safety factor on the CEC Container Shell flange ring, acting to hold the lid in-place, is:

SF (flange ring) = Closure Lid Weld Capacity/ Filtered Peak Impact Load > 6.9

Finally, a small missile entering the outlet duct will not damage the MPC because there is no direct line-of-sight to the MPC, and even if it arrives at the MPC, it will have undergone multiple impacts with the duct walls, and can only impact the thick MPC lid. Therefore, MPC damage from the small missile is not credible.

An assessment of all simulation results concludes that the postulated missile strikes will not preclude MPC retrievability, will not cause loss of confinement, and will not affect criticality. In no scenario, does the lid become dislodged.

3.I.4.8.2 Tornado Missile Protection during Construction

The number of VVMs in a HI-STORM 100U ISFSI may vary depending on a user's need. While there is a minimum spacing (pitch) requirement (see licensing drawing in Subsection 1.I.5), there is no limitation on the maximum spacing. Furthermore, a module array may have a non-rectangular external contour such as shown in the licensing drawing with a trapezoidal contour. Finally, an ISFSI may be constructed in multiple campaigns to allow the user to align the VVM cavity construction schedule with the plant's fuel storage needs. Any ISFSI constructed in one campaign shall have the following mandatory perimeter protection features:

i. The Radiation Protection Space (RPS) shall extend to an appropriate distance beyond the outer surface of the CEC shell (see licensing drawing in Subsection 1.I.5). Calculations have been performed [3.I.27] that confirm that a 10' distance beyond the outer surface of the CEC shell is sufficient to prevent the 8" diameter rigid cylindrical missile (defined in Table 2.I.1 and is the most penetrating of the missile types considered in this FSAR) from contacting the CEC shell should this missile strike the exposed cut from the adjacent construction. The penetration analysis conservatively assumed a subgrade with minimum resistance to missile penetration and the formulation described in [3.I.30].

ii. Unless a retaining wall (see licensing drawing) has been built to confine and retain the subgrade at the boundary of the RPS (or beyond) in the particular direction of excavation, an Excavation Exclusion Zone (EEZ) shall be defined within which any excavation activity during an operating ISFSI is prohibited (see Subsection 2.I.2). The retaining wall is the EEZ boundary if the retaining wall is located at or beyond the RPS.

3.I.4.9 HI-STORM 100U VVM Service Life

The VVM is engineered for 40 years of design life, while satisfying the conservative design requirements defined in Supplement 2.I. For information supporting the 40 year design life addressing chemical and galvanic reactions as well as other potentially degrading factors see Subsection 3.I.4.1. Requirements for periodic inspection and maintenance of the HI-STORM 100U VVM throughout the 40-year design life are defined in Supplement 9.I. The VVM is designed, fabricated, and inspected under the comprehensive Quality Assurance Program discussed in Chapter 13.

3.I.5 FUEL RODS

No new analysis of fuel rods is required for storage of an MPC in a HI-STORM 100U VVM.

3.I.6 SUPPLEMENTAL DATA

3.I.6.1 Additional Codes and Standards Referenced in HI-STORM 100 System Design and Fabrication

No additional Codes and Standards are added for the HI-STORM 100U system.

3.I.6.2 Computer Programs

ANSYS 5.7, 7.0, 9.0, 11.0, and LS-DYNA (previously known as DYNA3D) [3.I.2] are used for the finite element analyses prepared by Holtec and summarized in this supplement.

ANSYS

ANSYS is a public domain code, well benchmarked code, which utilizes the finite element method for structural analyses. It can simulate both linear and non-linear material and geometric behavior. It includes contact algorithms to simulate surfaces making and breaking contact, and can be used for both static and dynamic simulations. ANSYS has been independently QA validated at Holtec International. In this FSAR submittal, ANSYS is used within [3.1.27] and the element size used in the application follows the recommendation of the code developers.

LS-DYNA

LS-DYNA is a nonlinear, explicit, three-dimensional finite element code for solid and structural mechanics. It was originally developed at Lawrence Livermore Laboratories and is ideally suited for study of short-time duration, highly nonlinear impact problems in solid mechanics. LS-DYNA is commercially available and has been independently validated at Holtec following Holtec's QA procedures for commercial computer codes. This code has been used to analyze the Non-Mechanistic Storage tip-over for the HI-STORM 100 Part 72 general license. In this supplement, the code is used to establish the performance of the HI-STORM 100U under a design basis seismic event, and to evaluate the response to a design basis missile.

LS-DYNA is currently supported and distributed by Livermore Software. Each update is independently subject to QA validation at Holtec.

3.I.6.3 Appendices Included in Supplement 3.I

None.

3.I.6.4 Calculation Packages

A calculation package [3.1.27] containing the structural calculations supporting Supplement 3.I has been prepared and archived according to Holtec International's Quality Assurance program (see Chapter 13), and submitted with this application. A second calculation report [3.I.14], documenting the SASSI analyses, has been prepared by a Holtec subcontractor under the subcontractor's QA program.

3.I.7 COMPLIANCE WITH NUREG-1536

The material in this supplement for the HI-STORM 100U system provides the same information as previously provided for the aboveground HI-STORM 100 systems. Therefore, to the extent applicable, the information provided is in compliance with NUREG-1536.

3.I.8 REFERENCES

The references in Section 3.8 apply to the VVM to the extent that they are appropriate for use with an underground system. The additional references below are specific to Supplement 3.I.

[3.I.1] SHAKE2000, A Computer Program for the 1-D Analysis of Geotechnical Earthquake Engineering Problems, G.A. Ordonez, Dec. 2000.

[3.I.2] LS-DYNA, Version 971, Livermore Software, 2006.

[3.I.3] USNRC Interim Staff Guidance (ISG-15), "Materials Evaluation", Revision 0, January 2001.

[3.I.4] ANSI/AWWA C105/A21.5-99, "American National Standard (ANSI) for Polyethylene Encasement for Ductile-Iron Pipe Systems".

[3.I.5] M. B. Bruce and M. V. Davis, "Radiation Effects on Organic Materials in Nuclear Plants", Final Report, 1981. (Prepared by Georgia Institute of Technology for EPRI)

[3.I.6] ANSI D 4082-02, "American National Standard (ANSI) Standard Test Method for Effects of Gamma Radiation on Coatings for Use in Light Water Nuclear Power Plants".

[3.I.7] USNRC Regulatory Guide (RG-1.54), "Service Level I, II and III Protective Coatings Applied to Nuclear Power Plants, Revision 1, July, 2000.

[3.I.8] ANSI D 3843-00, "American National Standard (ANSI) Standard Practice for Quality Assurance for Protective Coatings Applied to Nuclear Facilities".

[3.I.9] ANSI C 210-03, "American National Standard (ANSI) Standard Practice for Liquid-Epoxy Coating Systems for the Interior and Exterior of Steel Water Pipelines".

[3.I.10] Keeler & Long Inc. Product Data Sheet for Kolor-Proxy™ Primer KL3200 Series, Product Code KL3200.

[3.I.11] Samuel A. Bradford, "Practical Handbook of Corrosion Control in Soils", ASM International and CASTI Publishing Inc., 2004.

[3.I.12] L. M. Poukhonto, "Durability of Concrete Structures and Constructions – Silos, Bunkers, Reservoirs, Water Towers, Retaining Walls", A. A. Balkema Publishers, 2003.

[3.I.13] 49CFR Part 195 Subpart H "Corrosion Control", Title 49 of the Code of Federal Regulations, Oct, 1 2004 Edition, Office of the Federal Register, Washington, D.C.

[3.I.14] HI-2084023, SSI Analysis of HI-STORM 100U Using SASSI, Rev. 0 (a Subcontractor report prepared for Holtec by International Civil Engineering

Consultants, Rev. 2, April 2008) (Holtec Proprietary) .

[3.I.15] S. Stojko, Application of DYNA3D to Non-Liner Soil Structure Interaction (SSI) Analysis of Retaining Wall Structures, International LS-DYNA3D Conference, March 1993.

[3.I.16] ASLB Hearings, Private Fuel Storage, LLC, Docket # 72-22-ISFSI, ASLBP 97-732-02-ISFSI, February 2005.

[3.I.17] Topical Report – Design of Structures for Missile Impact", BC-TOP-9A, Rev. 2, Bechtel Corporation, 9/74

[3.I.18] SAE Technical Paper 2000-01-0627, Development and Validation of High Fidelity Vehicle Crash Simulation Models, S.W. Kirkpatrick, Applied Research Associates, Inc.

[3.I.19] H. Boyer, Atlas of Stress Strain Curves, ASM International, 1987, p.189.

[3.I.20] Thermal Ceramics Inc., Product Data Sheet for Blanket Products (Kaowool® Blanket).

[3.I.21] NACE Standard RP0285-2002 "Corrosion Control of Underground Storage Tank Systems by Cathodic Protection", NACE International.

[3.I.22] API RP1632, "Cathodic Protection of Underground Petroleum Storage Tanks and Piping Systems", American Petroleum Institute.

[3.I.23] NACE RP0169-96, "Control of External Corrosion on Underground or Submerged Piping Systems", NACE International.

[3.I.24] 49CFR Part 192 Subpart I "Requirements for Corrosion Control, Title 49 of the Code of Federal Regulations, Oct, 1 2004 Edition, Office of the Federal Register, Washington, D.C.

[3.I.25] ACI 544.3R-93 (or latest), Guide for Specifying, Proportioning, Mixing, Placing, and Finishing Steel Fiber Reinforced Concrete.

[3.I.26] ASTM C1116-03 (or latest) Standard Specification for Fiber-Reinforced Concrete and Shotcrete.

[3.I.27] HI-2053389, Calculation Package Supporting Structural Evaluation of HI-STORM 100U, Revision 9, September 2010 (Holtec Proprietary).

[3.I.28] ASCE 4-98, Seismic Analysis of Safety-Related Nuclear Structures and Commentary, American Society of Civil Engineers, 2000.

[3.I.29] ASCE/SEI 43-05, Seismic Design Criteria for Structures, Systems, and Components in Nuclear Facilities, American Society of Civil Engineers, 2005.

[3.I.30] Sandia National Laboratory Contractor Report SAND97-2426, Penetration Equations, C.Y. Young, Applied Research Associates, Inc., Albuquerque NM 87110.

[3.I.31] Doug Ammerman and Gordon Bjorkman, "Strain-Based Acceptance Criteria for Section III of the ASME Boiler and Pressure Vessel Code", Proceedings of the 15th International Symposium on the Packaging and Transportation of Radioactive Materials, PATRAM 2007, October 21-26, 2007, Miami, Florida, USA.

[3.I.32] ACI-349 (2001), Code Requirements for Nuclear Safety Related Concrete Structures (ACI 349-01) and Commentary (ACI 349R-01), Appendix C, American Concrete Institute, 2001.

[3.I.33] ANSYS 11.0, ANSYS Inc., 2007 and ANSYS 13.0, Ansys Inc., 2010, Copyright SAS IP, Inc.

TABLE 3.I.1

HI-STORM 100U BOUNDING WEIGHT DATA

Item	Bounding Weight (lb)
MPCs	
• Without SNF	See Table 3.2.1
• Fully loaded with SNF and Fuel Spacers	90,000
HI-STORM 100U VVM	
• Closure Lid (with shielding concrete)	24,000
• CEC (empty without Closure Lid)	33,000
• Maximum Loaded Weight (with bounding MPC)	147,000
Loaded Transporter (Typical)	
• Carrying a loaded HI-TRAC	400,000
• Empty	160,000
• Length & width of each load patch (2 load patches per transporter)	197.1875 inch by 29.5 inch
• Computed average normal pressure on two load patches	34.4 psi
Loaded HI-TRAC and Mating Device	275,000
Note 1: CEC and Closure Lid include an overage up to 5% Note 2: Transporter weight is based on representative units used in the industry.	

TABLE 3.I.2

CENTER OF GRAVITY DATA FOR THE HI-STORM 100U SYSTEM

Component	Height of CG Above Datum (in)
MPC	See Table 3.2.3
HI-STORM 100U VVM CEC (empty without Closure Lid)	108.7
HI-STORM 100U VVM Closure Lid	20.26
Note: Datum for CEC is at the top surface of the foundation; datum for Closure Lid is at bottom surface of baseplate of lid.	

TABLE 3.I.3 (a)*
RELEVANT MATERIAL PROPERTIES FOR THE HI-STORM 100U
Yield, Ultimate, Linear Thermal Expansion, Young's Modulus

Temp. (Deg. F)	SA516 and SA515, Grade 70			
	S_y	S_u	α	E
-40	38.0	70.0	---	29.95
100	38.0	70.0	5.53 (5.73)	29.34
150	36.3	70.0	5.71 (5.91)	29.1
200	34.6	70.0	5.89 (6.09)	28.8
250	34.15	70.0	6.09 (6.27)	28.6
300	33.7	70.0	6.26 (6.43)	28.3
350	33.15	70.0	6.43 (6.59)	28.0
400	32.6	70.0	6.61 (6.74)	27.7
450	31.65	70.0	6.77 (6.89)	27.5
500	30.7	70.0	6.91 (7.06)	27.3
550	29.4	70.0	7.06 (7.18)	27.0
600	28.1	70.0	7.17 (7.28)	26.7
650	27.6	70.0	7.30 (7.40)	26.1
700	27.4	70.0	7.41 (7.51)	25.5
750	26.5	69.3	7.50 (7.61)	24.85
800	25.3	64.3	7.59 (7.71)	24.2

* Footnotes in corresponding table in Section 3.3 apply to the values in parentheses.

TABLE 3.I.3 (b)
DESIGN AND LEVEL A: ALLOWABLE STRESS FROM ASME NF
Material : **SA516 Grade 70, SA515 Grade 70**
Service Conditions: **Design and Level A Stress**
Item: **Stress**

Temp. (Deg. F)	Classification and Value (ksi)		
	S	Membrane Stress	Membrane plus Bending Stress
-20 to 650	17.5	17.5	26.3
700	16.6	16.6	24.9
750	14.8	14.8	22.2
800	12.0	12.0	18.0

TABLE 3.I.3 (c)
LEVEL D: STRESS INTENSITY

Code: **ASME NF**
Material: **SA516, Grade 70**
Service Conditions: **Level D**
Item: **Stress Intensity**

Temp. (Deg. F)	Classification and Value (ksi)		
	S_m	P_m	$P_m + P_b$
-20 to 100	23.3	45.6	68.4
200	23.1	41.5	62.3
300	22.5	40.4	60.6
400	21.7	39.1	58.7
500	20.5	36.8	55.3
600	18.7	33.7	50.6
650	18.4	33.1	49.7
700	18.3	32.9	49.3

TABLE 3.I.3 (d)

Code: ASME NB
Material: Alloy X
Service Conditions: Level D
Item: Stress Intensity

Temp. (Deg. F)	Classification and Value (ksi)		
	P_m	P_L	$P_L + P_b$
-20 to 100	48.0	72.0	72.0
200	48.0	72.0	72.0
300	46.2	69.3	69.3
400	44.9	67.4	67.4
500	42.0	63.0	63.0
600	39.4	59.1	59.1
650	38.4	57.6	57.6
700	37.4	56.1	56.1
750	36.5	54.8	54.8
800	35.8	53.7	53.7

TABLE 3.I.4
REFERENCE AND DERIVED PROPERTIES OF ISFSI REINFORCED CONCRETE, SUBGRADE, AND UNDERGRADE

Property	Value
Concrete Compressive Strength (psi)	4,500
Concrete Rupture Strength (psi)	335.4
Allowable Bearing Stress (psi)	4,972.5*
Mean Coefficient of Thermal Expansion (in/in-deg. F)	5.5E-06
Modulus of Elasticity (psi)	57,000 x (Concrete Compressive strength (in psi))$^{1/2}$
Subgrade Yield Stress (psi)	25¥
Subgrade Strain Compatible Modulus of Elasticity (ksi) (see Figure 2.I.5)	Space A: 18.8 Space B: 14.0 Spaces C and D: 17.7

* Per ACI-318 (2005), Sec. 10.17.1 and Sec. 9.3.2.4. Since the ISFSI concrete is always confined, the allowable value is doubled.

¥ Only applied to Space A.

TABLE 3.I.5
SOIL PROPERTIES, COMPUTED SETTLEMENT, AND CORRESPONDING ELASTIC MODULII FOR THE SUBGRADE

	Item	Value
1.	Characteristics for Subgrade Below SFP: Water Content 'w_n' Soil Parameter 'a' Soil Parameter 'b' Poisson's Ratio	 14% 0.18 0.13 0.45
2.	Derived Properties for the Subgrade Below SFP (Note 1): Computed Long-Term Settlement (in) (Note 2) Computed Elastic Modulus (psi)	 0.189 5,377
3.	Values used in the Structural Analyses Model for Subgrade Below SFP: Limiting Long-Term Settlement (in) Corresponding Elastic Modulus (psi)	 From Table 2.I.2 5,081
4.	Soil Characteristics for Subgrade Above SFP: Water Content 'w_n' Soil Parameter 'a' Soil Parameter 'b' Poisson's Ratio	 14% 0.09 0.13 0.45
5.	Derived Properties for the Subgrade Above SFP (Note 3): Computed Long-Term Settlement (in) (Note 2) Computed Elastic Modulus (psi)	 0.39 5,073
6.	Values used in the Structural Analyses Model for Subgrade Above SFP: Long-Term Settlement (in) Corresponding Elastic Modulus (psi)	 From Table 2.I.2 4,946

Note 1: The substrate characteristics are obtained using the density data from Table 2-3 and Table 5-1 of reference [2.I.7]. The soil compaction index 'Cc' is a direct function of soil parameters w_n, a, and b per [2.I.7]. The long-term settlement and the elastic modulus are derived using the relationships in [2.I.6].

Note 2: See Table 2.I.2 for the values of settlement (greater than those computed here for conservatism) used as the Design Basis data for qualification of the ISFSI structures.

Note 3: The Design Basis settlement has been set at a higher value than that computed for the TSP and SFP to allow for the variation in the soil parameters at a host site.

TABLE 3.I.6
MENU OF LS-DYNA RUNS (SSI ANALYSES)

No.	Case	Comment
1.	VVM array model (5x5 array) with 100% concrete modulus for the SFP	To obtain interface load for the ISFSI structures
2.	VVM array model (5x5 array) with 50% concrete modulus for the SFP	To obtain interface load for the ISFSI structures
3.	VVM array model (5x5 array) for the optional ISFSI design with retaining walls	To obtain interface load for the ISFSI structures
4.	Design Basis Single VVM seismic model	To qualify VVM components.

TABLE 3.I.7
ISFSI INTERFACE LOADS OBTAINED FROM LS-DYNA SSI SIMULATIONS

Interface Load	Case 1	Case 2	Case 3	Case 4
CEC to SFP Impact Load, lb	6.499×10^5	6.267×10^5	6.590×10^5	6.433×10^5
Transporter to TSP Contact Load per Track, lb	1.078×10^6	1.109×10^6	N/A	1.148×10^6
Soil Compressive Load on the Retaining Wall, lb	N/A	N/A	3.290×10^6	N/A
In-Plane Tensile Load on TSP from Retaining Wall, lb	N/A	N/A	9.672×10^5	N/A
In-Plane Tensile Load on SFP from Retaining Wall, lb	N/A	N/A	2.287×10^6	N/A

TABLE 3.I.8
LOADS APPLIED IN THE ISFSI STRUCTURAL EVALUTION†

Load on ISFSI	Simulation Models I, II and III	Simulation Model IV
Load on SFP at each VVM location ‡, lbf	660,000	660,000
Total Load on TSP due to Transporter ‡, lbf	$5.6 \times 400000 = 2.24 \times 10^6$	N/A
In-Plane Tensile Load on TSP Extreme Face, lbf	N/A	9.68×10^5
In-Plane Tensile Load on SFP Extreme Face, lbf	N/A	2.29×10^6

Notes:
† For conservatism, the loads used for ISFSI structural evaluation bound the peak loads obtained from SSI simulations (see Table 3.I.7).

‡ The listed load is a sum of dead and seismic components. These loads are appropriately divided as dead and seismic in ANSYS prior to applying the appropriate load factors and combinations per Table 2.I.11.

TABLE 3.I.9*

RESULTS FROM TORNADO MISSILE ANALYSIS (LOAD CASE 03 OF TABLE 2.I.5)			
Item	**Bounding Value, inch**	**Allowable Value, inch**	**Safety Factor**
Maximum Vertical Displacement of lid (inch) (inclined impact)	< 3	12**	> 4
Perforation of Inner Shield Dome Steel	Yes (see Fig. 3.I.7)	N/A	N/A
Maximum Peak Impact Force (kips)	< 1,000	1,849	**> 1**
* Details of the calculations can be found in [3.I.27]. ** This is the minimum distance between the Closure Lid bottom plate and the top lid of the MPC.			

TABLE 3.I.10
MOMENT RESULTS AND CORRESPONDING MINIMUM SAFETY FACTORS FOR THE ISFSI STRUCTURES

Support Foundation Pad (SFP) ‡				
ISFSI Load Configuration	Moment Induced (lbf-in/in)	Axial Force (lbf/in)	Corresponding Moment Capacity (lbf-in/in)	Minimum Safety Factor (Limiting Element No.)
Simulation Model I	192,000	-1529.8	263,270	1.371 (1766)
Simulation Model II	192,990	-2965.3	276,665	1.434 (3329)
Simulation Model III	230,920	-2541.3	272,710	1.181 (1766)
Simulation Model IV	168,140	-2158.8	269,141	1.601 (1520)
Simulation Model V	170,170	5,140	180,583	1.061 (1766)
Top Surface Pad (TSP) ‡				
Simulation Model I	318,070	-15713	347,755	1.093 (67115)
Simulation Model II	186,960	-4707.9	258,978	1.385 (147092)
Simulation Model III	293,240	-11386	312,850	1.067 (67115)
Simulation Model IV	277,670	-8660.1	290,860	1.048 (66996)
Simulation Model V	82,161	-966	228,791	2.785 (97531)
Retaining Wall †				
Fully Loaded (Case 3 of Table 3.I.6)	80,000	N/A	175,000	2.19

TABLE 3.I.10 (continued)
MOMENT RESULTS AND CORRESPONDING MINIMUM SAFETY FACTORS FOR THE ISFSI STRUCTURES

‡ The moment capacities for the SFP and TSP are calculated using axial-force-moment interaction diagram corresponding to the axial force and moment induced in the limiting element. An example showing the moment and axial force calculation for the limiting element, using the in-plane stresses, is included under Figure 3.I.18.b. Figures 3.I.18a through 3.I.22c also capture the stress plots for the governing load combination (LC-3 in Table 2.I.11) for all the ISFSI loading configurations analyzed. These figures also identify the limiting element (i.e., maximum loaded element) that corresponds with the results presented above.

Note that the flexural safety factors calculated above are based on the maximum moment induced in a single element, which is very conservative. Averaging over a width of the loaded section would result in much higher safety factors.

† The moment capacity for the Retaining Wall is based on the pure bending.

TABLE 3.I.11
PUNCHING SHEAR SAFETY FACTORS FOR ISFSI STRUCTURES

ISFSI Structure	Punching Safety Factor
SFP†	2.1
TSP	1.32
† Note that the punching shear calculation for the SFP is conservatively based on a bounding load of 950 kips.	

TABLE 3.I.12
PRESUMPTIVE SOIL BEARING

Computed Bearing Stress (psi)	Allowable Bearing Stress (psi)	Safety Factor	Minimum Safety Factor Required per [2.I.8]
42.8	90	2.1	2.0

TABLE 3.I.13
RESULTS OF STRENGTH EVALUATION FOR RETAINING WALL SHEAR CONNECTIONS

Component	Minimum Safety Factor
Top Shear Key	9.41
Bottom Dowels	1.56

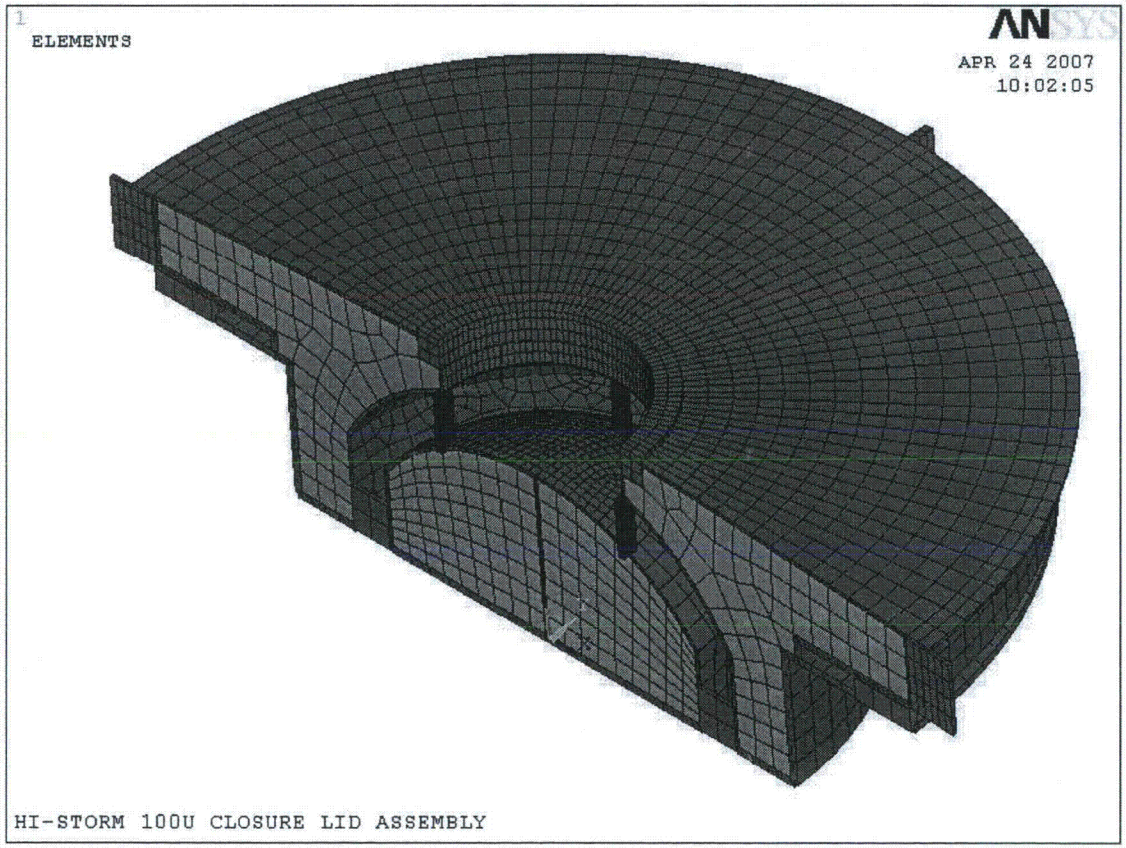

Figure 3.I.1; 3-D ANSYS/LSDYNA Finite Element Model of Closure Lid (Current Configuration)

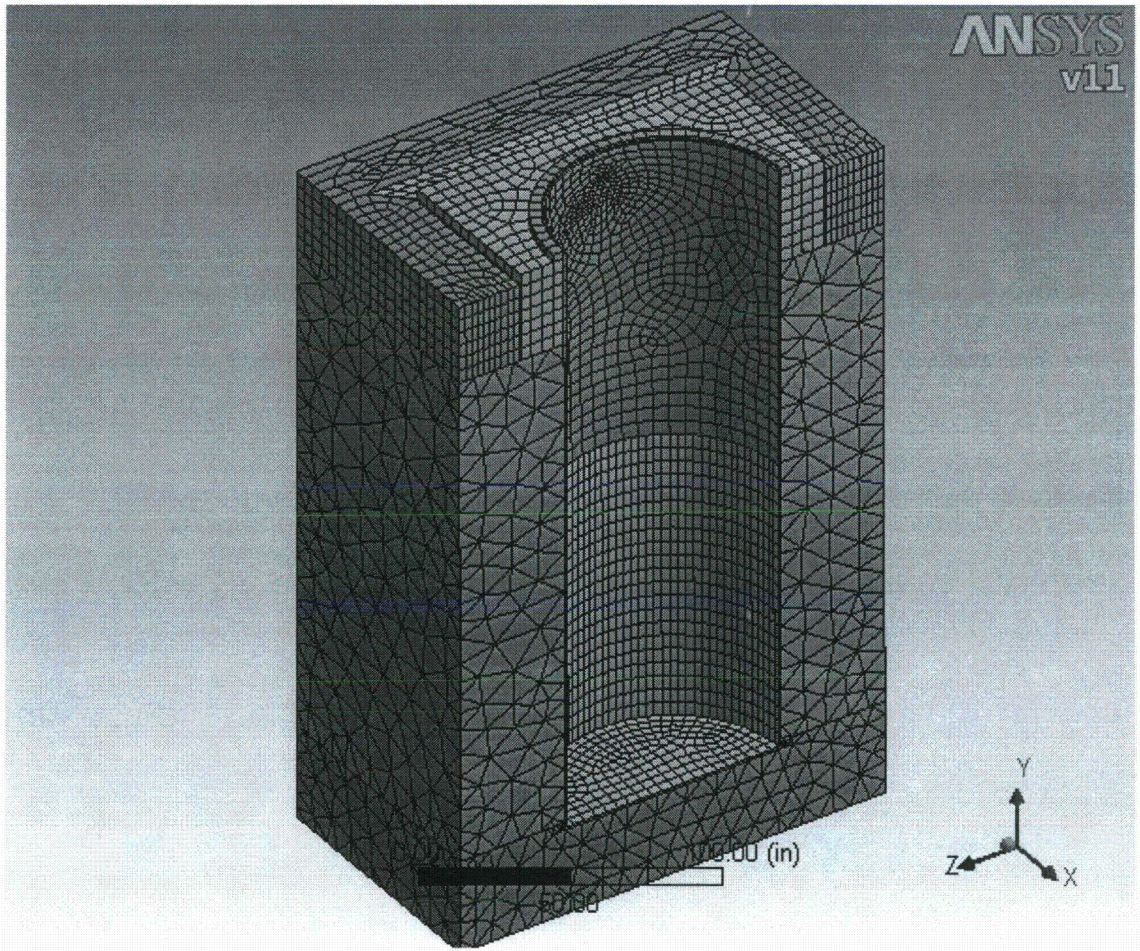

Figure 3.I.2; 3-D ANSYS Finite Element One-Half Model of Substrate Surrounding VVM, CEC Container Shell, TSP, and VIP

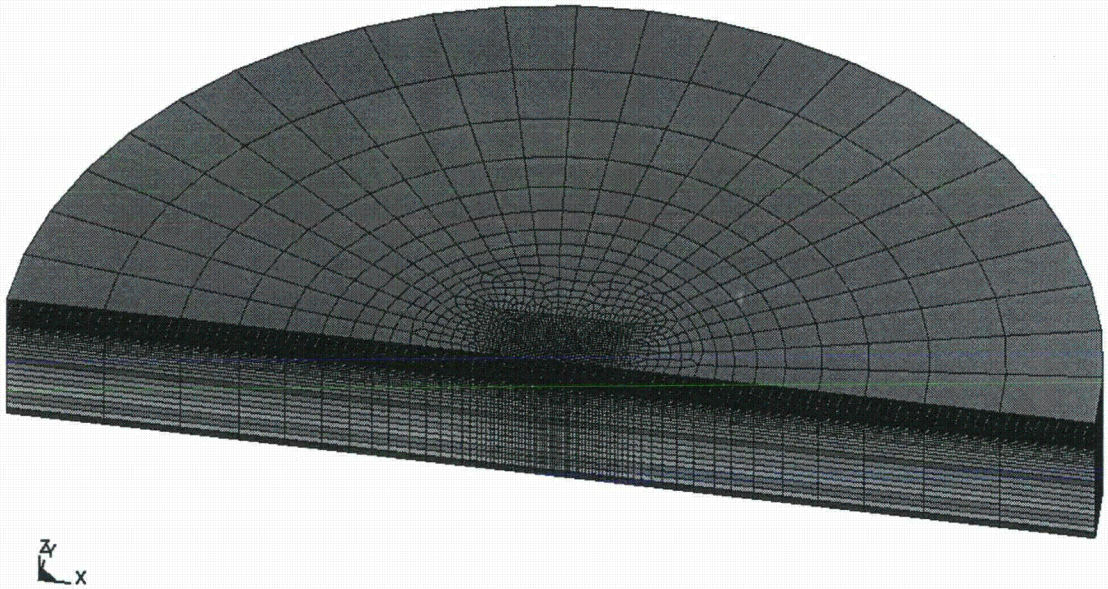

Figure 3.I.3-A; 3-D LSDYNA Soil Model for Design Basis Seismic Response Analysis

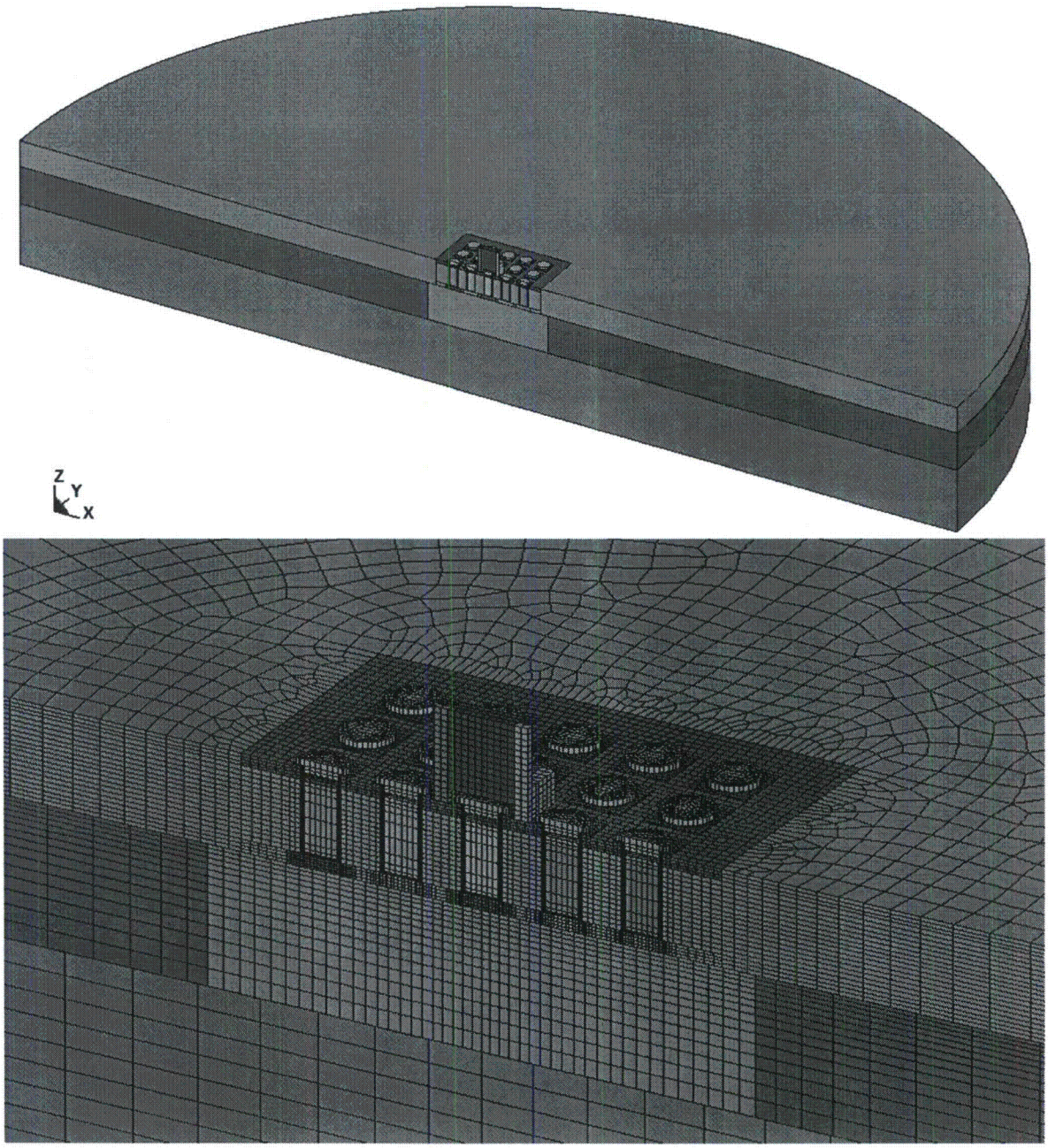

Figure 3.I.3-B; 3-D LSDYNA Model for Non-Linear SSI Analysis of 5x5 loaded VVMs on the Support Foundation

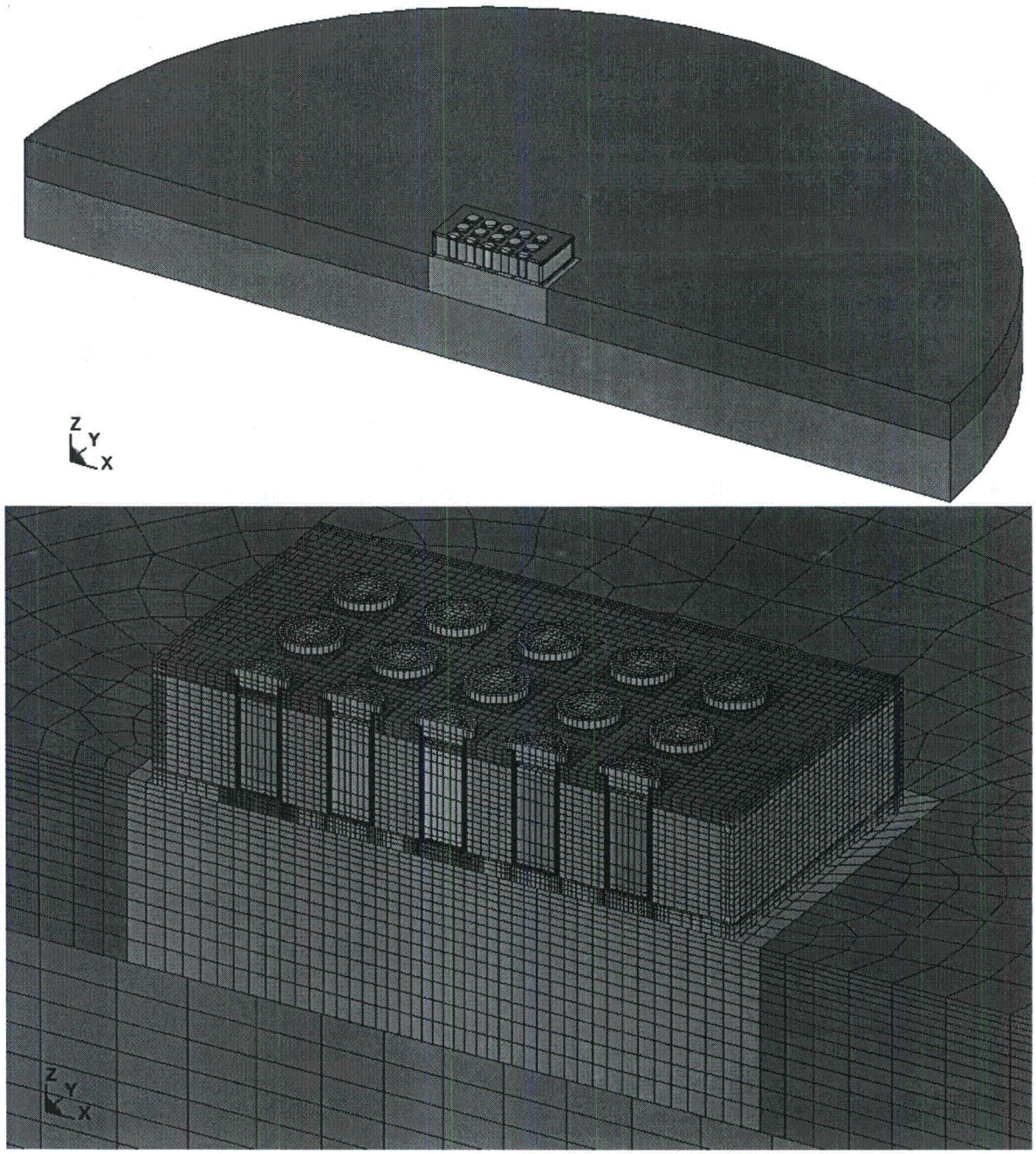

Figure 3.I.3-C; 3-D LSDYNA Model for Non-Linear SSI Analysis of 5x5 loaded VVMs on the Support Foundation with Retaining Walls

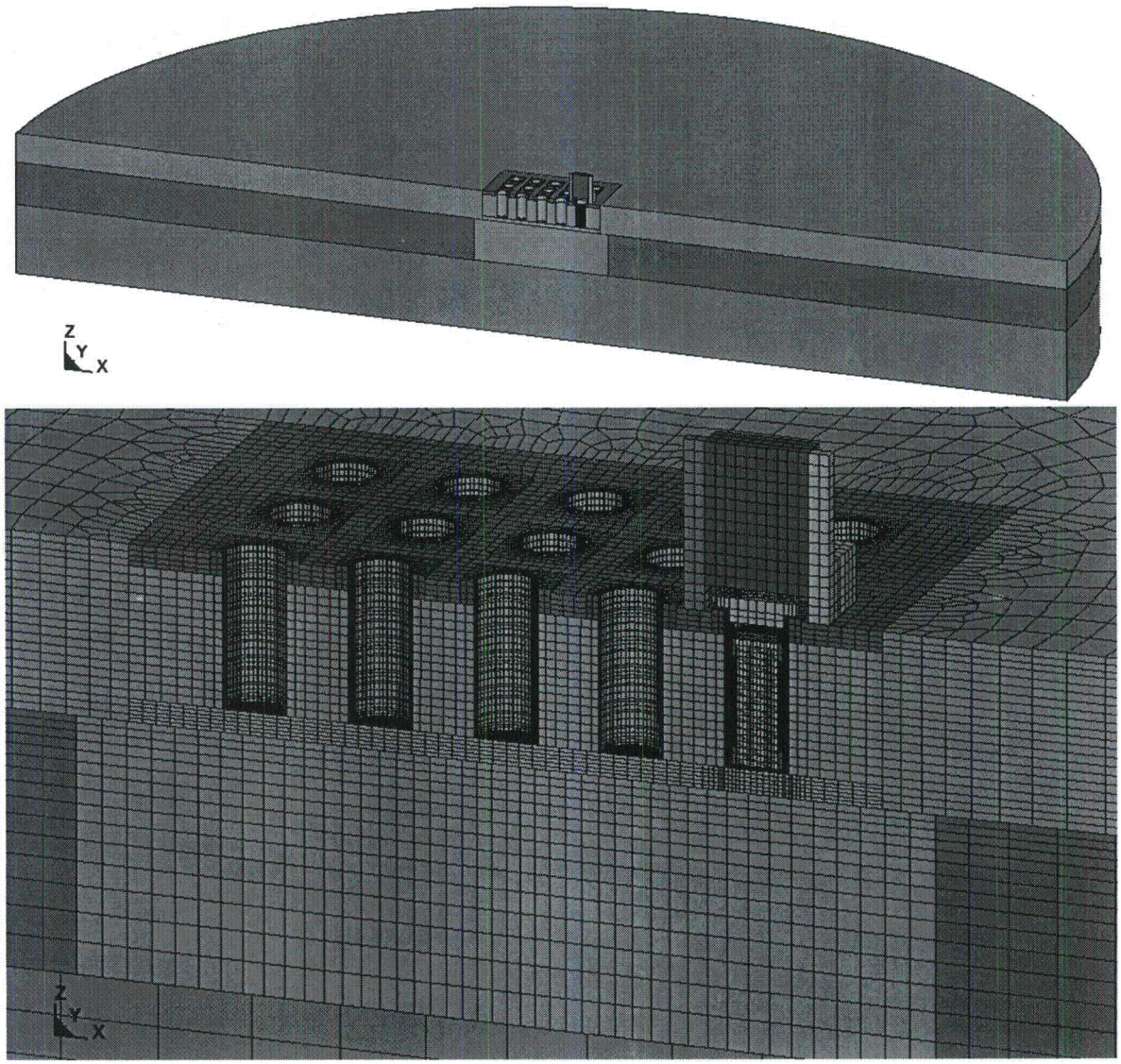

Figure 3.I.3-D; 3-D LSDYNA Model for Non-Linear SSI Analysis of a single VVM on Support Foundation

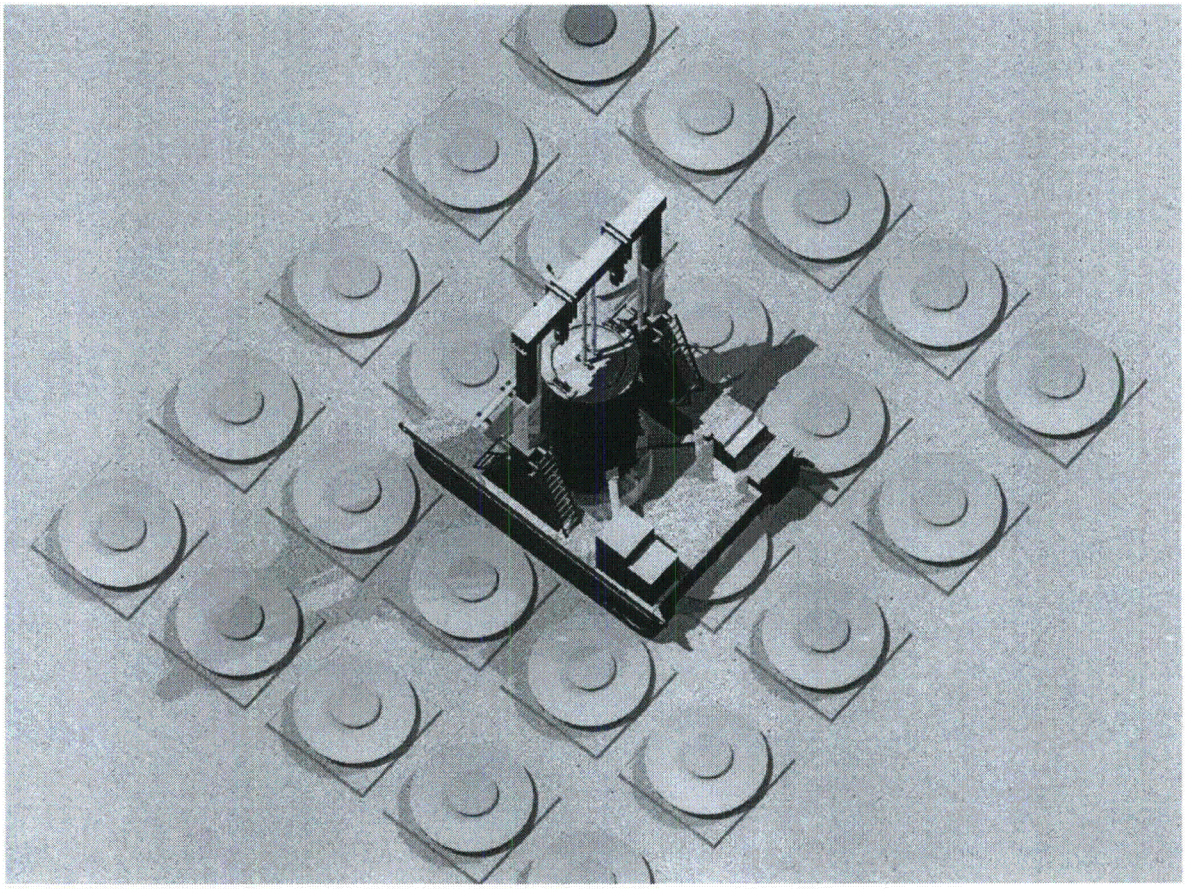

Figure 3.I.4; Cask Transporter on the ISFSI Positioned to Transfer MPC in the Central Cavity in the 5x5 VVM Array (illustrative analysis case)

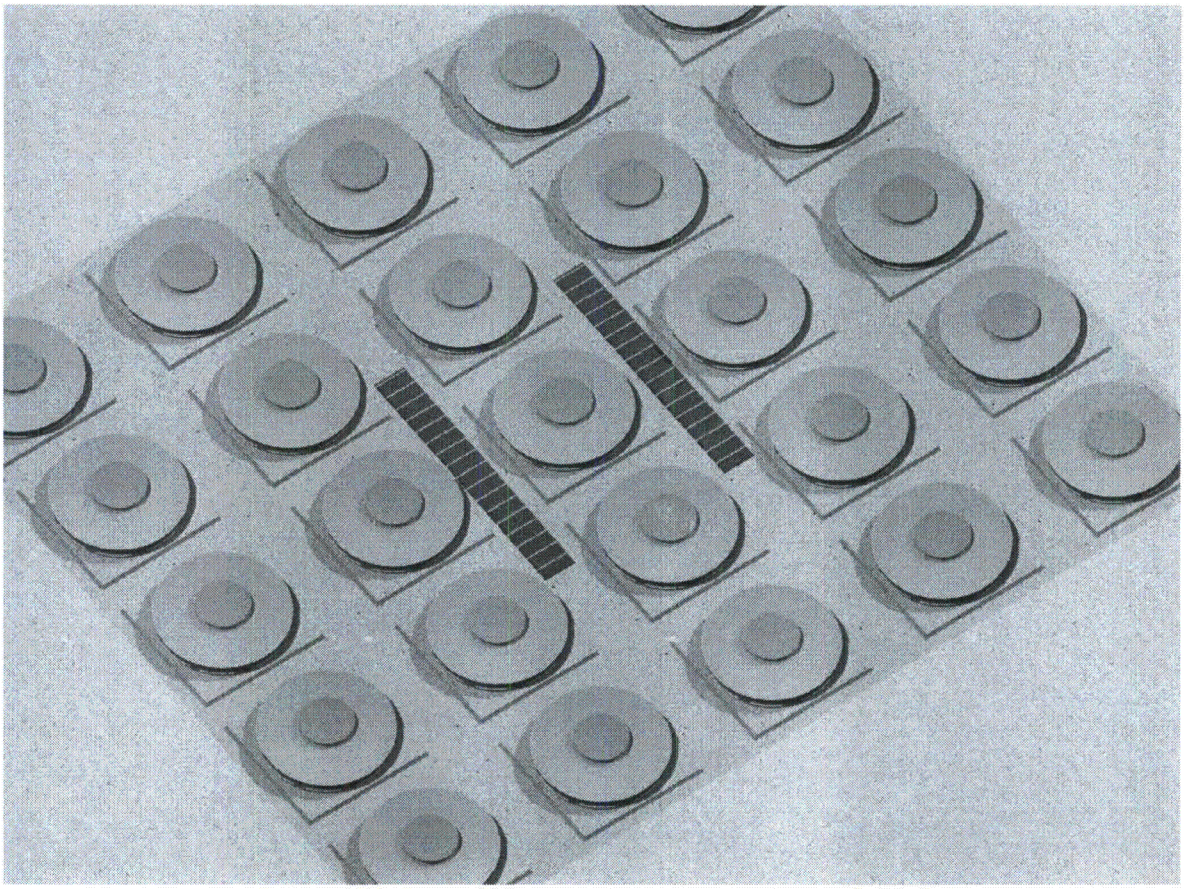

Figure 3.I.5; Load patch from the loaded Transporter in Figure 3.I.19
(Illustrative analysis case)

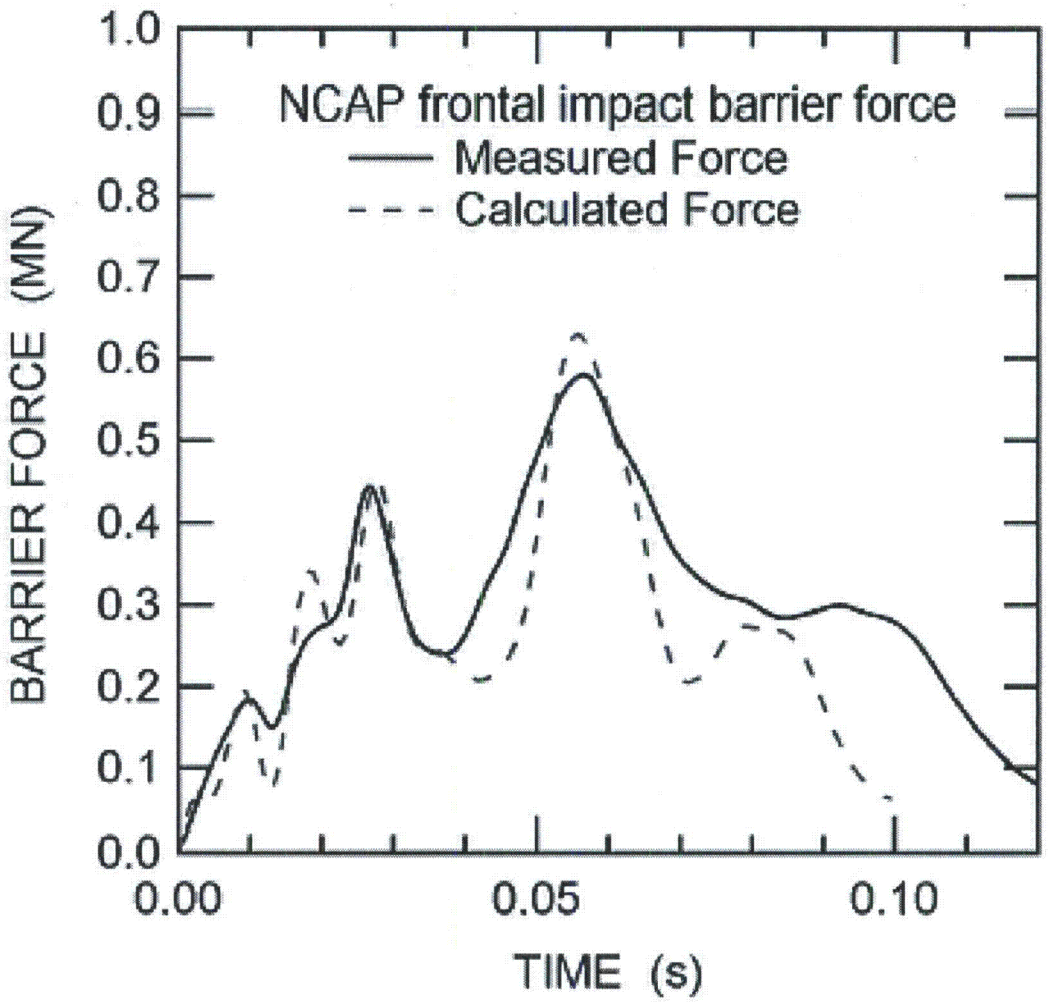

Figure 3.I.6; Test Results from 35mph Impact of a Ford (1705 Kg) Against a Rigid Wall

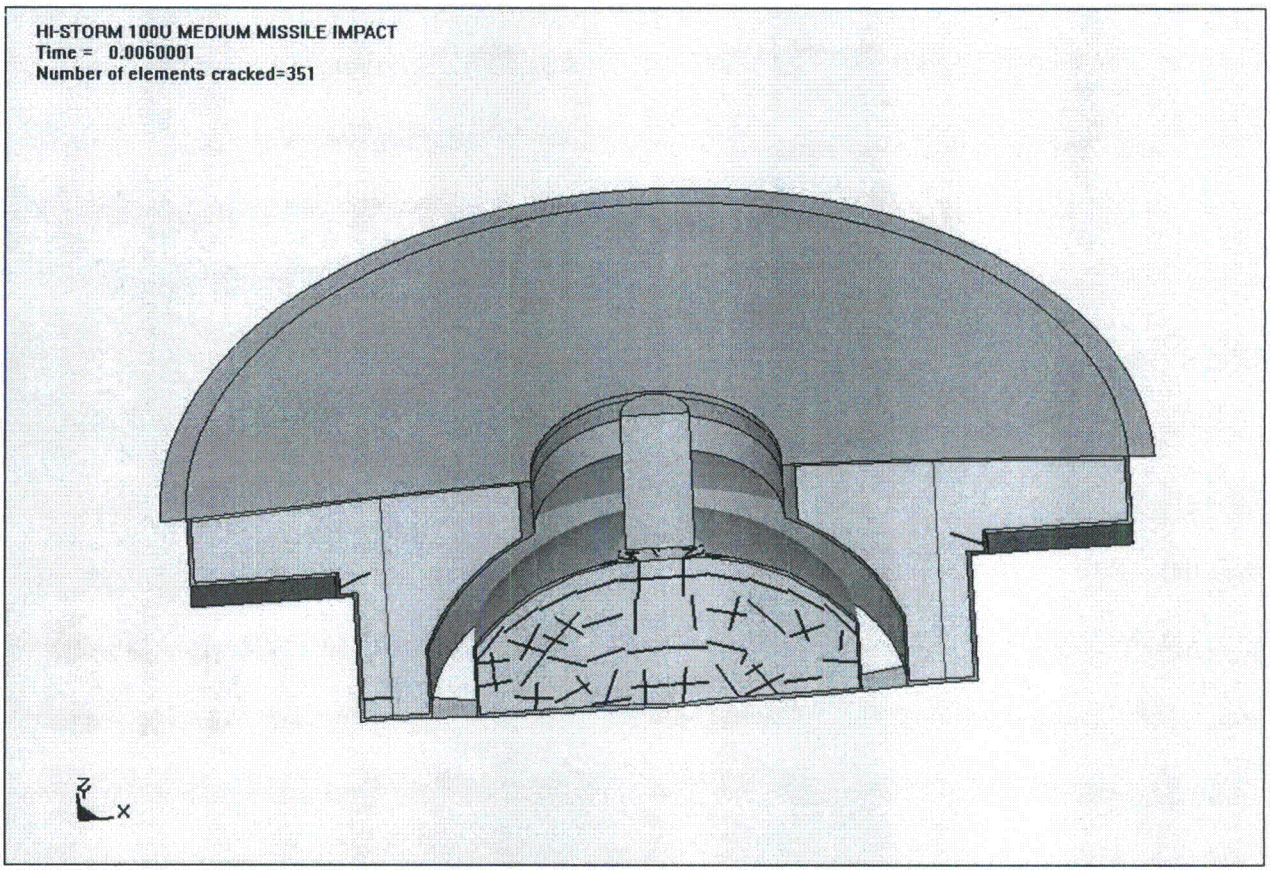

Figure 3.I.7; LSDYNA Model Section for Central Intermediate Missile Strike (subsequent to impact)

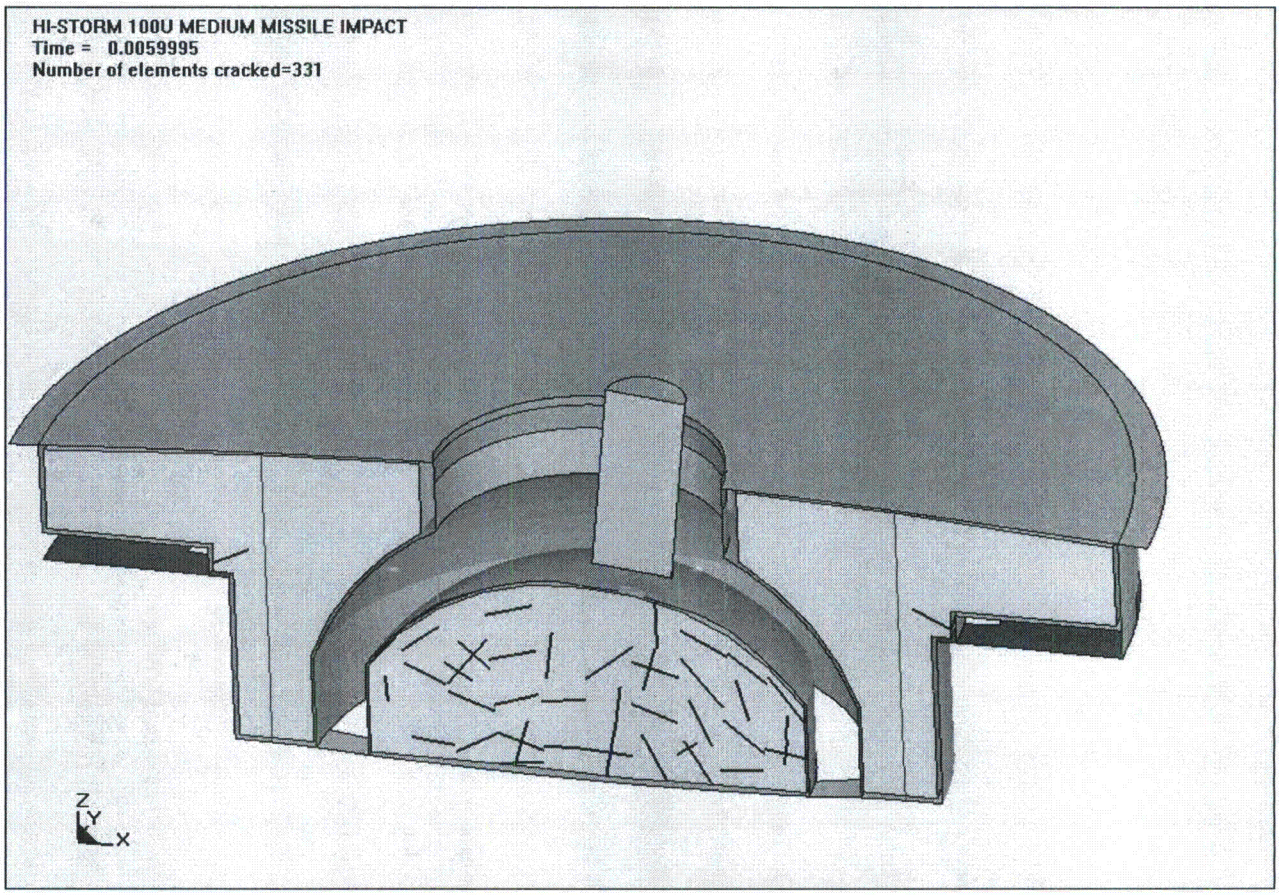

Figure 3.I.8; LSDYNA Model Section for Inclined Intermediate Missile Strike (subsequent to impact)

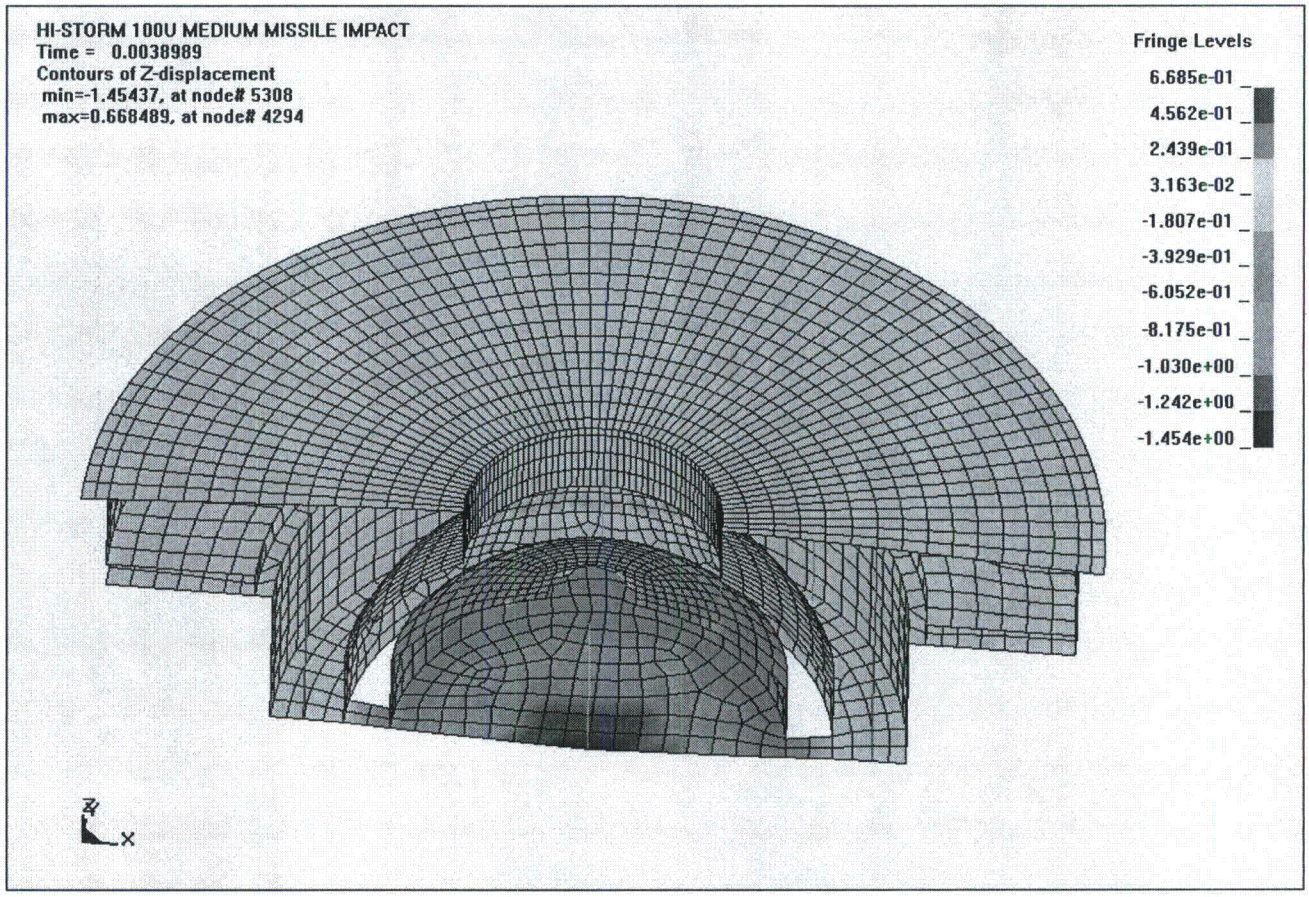

Figure 3.I.9; Deformation Profile at Time of Maximum Deformation – Central Strike

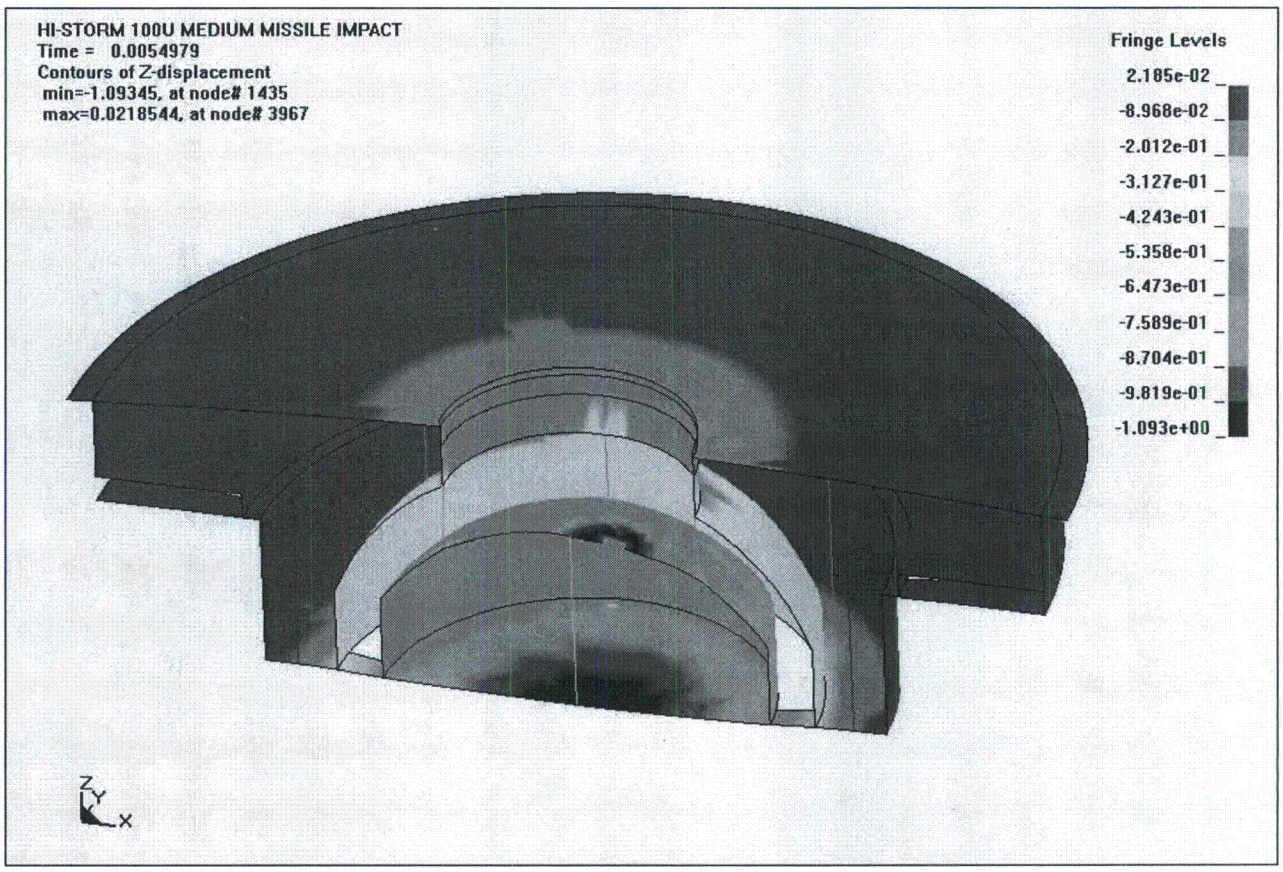

Figure 3.I.10; Deformation Profile at Time of Maximum Deformation – Inclined Strike

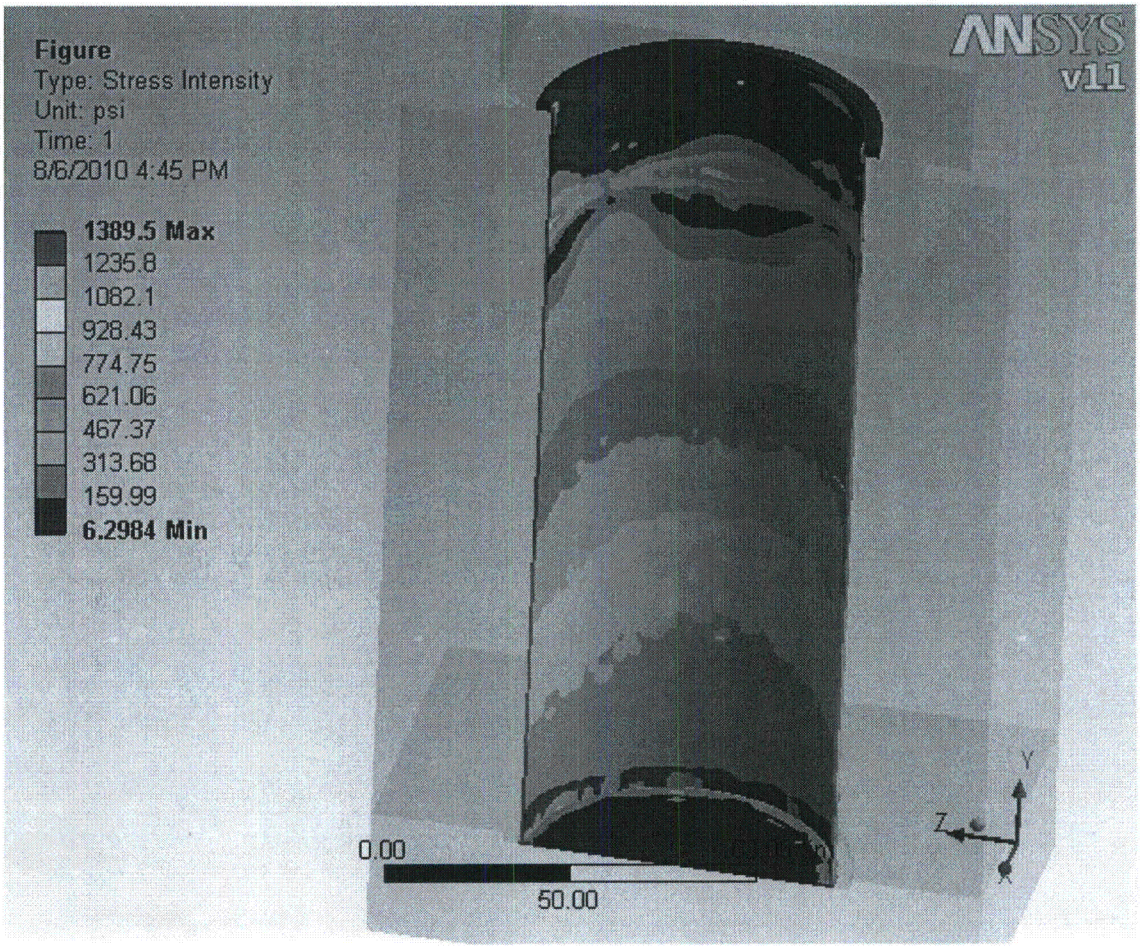

Figure 3.I.11; Stress Distribution in CEC Shell from Transporter and Substrate (Load Case 07)

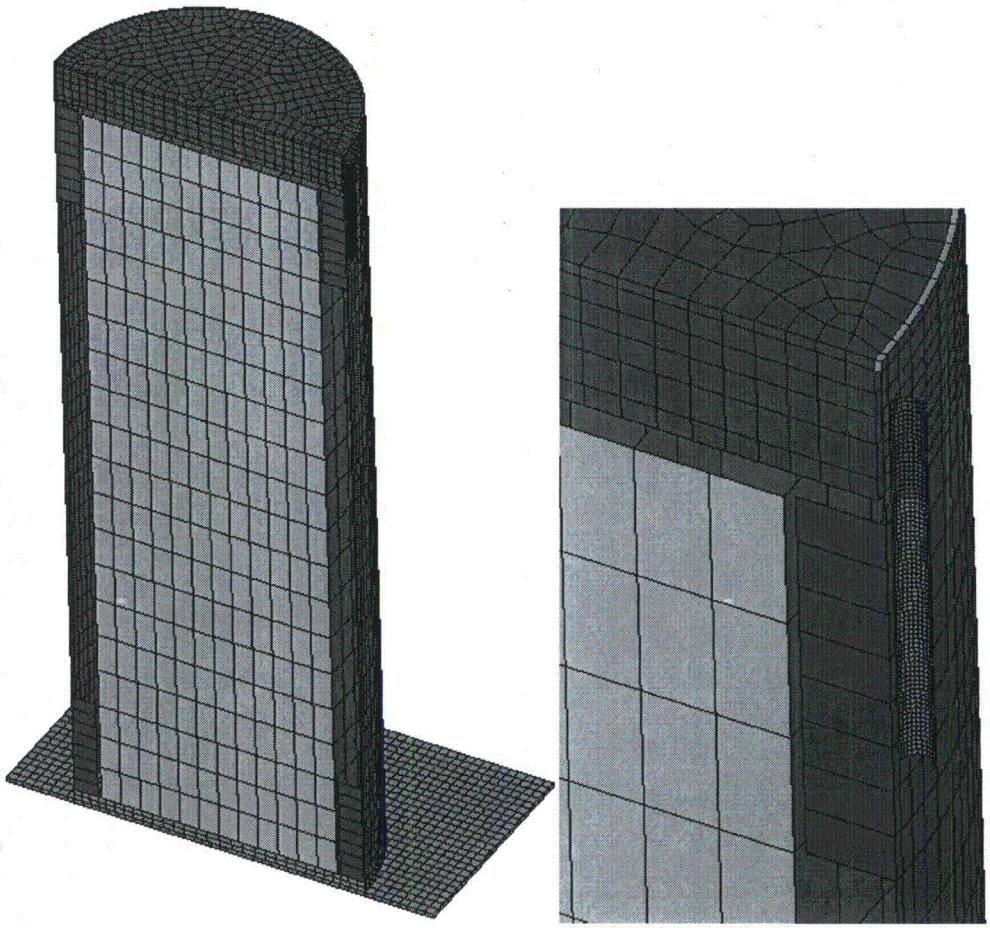

Figure 3.I.12; MPC Guide/MPC Impact LS-DYNA Model

Figure 3.I.13; Maximum Plastic Strain of the MPC Enclosure Members in the Impact Region

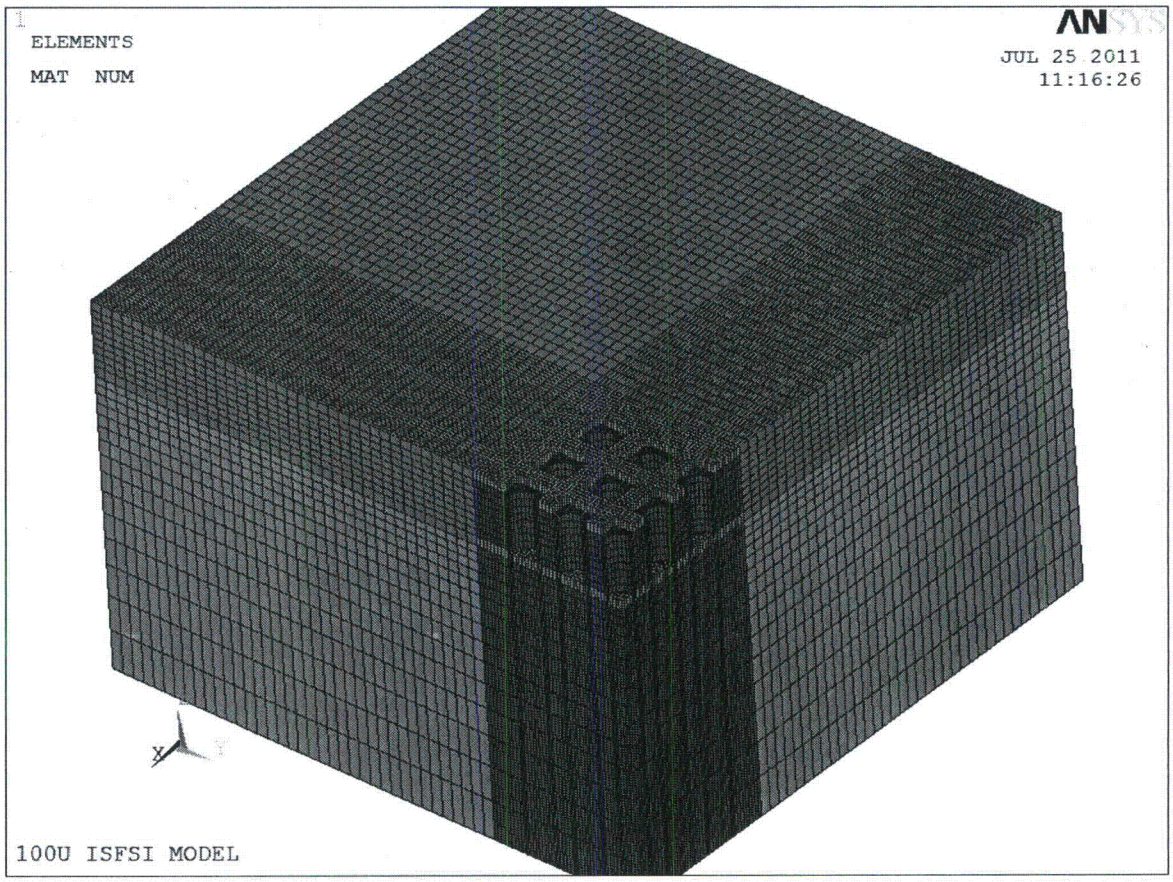

Figure 3.I.14; Finite Element Model of the ISFSI Reinforced Concrete Structures for Simulation Models I, III and IV

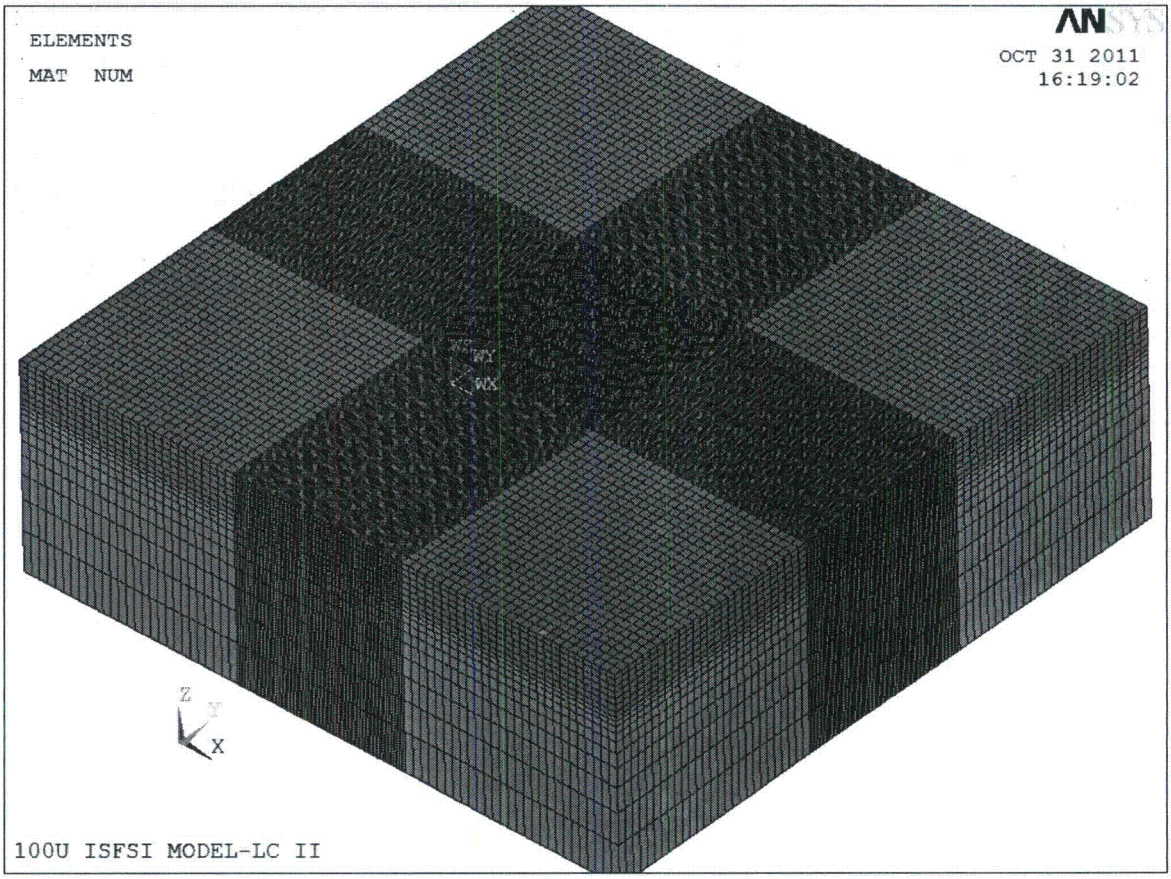

Note that Simulation Model II is identical to Models I, III and IV in all respects, except that this is a full FE model with coarser element mesh for the soil components (soil elements). Also note that the symmetric boundary constraint does not apply to the full model.

Figure 3.I.15; Finite Element Model of the ISFSI Reinforced Concrete Structures for Simulation Model II

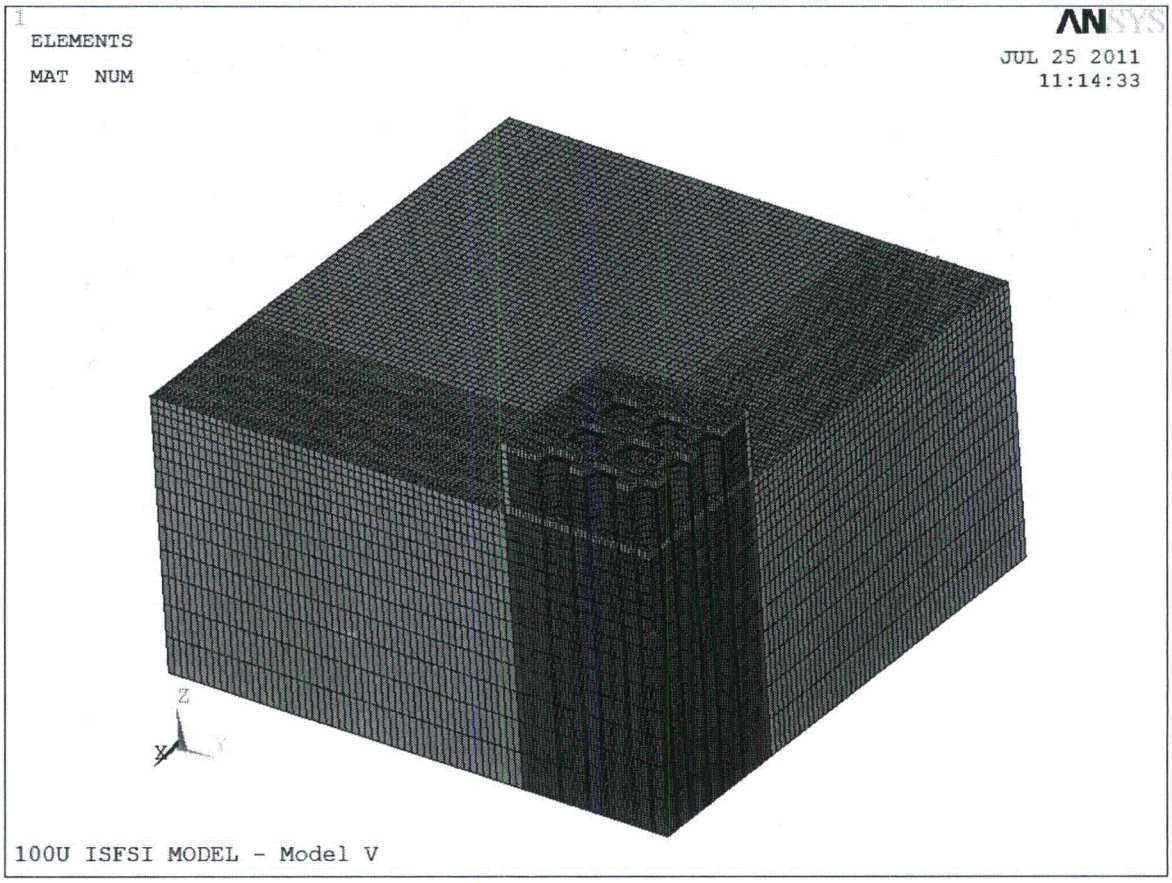

Figure 3.I.16; Finite Element Model of the ISFSI Reinforced Concrete Structures for Simulation Model V (with Optional Retaining Wall)

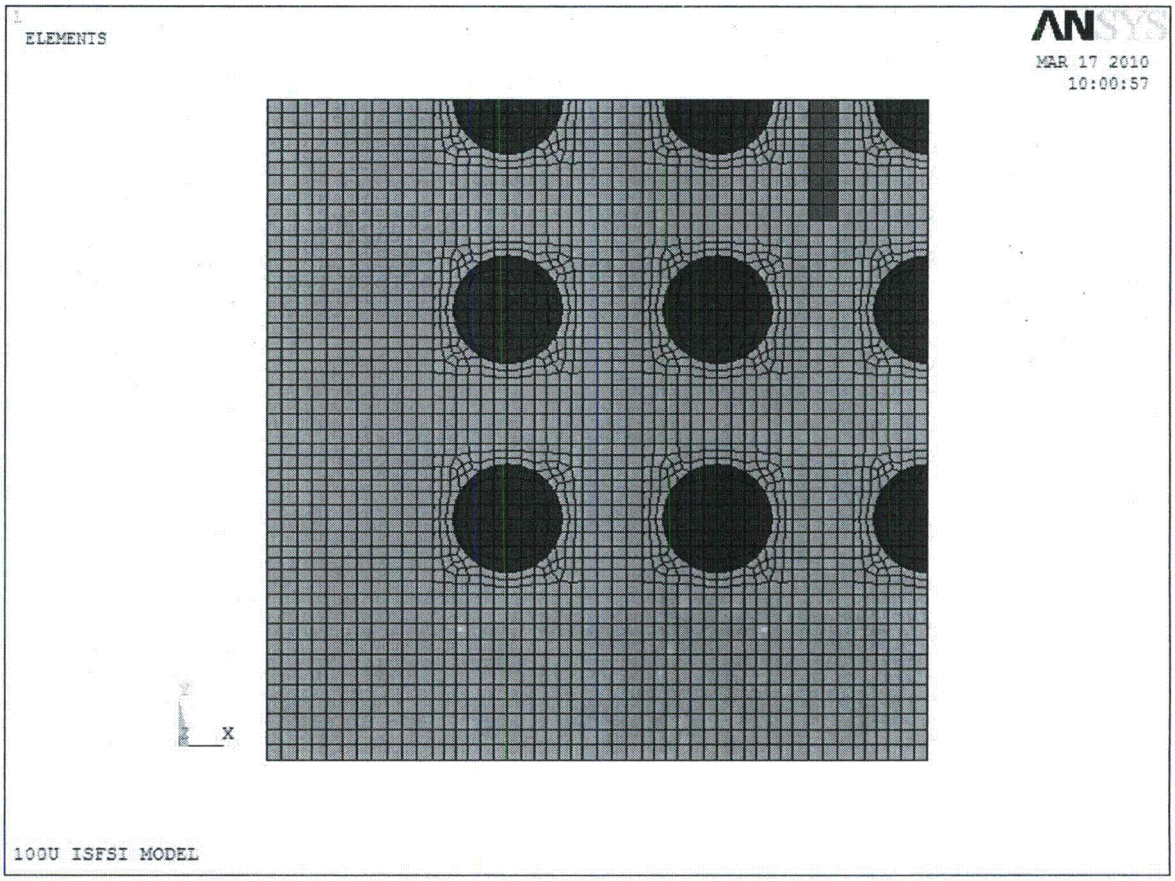

Note: The blue footprints show the SFP area loaded with the SSC's and the red footprint represents the loaded TSP area with the transporter (VCT). The soil extending beyond the SFP boundary is not shown in the above plot for clarity.

Figure 3.I.17; ANSYS Finite Element Model of ISFSI Showing the Fully Loaded Configuration (Simulation Model I)

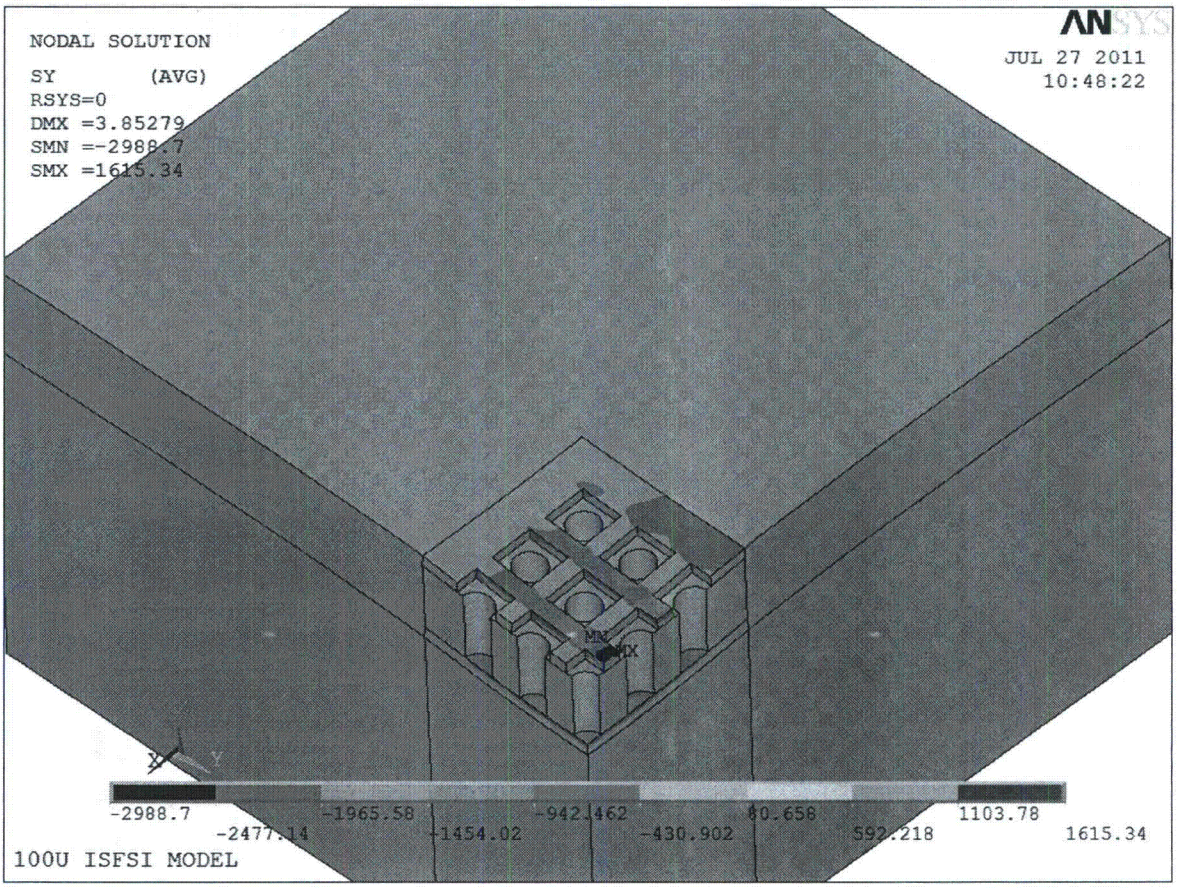

Figure 3.I.18a; Normal Stress (Sy) in the ISFSI in the Direction of the Transporter Path for Simulation Model I – Load Combination LC-3 from Table 2.I.11

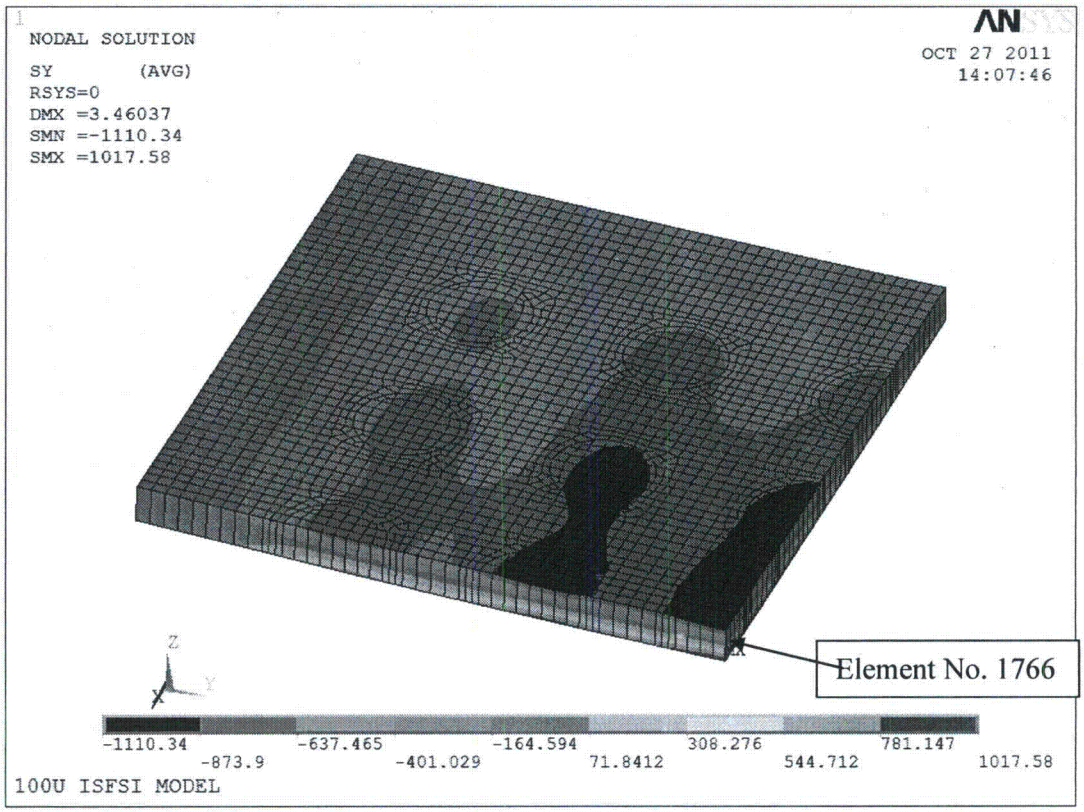

Notes:
Element 1766 realizes the maximum loading and produces the limiting safety factor.

Moment (Mx) in the limiting element is calculated as = {1017.6-(-1110.3)} x $33^2/12$ = 193,106.9 lbf-in/in, Axial Force (Fx) in the limiting element is calculated as = {(-1110.3)+1017.6} x 33/2 = -1529.6 lbf/in, where 33 represents the thickness of the SFP in inches. The axial force and moment values calculated here correspond well with the results shown in Table 3.I.10 for the SFP for Simulation Model I. The small deviation (less than 0.6%) from the results shown in Table 3.I.10 is due to the fact that the results in Table 3.I.10 are computed based on the average surface stresses (top and bottom) considering all 4 nodes that define each element surface. In the calculations above, the maximum and minimum stresses at a single node location (top and bottom) are considered for simplicity.

Figure 3.I.18b; Normal Stress (Sy) in SFP, Simulation Model I – Load Combination LC-3 from Table 2.I.11

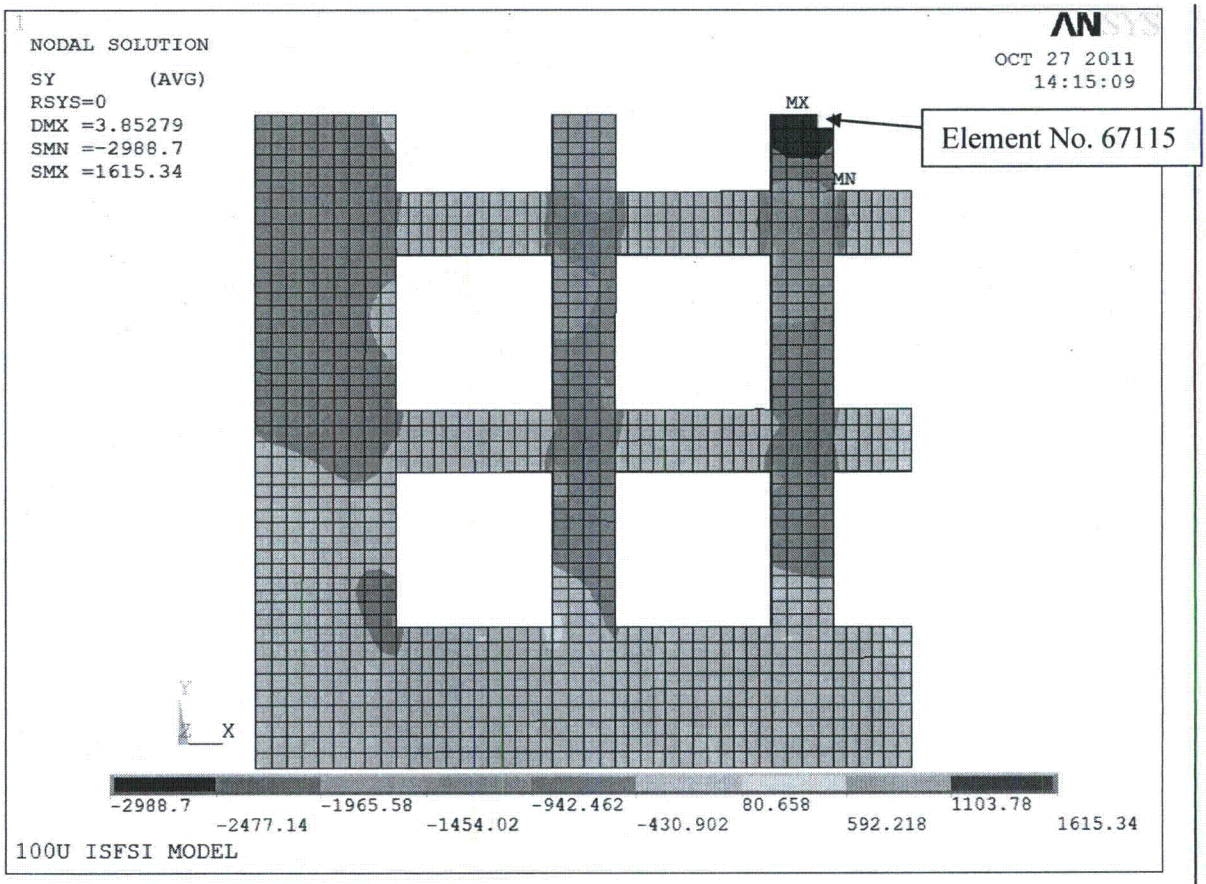

Note: Element 67115 realizes the maximum loading and produces the limiting safety factor.

Figure 3.I.18c; Normal Stress (Sy) in TSP Simulation Model I – Load Combination LC-3 from Table 2.I.11

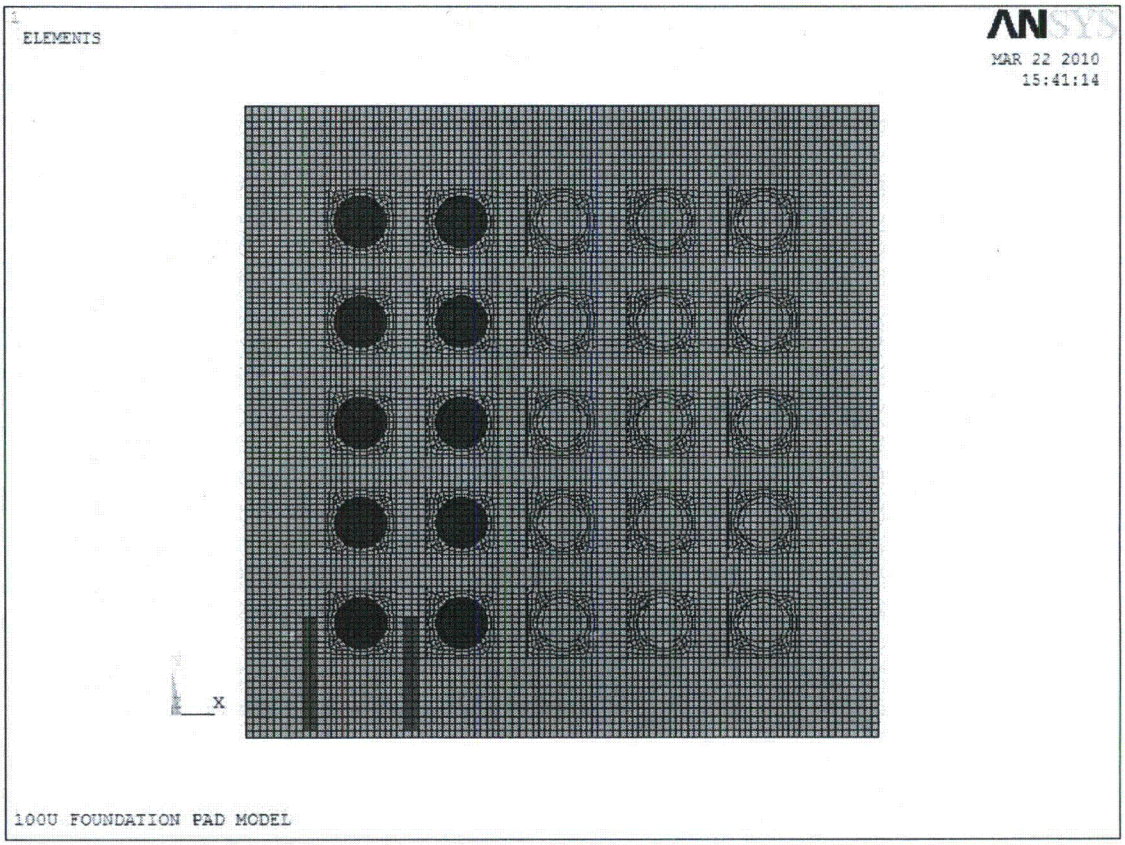

Note: The blue footprints show the SFP area loaded with the SSC's and the red footprint represents the loaded TSP area with the transporter (VCT). The soil extending beyond the pad (SFP/TSP) boundary is not shown in the above plot for clarity.

Figure 3.I.19; ANSYS Finite Element Model of ISFSI Showing the Partially Loaded Configuration (Simulation Model II)

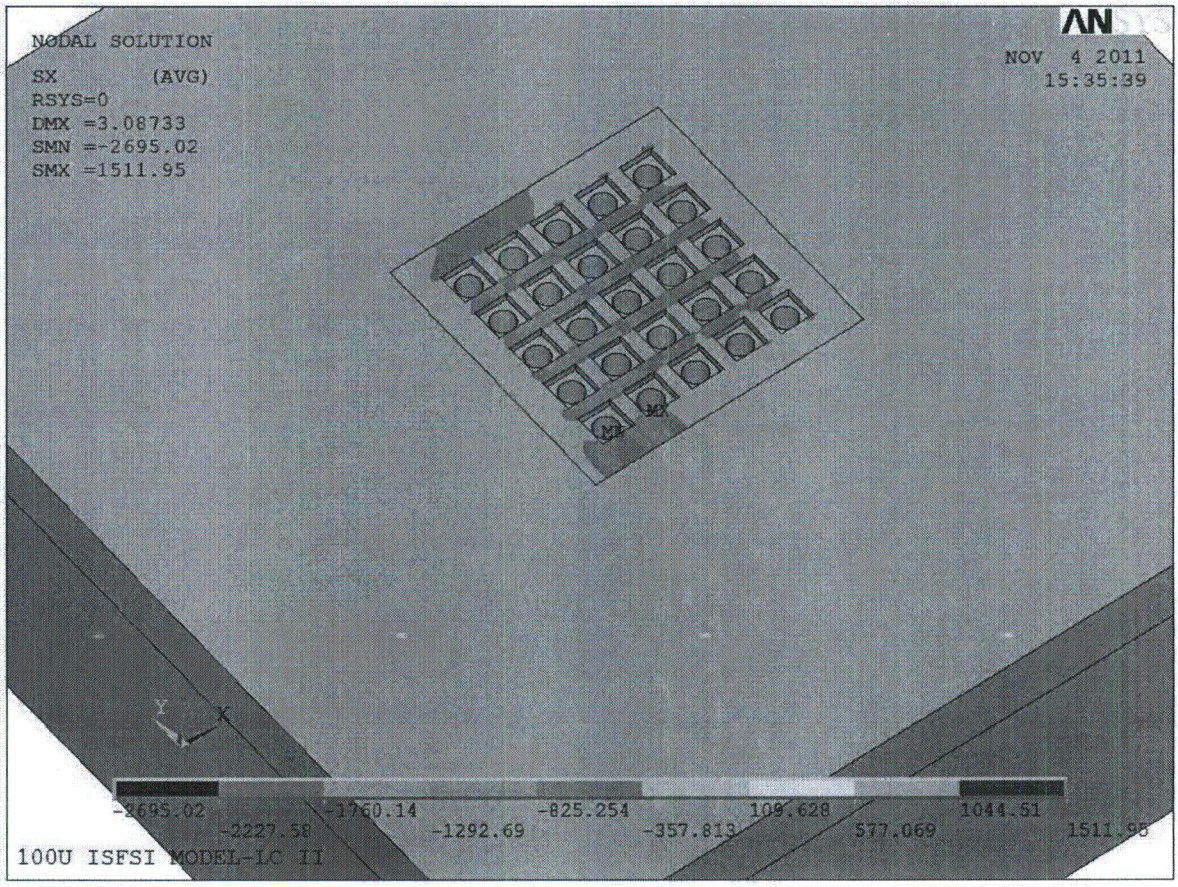

Figure 3.I.19a; Normal Stress in the ISFSI in the Direction of the Transporter Path for Simulation Model II – Load Combination LC-3 from Table 2.I.11

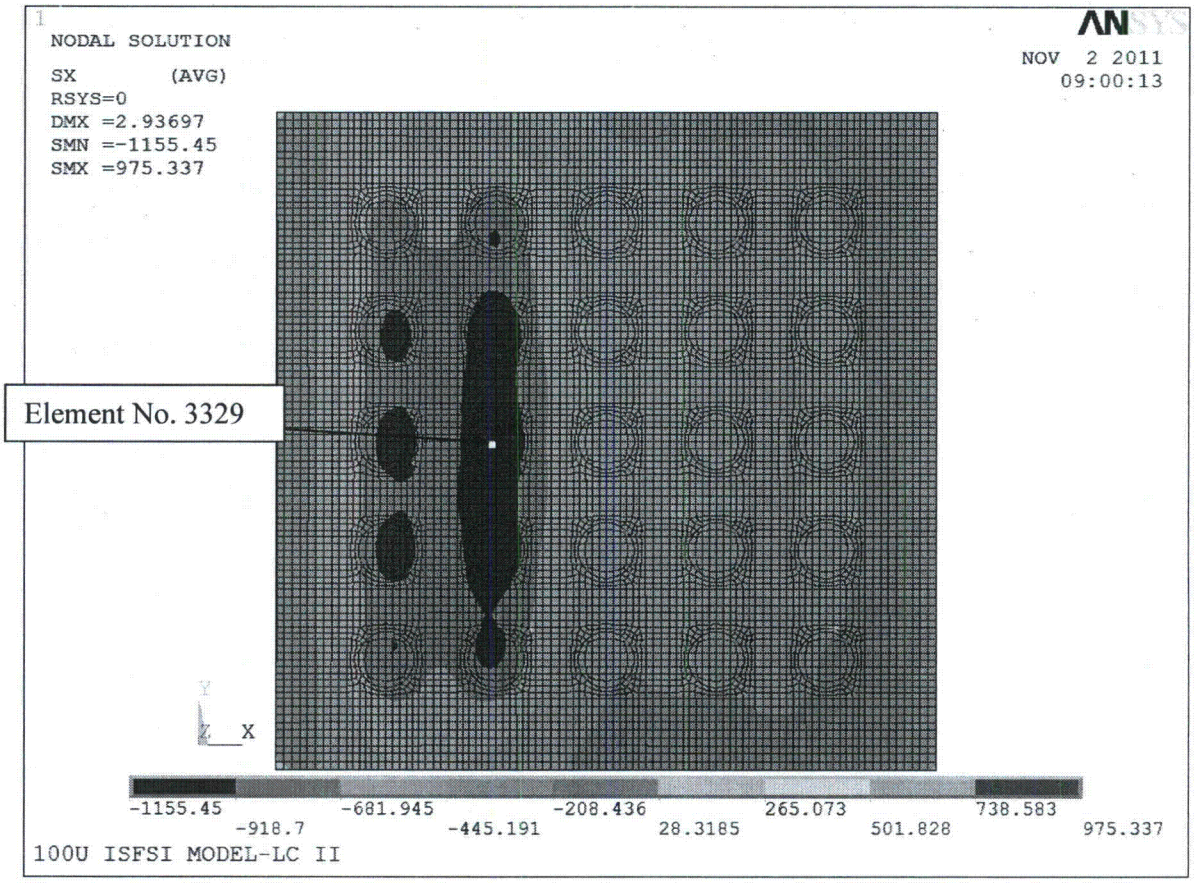

Note: Element 3329 realizes the maximum loading and produces the limiting safety factor.

Figure 3.I.19b; Normal Stress (Sx) in SFP, Simulation Model II – Load Combination LC-3 from Table 2.I.11

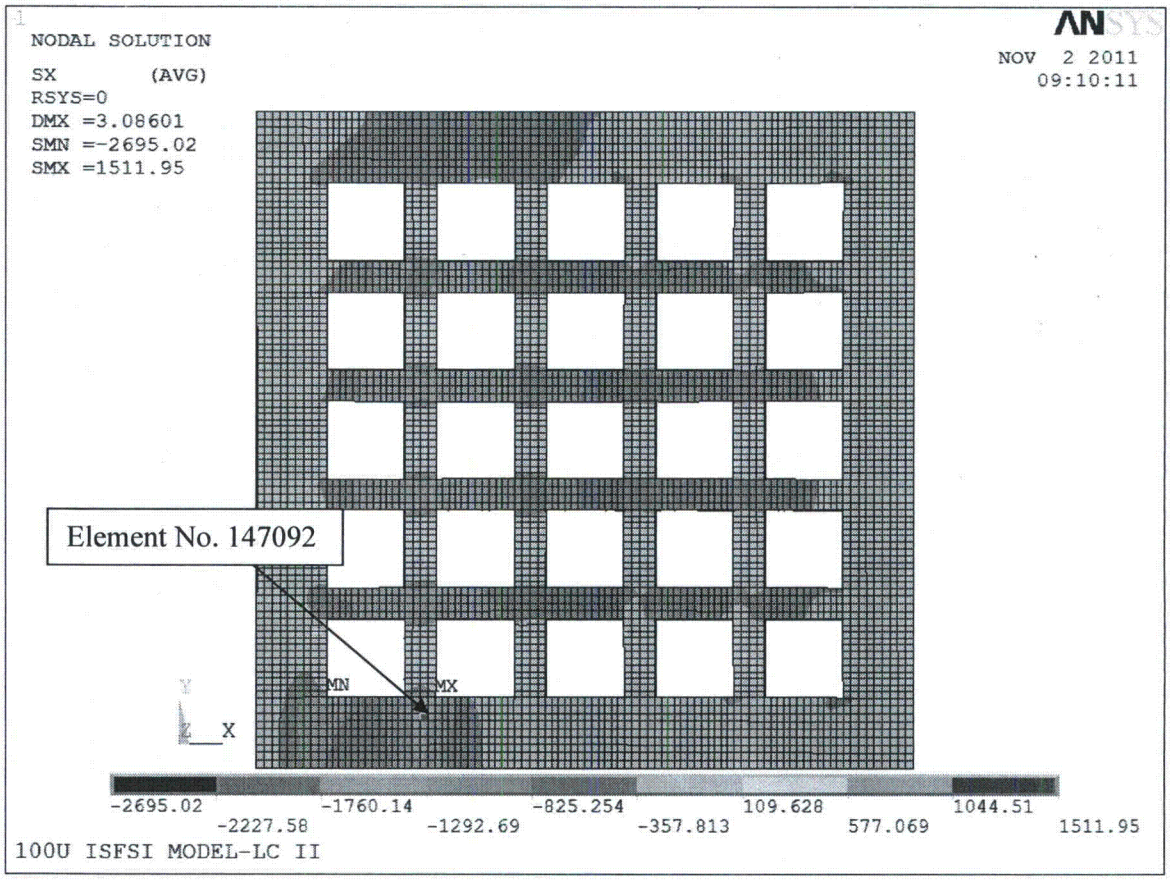

Note: Element 147092 realizes the maximum loading and produces the limiting safety factor.

Figure 3.I.19c; Normal Stress (Sx) in TSP, Simulation Model II – Load Combination LC-3 from Table 2.I.11

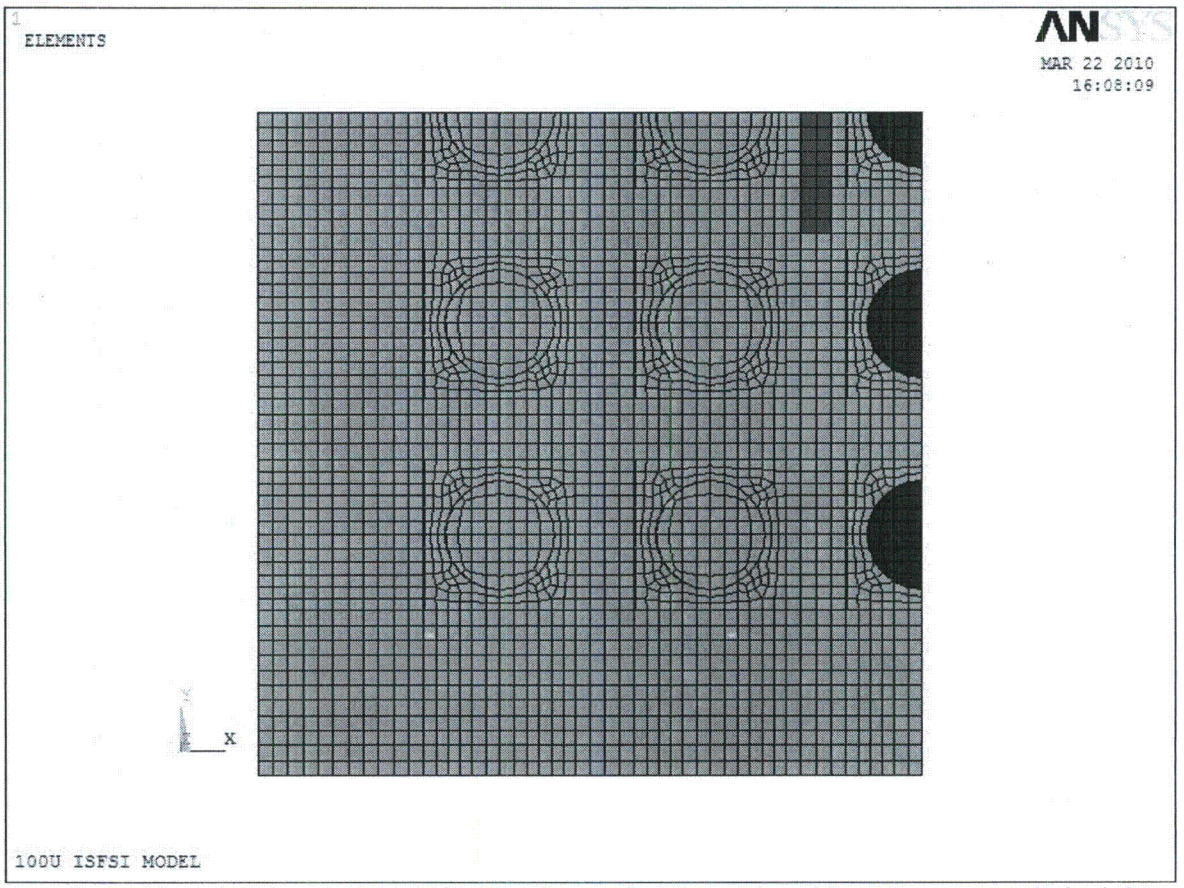

Note: The blue footprints show the loaded VVM locations on the SFP and the red footprint represents the loaded TSP area with the transporter.

Figure 3.I.20; ANSYS Finite Element of ISFSI Showing the Center Row Loading (Simulation Model III)

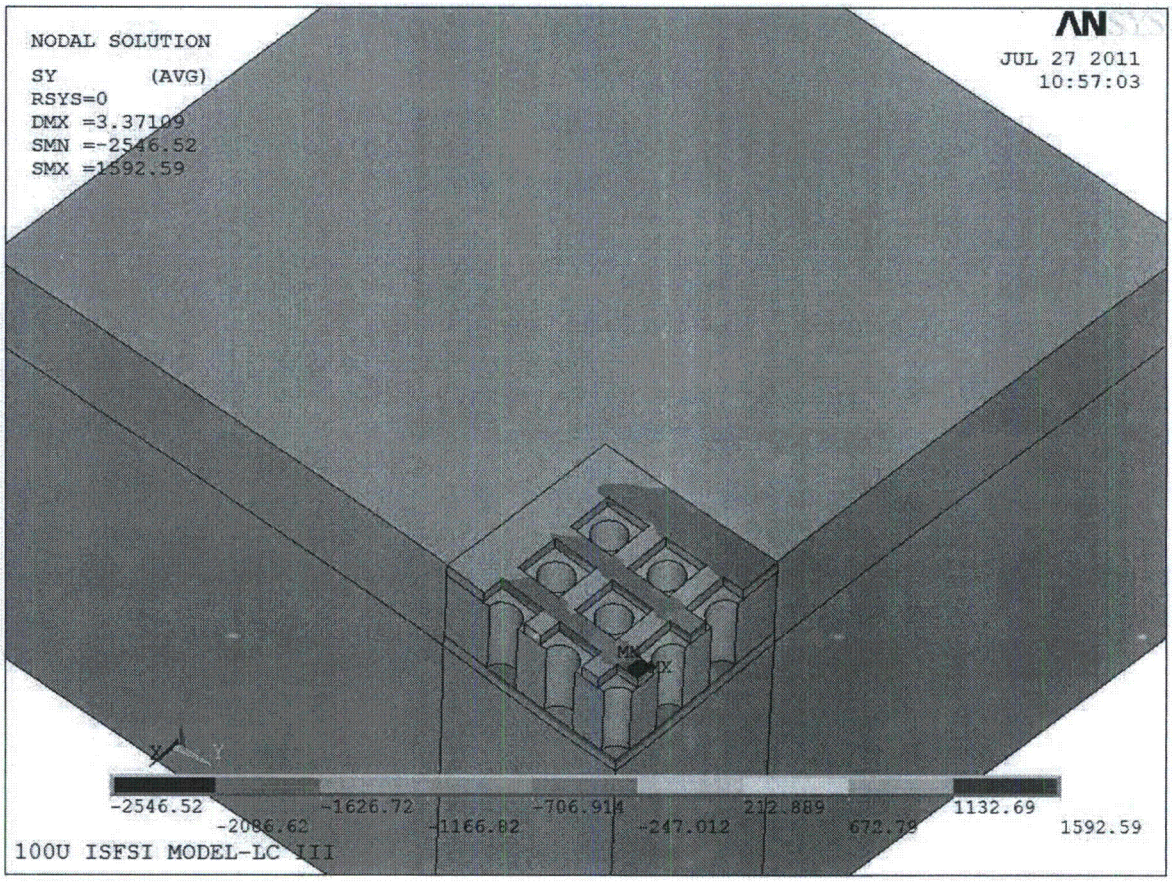

Figure 3.I.20a; Normal Stress in the ISFSI in the Direction of the Transporter Path for Simulation Model III – Load Combination LC-3 from Table 2.I.11

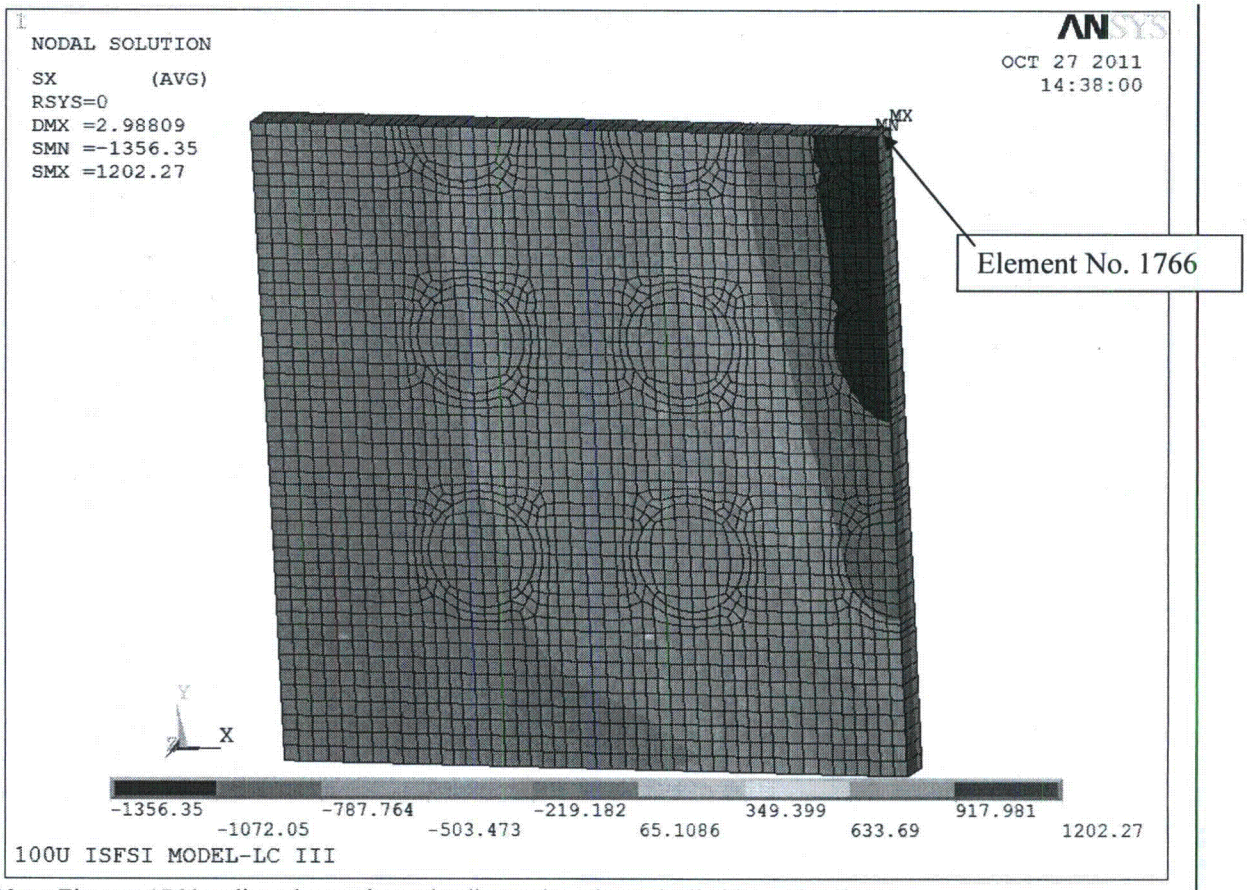

Note: Element 1766 realizes the maximum loading and produces the limiting safety factor.

Figure 3.I.20b; Normal Stress (Sx) in SFP, Simulation Model III – Load Combination LC-3 from Table 2.I.11

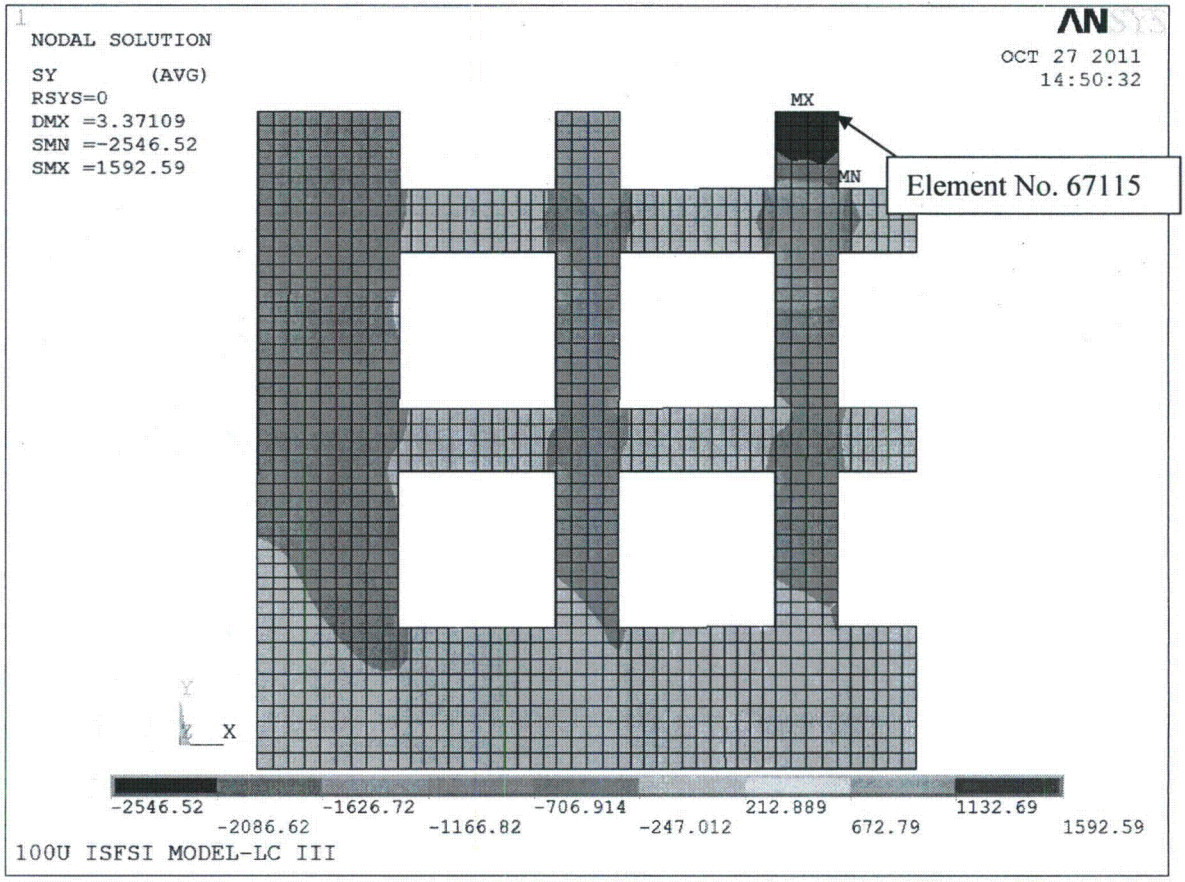

Note: Element 67115 realizes the maximum loading and produces the limiting safety factor.

Figure 3.I.20c; Normal Stress (Sy) in TSP, Simulation Model III – Load Combination LC-3 from Table 2.I.11

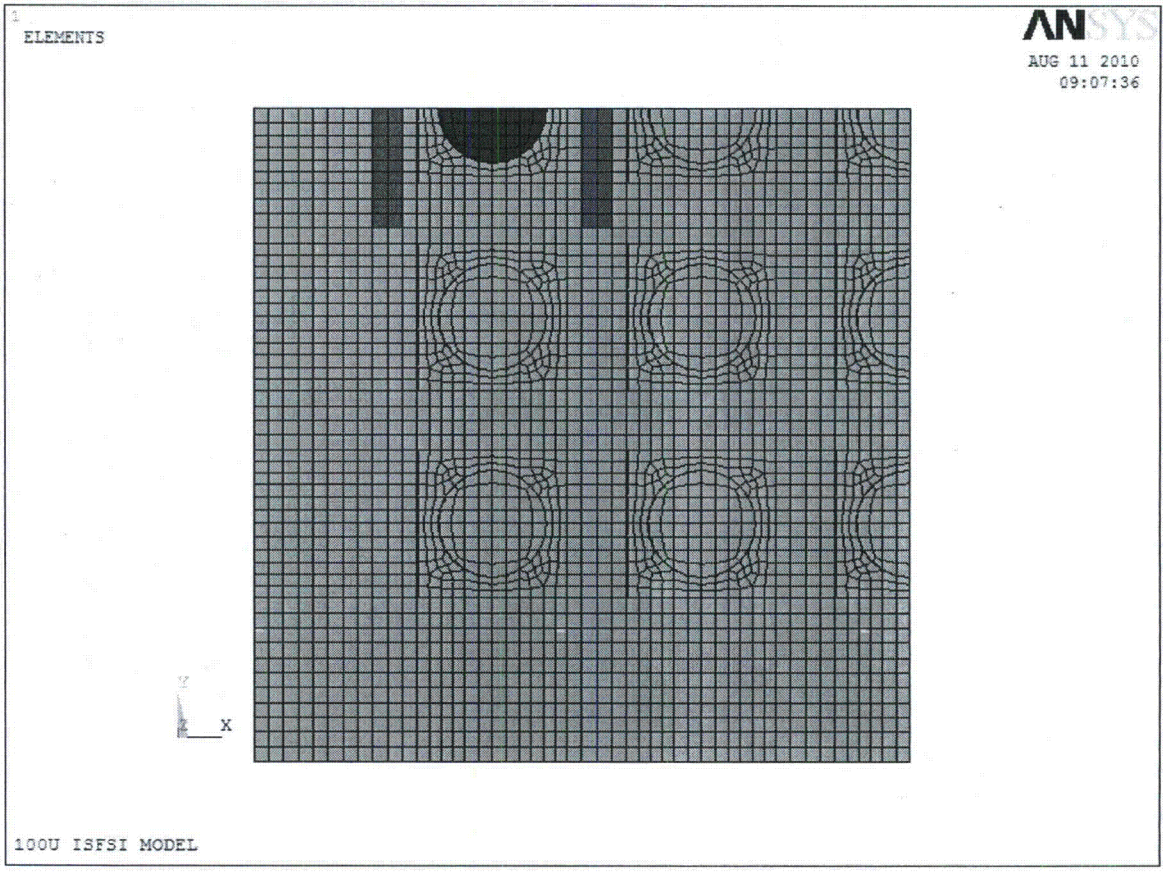

Note: The blue footprints show the loaded VVM locations on the SFP and the red footprint represents the loaded TSP area with the transporter.

Figure 3.I.21; ANSYS Finite Element of ISFSI Showing the Single VVM Loaded (Simulation Model IV)

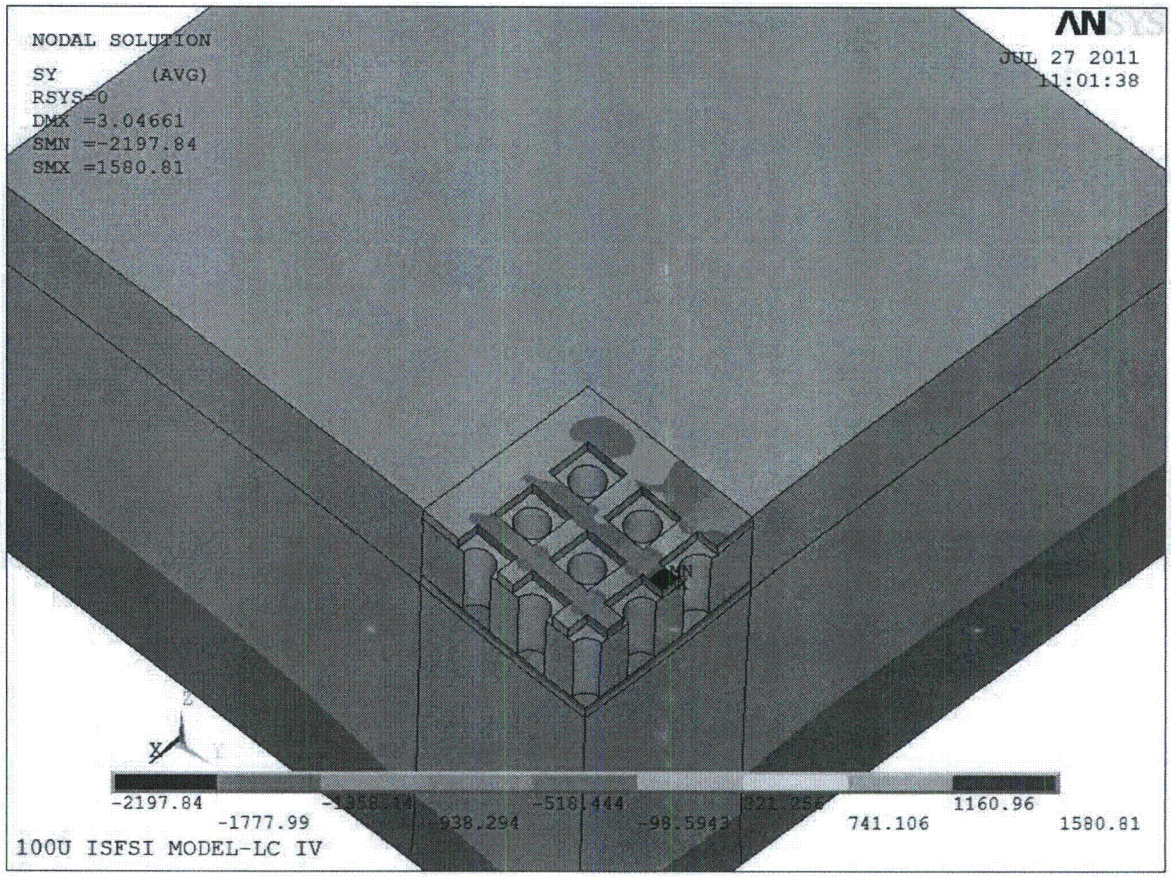

Figure 3.I.21a; Normal Stress in the ISFSI in the Direction of the Transporter Path for Simulation Model IV – Load Combination LC-3 from Table 2.I.11

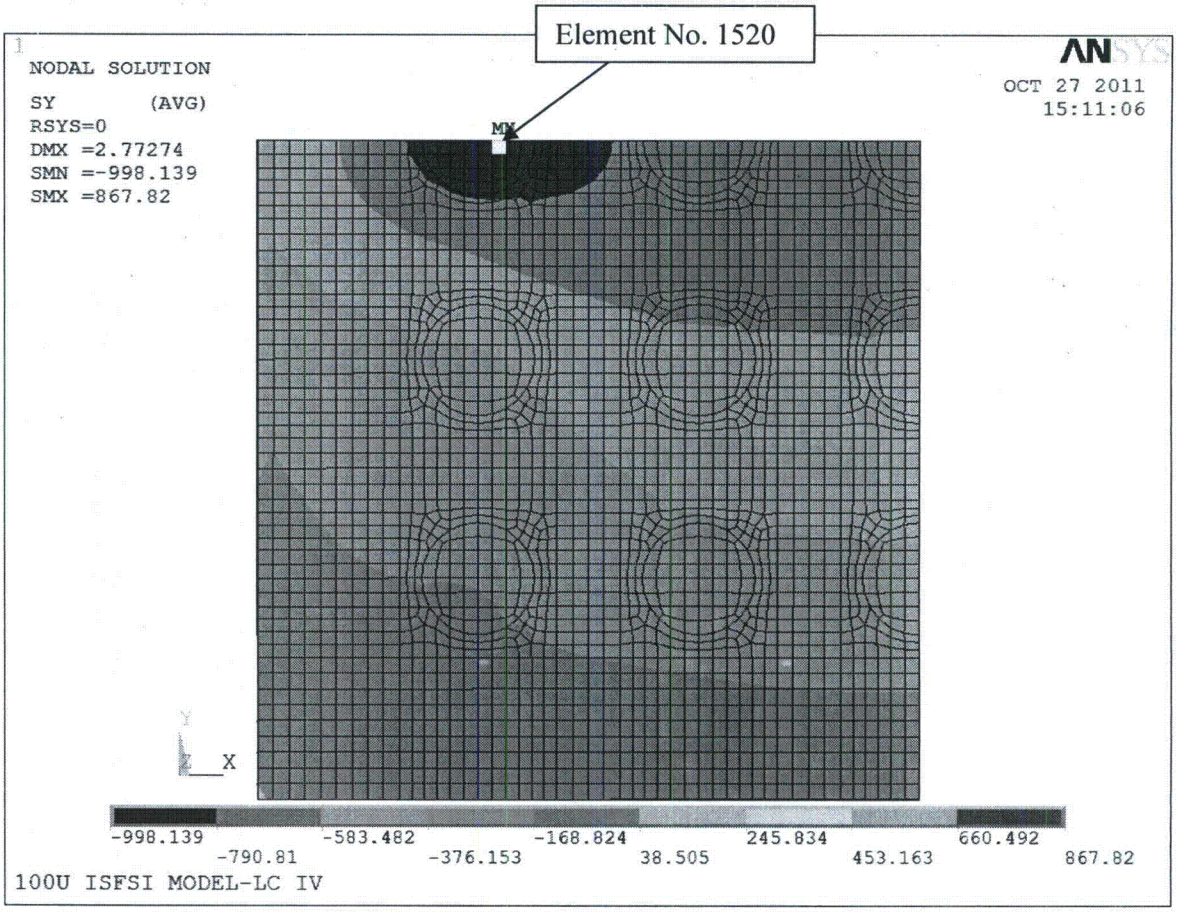

Note: Element 1520 realizes the maximum loading and produces the limiting safety factor.

Figure 3.I.21b; Normal Stress (Sy) in SFP, Simulation Model IV – Load Combination LC-3 from Table 2.I.11

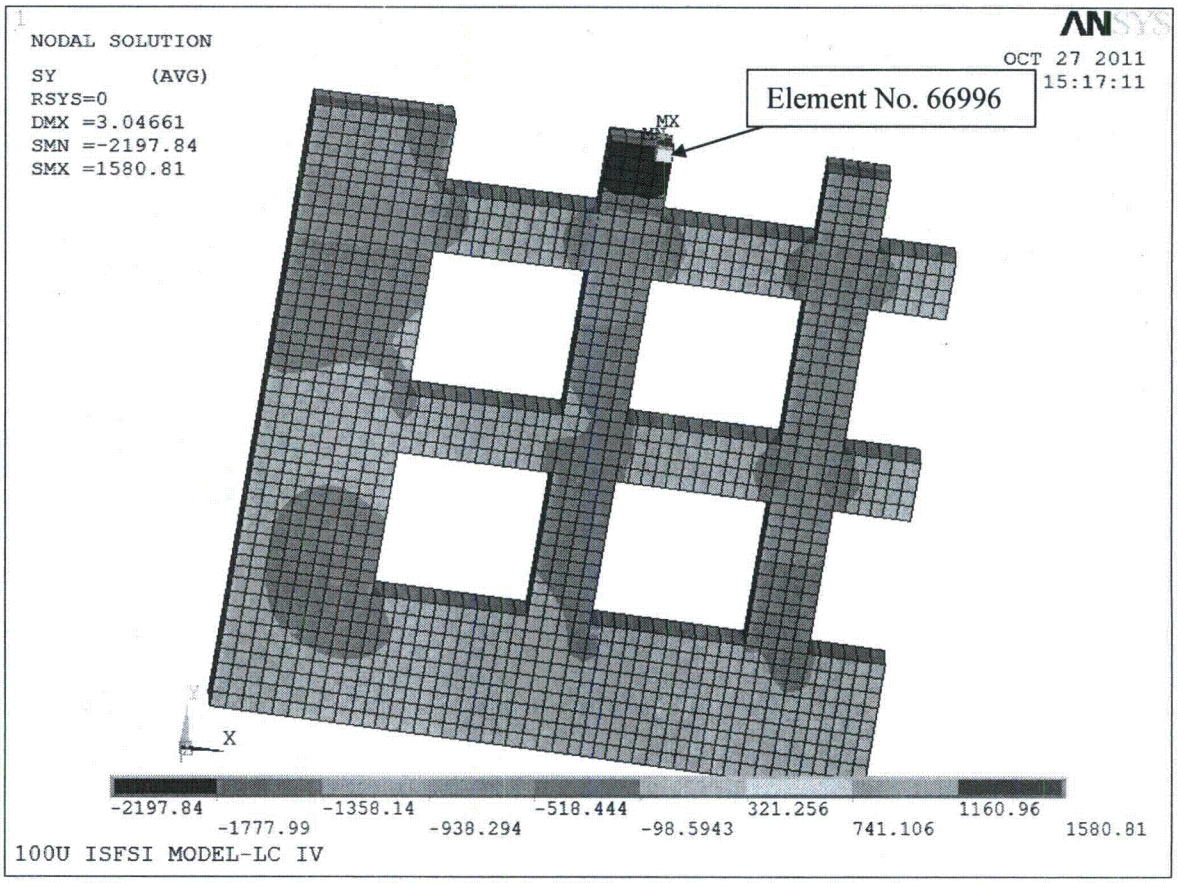

Note: Element 66996 realizes the maximum loading and produces the limiting safety factor.

Figure 3.I.21c; Normal Stress (Sy) in TSP, Simulation Model IV – Load Combination LC-3 from Table 2.I.11

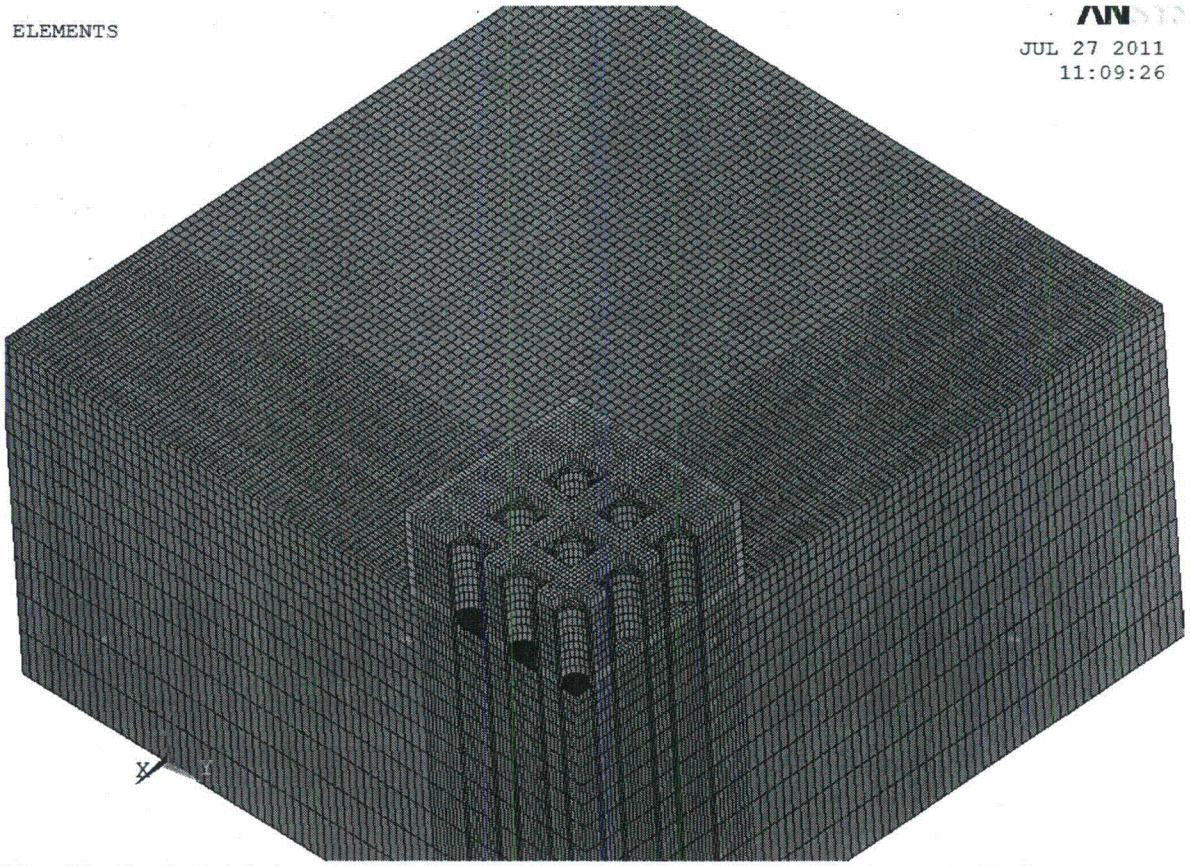

Note: The blue footprints show the loaded VVM locations on the SFP and there is no transporter load.

Figure 3.I.22; ANSYS Finite Element of ISFSI with Retaining Wall Optional Design (Simulation Model V)

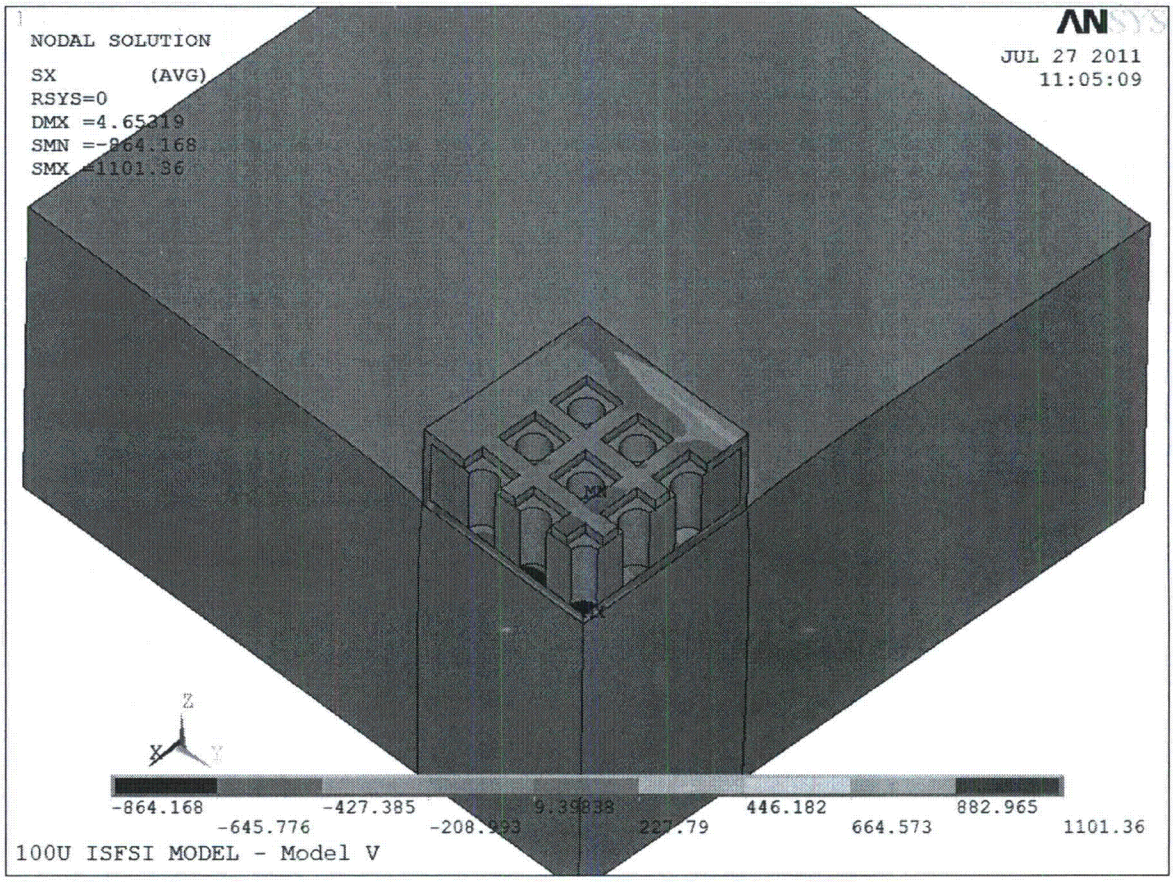

Figure 3.I.22a; Normal Stress in the ISFSI in the Direction for Simulation Model V – Load Combination LC-3 from Table 2.I.11

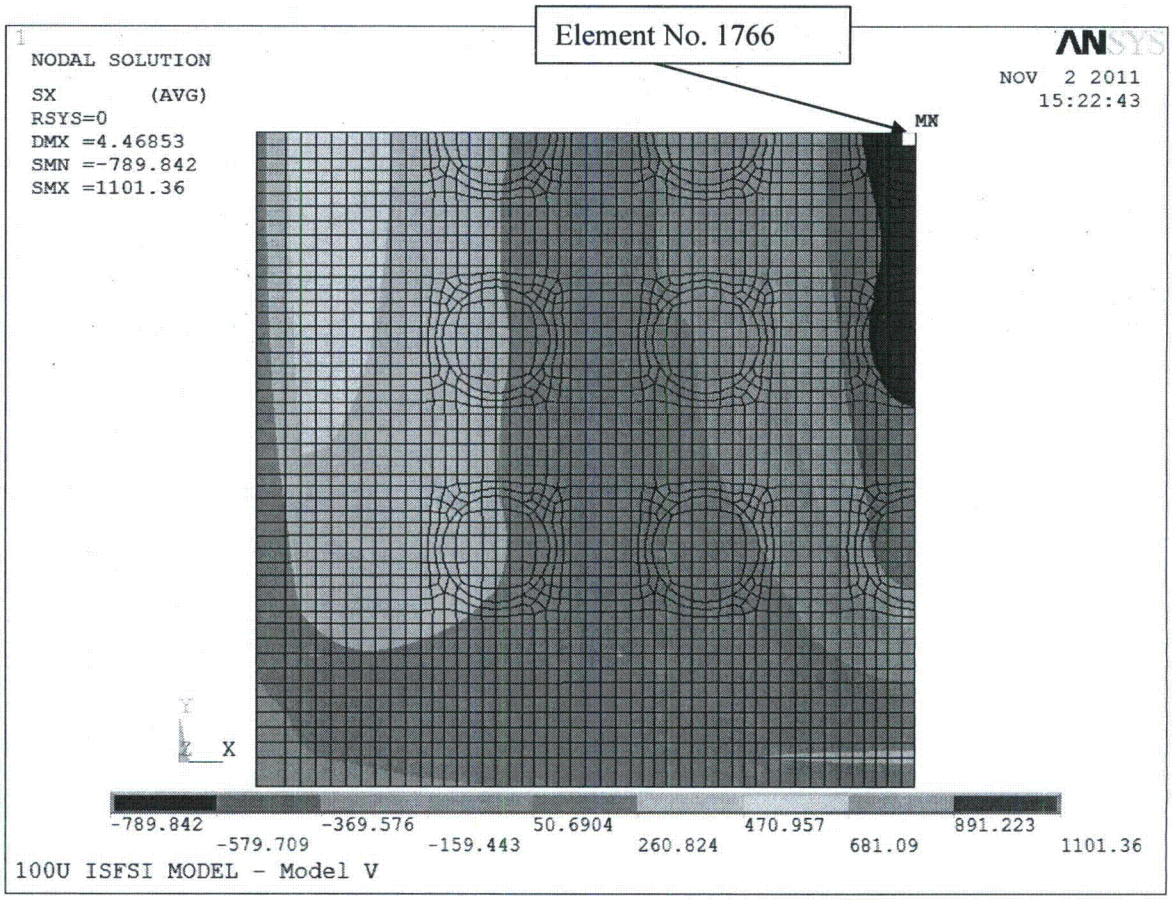

Note: Element 1766 realizes the maximum loading and produces the limiting safety factor.

Figure 3.I.22b; Normal Stress (Sx) in SFP, Simulation Model V – Load Combination LC-3 from Table 2.I.11

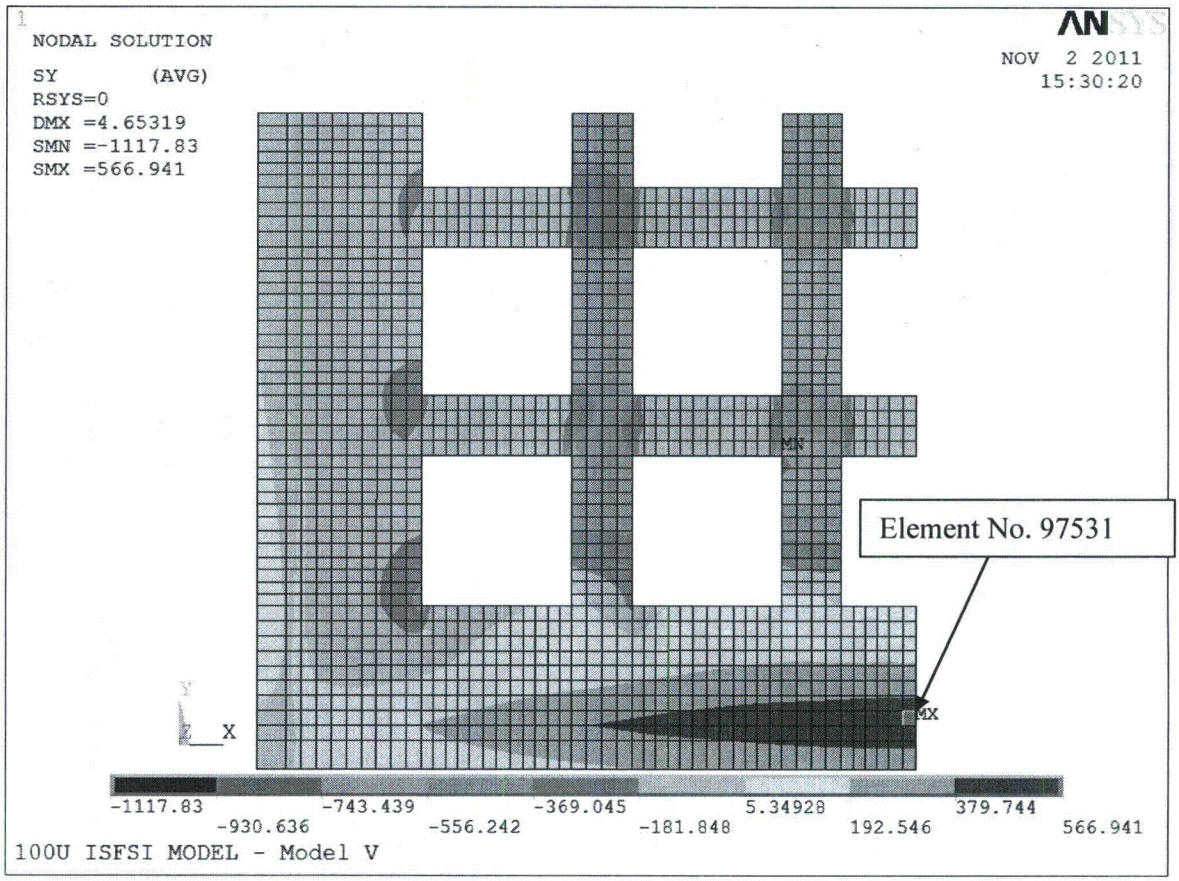

Note: Element 97531 realizes the maximum loading and produces the limiting safety factor.

Figure 3.I.22c; Normal Stress (Sy) in TSP, Simulation Model V – Load Combination LC-3 from Table 2.I.11

Figure 3.I.23-A; Divider and CEC Shell Displacement Distribution at the End of the Earthquake

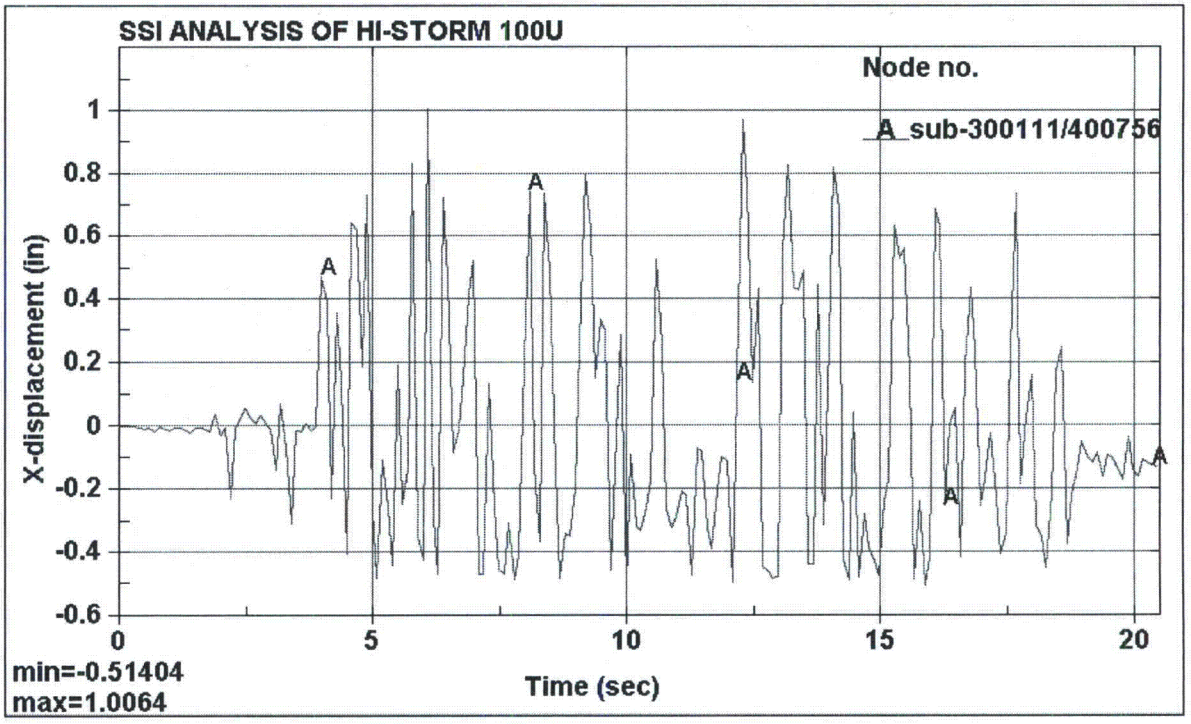

Figure 3.I.23-B; Changes of the Radial Gap between CEC Shell and Divider Shell Measured at the Top Guide Elevation
(Radial gap change at the end of earthquake = 0.1325 inches)

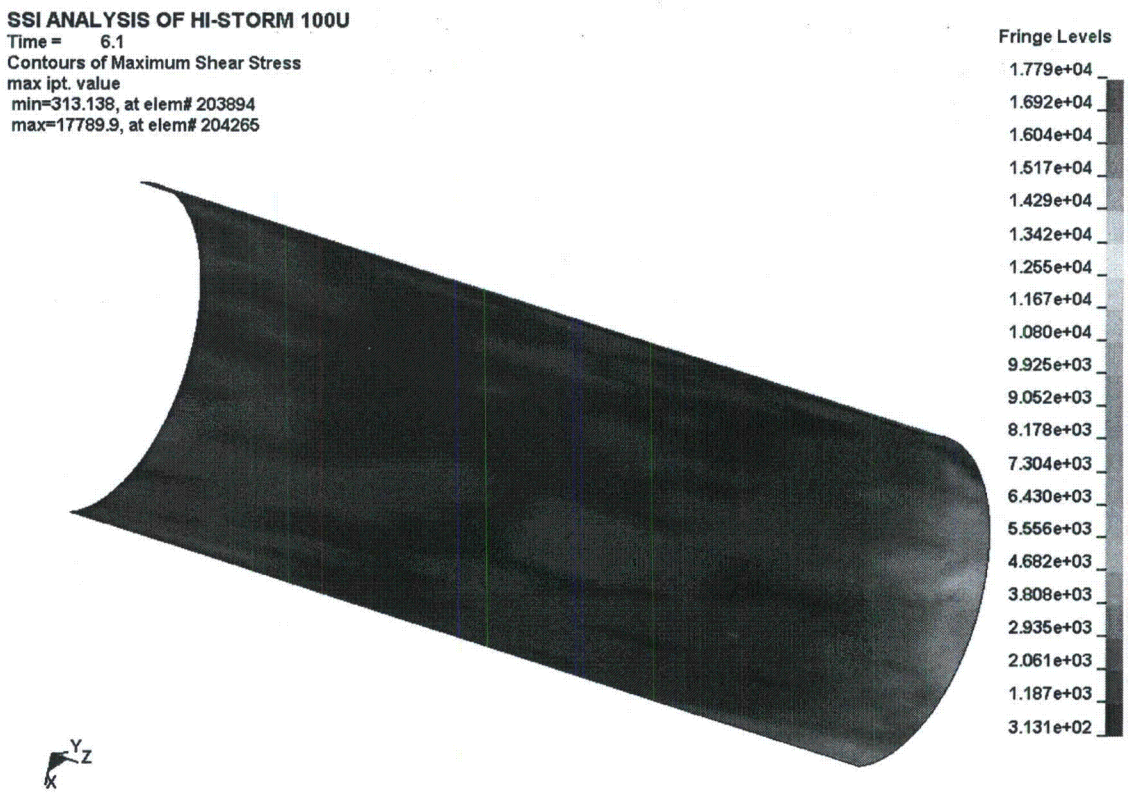

Figure 3.I.24; Maximum Shear Stress of the MPC Shell
(Maximum Primary Stress Intensity = 2×6,430 psi = 12,860 psi)

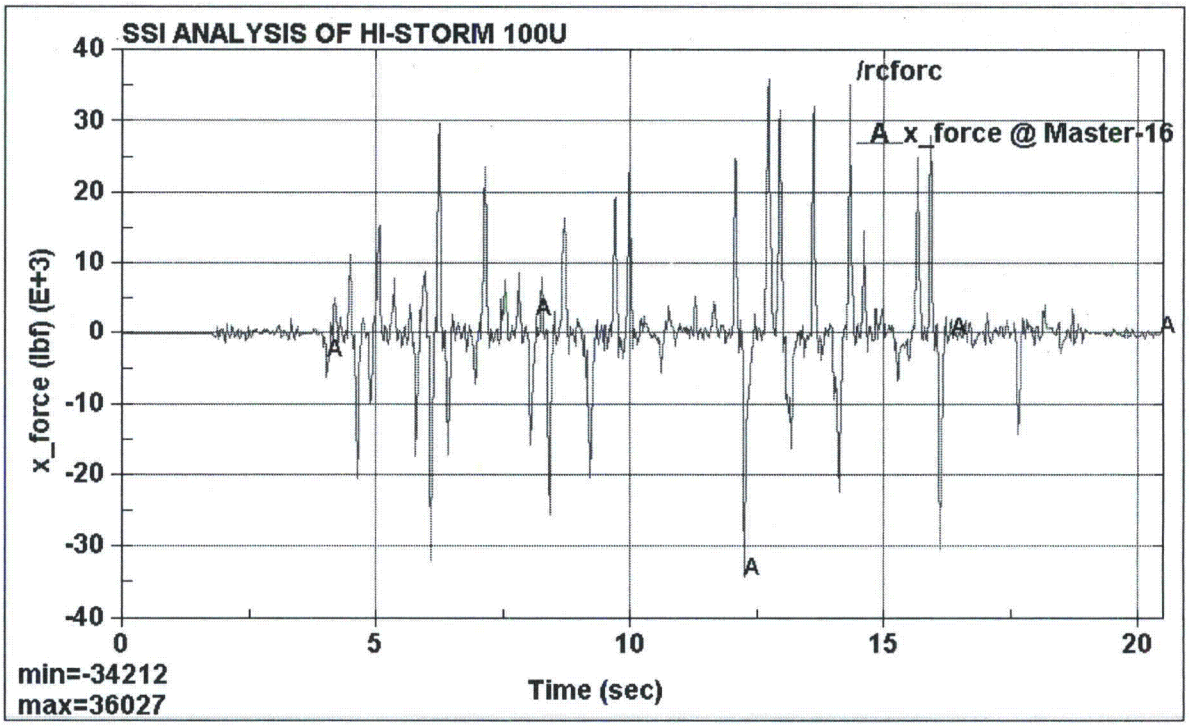

Figure 3.I.25-A; Impact Force between the MPC and MPC Top Guides
(Maximum Impact Force = 2×36,027 lb = 72,054 lb to account for half-symmetric model)

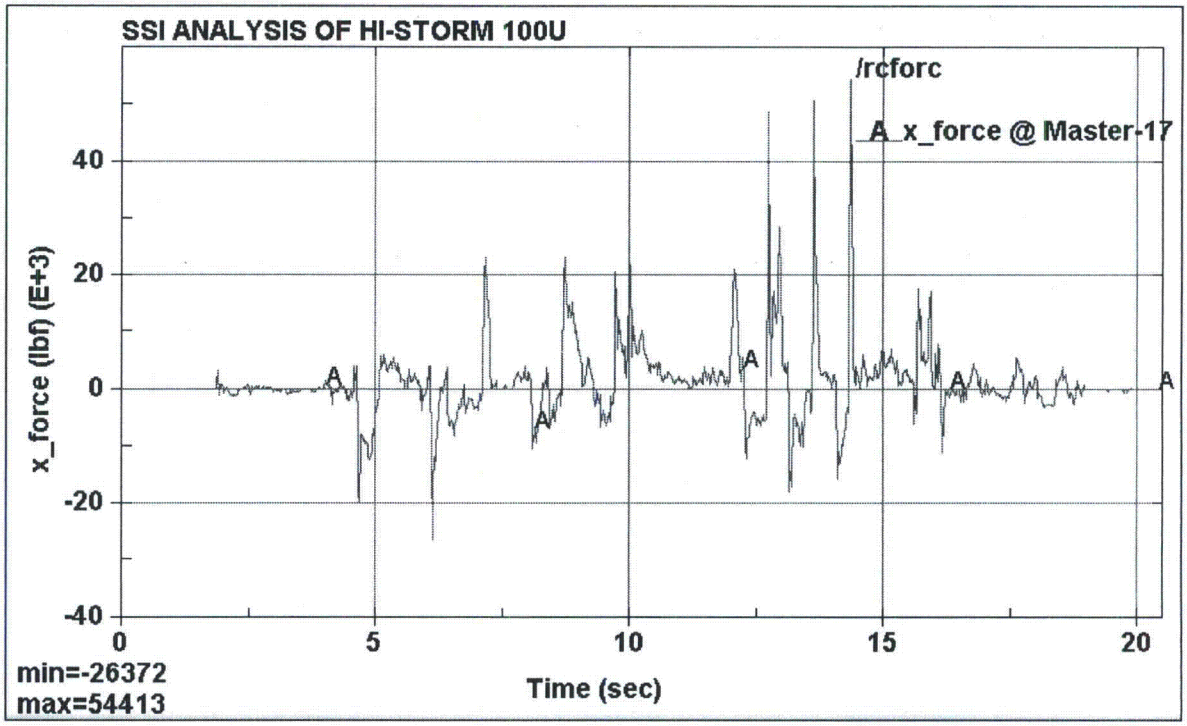

Figure 3.I.25-B; Impact Force between the MPC and MPC Bottom Guides
(Maximum Impact Force = 2×54,413 lb = 108,826 lb to account for half-symmetric model)

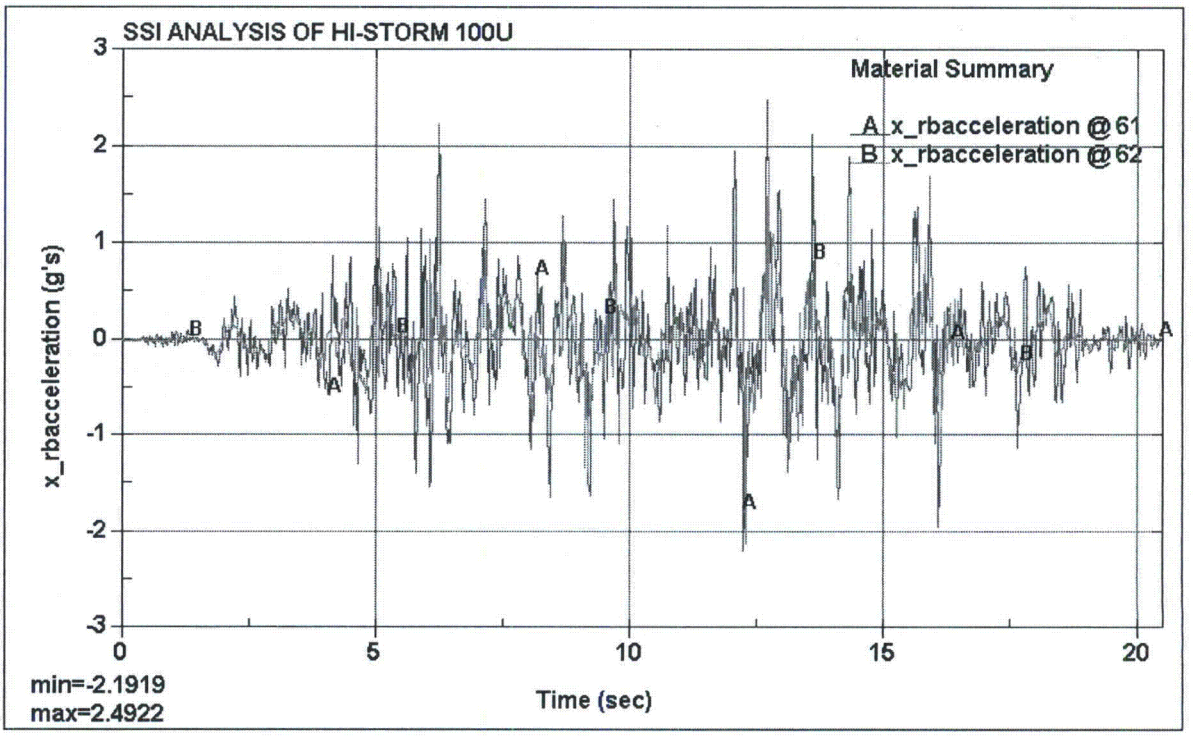

Figure 3.I.26; MPC Lid and Baseplate Lateral Acceleration Time Histories
(A - MPC Lid; B - MPC Baseplate)

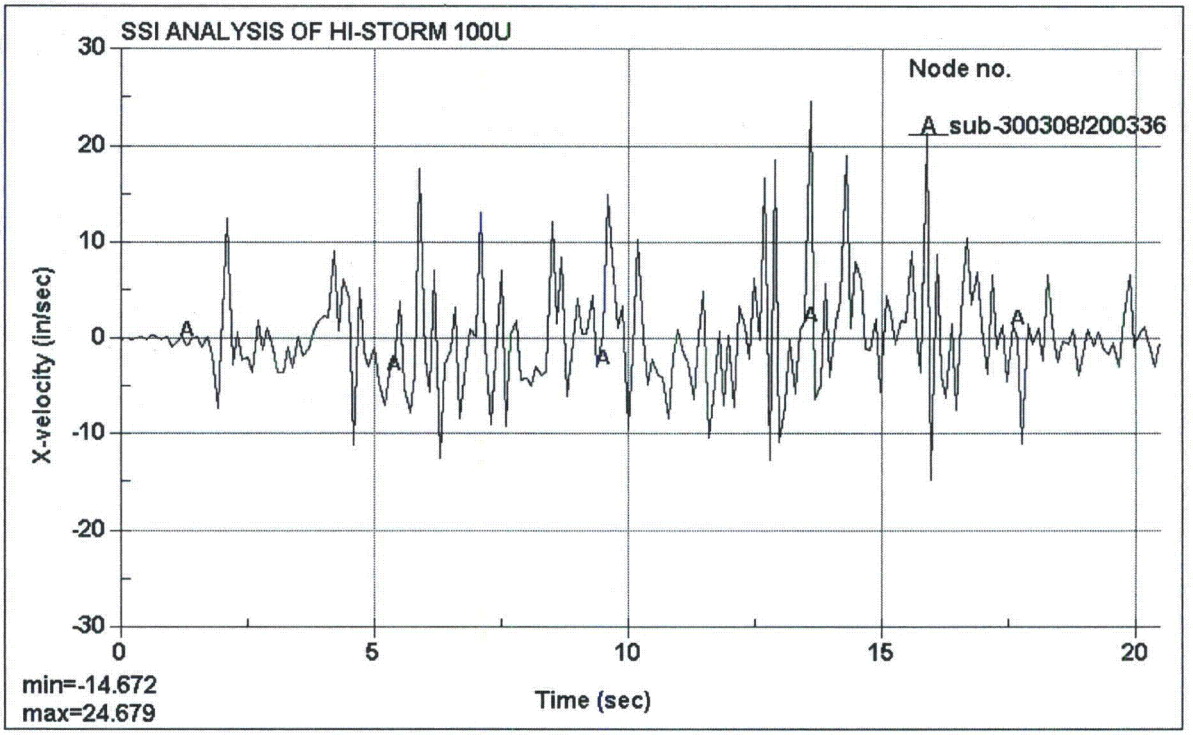

Figure 3.I.27; MPC Lid to MPC Top Guide Approaching Velocity Time History

SUPPLEMENT 3.III

STRUCTURAL EVALUATION OF THE MPC-68M

3.III.0 OVERVIEW

In this supplement, the structural adequacy of the MPC-68M is evaluated pursuant to the guidelines of NUREG-1536.

The organization of technical information in this supplement mirrors the format and content of Chapter 3 except that it only contains material directly pertinent to the MPC-68M.

The MPC-68M consists of a stainless steel (Alloy X) Enclosure Vessel, which is identical to that of the MPC-68, a BWR fuel basket made from Metamic-HT, and aluminum basket shims. Section 1.III.2 contains a complete description of the MPC-68M components.

The applicable codes, standards, and practices governing the structural analysis of the MPC-68M as well as the design criteria, are presented in Supplement 2.III. Throughout this supplement, the term "*safety factor*" is defined as the *ratio of the allowable stress (load) or displacement for the applicable load combination to the maximum computed stress (load) or displacement.* Where applicable, bounding safety factors are computed using values that bound the calculated results.

3.III.1 STRUCTURAL DESIGN

3.III.1.1 Discussion

A general discussion of the structural features of the MPC is provided in Subsection 3.1.1, and in general it applies to the MPC-68M with one notable exception. The MPC-68M fuel basket is qualified using a deflection-based acceptance criterion (see Subsection 2.III.0.1) as opposed to a stress-based criterion. The drawings of the MPC-68M fuel basket and MPC Enclosure Vessel are provided in Section 1.5.

3.III.1.2 Design Criteria

Same as in Subsection 3.1.2, including all of its paragraphs, except as modified in Subsection 2.III.0.1 for the MPC-68M fuel basket.

3.III.2 WEIGHTS AND CENTERS OF GRAVITY

Since the weight density of Metamic-HT is significantly less than that of Alloy X, the MPC-68M weighs less than the MPCs listed in Table 3.2.1. The bounding weights for the MPC-68M are provided in Table 3.III.1.

The center of gravity (CG) height of the empty MPC-68M, and various other configurations involving the MPC-68M, is provided in Table 3.III.2.

3.III.3 MECHANICAL PROPERTIES OF MATERIALS

The strength properties of Metamic-HT have been characterized through a comprehensive test program, and Minimum Guaranteed Values suitable for structural design are provided in Appendix 1.III.A and also archived in [1.III.A.3].

The fuel basket shims are made of an aluminum alloy (ASTM B221 2219-T851). Representative mechanical properties for the fuel basket shims are tabulated in Table 3.III.3. Strictly speaking, the shim is not a structural material because it does not withstand any tensile loads and is located in a confined space which would prevent its uncontrolled deformation under load. The simulation of the shim in the basket's structural model, however, utilizes its mechanical properties of which only the Yield Strength has a meaningful (but secondary) role. Accordingly, in this FSAR, the nominal value of the Yield Strength specified in Table 3.III.3 herein, is set down as a "critical characteristic" for the shim material. The minimum value of the Yield Strength reported in the material supplier's CoC must be at least 90% of the nominal value in the above referenced table to ensure that the non-mechanistic tip-over analysis will not have to be revisited.

The mechanical properties for all other materials of construction are the same as in Section 3.3 (including all subsections and tables).

3.III.4 GENERAL STANDARDS FOR CASKS

3.III.4.1 Chemical and Galvanic Reactions

The materials used in the HI-STORM 100 System are examined in Subsection 3.4.1 to establish that they do not participate in any chemical or galvanic reactions when exposed to the various environments during all normal operating conditions and off-normal and accident events. The only new materials that are introduced in the MPC-68M are Metamic-HT (for the fuel basket) and aluminum (for the basket shims). The environmental compatibility of these materials is examined below.

The MPC-68M is principally constructed of stainless steel shell, aluminum basket shims, and Metamic-HT. Borated aluminum and stainless steel have been used in close proximity in wet storage for over 30 years. Many spent fuel pools at nuclear plants contain fuel racks, which are fabricated from Metamic (classic) and stainless steel materials. Not one case of chemical or galvanic degradation has been found in such fuel racks. This experience provides a sound basis to conclude that chemical and galvanic corrosion of these materials will be negligible. For further protection, both Metamic-HT and aluminum basket shims are installed in the anodized state in the MPC.

Furthermore, galvanic corrosion is not an applicable corrosion mechanism during long-term storage since the interior of the MPC during normal operation is both inerted with helium and essentially devoid of any moisture while the MPC shell surfaces are expected to be practically

free from condensation and gross environmental contaminants. The cleanliness requirements and inspections during fabrication and fuel loading operations also ensure that the MPC has minimal surface debris and impurities.

Tests on Metamic-HT

Extensive tests [1.III.A.3] have been conducted to establish material properties of Metamic-HT including its corrosion-resistance characteristics. The Metamic-HT specimens were used for corrosion testing in demineralized water and in 2000 ppm boric acid solution. The tests concluded that the Metamic-HT panels will sustain no discernible degradation due to corrosion when subjected to the severe thermal and aqueous environment that exists around a fuel basket during fuel loading or unloading conditions.

Aluminum Alloy

Aluminum alloy used in the fuel basket shims are hard anodized to achieve the desired emissivity specified in Supplement 3.III. The anodizing is an electrolytic passivation process used to increase the thickness of the natural oxide layer on the surface of metal parts. Anodizing increases corrosion resistance and wear resistance of the material surface. There is no mechanistic process for the basket shims with hard anodized surface to react with borated water or demineralized water during fuel loading operation. Under the long-term storage condition, the basket shims are exposed to dry and inert helium with no potential for reaction.

Finally, to ensure safe fuel loading operation, the operating procedure described in Chapter 8 provides for the monitoring of hydrogen gas in the area around the MPC lid prior to and during welding or cutting activities. Although the aluminum surfaces (Metamic-HT fuel basket and aluminum basket shims) are anodized, there is still a potential for generation of hydrogen in minute amounts when immersed in spent fuel pool water for an extended period. Accordingly, as a defense-in-depth measure, the lid welding procedure requires purging the space below the MPC lid prior to and during welding or cutting operation to eliminate any potential for formation of any combustible mixture of hydrogen and oxygen. Following the completion of the MPC lid welding and hydrostatic testing, the MPC-68M is drained and dried. After the completion of the drying operation, there is no credible mechanism for any combustible gases to be generated within the MPC-68M.

3.III.4.2 Positive Closure

Same as in Subsection 3.4.2.

3.III.4.3 Lifting Devices

The structural analyses of the lifting devices in Subsection 3.4.3 (including all paragraphs) are bounding for the MPC-68M for the following reasons:

i. the MPC-68M does not require any changes to the HI-STORM overpacks or the HI-TRAC transfer casks for loading operations or long-term storage;

ii. the MPC-68M utilizes the same MPC Enclosure Vessel design as all MPCs;

iii. the fully loaded weight of the MPC-68M (Table 3.III.1) is less than bounding MPC weight analyzed in Chapter 3 (Table 3.2.1).

3.III.4.4 Heat

The thermal evaluation of the MPC-68M is reported in Supplement 4.III.

3.III.4.4.1 Summary of Pressures and Temperatures

The design pressures and design temperatures listed in Tables 2.2.1 and 2.2.3, respectively, are applicable to the MPC-68M. Temperature limits of MPC-68M fuel basket and basket shim materials are specified in Table 4.III.2.

3.III.4.4.2 Differential Thermal Expansion

The material presented in Supplement 4.III demonstrates that a physical interference between discrete components of the MPC-68M (e.g., fuel basket and enclosure vessel) will not develop due to differential thermal expansion during any operating condition.

3.III.4.4.3 Stress Calculations

The majority of the stress calculations reported in Paragraph 3.4.4.3 are unaffected by or bound the addition of the MPC-68M to the HI-STORM 100 System for the following reasons:

i. the MPC-68M does not require any changes to the HI-STORM overpacks or the HI-TRAC transfer casks for loading operations or long-term storage;

ii. the MPC-68M utilizes the same MPC Enclosure Vessel design as all MPCs;

iii. the fully loaded weight of the MPC-68M (Table 3.III.1) is less than the bounding MPC weight analyzed in Chapter 3 (Table 3.2.1);

Therefore, the stress calculations reported in Paragraph 3.4.4.3 are not repeated here unless material, geometry, or load changes warrant new analysis or discussion. In other words, unless a new analysis is presented in this subsection, the results in Paragraph 3.4.4.3 for the HI-STORM 100 System are also valid for the MPC-68M either inside the HI-STORM overpack or the HI-TRAC transfer cask.

3.III.4.4.3.1 Analysis of Load Cases F.3.b and F.3.c (Table 3.1.3)

During a non-mechanistic tip-over event, the fuel assemblies exert a lateral force on the fuel basket panels as the overpack impacts the ground and decelerates. The lateral force causes the fuel basket panels to deflect potentially affecting the spacing between stored fuel assemblies. To maintain the fuel in a subcritical configuration, a deflection limit for the fuel basket panels is set in Subsection 2.III.0.1, which is supported by the criticality safety analysis in Supplement 6.III. Here a finite element analysis is performed using ANSYS to demonstrate that the maximum lateral deflection in the fuel basket panels under a bounding deceleration of 70g is less than the limit specified in Section 2.III.0.1. The 70g input deceleration is bounding because it exceeds the design basis deceleration limit of 45g for the non-mechanistic tip over of the HI-STORM storage overpack (see Subsection 3.III.4.10), as well as the design basis lateral deceleration limit of 60g for the HI-STAR transport cask [1.1.3] for future considerations. The analysis methodology presented in this subsection is identical to the methodology used in [2.III.6.2] to qualify the F-37 fuel basket.

As shown in Figure 3.III.1, a representative slice of the MPC-68M fuel basket, consisting of a smaller end section and a full section, is modeled in detail including the contained fuel assemblies and supporting basket shims. The fuel basket panels are modeled with SOLSH190 solid shell elements. The basket shims and each fuel assembly are modeled with SOLID45 solid elements. Standard contact pairs using CONTA173/TARGE170 elements are defined at the interfaces of fuel assembly/basket panel, shim/basket panel, and between stacked basket panels including all the intersecting slot locations. The fuel basket material model is implemented with true stress-true strain multi-linear isotropic hardening plasticity model. An elastic material model is used for the basket shims since no plastic deformation is expected. To accommodate large plastic deformation in the fuel basket panels, sufficiently small element sizes (< 0.40 in) are used and 9 integration points through the thickness are specified. A sensitivity study was performed in [2.III.6.2] to confirm that the panel stresses and displacements obtained using solid shell elements are converged and comparable to those obtained using 5 solid elements through the thickness of the panel.

The 70g deceleration is applied to the model with the basket in the so-called 0° orientation (see Figure 3.III.5). This orientation is chosen for analysis because it maximizes the lateral load on a single basket panel, which in turn maximizes the lateral deflection of the panel. In the 0° orientation, the amplified weight of each stored fuel assembly (during the 70g impact event) bears entirely on one basket panel. Conversely, in the 45° orientation, the amplified weight of each stored fuel assembly is equally supported by two basket panels. The difference in loading between these two basket orientations is pictorially shown in Figure 3.III.5, where "m" denotes the fuel assembly mass, "a" denotes the maximum lateral deceleration, and "d" denotes the enveloping size of the fuel assembly. For comparison purposes, the pressure loads on the basket panels are defined as "p" and "q", respectively, for the 0° and 45° orientations. From the figure, the pressure load p that develops in the 0° orientation is 41% greater than the pressure load q that develops in the 45° orientation. Hence, the lateral deflection of a basket panel is much greater for the 0° orientation (which is why it is chosen for detailed analysis). It is also noted that the 90° corners where the basket panels intersect do not provide any additional moment resistance because of the slotted joint construction (see Figure 1.III.1); therefore, the 45° orientation (or any other orientation between 0° and 45°) does not give rise to any prying loads at the cell corners.

Finally, to ensure that the analysis for the 0° orientation is conservative and bounds all other basket orientations, the analysis is performed based on a lateral impact deceleration of 70g even though, according to the results presented in Section 3.III.4.10, the maximum impact deceleration due to the non-mechanistic tip over event (measured at the top of the overpack lid) is less than 45g.

The stress and strain distributions in the fuel basket panels at 70g are shown in Figures 3.III.2 and 3.III.3, respectively. These figures show that the state of stress in the fuel basket panels is primarily elastic. The fuel basket displacements are plotted in Figure 3.III.4. Table 3.III.4 compares the maximum lateral displacement in a fuel basket panel (relative to its end supports) with the deflection limit specified in Subsection 2.III.0.1.

Per the licensing drawing, the nominal width of fuel basket panels in the vertical direction may be increased or decreased provided that the length of the panel slots is increased or decreased proportionally. This means that the fixed-height fuel basket may be assembled using more (or fewer) panels than the number depicted on the licensing drawing. The results of the ANSYS static analysis for the fuel basket presented herein are valid for any panel width since (a) the lateral load on the fuel basket per unit (vertical) length remains the same and (b) the length of the slots measured as a percentage of the panel width remains the same.

Finally, to evaluate the potential for crack propagation and growth for the MPC-68M fuel basket under the non-mechanistic tipover event, a crack propagation analysis is carried out for the MPC-68M fuel basket using the same methodology utilized in Attachment D of [1.III.A.3] to evaluate the HI-STAR 180 F-37 fuel basket in support of the HI-STAR 180 Transport Package [2.III.6.2].

The crack propagation analysis is informed by the results from the ANSYS finite element analysis of the MPC-68M fuel basket under a bounding load of 70-g, which is described above. In particular, the stress distribution in the Metamic-HT basket panels, as determined by ANSYS, is shown in Figure 3.III.2. The maximum stress occurs at one of the basket notches, which are conservatively modeled as sharp (90 degree) corners in the finite element model. This peak stress is used as input to the following crack propagation analysis.

Per [1.III.A.3] the critical stress intensity factor of Metamic-HT panels is estimated to be

$$K_{IC} = 30ksi\sqrt{in}$$

based on Charpy V-notch absorbed energy (CVE) correlations for steels. The estimated value is consistent with the range for aluminum alloys, which is 20 to 50 $MPa\sqrt{m}$ or 18.2 to 45 $ksi\sqrt{in}$ per Table 3 of [3.III.4]. Next the minimum crack size, a_{min}, for crack propagation to occur is calculated below using the formula for a through-thickness edge crack given in [3.1.5]. Although the formula is derived for a straight-edge specimen, the use of the peak stress, σ_{max}, at a notch in the fuel basket panel (instead of the average stress in the panel as required by the formula) essentially compensates for the geometric difference between the basket panel and the specimen. Moreover, the maximum size of a pre-existing crack (1/16") in the fuel basket panel is less than

1/6th of the basket panel thickness (0.40"). Thus, the assumption of a through-thickness edge crack is very conservative. The result is

$$a_{min} = \frac{\left(\frac{K_{IC}}{1.12\sigma_{max}}\right)^2}{\pi} = \frac{\left[\frac{30ksi\sqrt{in}}{1.12(18.025ksi)}\right]^2}{\pi} = 0.703in$$

and the safety factor against crack propagation (based on a 1/16" minimum detectable flaw size) is

$$SF = \frac{a_{min}}{a_{det}} = \frac{0.703in}{0.0625in} = 11.2$$

The calculated minimum crack size is more than 11 times greater than the maximum possible pre-existing crack size in the fuel basket (based on 100% surface inspection of each panel). The large safety factor ensures that crack propagation in the MPC-68M fuel basket will not occur due to the non-mechanistic tipover event.

3.III.4.4.3.2 Elastic Stability and Yielding of the MPC-68M Fuel Basket under Compression Loads (Load Case F3 in Table 3.1.3)

Under certain conditions, the fuel basket plates may be under direct compressive load. Although the finite element simulations can predict the onset of an instability and post-instability behavior, the computation in this subsection uses (the more conservative) classical instability formulations to demonstrate that an elastic instability of the basket plates is not credible.

A solution for the stability of the fuel basket plate is obtained using the classical formula for buckling of a wide bar [3.III.1]. Material properties are selected corresponding to a metal temperature of 325°C, which bounds the computed metal temperatures anywhere in the fuel basket (see Table 4.III.3). The critical buckling stress for a pin-ended bar is:

$$\sigma_{cr} = (\pi)^2 \frac{E}{12(1-\nu^2)}\left(\frac{h}{a}\right)^2$$

where h is the plate thickness, a is the unsupported plate length, E is the Young's Modulus of Metamic-HT at 325°C, ν is Poisson's Ratio (use 0.3 for this calculation)

From the drawings in Section 1.5, h = 0.40 in, a = 6.05 in, and E = 8,050 ksi (Table 1.III.A.1). Then, the classical critical buckling stress is computed as 31.8 ksi, which exceeds the yield strength of the material. This demonstrates that basket plate instability by elastic buckling is not possible.

3.III.4.5 Cold

Same as in Subsection 3.4.5.

3.III.4.6 HI-STORM 100 Kinematic Stability under Flood Condition (Load Case A in Table 3.1.1)

The stability evaluation of the HI-STORM 100 overpack under flood conditions in Subsection 3.4.6 bounds the scenario of a loaded MPC-68M inside a HI-STORM overpack. The previous analysis is bounding because it uses as input the empty weight of the HI-STORM overpack (i.e., no MPC inside) combined with the maximum CG height from Table 3.2.3.

3.III.4.7 Seismic Event and Explosion

Since there are no physical changes to the HI-STORM overpacks and the MPC-68M reduces the CG height of the loaded HI-STORM overpacks, relative to those analyzed in Chapter 3, the seismic event and explosion analyses presented in Subsection 3.4.7 (including all paragraphs) bound the scenario of a loaded MPC-68M inside a HI-STORM overpack.

3.III.4.8 Tornado Wind and Missile Impact (Load Case B in Table 3.1.1 and Load Case 04 in Table 3.1.5)

The results for the post-impact response of the HI-STORM 100 overpack in Subsection 3.4.8 for the combination of tornado missile plus either steady tornado wind or instantaneous tornado pressure drop bound the results for a loaded MPC-68M inside a HI-STORM overpack. The results are bounding because they are calculated assuming a lower bound weight for the loaded HI-STORM and an upper bound CG height (as compared to a loaded MPC-68M inside a HI-STORM).

In addition, since the MPC-68M does not require any physical changes to the HI-STORM overpacks or the HI-TRAC transfer casks for MPC loading, the missile penetration analyses presented in Subsection 3.4.8 remain valid.

3.III.4.9 HI-TRAC Drop Events

The HI-TRAC drop analyses presented in Subsection 3.4.9 (including all paragraphs) are valid for a loaded MPC-68M inside a HI-TRAC for the following reasons:

i. the MPC-68M does not require any changes to the HI-TRAC transfer casks for MPC loading;

ii. the MPC and its contents are modeled as a solid body (i.e., no explicit modeling of MPC fuel basket);

iii. the difference in weight between a fully loaded MPC-68M and the MPC analyzed in Subsection 3.4.9 is less than 5% of the total drop weight.

3.III.4.10 HI-STORM 100 Non-Mechanistic Tip-over and Vertical Drop Event (Load Cases 02.a and 02.c in Table 3.1.5)

Pursuant to the provision in NUREG-1536, a non-mechanistic tip-over of a loaded MPC-68M inside a HI-STORM overpack on to the ISFSI pad is considered in this supplement. Calculations are also performed to determine the maximum vertical carry height limit such that the deceleration sustained by a vertical free fall of a HI-STORM overpack carrying a loaded MPC-68M onto the ISFSI pad is less than design basis deceleration limit specified in Table 3.1.2.

The tip-over analysis performed in Appendix 3.A is based on the HI-STORM 100 geometry and a bounding weight. Since the MPC-68M has a slightly higher center of gravity and weighs less than the MPC modeled in Appendix 3.A, it is not a foregone conclusion that the maximum rigid body deceleration level is, in fact, reduced if a HI-STORM 100, with a loaded MPC-68M inside, suffers a non-mechanistic tip-over onto the identical target. In what follows, we present a summary of the analysis undertaken to demonstrate conclusively that the result for maximum deceleration level is less than design basis deceleration limit specified in Table 3.1.2 when the MPC-68M is stored inside the HI-STORM 100 overpack. The analysis employs the methodology previously established in Subsection 3.4.10 for analyzing the HI-STORM 100S overpack.

Appendix 3.A presents a result for the angular velocity of the cylindrical body representing a HI-STORM 100 just prior to impact with the defined target. The result is expressed in Subsection 3.A.6 in terms of the cask geometry, and the ratio of the mass divided by the mass moment of inertia about the corner point that serves as the rotation origin. Since the mass moment of inertia is also linearly related to the mass, the angular velocity at the instant just prior to target contact is independent of the cask mass. Subsequent to target impact, we investigate post-impact response by considering the cask as a cylinder rotating into a target that provides a resistance force that varies linearly with distance from the rotation point. We measure "time" as starting at the instant of impact, and develop a one-degree-of freedom equation for the post-impact response (for the rotation angle into the target) as:

$$\ddot{\theta} + \omega^2\theta = 0$$

where

$$\omega^2 = \frac{kL^3}{3I_A}$$

The initial conditions at time zero are: the initial angle is zero and the initial angular velocity is equal to the rigid body angular velocity acquired by the tip-over from the center-of-gravity over corner position. In the above relation, L is the length of the overpack, I is the mass moment of inertia defined in Appendix 3.A, and k is a "spring constant" associated with the target

resistance. If we solve for the maximum angular acceleration subsequent to time zero, we obtain the result in terms of the initial angular velocity as:

$$\ddot{\theta}_{max} = \omega\dot{\theta}_0$$

If we form the maximum linear acceleration at the top of the overpack lid, we can finally relate the decelerations of the HI-STORM 100 configuration analyzed in Appendix 3.A and the HI-STORM 100/MPC-68M configuration solely in terms of their geometry properties and their mass ratio. The value of "k", the target spring rate is the same for both overpacks so it does not appear in the relationship between the two decelerations. After substituting the appropriate geometry and calculated masses, we determine that the ratio of maximum rigid body decelerations at the top surface of the lids is:

$$A_{\text{HI-STORM 100-68M}}/A_{\text{HI-STORM 100}} = 1.01$$

The fact that the calculated ratio is only marginally above 1.0 indicates that the MPC-68M has a minor effect on the non-mechanistic tip-over analysis performed in Appendix 3.A. The maximum rigid body deceleration for the HI-STORM 100/MPC-68M configuration is determined by scaling the calculated result from Appendix 3.A as follows:

$$A_{\text{HI-STORM 100-68M}} = 1.01 \times A_{\text{HI-STORM 100}} = 1.01 \times 42.98g = 43.42g$$

This demonstrates that when the MPC-68M is stored inside the HI-STORM 100 overpack the result for maximum deceleration level is less than the design basis deceleration limit specified in Table 3.1.2. Based on the comparative evaluations in Subsection 3.4.10, the HI-STORM 100 overpack is the limiting overpack for the non-mechanistic tip-over event. Therefore, when the MPC-68M is inside the HI-STORM 100S or the HI-STORM 100S Version B overpack, the maximum rigid body deceleration at the top surface of the lid is less than the deceleration above.

Next we demonstrate that the deceleration sustained by a vertical free fall of a HI-STORM overpack carrying a loaded MPC-68M onto the ISFSI pad is less than the design basis deceleration limit specified in Table 3.1.2. According to Appendix 3.A, analysis of a single mass impacting a spring with a given initial velocity shows that the maximum deceleration "a_M" of the mass is related to the dropped weight "w" and the drop height "h" as follows:

$$a_M \sim \frac{\sqrt{h}}{\sqrt{w}}$$

In other words for a fixed drop height, as the dropped weight decreases, the maximum deceleration of the mass increases. Since the MPC-68M weighs less than the MPC analyzed in Appendix 3.A, the maximum deceleration calculated in Appendix 3.A is not bounding. From the above relationship, the maximum deceleration for the HI-STORM 100/MPC-68M configuration is determined as:

$$a_{100-68M} = \sqrt{\frac{w_{100}}{w_{100-68M}}} a_{100}$$

where $w_{100-68M}$ is the weight of a HI-STORM 100 carrying a loaded MPC-68M, w_{100} is the weight of a loaded HI-STORM 100 overpack as analyzed in Appendix 3.A, and a_{100} is the maximum deceleration of the HI-STORM 100 calculated in Appendix 3.A for an 11" vertical drop. The above equation yields the following result:

$$a_{100-68M} = 44.39g$$

Although the result is higher than the maximum deceleration calculated in Appendix 3.A, it is still less than the design basis vertical deceleration limit specified in Table 3.1.2. Therefore, the previously established lift height limit of 11 inches for a loaded HI-STORM overpack is also applicable to HI-STORM overpacks carrying the MPC-68M. Note that depending on site-specific conditions, a lower lift height limit may be required. See Section 2.2.3.1.

Finally, Subsection 3.4.10 provides the results of a simple elastic strength of materials calculation, which demonstrates that the cylindrical storage overpack will not permanently deform to the extent that the MPC cannot be removed by normal means after a tip-over event. Those results are valid for the MPC-68M since:

i. there are no changes to the HI-STORM overpack stemming from the MPC-68M;

ii. the external dimensions of the MPC-68M are the same as all other MPC types;

iii. the results are calculated using upper bound impact decelerations.

3.III.4.11 Storage Overpack and HI-TRAC Transfer Cask Service Life

Same as in Subsection 3.4.11 (including all paragraphs).

3.III.4.12 MPC Service Life

Same as in Subsection 3.4.12 and with the following supplementary information provided herein.

3.III.4.12.1 Metamic-HT Considerations

Metamic-HT has been extensively tested as indicated in Appendix A of Supplement 1.III. Testing has included extensive tests for creep, irradiation and corrosion to ensure long-term fuel basket performance under normal conditions of storage. The Metamic-HT is also not susceptible to structural fatigue and brittle fracture under long term conditions of storage. Corrosion is discussed further in Subsection 3.III.4.1. Creep and boron depletion are further discussed below.

i) Fuel Basket Creep

The Metamic sourcebook contains data on the testing to determine the creep characteristics of the Metamic-HT under both unirradiated and irradiated conditions. A creep equation to estimate a bounding estimate of total creep as a function of stress and temperature is also provided. The creep equation developed from this test provides a conservative prediction of accumulated creep strain by direct comparison to measured creep in unirradiated and irradiated coupons.

The creep equation for Metamic-HT that bounds *all* measured data (tests run for 20,000 hours) is of the classical exponential form in stress and temperature (see Appendix A of Supplement 1.III), which is written symbolically as $\varepsilon = f(\sigma,T)$.

Creep in the MPC-68M fuel basket will not be a reactivity modifier because the basket is arrayed in the vertical orientation. The lateral loading of the fuel basket walls is insignificant and hence no mechanistic means for the basket panels to undergo lateral deformation from creep exists, even if the panel material were susceptible to creep.

The creep effect would tend to shorten the fuel basket under the self-weight of the basket. An illustrative calculation of the cumulative reduction of the basket length is presented below to demonstrate the insignificant role of creep in the MPC-68M fuel basket.

The in-plane compressive stress, σ, at height x in the basket panel is given by

$$\sigma = \rho(H-x) \qquad (3.III.1)$$

where:
ρ = weight density of Metamic-HT
H = height of the fuel basket

Using the above stress equation, the total creep shrinkage, δ, is given by

$$\delta = \int_0^H f(\sigma,T)dx \qquad (3.III.2)$$

where:
T = panel's metal temperature (conservatively assumed to be 350°C for a period of 60 years)
H = height of the basket (conservatively assumed to be 200 inches)

Using the creep equation (provided in Appendix A of Supplement 1.III) and performing the above integration numerically yields $\delta = 0.095$ inch. In other words, the computed shrinkage of the basket is less than 0.048% of its original length. Therefore, it is concluded that for the vertical storage configuration the creep effects of the MPC-68M fuel basket are insignificant due to absence of any meaningful loads on the panels. Therefore, creep in the Metamic-HT fuel basket is not a matter of safety concern.

ii) Fuel Basket Boron Depletion

The similarities between Metamic-HT and Metamic (classic) neutron absorbers and their exposure to the same long-term conditions of storage in the HI-STORM 100 system provide a logical basis to expect negligible neutron absorber boron depletion in Metamic-HT. However, to assure criticality safety during worst case design basis conditions over the 40-year design life, the analysis discussed in Subsection 6.III demonstrates that the boron depletion in the Metamic-HT is negligible over a 50-year duration. Thus, sufficient levels of boron are present in the fuel basket to maintain criticality safety over the 40-year design life of the MPC.

3.III.4.12.2 Basket Shim Considerations:

i) Basket Shim Creep

Like the fuel basket, the basket shims are not subject to any significant loading during storage. The ability of the basket shims (made of a creep resistant aluminum alloy) has been evaluated and qualified in Docket No. 71-9325 [2.III.6.2] for transport applications where the stress level (in horizontal configuration) is significant. Therefore, in light of the minuscule stress levels from self-weight in long-term storage, creep is ruled out as a viable concern for the basket shims.

ii) Basket Shim Corrosion

Basket shim corrosion is discussed in Subsection 3.III.4.1.

3.III.4.13 Design and Service Life

Same as in Subsection 3.4.13.

3.III.5 FUEL RODS

Same as in Section 3.5.

3.III.6 SUPPLEMENTAL DATA

3.III.6.1 Additional Codes and Standards Referenced in HI-STORM 100 System Design and Fabrication

Same as in Subsection 3.6.1.

3.III.6.2 Computer Programs

ANSYS 11.0, which is a public domain finite element code, has been utilized to perform structural analyses documented in this supplement.

3.III.6.3 Appendices Included in Supplement 3.III

None.

3.III.6.4 Calculation Packages

A calculation package containing the structural calculations supporting Supplement 3.III has been prepared, reviewed, and archived according to Holtec International's quality assurance program (see Chapter 13).

3.III.7 COMPLIANCE WITH NUREG-1536

The material in this supplement for the MPC-68M provides the same information as previously provided for the other MPC types in Chapter 3. Therefore, to the extent applicable, the information provided is in compliance with NUREG-1536.

3.III.8 REFERENCES

[3.III.1] Buckling of Bars, Plates, and Shells, D.O. Brush and B.O. Almroth, McGraw-Hill, 1975, p.22.

[3.III.2] Properties of Aluminum Alloys, Tensile, Creep, and Fatigue Data at High and Low Temperatures, ASM International, November 2006.

[3.III.3] ASME Boiler & Pressure Vessel Code, Section II, Parts A and D, American Society of Mechanical Engineers, 2007.

[3.III.4] "Mechanical Testing and Evaluation", ASM Handbook, Volume 8, 2000.

[3.III.5] ASTM Specification B221M-07, "Standard Specification for Aluminum and Aluminum-Alloy Extruded Bars, Rods, Wire, Profiles, and Tubes (Metric)".

TABLE 3.III.1
WEIGHT DATA FOR MPC-68M

Item	Bounding Weight (lb)
MPC-68M	
• Without SNF	30,000
• Fully loaded with SNF and Fuel Spacers	90,000

TABLE 3.III.2
CENTERS OF GRAVITY OF HI-STORM SYSTEM CONFIGURATIONS INVOLVING MPC-68M

Component	Height of CG Above Datum (in)
MPC-68M (empty)	114.9
HI-STORM 100 Overpack w/ fully loaded MPC-68M	118.4
HI-STORM 100S(232) Overpack w/ fully loaded MPC-68M	113.3
HI-STORM 100S(243) Overpack w/ fully loaded MPC-68M	117.7
HI-STORM 100S Version B(218) Overpack w/ fully loaded MPC-68M	108.5
HI-STORM 100S Version B(229) Overpack w/ fully loaded MPC-68M	112.8
HI-TRAC 125 Transfer Cask w/ Top Lid, Pool Lid, and fully loaded MPC-68M (water jacket filled)	97.4
HI-TRAC 100 Transfer Cask w/ Top Lid, Pool Lid, and fully loaded MPC-68M (water jacket filled)	96.5
HI-TRAC 125D Transfer Cask w/ Top Lid, Pool Lid, and fully loaded MPC-68M (water jacket filled)	96.9
HI-TRAC 100D Transfer Cask w/ Top Lid, Pool Lid, and fully loaded MPC-68M (water jacket filled)	94.3

Notes:

1. The datum used for calculations involving the HI-STORM is the bottom of the overpack baseplate. The datum used for calculations involving the HI-TRAC is the bottom of the pool lid.

2. The datum used for calculations involving only the MPC is the bottom of the MPC baseplate.

3. The CG height of the HI-STORM overpack is calculated based on standard density concrete (i.e., 166 pcf dry) in the radial cavity. At higher densities, the CG height is slightly lower, which makes the HI-STORM overpack less prone to tipping.

TABLE 3.III.3
FUEL BASKET SHIMS – NOMINAL MECHANICAL PROPERTIES

Aluminum Alloy (B221 2219-T8511)					
Temp. °C (°F)	S_y	S_u	E	α	% Elongation
25 (75)	290 (42)	400 (58)	7.2 (10.5)	–	5
150 (300)	243 (35)	307 (44)	6.8 (9.8)	23.9 (13.3)	6.4
204 (400)	188 (27)	231 (34)	6.3 (9.1)	24.5 (13.6)	8.2
230 (450)	171 (25)	209 (30)	6.1 (8.8)	24.8 (13.8)	8.6
260 (500)	154 (22)	182 (26)	5.9 (8.5)	25.0 (13.9)	8.6
290 (550)	98 (14)	116 (17)	5.5 (8.0)	25.4 (14.1)	10.5

Definitions:

S_y = Yield Stress, MPa (ksi)
α = Mean Coefficient of thermal expansion, cm/cm-°C x 10^{-6} (in/in-°F x 10^{-6})
S_u = Ultimate Stress, MPa (ksi)
E = Young's Modulus, MPa x 10^4 (psi x 10^6)

Notes:

1. Source for E values is "Properties of Aluminum Alloys", page 82 [3.III.2] (properties listed in the table above are not affected by time at temperature).
2. Source for α is Table TE-2 of [3.III.3] (values listed in TE-2 are also considered representative of Aluminum Alloy (2219-T8511) (UNS No. A92219)).
3. Source for Sy, Su, and % Elongation values at room temperature is ASTM Specification B221M [3.III.5]. Values at elevated temperatures are obtained by scaling the room temperature values using the data from [3.III.3].

TABLE 3.III.4
MAXIMUM DISPLACEMENT IN MPC-68M FUEL BASKET

Maximum Lateral Displacement in Fuel Basket Panel, θ (dimensionless) (Note 1)	Maximum Allowable Value of θ (from Table 2.III.4)	Safety Factor
9.6×10^{-4}	0.005	5.21

Notes:

1. See Subsection 2.III.0.1 for definition of θ.

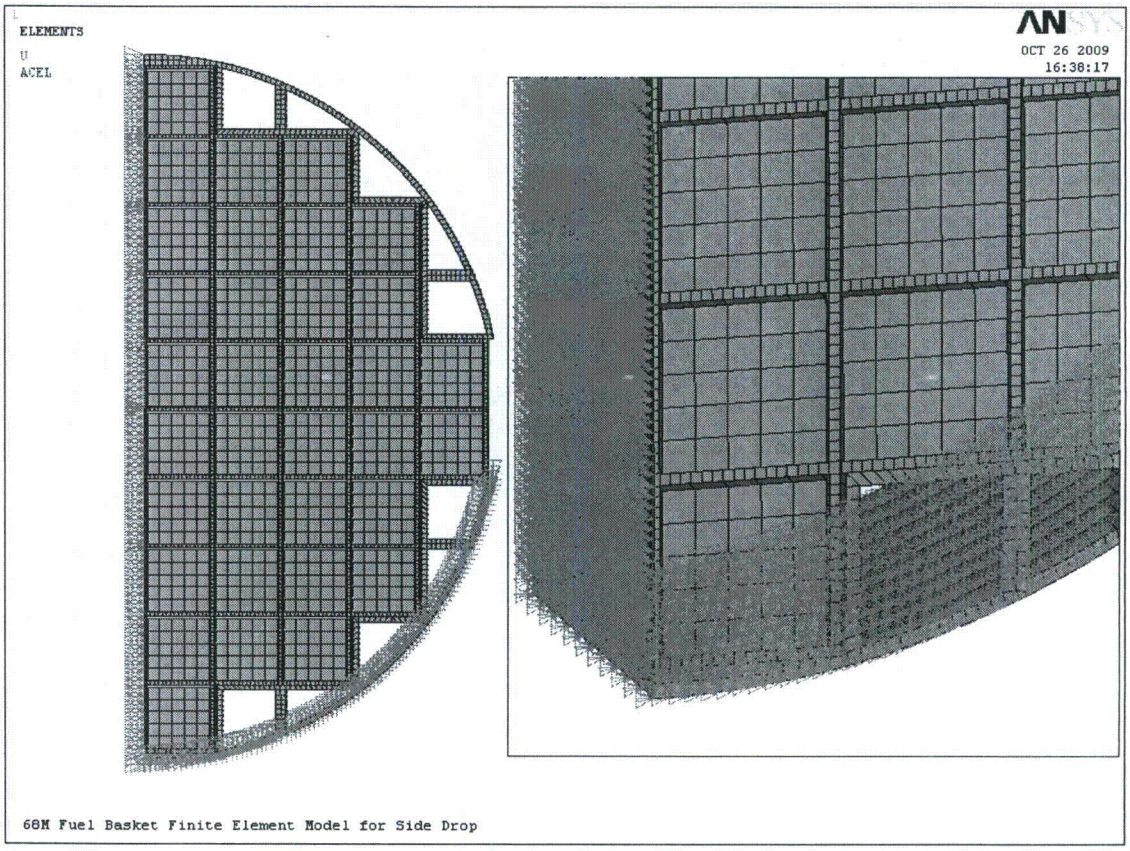

FIGURE 3.III.1: FINITE ELEMENT MODEL OF MPC-68M FUEL BASKET

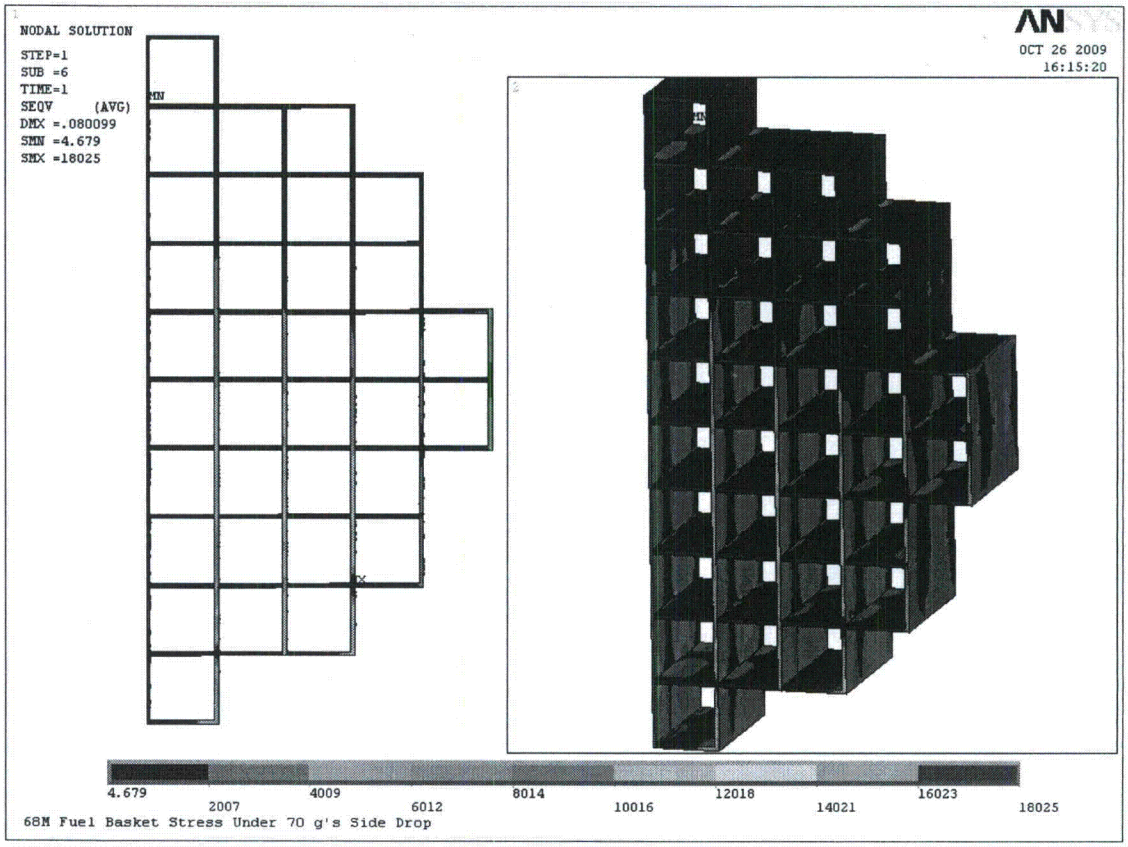

FIGURE 3.III.2: VON MISES STRESS DISTRIBUTION IN MPC-68M FUEL BASKET UNDER 70g LOAD

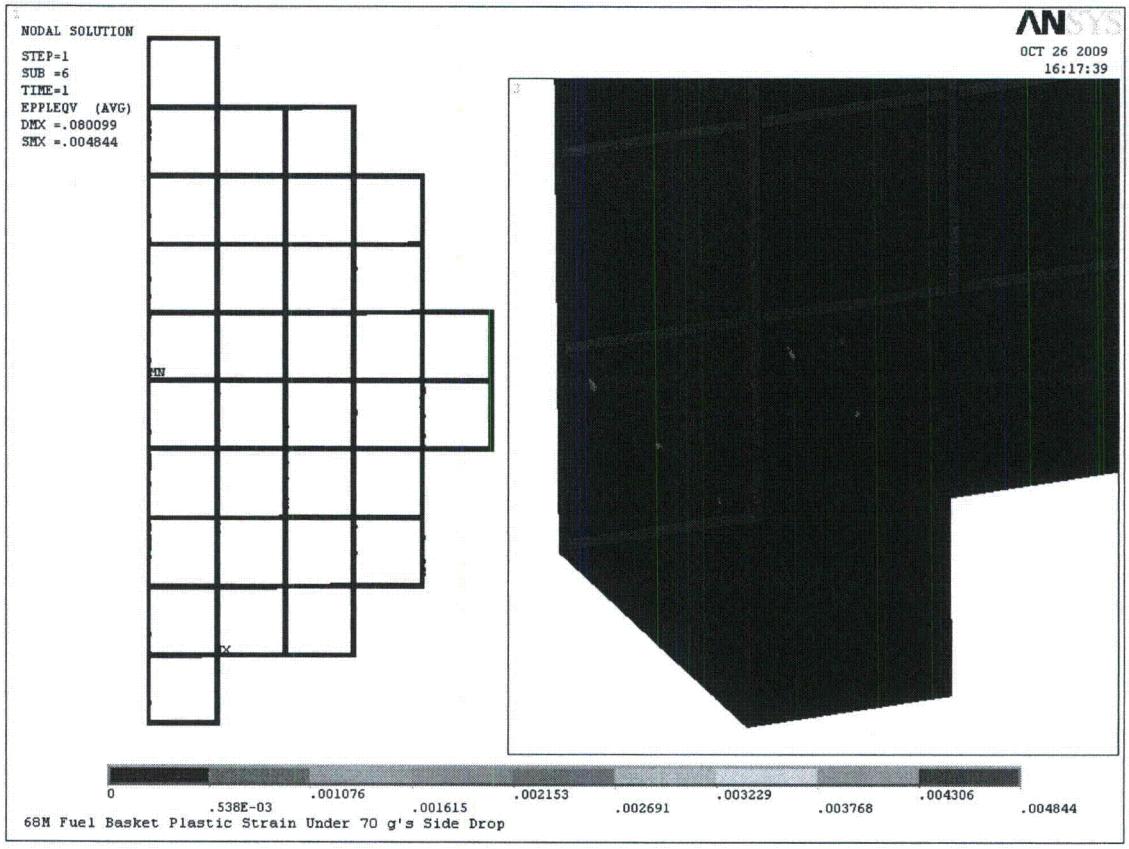

FIGURE 3.III.3: PLASTIC STRAIN DISTRIBUTION IN MPC-68M FUEL BASKET UNDER 70g LOAD

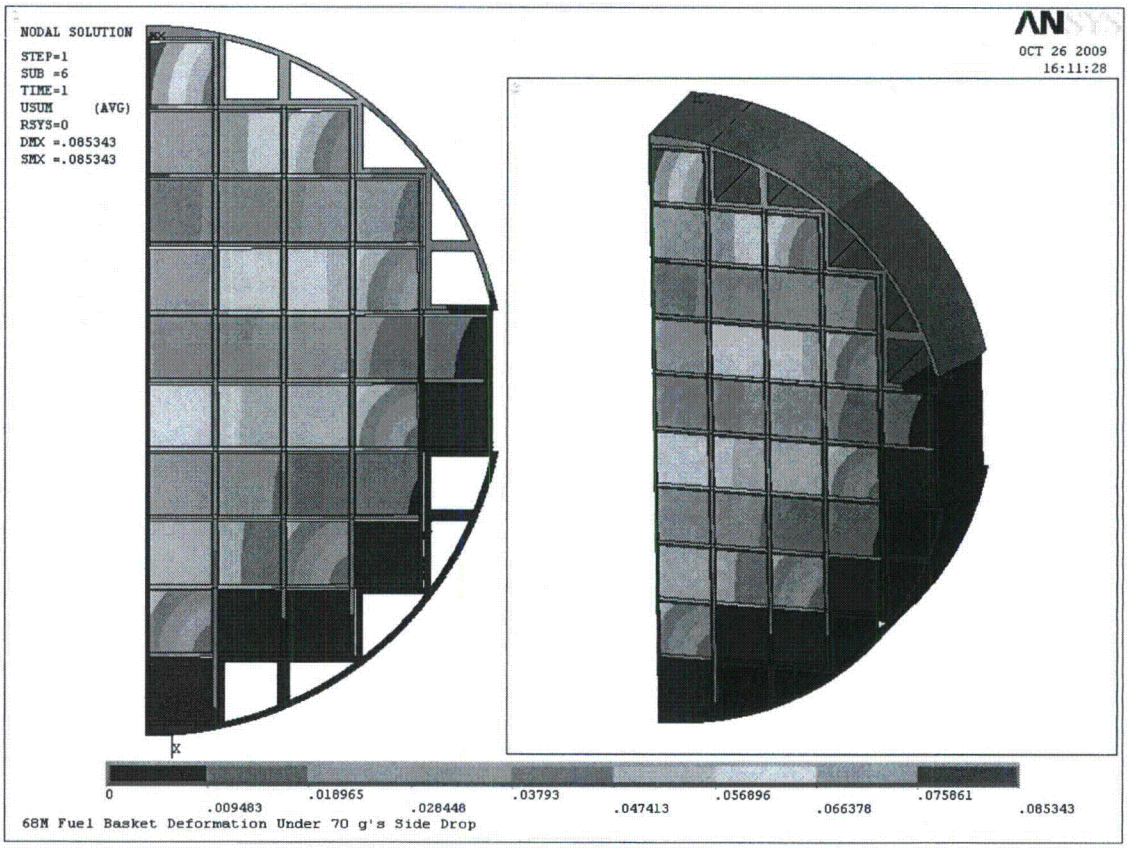

FIGURE 3.III.4: DISPLACEMENT CONTOURS IN MPC-68M FUEL BASKET UNDER 70g LOAD

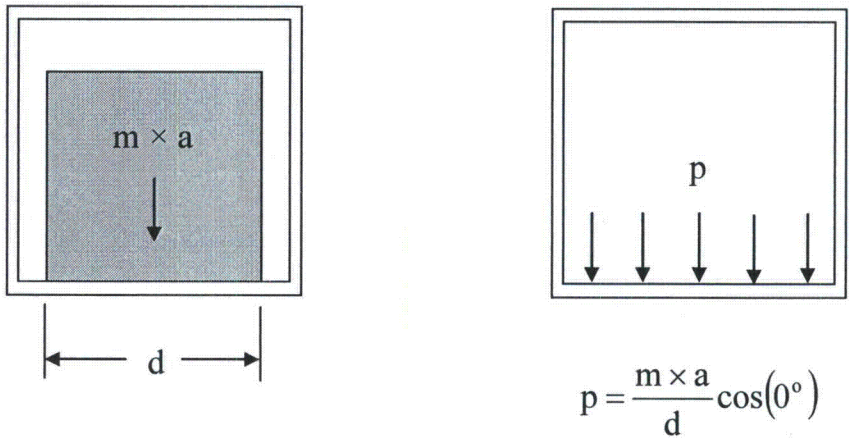

(a) 0° Orientation

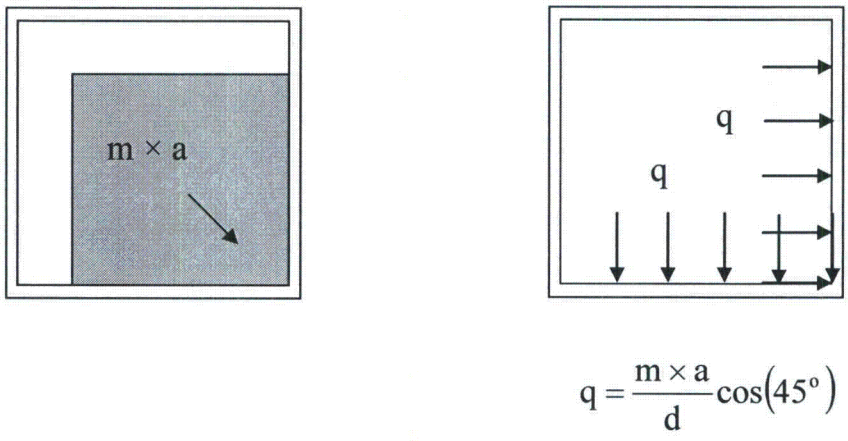

(b) 45° Orientation

FIGURE 3.III.5: FUEL LOADING FOR 0° AND 45° BASKET ORIENTATIONS

CHAPTER 4[1] THERMAL EVALUATION

4.0 OVERVIEW

The HI-STORM System is designed for long-term storage of spent nuclear fuel (SNF) in a vertical orientation. An array of HI-STORM Systems laid out in a rectilinear pattern will be stored on a concrete ISFSI pad in an open environment. In this section, compliance of the HI-STORM thermal performance to 10CFR72 requirements for outdoor storage at an ISFSI is established. The analysis considers passive rejection of decay heat from the stored SNF assemblies to the environment under normal, off-normal, and accident conditions of storage. Effects of incident solar radiation (insolation) and partial radiation blockage due to the presence of neighboring casks at an ISFSI site are included in the analyses. Finally, the thermal margins of safety for long-term storage of both moderate burnup (up to 45,000 MWD/MTU) and high burnup spent nuclear fuel (greater than 45,000 MWD/MTU) in the HI-STORM 100 system are quantified. Safe thermal performance during on-site loading, unloading and transfer operations utilizing the HI-TRAC transfer cask is also demonstrated.

The HI-STORM thermal evaluation follows the guidelines of NUREG-1536 [4.4.1] and ISG-11 [4.1.4] to demonstrate thermal compliance of the HI-STORM system. . These guidelines provide specific limits on the permissible maximum cladding temperature in the stored commercial spent fuel (CSF)[2] and other confinement boundary components, and on the maximum permissible pressure in the confinement space under certain operating scenarios. Specifically, the requirements are:

1. The fuel cladding temperature for long-term storage shall be limited to 752°F (400°C).

2. The fuel cladding temperature for short-term operations shall be limited to 752°F (400°C) for high burnup fuel and 1058°F (570°C) for moderate burnup fuel.

3. The fuel cladding temperature should be maintained below 1058°F (570°C) for accident and off-normal event conditions.

4. The maximum internal pressure of the MPC should remain within its design pressures for normal, off-normal, and accident conditions.

---

1 This chapter has been prepared in the format and section organization set forth in Regulatory Guide 3.61. However, the material content of this chapter also fulfills the requirements of NUREG-1536. Pagination and numbering of sections, figures, and tables are consistent with the convention set down in Chapter 1, Section 1.0, herein. Finally, all terms-of-art used in this chapter are consistent with the terminology of the glossary (Table 1.0.1) . This chapter has been substantially re-written in support of LAR #3 to improve clarity and to incorporate the 3-D thermal model. Because of extensive editing a clean chapter is issued with this amendment.

2 Defined as nuclear fuel that is used to produce energy in a commercial nuclear reactor (See Table 1.0.1).

4. The cask materials should be maintained within their minimum and maximum temperature criteria for normal, off-normal, and accident conditions.

5. For fuel assemblies proposed for storage, the cask system should ensure a very low probability of cladding breach during long-term storage.

6. The HI-STORM System should be passively cooled.

7. The thermal performance of the cask shall be in compliance with the design criteria specified in FSAR Chapters 1 and 2 for normal, off-normal, and accident conditions.

As demonstrated in this chapter, the HI-STORM System is designed to comply with all of the criteria listed above. Sections 4.1 through 4.3 describe thermal analyses and input data that are common to all conditions. All thermal analyses to evaluate normal conditions of storage in a HI-STORM storage module are described in Section 4.4. All thermal analyses to evaluate normal handling and on-site transfer in a HI-TRAC transfer cask are described in Section 4.5. All thermal analyses to evaluate off-normal and accident conditions are described in Section 4.6. This FSAR chapter is in full compliance with ISG-11 and with NUREG-1536 guidelines, subject to the exceptions and clarifications discussed in Chapter 1, Table 1.0.3.

The HI-STORM thermal evaluations for CSF are grouped in two categories of fuel assemblies. The two groups are classified as Low Heat Emitting (LHE) fuel assemblies and Design Basis (DB) fuel assemblies. The LHE group of fuel assemblies are characterized by low burnup, long cooling time, and short active fuel lengths. Consequently, their heat loads are dwarfed by the DB group of fuel assemblies. All Dresden-1 (6x6 and 8x8 and a thoria rod canister constituted as part of an 8x8 fuel assembly), Quad+, Humboldt Bay (7x7 and 6x6), Indian Point, Haddam Neck and all stainless-steel clad fuel assemblies are classified as LHE fuel. The low heat emitting characteristics of these fuel assemblies render them non-governing for thermal evaluation. The HI-STORM System temperatures for MPCs loaded with LHE fuel are bounded by design basis evaluations reported in this chapter.

The HI-STORM System is evaluated for two fuel storage scenarios. In one scenario, designated as uniform loading, every basket cell is assumed to be occupied with fuel producing heat at the maximum rate. As discussed in Chapter 2, this storage specification is extremely conservative, and virtually impossible to realize in actual practice. A less unrealistic, yet conservative idealization of storage scenario, designated as regionalized loading, involves defining two discrete regions within the basket. The two regions are designated as Region 1 (inner region) and Region 2 (outer region). Regionalized storage is designed to recognize storage of fuel assemblies having wide disparity in heat emission rates. For further discussion of regionalized storage, Section 2.1 of Chapter 2 should be consulted.

The HI-STORM System is designed for one reference storage condition defined in Table 4.0.1. This condition establishes the required helium backfill pressures computed later in this chapter (See Subsection 4.4.5.1). Having defined the helium backfill pressures an array of analyses are performed to evaluate the range of storage configurations specified in Chapter 2 and results reported in Section 4.4.

Table 4.0.1

REFERENCE HI-STORM OPERATING CONDITIONS

Condition	Value
MPC Decay Heat	Table 2.1.26
MPC Operating Pressure	7 atm (absolute)
Normal Ambient Temperature	Table 2.2.2

4.1 DISCUSSION

The HI-STORM FSAR seeks to establish complete compliance with the provisions of ISG-11 [4.1.4]. For this purpose the HI-STORM normal storage fuel cladding temperatures are required to meet the 752°F (400°C) temperature limit for all CSF (See Section 4.3). Additionally, when the MPCs are deployed for storing High Burnup Fuel (HBF) further restrictions during certain fuel loading activities (vacuum drying) are set forth to preclude fuel temperatures from exceeding the normal temperature limits. To ensure explicit compliance, a specific term "short term operations" is defined in Chapter 2 to cover all fuel loading activities. ISG-11 fuel cladding temperature limits are applied for short-term operations (see Table 4.3.1).

Potential thermally challenging states for the spent fuel arise if the fuel drying process utilizes the pressure reduction process (i.e., vacuum drying). The short-term evolutions that may be thermally limiting and warrant analysis are:

i. Vacuum Drying
ii. Loaded MPC in HI-TRAC in the Vertical Orientation

The threshold MPC heat generation rate at which the HI-STORM peak cladding temperature reaches a steady state equilibrium value approaching the normal storage peak clad temperature limit is computed in this chapter. Likewise, the MPC heat generation rates that produce the steady state equilibrium temperature approaching the normal storage peak clad temperature limit for the MPC in HI-TRAC are computed in this chapter. These computed heat generation rates directly bear upon the compliance of the system with ISG-11 [4.1.4] and are, accordingly, adopted in the system Technical Specifications for high burnup fuel (HBF).

The aboveground HI-STORM system consists of a sealed MPC situated inside a vertically-oriented, ventilated storage overpack. Air inlet and outlet ducts that allow for air cooling of the stored MPC are located at the bottom and top, respectively, of the cylindrical overpack. The SNF assemblies reside inside the MPC, which is sealed with a welded lid to form the confinement boundary. The MPC contains a stainless-steel honeycomb fuel basket structure with square-shaped compartments of appropriate dimensions to allow insertion of the fuel assemblies prior to welding of the MPC lid and closure ring. Each fuel basket panel, with the exception of exterior panels on the MPC-68 and MPC-32, is equipped with a thermal neutron absorber panel sandwiched between an Alloy X steel sheathing plate and the fuel basket panel, along the entire length of the active fuel region. The MPC is backfilled with helium up to the design-basis initial fill level (Table 1.2.2). This provides a stable, inert environment for long-term storage of the SNF. Heat is rejected from the SNF in the HI-STORM System to the environment by passive heat transport mechanisms only.

The helium backfill gas plays an important role in the MPC's thermal performance. The helium fills all the spaces between solid components and provides an improved conduction medium (compared to air) for dissipating decay heat in the MPC. Within the MPC the pressurized helium environment sustains a closed loop thermosiphon action, removing SNF heat by an upward flow of helium through the storage cells. This MPC internal convection heat dissipation mechanism is illustrated in

Figure 4.1.1. On the outside of the MPC a ducted overpack construction with a vertical annulus facilitates an upward flow of air by buoyancy forces. The annulus ventilation flow cools the hot MPC surfaces and safely transports heat to the outside environment. The annulus ventilation cooling mechanism is illustrated in Figure 4.1.2. To ensure that the helium gas is retained and is not diluted by lower conductivity air, the MPC confinement boundary is designed and fabricated in accordance with the ASME B&PV Code Section III, Subsection NB as an all-seal-welded pressure vessel with redundant closures. It is demonstrated in Section 11.1.3 that the failure of one field-welded pressure boundary seal will not result in a breach of the pressure boundary. The helium gas is therefore assumed to be retained in an undiluted state, and may be credited in the thermal analyses.

An important thermal design criterion imposed on the HI-STORM System is to limit the maximum fuel cladding temperature to within design basis limits (Table 4.3.1) for long-term storage of design basis SNF assemblies. An equally important requirement is to minimize temperature gradients in the MPC so as to minimize thermal stresses. In order to meet these design objectives, the MPC baskets are designed to possess certain distinctive characteristics, which are summarized in the following.

The MPC design minimizes resistance to heat transfer within the basket and basket periphery regions. This is ensured by an uninterrupted panel-to-panel connectivity realized in the all-welded honeycomb basket structure. The MPC design incorporates top and bottom plenums with interconnected downcomer paths. The top plenum is formed by the gap between the bottom of the MPC lid and the top of the honeycomb fuel basket, and by elongated semicircular holes in each basket cell wall. The bottom plenum is formed by large elongated semicircular holes at the base of all cell walls. The MPC basket is designed to eliminate structural discontinuities (i.e., gaps) which introduce added thermal resistances to heat flow. Consequently, temperature gradients are minimized in the design, which results in lower thermal stresses within the basket. Low thermal stresses are also ensured by an MPC design that permits unrestrained axial and radial growth of the basket. The possibility of stresses due to restraint on basket periphery thermal growth is eliminated by providing adequate basket-to-canister shell gaps to allow for basket thermal growth during all operational modes.

The MPCs design maximum decay heat loads for storage of zircaloy clad fuel are listed in Table 4.0.1. Storage of stainless steel clad fuel is permitted for a low decay heat limit set forth in Chapter 2 (Tables 2.1.17 through 2.1.24). Storage of zircaloy clad fuel with stainless steel clad fuel in an MPC is permitted. In this scenario, the zircaloy clad fuel must meet the lower decay heat limits for stainless steel clad fuel. The axial heat distribution in each fuel assembly is conservatively assumed to be non-uniformly distributed with peaking in the active fuel mid-height region (See axial burnup Table 2.1.11).

The HI-STORM System (i.e., HI-STORM overpack, HI-TRAC transfer cask and MPC) is evaluated under normal storage (HI-STORM overpack), during off-normal and accident events and during short term operations in a HI-TRAC. Results of HI-STORM thermal analysis during normal (long-term) storage are obtained and reported in Section 4.4. Results of off-normal and accident events are reported in Section 4.6. Results of HI-TRAC short term operations (fuel loading, vacuum drying)

are reported in Section 4.5.

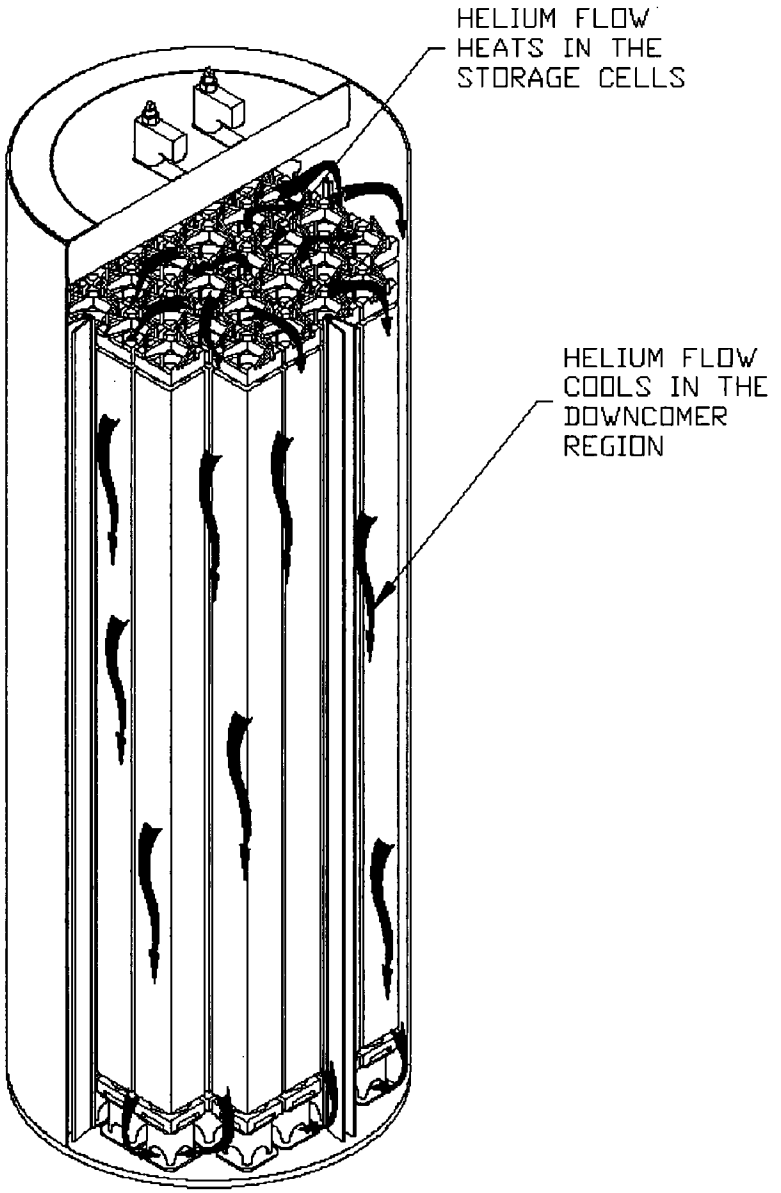

FIGURE 4.1.1: MPC INTERNAL HELIUM CIRCULATION

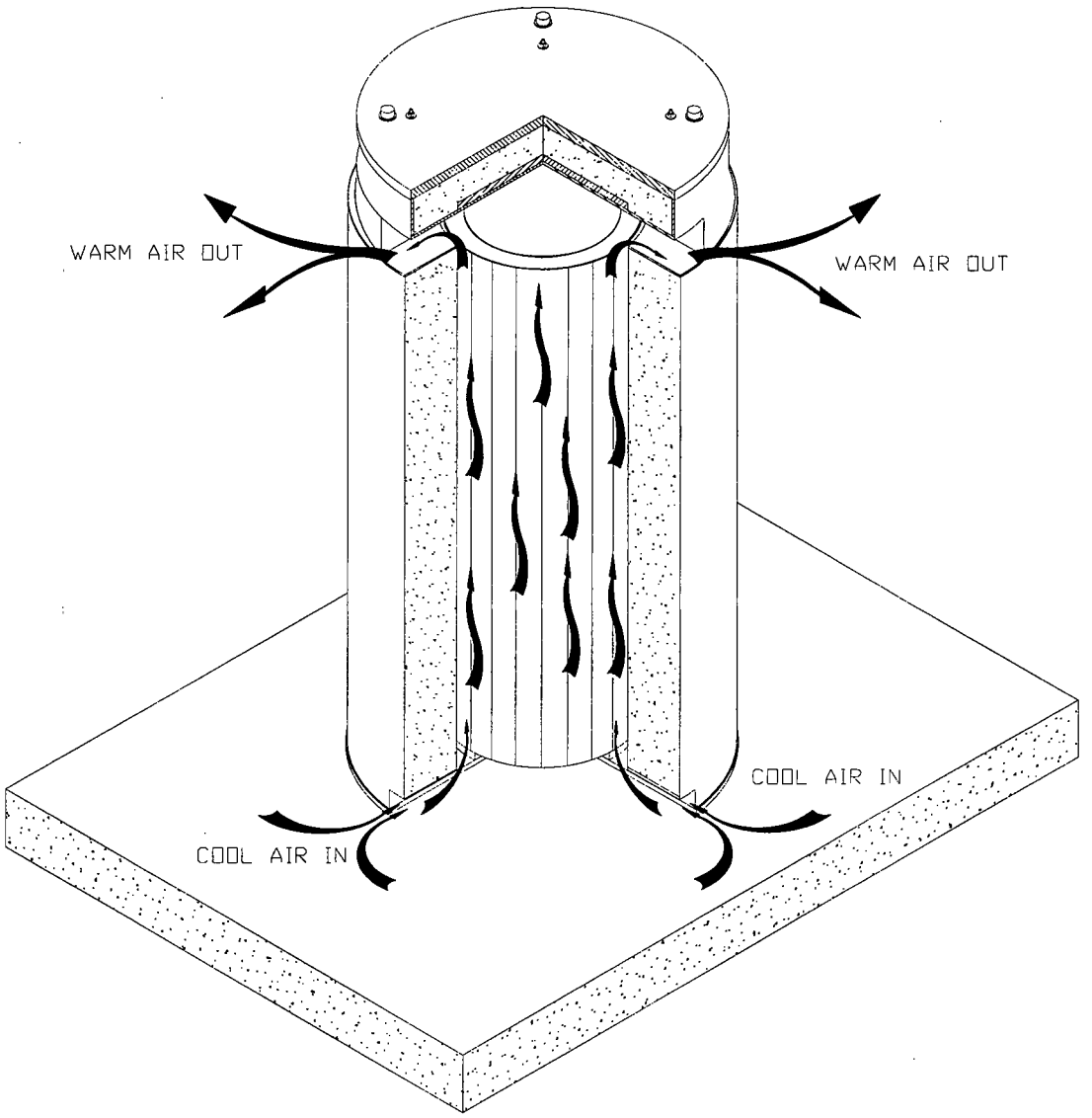

FIGURE 4.1.2: VENTILATION COOLING OF A HI-STORM SYSTEM

4.2 SUMMARY OF THERMAL PROPERTIES OF MATERIALS

Materials present in the MPCs include stainless steels (Alloy X), neutron absorber (Boral or METAMIC) and helium. Materials present in the HI-STORM storage overpack include carbon steels and concrete. Materials present in the HI-TRAC transfer cask include carbon steel, lead, Holtite-A neutron shield, paints (See Appendix 1.C) and demineralized water. In Table 4.2.1, a summary of references used to obtain cask material properties for performing all thermal analyses is presented.

Individual thermal conductivities of the alloys that comprise the Alloy X materials and the bounding Alloy X thermal conductivity are reported in Appendix 1.A of this report. Tables 4.2.2 and 4.2.3 provide numerical thermal conductivity data of materials at several representative temperatures. The currently approved neutron absorber materials, (Boral™ and Metamic™) are both made of aluminum powder and boron carbide powder. Although their manufacturing processes differ, from a thermal standpoint, their ability to conduct heat is virtually identical. Therefore, the values of conductivity of the original neutron absorber (Boral) continue to be used in the thermal calculations.

For the HI-STORM overpack, the thermal conductivity of concrete and the emissivity/absorptivity of painted surfaces are particularly important. Recognizing the considerable variations in reported values for these properties, the values that are conservative with respect to both authoritative references and values used in analyses on previously licensed cask dockets have been selected. Specific discussions of the conservatism of the selected values are included in the following paragraphs.

As specified in Table 4.2.1, the concrete thermal conductivity is taken from Marks' Standard Handbook for Mechanical Engineers, which is conservative compared to a variety of recognized concrete codes and references. Neville, in his book "Properties of Concrete" (4^{th} Edition, 1996), gives concrete conductivity values as high as 2.1 Btu/(hr×ft×°F). For concrete with siliceous aggregates, the type to be used in HI-STORM overpacks, Neville reports conductivities of at least 1.2 Btu/(hr×ft×°F). Data from Loudon and Stacey, extracted from Neville, reports conductivities of 0.980 to 1.310 Btu/(hr×ft×°F) for normal weight concrete protected from the weather. ACI-207.1R provides thermal conductivity values for seventeen structures (mostly dams) at temperatures from 50-150°F. Every thermal conductivity value reported in ACI-207.1R is greater than the value used in the HI-STORM thermal analyses. Additionally, the NRC has previously approved analyses that use higher conductivity values than those applied in the HI-STORM thermal analysis. For example, thermal calculations for the NRC approved Vectra NUHOMS cask system (June 1996, Rev. 4A) used thermal conductivities as high as 1.17 Btu/(hr×ft×°F) at 100°F. Based on these considerations, the concrete thermal conductivity value chosen for HI-STORM thermal analyses is considered to be conservative.

Holtite-A is a composite material consisting of approximately 37 wt% epoxy polymer, 1 wt% B_4C and 62 wt% aluminum trihydrate. While polymers are generally characterized by a low conductivity (0.05 to 0.2 Btu/ft-hr-°F), the addition of fillers in substantial amounts can raise the mixture conductivity by up to a factor of ten. The thermal conductivity of epoxy filled resins with alumina is

reported in the technical literature[1] as approximately 0.5 Btu/ft-hr-°F and higher. A conservatively postulated conductivity of 0.3 Btu/ft-hr-°F is used in the thermal models for the neutron shield region[2] (in the HI-TRAC transfer cask). As the thermal inertia of the neutron shield is not credited in the analyses, the density and heat capacity properties are not reported herein.

Surface emissivity data for key materials of construction are provided in Table 4.2.4. The emissivity properties of painted external surfaces are generally excellent. Kern [4.2.5] reports an emissivity range of 0.8 to 0.98 for a wide variety of paints. In the HI-STORM thermal analysis, an emissivity of 0.85[3] is applied to painted surfaces. A conservative solar absorptivity coefficient of 1.0 is applied to all exposed overpack surfaces.

In Table 4.2.5, the heat capacity and density of the MPC, overpack and CSF materials are presented. These properties are used in performing transient (i.e., hypothetical fire accident condition) analyses. The temperature-dependent values of the viscosities of helium and air are provided in Table 4.2.6.

The heat transfer coefficient for exposed surfaces is calculated by accounting for both natural convection and thermal radiation heat transfer. The natural convection coefficient depends upon the product of Grashof (Gr) and Prandtl (Pr) numbers. Following the approach developed by Jakob and Hawkins [4.2.9], the product Gr×Pr is expressed as $L^3\Delta TZ$, where L is height of the overpack, ΔT is overpack surface temperature differential and Z is a parameter based on air properties, which are known functions of temperature, evaluated at the average film temperature. The temperature-dependent values of Z are provided in Table 4.2.7.

1 "Principles of Polymer Systems", F. Rodriguez, Hemisphere Publishing Company (Chapter 10).

2 The thermal conductivity value used in the thermal models for the neutron shield region is confirmed to be bounded by the Holtite-A test data [4.2.13] with a margin.

3 This is conservative with respect to prior cask industry practice, which has historically utilized higher emissivities [4.2.16].

Table 4.2.1

SUMMARY OF HI-STORM SYSTEM MATERIALS
THERMAL PROPERTY REFERENCES

Material	Emissivity	Conductivity	Density	Heat Capacity
Helium	N/A	Handbook [4.2.2]	Ideal Gas Law	Handbook [4.2.2]
Air	N/A	Handbook [4.2.2]	Ideal Gas Law	Handbook [4.2.2]
Zircaloy	[4.2.3], [4.2.17], [4.2.18], [4.2.7]	NUREG [4.2.6]	Rust [4.2.4]	Rust [4.2.4]
UO_2	Note 1	NUREG [4.2.6]	Rust [4.2.4]	Rust [4.2.4]
Stainless Steel (machined forgings)[4]	Kern [4.2.5]	ASME [4.2.8]	Marks' [4.2.1]	Marks' [4.2.1]
Stainless Steel Plates[5]	ORNL [4.2.11], [4.2.12]	ASME [4.2.8]	Marks' [4.2.1]	Marks' [4.2.1]
Carbon Steel	Kern [4.2.5]	ASME [4.2.8]	Marks' [4.2.1]	Marks' [4.2.1]
Boral	Note 1	Test Data (Note 2)	Test Data (Note 2)	Test Data (Note 2)
Holtite-A	Note 1	[4.2.13]	Not Used	Not Used
Concrete	Note 1	Marks' [4.2.1]	Appendix 1.D	Handbook [4.2.2]
Lead	Note 1	Handbook [4.2.2]	Handbook [4.2.2]	Handbook [4.2.2]
Water	Note 1	ASME [4.2.10]	ASME [4.2.10]	ASME [4.2.10]
METAMIC	Note 1	Test Data [4.2.14], [4.2.15]	Test Data [4.2.14], [4.2.15]	Test Data [4.2.14], [4.2.15]

Note 1: Emissivity not reported as radiation heat dissipation from these surfaces is conservatively neglected.
Note 2: AAR Structures Boral thermophysical test data.

4 Used in the top lid of the MPC.
5 Used in the basket panels, neutron absorber sheathing, MPC shell, and MPC baseplate.

Table 4.2.2

SUMMARY OF HI-STORM SYSTEM MATERIALS
THERMAL CONDUCTIVITY DATA

Material	**At 200°F (Btu/ft-hr-°F)**	**At 450°F (Btu/ft-hr-°F)**	**At 700°F (Btu/ft-hr-°F)**	**At 1000°F (Btu/ft-hr-°F)**
Helium	0.0976	0.1289	0.1575	0.1890
Air*	0.0173	0.0225	0.0272	0.0336
Alloy X	8.4	9.8	11.0	12.4
Carbon Steel	24.4	23.9	22.4	20.0
Concrete**	1.05	1.05	1.05	1.05
Lead	19.4	17.9	16.9	N/A
Water	0.392	0.368	N/A	N/A

* At lower temperatures, Air conductivity is between 0.0139 Btu/ft-hr-°F at 32°F and 0.0176 Btu/ft-hr-°F at 212°F.

** Conservatively assumed to be constant for the entire range of temperatures.

Table 4.2.3

SUMMARY OF FUEL ELEMENT COMPONENTS
THERMAL CONDUCTIVITY DATA

Zircaloy Cladding		**Fuel (UO_2)**	
Temperature (°F)	Conductivity (Btu/ft-hr-°F)	Temperature (°F)	Conductivity (Btu/ft-hr-°F)
392	8.28*	100	3.48
572	8.76	448	3.48
752	9.60	570	3.24
932	10.44	793	2.28*

* Lowest values of conductivity used in the thermal analyses for conservatism.

Table 4.2.4

SUMMARY OF MATERIALS SURFACE EMISSIVITY DATA*

Material	Emissivity
Zircaloy	0.80
Painted surfaces	0.85
Stainless steel (machined forgings)	0.36
Stainless Steel Plates	0.587**
Carbon Steel	0.66

* See Table 4.2.1 for cited references.

** Lowerbound value from the cited references in Table 4.2.1.

Table 4.2.5

DENSITY AND HEAT CAPACITY PROPERTIES SUMMARY*

Material	Density (lbm/ft^3)	Heat Capacity (Btu/lbm-°F)
Helium	(Ideal Gas Law)	1.24
Zircaloy	409	0.0728
Fuel (UO_2)	684	0.056
Carbon steel	489	0.1
Stainless steel	501	0.12
Boral	154.7	0.13
Concrete	140**	0.156
Lead	710	0.031
Water	62.4	0.999
METAMIC	163.4**	0.22**

* See Table 4.2.1 for cited references.

** Lowerbound values reported for conservatism.

Table 4.2.6

GASES VISCOSITY* VARIATION WITH TEMPERATURE

Temperature (°F)	Helium Viscosity (Micropoise)	Temperature (°F)	Air Viscosity (Micropoise)
167.4	220.5	32.0	172.0
200.3	228.2	70.5	182.4
297.4	250.6	260.3	229.4
346.9	261.8	338.4	246.3
463.0	288.7	567.1	293.0
537.8	299.8	701.6	316.7
737.6	338.8	1078.2	377.6
921.2	373.0	-	-
1126.4	409.3	-	-
* Obtained from Rohsenow and Hartnett [4.2.2].			

Table 4.2.7

VARIATION OF NATURAL CONVECTION PROPERTIES
PARAMETER "Z" FOR AIR WITH TEMPERATURE

Temperature (°F)	Z ($ft^{-3}°F^{-1}$)*
40	2.1×10^{6}
140	9.0×10^{5}
240	4.6×10^{5}
340	2.6×10^{5}
440	1.5×10^{5}
* Obtained from Jakob and Hawkins [4.2.9]	

4.3 SPECIFICATIONS FOR COMPONENTS

HI-STORM System materials and components designated as "Important to Safety" (i.e., required to be maintained within their safe operating temperature ranges to ensure their intended function) which warrant special attention are summarized in Table 4.3.1. The neutron shielding ability of Holtite-A neutron shield material used in the HI-TRAC transfer cask is ensured by demonstrating that the material exposure temperatures are maintained below the maximum allowable limit. Long-term integrity of SNF is ensured by the HI-STORM System thermal evaluation which demonstrates that fuel cladding temperatures are maintained below design basis limits. Neutron absorber materials used in MPC baskets for criticality control (made from B_4C and aluminum) are stable in excess of 1000°F[1]. Accordingly 1000°F is conservatively adopted as the short-term temperature limit for neutron absorber materials. The overpack concrete, the primary function of which is shielding, will maintain its structural, thermal and shielding properties provided that American Concrete Institute (ACI) guidance on temperature limits (see Appendix 1.D) is followed.

Compliance to 10CFR72 requires, in part, identification and evaluation of short-term off-normal and severe hypothetical accident conditions. The inherent mechanical characteristics of cask materials and components ensure that no significant functional degradation is possible due to exposure to short-term temperature excursions outside the normal long-term temperature limits. For evaluation of HI-STORM System thermal performance, material temperature limits for long-term normal, short-term operations, and off-normal and accident conditions are provided in Table 4.3.1. In Table 4.3.1, ISG-11 [4.1.4] temperature limits are adopted for Commercial Spent Fuel (CSF). These limits are applicable to all fuel types, burnup levels and cladding materials approved by the NRC for power generation.

4.3.1 Evaluation of Moderate Burnup Fuel

It is recognized that hydrides present in irradiated fuel rods (predominantly circumferentially oriented) dissolve at cladding temperatures above 400°C [4.3.1]. Upon cooling below a threshold temperature (T_p), the hydrides precipitate and reorient to an undesirable (radial) direction if cladding stresses at the hydride precipitation temperature T_p are excessive. For moderate burnup fuel, T_p is conservatively estimated as 350°C [4.3.1]. In a recent study, PNNL has evaluated a number of bounding fuel rods for reorientation under hydride precipitation temperatures for MBF [4.3.1]. The study concludes that hydride reorientation is not credible during short-term operations involving low to moderate burnup fuel (up to 45 GWD/MTU). Accordingly, the higher ISG-11 temperature limit is justified for moderate burnup fuel and is adopted in the HI-STORM FSAR for short-term operations for MBF fueled MPCs (see Table 4.3.1).

---

1 B_4C is a refractory material that is unaffected by high temperature (on the order of 1000°F) and aluminum is solid at temperatures in excess of 1000°F.

Table 4.3.1

HI-STORM SYSTEM MATERIAL TEMPERATURE LIMITS[2]

Material	**Normal Long-Term Temperature Limits [°F]**	**Short-Term Temperature Limits [°F]**
CSF cladding (zirconium alloys and stainless steel)	752	Short-Term Operations 752 (HBF) 1058 (MBF) Off-Normal and Accident 1058
Neutron Absorber	800	1000
Holtite-A[3]	N/A (Not Used)	350 (Short Term Operations)
Concrete[4]	300	350
Water	N/A	307[5] (Short Term Operations) N/A (Off-Normal and Accident)

2 This table specifies temperature limits for non-ASME Code materials. Temperature limits of ASME Code materials (structural steels) are specified in Table 2.2.3.
3 See Chapter 1, Appendix 1.B.
4 These values are applicable for concrete in the overpack body, overpack lid and overpack pedestal. As stated in Chapter 1 (Appendix 1.D), these limits are compared to the through-thickness section average temperature.
5 Saturation temperature at HI-TRAC water jacket design pressure specified in Table 2.2.1.

4.4 THERMAL EVALUATION FOR NORMAL CONDITIONS OF STORAGE

The HI-STORM System (i.e., HI-STORM overpack, HI-TRAC transfer cask and MPC) thermal evaluation is performed in accordance with the guidelines of NUREG-1536 [4.4.1] and ISG-11 [4.1.4]. To ensure a high level of confidence in the thermal evaluation, 3-Dimensional models of the MPC, HI-STORM overpack and HI-TRAC transfer cask are constructed to evaluate fuel integrity under normal (long-term storage), off-normal and accident conditions and in the HI-TRAC transfer cask under short-term operation and hypothetical accidents. The thermal models incorporate an array of conservatisms to ensure robustly bounding thermal solutions. The principal features of these models are described in this section for HI-STORM and Section 4.5 for HI-TRAC. Thermal analysis results for the long-term storage scenarios are obtained and reported in this section.

4.4.1 Overview of the Thermal Model

The MPC basket design consists of four distinct geometries to hold 24 or 32 PWR, or 68 BWR fuel assemblies. The basket is a matrix of interconnected square compartments designed to hold the fuel assemblies in a vertical position under long term storage conditions. The basket is a honeycomb structure of stainless steel (Alloy X) plates with full-length edge-welded intersections to form an integral basket configuration. All individual cell walls, except outer periphery cell walls in the MPC-68 and MPC-32, are provided with neutron absorber plates sandwiched between the box wall and a stainless steel sheathing plate over the full length of the active fuel region. The neutron absorber plates used in all MPCs are made of an aluminum-based, boron carbide-containing material to provide criticality control, while maximizing heat conduction capabilities.

Thermal analysis of the HI-STORM System is performed for an array of limiting heat load scenarios defined in Chapter 2 for uniform and regionalized fuel loading (wherein each fuel assembly in a region is assumed to be generating heat at the maximum permissible rate). While the assumption of limiting heat generation in each storage cell imputes a certain symmetry to the cask thermal problem, it grossly overstates the total heat duty of the system in most cases because it is unlikely that any basket would be loaded with fuel emitting heat at their limiting values (see for example a fuel loading scenario discussed in Section 2.1). The principal attributes of the thermal model are described in the following:

i. While the rate of heat conduction through metals is a relatively weak function of temperature, radiation heat exchange is a highly nonlinear function of surface temperatures.

ii. Heat generation in the MPC is axially non-uniform due to non-uniform axial burnup profiles in the fuel assemblies.

iii. Inasmuch as the transfer of heat occurs from inside the basket region to the outside, the temperature field in the MPC is spatially distributed with the maximum values reached in the central core region.

4.4.1.1 Description of the 3-D Thermal Model

i. Introduction

The interior of the MPC is a 3-D array of square shaped cells inside an irregularly shaped basket outline confined inside the cylindrical space of the MPC cavity. To ensure an adequate representation of these features, a 3-D geometric model of the MPC is constructed using the FLUENT CFD code pre-processor [4.1.2]. Other than representing the composite cell walls (made up of Alloy X panels, neutron absorber panels and Alloy X sheathing) by a homogeneous panel with equivalent orthotropic (thru-thickness and parallel plates direction) thermal conductivities, the 3-D model requires no idealizations of the fuel basket structure. Further, since it is impractical to model every fuel rod in every stored fuel assembly explicitly, the cross section bounded by the inside of the storage cell (inside of the fuel channel in the case of BWR MPCs), which surrounds the assemblage of fuel rods and the interstitial helium gas (also called the "rodded region"), is replaced with an "equivalent" square homogeneous section characterized by an effective thermal conductivity. Homogenization of the storage cell cross-section is illustrated in Figure 4.4.1. As the effective conductivity of the rodded region includes radiation heat transfer the conductivities will be a strong function of temperature because radiation heat transfer (a major component of the heat transport between the fuel rods and the surrounding basket cell metal) rises as the fourth power of absolute temperature. Therefore, in effect, the effective conductivity of the equivalent square section (depending on the coincident temperature) will be different throughout the basket. For thermal-hydraulic simulation, each fuel assembly in its storage cell is represented by an equivalent porous medium. For BWR fuel, the presence of the fuel channel divides the storage cell space into two distinct axial flow regions, namely, the in-channel (rodded) region and the square prismatic annulus region (in the case of PWR fuel this modeling complication does not exist).

ii. Details of the 3-D Model

The 3-D model implemented to analyze the HI-STORM system has the following key attributes:

a. As mentioned above, the composite walls in the fuel basket consisting of the Alloy X structural panels, the aluminum-based neutron absorber, and the Alloy X sheathing, are represented by an orthotropic homogeneous panel of equivalent thermal conductivity in the three principal directions. The in-plane and thru-thickness thermal conductivities of the composite wall are computed using a standard procedure for such shapes with certain conservatisms, as described below.

   During fabrication, a uniform normal pressure is applied to each "Box Wall - Neutron Absorber - Sheathing" sandwich in the assembly fixture during welding of the sheathing periphery on the box wall. This ensures adequate surface-to-surface contact between the neutron absorber and the adjacent Alloy X surfaces. The mean coefficient of linear expansion of the neutron absorber is higher than the thermal expansion coefficients of the basket and sheathing materials. Consequently, basket heat-up from the stored SNF will further ensure a tight fit of the neutron absorber plate in the sheathing-to-box pocket. Nevertheless the possible presence of small microscopic gaps due to less than perfect

surface-to-surface contact requires consideration of an interfacial contact resistance between the neutron absorber and box-sheathing surfaces. In the thermal analysis a 2 mil neutron absorber to pocket gap has been used. This is conservative as the sandwich is engineered to ensure an essentially no-gap fitup and assembly of the neutron-absorber panels. Furthermore, no credit is taken for radiative heat exchange across the neutron absorber to sheathing or neutron absorber to box wall gaps.

The heat conduction properties of the composite "Box Wall - Neutron Absorber - Sheathing" sandwich panels in the two principal basket cross sectional directions (i.e., thru-thickness and parallel plates direction) are unequal. In the thru-thickness direction, heat is transported across layers of sheathing, helium-gap, neutron absorber and box wall resistances that are essentially in series. Heat conduction in the parallel plates direction, in contrast, is through an array of essentially parallel resistances comprised of these several layers listed above. In this manner the composite walls of the fuel basket storage cells are replaced with a solid wall of equivalent through thickness and parallel plates direction conductivities. Table 4.4.1 provides the values of the conductivities as a function of temperature for the different MPC types.

b. In the case of a BWR CSF, the fuel bundle and the small surrounding spaces inside the fuel "channel" are replaced by an equivalent porous media having the flow impedance properties computed using a conservatively articulated 3-D CFD model [4.4.2]. The space between the BWR fuel channel and the storage cell is represented as an open flow annulus. The fuel channel is also explicitly modeled. The porous medium within the channel space is also referred to as the "rodded region". The fuel assembly is assumed to be positioned coaxially with respect to its storage cell. The 3-D model of an MPC-68 storage cell occupied with channeled BWR fuel is shown in Figure 4.4.4.

   In the case of the PWR CSF, the porous medium extends to the entire cross-section of the storage cell. As described in [4.4.2], the CFD model for both the BWR and PWR case is prepared for the Design Basis fuel in comprehensive detail, which includes grid straps, BWR water rods and PWR guide and instrument tubes (assumed to be plugged for conservatism).

c. Every MPC fuel storage cell is assumed to be occupied by design basis PWR or BWR fuel assemblies specified in Chapter 2 (Table 2.1.5). The in-plane thermal conductivity of the design basis fuel assemblies are obtained using ANSYS [4.1.1] finite element models of an array of fuel rods enclosed by a square box. Radiation heat transfer from solid surfaces (cladding and box walls) are enabled in these models. Using these models the effective conduction-radiation conductivities are obtained and reported in Table 4.4.2. For heat transfer in the axial direction an area weighted mean of cladding and helium conductivities are computed (see Table 4.4.2). Axial conduction heat transfer in the fuel pellets and radiation heat dissipation in the axial direction are conservatively ignored. Thus, the thermal conductivity of the rodded region, like the porous media simulation for helium flow, is represented by a 3-D continuum having effective planar and axial conductivities.

d. The internals of the MPC, including the basket cross section, bottom mouse holes, top plenum, and circumferentially irregular downcomer are modeled explicitly. For simplicity, the mouse holes are modeled as rectangular openings with understated flow area.

e. The inlet and outlet vents in the HI-STORM overpack are modeled explicitly to incorporate any effects of non-axisymmetry of inlet air passages on the system's thermal performance.

f. The air flow in the HI-STORM/MPC annulus is simulated by a k-ω turbulence model with the transitional option enabled.

The 3-D model described above is illustrated in the cross section for the MPC-68 in Figure 4.4.3. A closeup of the fuel cell spaces which explicitly include the channel-to-cell gap in the 3-D model is shown in Figure 4.4.4. The principal 3-D modeling conservatisms are listed below:

1) The storage cell spaces are loaded with design basis fuel having the highest axial flow resistance (See Table 2.1.5).
2) Each storage cell is generating heat at its limiting value under uniform or regionalized storage scenarios as defined in Chapter 2, Section 2.1.
3) Axial dissipation of heat by the fuel pellets is neglected.
4) Axial dissipation of heat by radiation in the fuel bundle is neglected.
5) The fuel assembly channel length for BWR fuel is overstated.
6) The most severe environmental factors for long-term normal storage - ambient temperature of 80°F and 10CFR71 insolation levels - were coincidentally imposed on the system.
7) The absorbtivity of the external surfaces of the HI-STORM is conservatively assumed to be unity.
8) To understate MPC internal convection heat transfer, the helium pressure is understated.
9) No credit is taken for contact between fuel assemblies and the MPC basket wall or between the MPC basket and the basket supports.
10) Heat dissipation by fuel basket peripheral supports is neglected.
11) Fuel basket and MPC shell emissivities are understated (see Table 4.2.4).
12) The k-ω model used for simulating the HI-STORM annulus flow yields uniformly conservative results [4.1.6].

The effect of crud resistance on fuel cladding surfaces has been evaluated and found to be negligible. The evaluation assumes a thick crud layer (130 μm) with a bounding low conductivity (conductivity of helium). The crud resistance increases the clad temperature by a very small amount (~0.1°F). Accordingly this effect is neglected in the thermal evaluations.

4.4.1.2 Fuel Assembly 3-Zone Flow Resistance Model

The HI-STORM System is evaluated for storage of bounding PWR (W-17x17) and BWR (GE-10x10) fuel assemblies. During fuel storage helium enters the MPC fuel cells from the bottom

plenum and flows upwards through the open spaces in the fuel storage cells and exits in the top plenum. Because of the low flow velocities the helium flow in the fuel storage cells and MPC spaces is in the deep laminar regime (Re < 100). The bottom and top plenums are essentially open spaces engineered in the fuel basket ends to facilitate helium circulation. In the case of BWR fuel storage, a channel enveloping the fuel bundle divides the flow in two parallel paths. One flow path is through the in-channel or rodded region of the storage cell and the other flow path is in the square annulus area outside the channel. In the global thermal modeling of the HI-STORM System the following approach is adopted:

(i) In BWR fueled MPCs an explicit channel-to-cell gap is modeled.
(ii) The fuel assembly enclosed in a square envelope (fuel channel for BWR fuel or fuel storage cell for PWR fuel) is replaced by porous media with equivalent flow resistance.

The above modeling approach is illustrated in Figure 4.4.4.

In the FLUENT program, porous media flow resistance is modeled as follows:

$$\Delta P = D\mu VL \qquad \text{(Eq. 1)}$$

where ΔP is the hydraulic pressure loss, D is the flow resistance coefficient, μ is the fluid viscosity, V is the superficial fluid velocity and L is the porous media length. In the HI-STORM thermal models the fuel storage cell length between the bottom and top plenums[1] is replaced by porous media. As discussed below the porous media length is partitioned in three zones with discrete flow resistances.

To characterize the flow resistance of fuel assemblies inside square envelopes (fuel channel for BWR fuel or fuel storage cell for PWR fuel) 3D models of W-17x17 and GE-10x10 fuel assemblies are constructed using the FLUENT CFD program. These models are embedded with several pessimistic assumptions to overstate flow resistance. These are:

(a) Water rods (BWR fuel) and guide tubes (PWR fuel) are assumed to be completely blocked
(b) Fuel rods assumed to be full length
(c) Channel length (BWR fuel) overstated
(d) Bounding grid thickness used
(e) Bottom fittings resistance overstated
(f) Bottom nozzle lateral flow holes (BWR fuel) assumed to be blocked

Using the 3D fuel assembly models flow solutions under an impressed pressure differential between the two extremities of the fuel storage cell are computed at reference conditions (7 atmosphere

1 These are the mousehole openings at the ends of the fuel basket to facilitate helium circulation. The mouseholes are explicitly included in the 3D thermal models with an understated flow area.

absolute pressure and 450°F temperature). The results of the 3D flow solutions are post-processed as described next and equivalent porous media flow resistances obtained.

Because of the narrow flow passages in the bare rods and gridded regions of the fuel assembly the flow resistance of the fueled length to axial helium flow is greater than the flow resistance from the fuel assembly ends (bottom nozzle, top fitting, handle etc.). This physical fact is duly recognized by defining three distinct axial zones as follows:

Zone 1: Length below the active fuel region
Zone 2: Active fuel region
Zone 3: Length above the active fuel region

In the 3-Zone flow resistance modeling, the flow resistance of each zone is characterized by post-processing the 3D fuel flow model solutions. For this purpose two approaches to flow resistance characterization are adopted. The first approach is the pressure drop method. This method is suitable when a zone is characterized by irregular geometries and the objective is to obtain a lumped resistance to duplicate the pressure drop. The second method is the shear stress method, which is suitable for flow zones characterized by regular geometries. For the 3-Zone flow resistance modeling the pressure drop method is adopted for the inactive regions (Zone 1 and Zone 3). The flow resistance coefficients are computed by post-processing the fuel assemblies 3D model flow solutions as follows:

Step 1: Obtain the helium volumetric flow Q under the impressed pressure differential.
Step 2: Compute helium superficial velocity, V = Q/A where A is the square envelope cross-sectional area.
Step 3: Obtain the individual Zone 1 and Zone 3 lengths (L_1 and L_3) and pressure drops (ΔP_1 and ΔP_3) from the FLUENT solutions.
Step 4: Compute Zone 1 and Zone 3 resistance coefficients D_1 and D_3 using Eq. 1, V, L_1, L_3, ΔP_1 and ΔP_3 from above steps.

The shear stress method is suitable for the active fuel region (Zone 2) as this region is characterized by an ordered array of entities (rods and grids). This method uses area averaged wall shear stresses post-processed from the active region (Zone 2) of the fuel assembly. Using hydraulic flow principles the wall shear stresses are mapped to flow resistance coefficients. To account for geometric discontinuities the active fuel region is sliced in a suitable number of constant geometry (bare rods and grids) sub-regions. Based on the fuel bundle layout, a total of 17 slices are identified for GE-10x10 fuel and 20 slices for W-17x17 fuel. In each sub-region an area averaged shear stress over all wetted surfaces (fuel rods, non-fuel rods, square envelope and grids) is post-processed and flow resistance coefficients of each slice are computed. The flow resistance of Zone 2 is obtained by computing the length-weighted average of the slice resistance coefficients.

4.4.2 [deleted]

4.4.3 Test Model

The HI-STORM thermal analysis is performed on the FLUENT [4.1.2] Computational Fluid Dynamics (CFD) program. To ensure a high degree of confidence in the HI-STORM thermal evaluations, the FLUENT code is benchmarked using data from tests conducted with casks loaded with irradiated SNF ([4.1.3],[4.1.7]). The benchmark work is archived in QA validated Holtec reports ([4.1.5],[4.1.6]).These evaluations show that the FLUENT solutions are conservative in all cases. In view of these considerations, additional experimental verification of the thermal design is not necessary.

4.4.4 Maximum and Minimum Temperatures

4.4.4.1 Maximum Temperatures

The 3-D model from the previous subsection is used to determine temperature distributions under long-term normal storage conditions for an array of cases covering PWR and BWR fuel storage in uniform and regionalized loading configurations. For this purpose one bounding MPC design in each of the two fuel classes – MPC-68 for BWR and MPC-32 for PWR – are analyzed and results obtained and summarized in this subsection. For a bounding evaluation the MPCs are assumed to be emplaced in a limiting overpack (HI-STORM 100S Version B).

The HI-STORM 100S Version B is the limiting overpack by virtue of the inlet and outlet vents design. Compared to two other overpack designs (i.e., HI-STORM 100 and HI-STORM 100S), the HI-STORM 100S Version B has smaller inlet and outlet vents. Thus Version B vent airflow resistances are bounding. Also, the HI-STORM 100S Version B is the shortest of the overpacks. This reduces the chimney height which minimizes the driving head for air flow. Because the HI-STORM 100S Version B will have the least cooling air flow, it will yield bounding results.

A cross-reference of HI-STORM thermal analyses is provided in Table 4.4.5. Under regionalized loading, an array of runs covering a range of regionalized storage configurations specified in Chapter 2 (X=0.5 to X=3) are analyzed. The results are graphed in Figures 4.4.6 and 4.4.7 for PWR and BWR fuel storage respectively. Based on this array of runs the fuel storage condition corresponding to X = 0.5 is determined to be limiting for both PWR and BWR MPCs. Accordingly HI-STORM MPC and overpack temperatures are reported for this storage condition in Tables 4.4.6 and 4.4.7.

It should be noted that the 3-D FLUENT cask model incorporates the effective conductivity of the fuel assembly submodell. Therefore the FLUENT models report the peak temperature in the fuel storage cells Thus, as the fuel assembly models include the fuel pellets, the FLUENT calculated peak temperatures are actually peak pellet centerline temperatures which bound the peak cladding temperatures with a margin.

The following observations can be derived by inspecting the temperature field obtained from the thermal models:

- The fuel cladding temperatures are below the regulatory limit (ISG-11 [4.1.4]) under all storage scenarios (uniform and regionalized) in all MPCs.
- The maximum temperature of the basket structural materials are within their design limits.
- The maximum temperature of the neutron absorbers are below their design limits.
- The maximum temperatures of the MPC pressure boundary materials are below their design limits.
- The maximum temperatures of concrete is within the guidance of the governing ACI Code (see Table 4.3.1).

The above observations lead us to conclude that the temperature field in the HI-STORM System with a loaded MPC containing heat emitting SNF complies with all regulatory temperature limits. In other words, the thermal environment in the HI-STORM System is in compliance with Chapter 2 Design Criteria.

4.4.4.2 Minimum Temperatures

In Table 2.2.2 of this report, the minimum ambient temperature condition for the HI-STORM storage overpack and MPC is specified to be -40°F. If, conservatively, a zero decay heat load with no solar input is applied to the stored fuel assemblies, then every component of the system at steady state would be at a temperature of -40°F. Low service temperature (-40°F) evaluation of the HI-STORM is provided in Chapter 3. All HI-STORM storage overpack and MPC materials of construction will satisfactorily perform their intended function in the storage mode at this minimum temperature condition.

4.4.4.3 Effects of Elevation

The reduced ambient pressure at site elevations significantly above the sea level will act to reduce the ventilation air mass flow, resulting in a net elevation of the peak cladding temperature. However, the ambient temperature (i.e., temperature of the feed air entering the overpack) also drops with the increase in elevation. Because the peak cladding temperature also depends on the feed air temperature (the effect is one-for-one within a small range, i.e., 1°F drop in the feed air temperature results in ~1°F drop in the peak cladding temperature), the adverse ambient pressure effect of increased elevation is partially offset by the ambient air temperature decrease. The table below illustrates the variation of air pressure and corresponding ambient temperature as a function of elevation.

Elevation (ft)	Pressure (psia)	Ambient Temperature Reduction versus Sea Level
Sea Level (0)	14.70	0°F
2000	13.66	7.1°F
4000	12.69	14.3°F

A survey of the elevation of nuclear plants in the U.S. shows that nuclear plants are situated near about sea level or elevated slightly (~1000 ft). The effect of the elevation on peak fuel cladding temperatures is evaluated by performing calculations for a HI-STORM 100 System situated at an elevation of 1500 feet. At this elevation the ambient temperature would decrease by approximately 5°F (See Table above). The peak cladding temperatures are calculated for a bounding configuration (non-uniform storage at X = 0.5), and conservatively assuming no reduction in ambient temperature using the 3D model described in Subsection 4.4.1.1 and compared to the sea level conditions. The results are given in the following table.

MPC Design	PCT at Sea Level	PCT at 1500 feet
MPC-68 BWR	711.4°F	723.8°F
MPC-32 PWR	697.1°F	718.2°F

These results show that the PCT, including the effects of site elevation, continues to be well below the regulatory cladding temperature limit of 752°F. In light of the above evaluation, it is not necessary to place any ISFSI elevation constraints for HI-STORM deployment at elevations up to 1500 feet. If, however, an ISFSI is sited at an elevation greater than 1500 feet, the effect of altitude on the PCT shall be quantified as part of the 10 CFR 72.212 evaluation for the site using the site ambient conditions.

4.4.5 Maximum Internal Pressure

4.4.5.1 MPC Helium Backfill Pressure

[TM1]For design basis heat load, the helium backfill shall be sufficient to produce the required operating pressure of 7 atmospheres (absolute) during normal storage at reference conditions (See Table 4.0.1). Thermal analyses performed on the different MPC designs indicate that this operating pressure requires a certain helium backfill pressure specified at a reference temperature (70°F). The minimum backfill pressure to attain this operating pressure for each MPC type is provided in Table 4.4.11. An upper limit on the helium backfill pressure corresponds to the design pressure of the MPC vessel (Table 2.2.1). The upper limit on the backfill pressure is also reported in Table 4.4.11. To bound the minimum and maximum backfill pressures listed in Table 4.4.11 with margin, a helium backfill specification is set forth in Table 4.4.12. These values support the technical specification of the system for the design basis heat load of the MPC.

In addition the technical specifications allow for using a wider range on the backfill pressure if the heat load of the MPC is less than 28.74 kW. The minimum of this range corresponds to an operating

pressure of 5 atm. The heat loads for this condition are provided in Table 4.5.7 and Table 4.5.8. If the MPC is loaded such that either Table 4.5.7 or 4.5.8 are satisfied, the lower pressure range in the technical specifications may be used.

It is conservative to backfill the MPC to the higher pressure range regardless of MPC heat load.

Two methods are available for ensuring that the appropriate quantity of helium has been placed in an MPC:

i. By pressure measurement
ii. By measurement of helium backfill volume (in standard cubic feet)

The direct pressure measurement approach is more convenient if FHD is used to dry the MPC cavity. In this case, a certain quantity of helium is already in the MPC. Because the helium is mixed inside the MPC during the FHD operation, the temperature of the helium gas at the exit of the MPC, along with the pressure provides a reliable means to compute the inventory of helium. A shortfall or excess of helium is adjusted by a calculated raising or lowering of the MPC pressure such that the MPC backfill pressure is within the specifications.

When vacuum drying is used to dry the MPC cavity it is more convenient to fill the MPC by introducing a known quantity of helium by measuring the quantity of helium introduced using a calibrated mass flow meter or other measuring apparatus. The required quantity of helium is computed by the product of net free volume and helium specific volume at the reference temperature (70°F) and a target pressure that lies in the mid-range of the specifications.

The net free volume of the MPC is obtained by subtracting B from A, where

A = MPC cavity volume in the absence of fuel and any DFC and/or NFH as computed from nominal design dimensions.

B = Total volume of the fuel and any DFC and/or NFHas computed from nominal design dimensions

4.4.5.2 MPC Pressure Calculations

The MPC pressure calculations are performed using the reference conditions in Table 4.0.1 since this condition always results in the highest pressure in the MPC and bounds the allowed pressure range for the lower MPC heat load as described above.

During normal storage, the gas temperature within the MPC rises to its maximum operating basis temperature. The gas pressure inside the MPC will also increase with rising temperature to its maximum operating pressure. The pressure rise is determined using the ideal gas law.

Table 4.4.8 presents a summary of the minimum MPC free volumes determined for each MPC type (MPC-24, MPC-68, MPC-32, and MPC-24E). The MPC maximum gas pressure is computed for a postulated release of fission product gases from fuel rods into this free space. For these scenarios, the amounts of each of the release gas constituents in the MPC cavity are summed and the resulting total pressures determined from the ideal gas law. Based on fission gases release fractions in NUREG-1536 [4.4.1] and the net free volume and initial fill gas pressure of the fuel rods, maximum gas pressures with 1% (normal), 10% (off-normal) and 100% (accident condition) rod rupture are calculated and provided in Table 4.4.9. The maximum computed gas pressures reported in Table 4.4.9 are all below the MPC internal design pressures for normal, off-normal and accident conditions specified in Table 2.2.1.

Evaluation of Non-Fuel Hardware

The inclusion of PWR non-fuel hardware (BPRA control elements and thimble plugs) to the PWR baskets influences the MPC internal pressure through two distinct effects. The presence of non-fuel hardware increases the effective basket conductivity, thus enhancing heat dissipation and lowering fuel temperatures as well as the temperature of the gas filling the space between fuel rods. The gas volume displaced by the mass of non-fuel hardware lowers the cavity free volume. These two effects, namely, temperature lowering and free volume reduction, have opposing influence on the MPC cavity pressure. The first effect lowers gas pressure while the second effect raises it. In the HI-STORM thermal analysis, the computed temperature field (with non-fuel hardware excluded) has been determined to provide a conservatively bounding temperature field for the PWR baskets (MPC-24, MPC-24E, and MPC-32). The MPC cavity free space is computed based on volume displacement by the heaviest fuel (bounding weight) with non-fuel hardware included. This approach ensures conservative bounding pressures.

During in-core irradiation of BPRAs, neutron capture by the B-10 isotope in the neutron absorbing material produces helium. Two different forms of the neutron absorbing material are used in BPRAs: Borosilicate glass and B_4C in a refractory solid matrix (At_2O_3). Borosilicate glass (primarily a constituent of Westinghouse BPRAs) is used in the shape of hollow pyrex glass tubes sealed within steel rods and supported on the inside by a thin-walled steel liner. To accommodate helium diffusion from the glass rod into the rod internal space, a relatively high void volume (~40%) is engineered in this type of rod design. The rod internal pressure is thus designed to remain below reactor operation conditions (2,300 psia and approximately 600°F coolant temperature). The B_4C- Al_2O_3 neutron absorber material is principally used in B&W and CE fuel BPRA designs. The relatively low temperature of the poison material in BPRA rods (relative to fuel pellets) favor the entrapment of helium atoms in the solid matrix.

Several BPRA designs are used in PWR fuel that differ in the number, diameter, and length of poison rods. The older Westinghouse fuel (W-14x14 and W-15x15) has used 6, 12, 16, and 20 rods per assembly BPRAs and the later (W-17x17) fuel uses up to 24 rods per BPRA. The BPRA rods in the older fuel are much larger than the later fuel and, therefore, the B-10 isotope inventory in the 20-rod BPRAs bounds the newer W-17x17 fuel. Based on bounding BPRA rods internal pressure, a large hypothetical quantity of helium (7.2 g-moles/BPRA) is assumed to be available for release into

the MPC cavity from each fuel assembly in the PWR baskets. The MPC cavity pressures (including helium from BPRAs) are summarized in Table 4.4.9.

4.4.6 Engineered Clearances to Eliminate Thermal Interferences

Thermal stress in a structural component is the resultant sum of two factors, namely: (i) restraint of free end expansion and (ii) non-uniform temperature distribution. To minimize thermal stresses in load bearing members, the HI-STORM System is engineered with adequate gaps to permit free thermal expansion of the fuel basket and MPC in axial and radial directions. In this subsection, differential thermal expansion calculations are performed to demonstrate that engineered gaps in the HI-STORM System are adequate to accommodate thermal expansion of the fuel basket and MPC.

The HI-STORM System is engineered with gaps for the fuel basket and MPC to expand thermally without restraint of free end expansion. Differential thermal expansion of the following gaps are evaluated:

a. Fuel Basket-to-MPC Radial Gap
b. Fuel Basket to MPC Axial Gap
c. MPC-to-Overpack Radial Gap
d. MPC-to-Overpack Axial Gap

To demonstrate that the fuel basket and MPC are free to expand without restraint, it is required to show that differential thermal expansion from fuel heatup is less than the as-built gaps that exist in the HI-STORM System. For this purpose a suitably bounding temperature profile (T(r)) for the fuel basket is established in Figure 4.4.5 wherein the center temperature (TC) is set at the limit (752°F) for fuel cladding (conservatively bounding assumption) and the basket periphery (TP) conservatively postulated at an upperbound of 610°F (see Table 4.4.6 for the maximum fuel and basket periphery temperatures). To maximize the fuel basket differential thermal expansion, the basket periphery-to-MPC shell temperature difference is conservatively maximized ($\Delta T = 175°F$). From the bounding temperature profile T(r) and ΔT, the mean fuel basket temperature (T1) and MPC shell temperature (T2) are computed as follows:

$$T1 = \frac{\int_0^1 rT(r)dr}{\int_0^1 rdr} = 676°F$$

$$T2 = TP - \Delta T = 425°F$$

The differential radial growth of the fuel basket (Y1) from an initial reference temperature (To = 70°F) is computed as:

$$Y1 = R \times [A1 \times (T1 - To) - A2 \times (T2 - To)]$$

where:

R = Basket radius (conservatively assumed to be the MPC radius)
A1, A2 = Coefficients of thermal expansion for fuel basket and MPC shell at T1 and T2 respectively for Alloy X (Chapter 1 and Table 3.3.1)

For computing the relative axial growth of the fuel basket in the MPC, bounding temperatures for the fuel basket (TC) and MPC shell temperature T2 utilized above are adopted. The differential expansion is computed by a formula similar to the one for radial growth after replacing R with basket height (H), which is conservatively assumed to be that of the MPC cavity.

For computing the radial and axial MPC-to-overpack differential expansions, the MPC shell is postulated at its design temperature (Chapter 2, Table 2.2.3) and thermal expansion of the overpack is ignored. Even with the conservative computation of the differential expansions in the manner of the foregoing, it is evident from the data compiled in Table 4.4.10 that the differential expansions are a fraction of their respective gaps.

4.4.7 Evaluation of System Performance for Normal Conditions of Storage

The HI-STORM System thermal analysis is based on a detailed and complete heat transfer model that conservatively accounts for all modes of heat transfer in various portions of the MPC and overpack. The thermal model incorporates conservative features that render the results for long-term storage to be extremely conservative.

Temperature distribution results obtained from this highly conservative thermal model show that the maximum fuel cladding temperature limits are met with adequate margins. Expected margins during normal storage will be much greater due to the conservative assumptions incorporated in the analysis. The long-term impact of decay heat induced temperature levels on the HI-STORM System structural and neutron shielding materials is considered to be negligible. The maximum local MPC basket temperature level is below the recommended limits for structural materials in terms of susceptibility to stress, corrosion and creep-induced degradation. Furthermore, stresses induced due to imposed temperature gradients are within Code limits (See Structural Evaluation Chapter 3). Therefore, it is concluded that the HI-STORM System thermal design is in compliance with 10CFR72 requirements.

Table 4.4.1

EFFECTIVE CONDUCTIVITY OF THE COMPOSITE FUEL BASKET WALLS
(Btu/hr-ft-°F)

	MPC-32		MPC-24/MPC-24E*		MPC-68	
Temperature (°F)	Thru-Thickness Direction	Parallel Plates Direction	Thru-Thickness Direction	Parallel Plates Direction	Thru-Thickness Direction	Parallel Plates Direction
200	6.000	14.65	5.676 4.800**	13.85 11.17**	5.544	12.06
450	7.260	16.12	6.864 5.808**	15.32 12.54**	6.708	13.45
700	8.316	17.20	7.884 6.672**	16.44 13.62**	7.680	14.52

* Lowerbound values reported.
** Effective conductivities of basket peripheral panels.

Table 4.4.2

LIMITING EFFECTIVE CONDUCTIVITIES OF THE RODDED REGION
(Btu/hr-ft-°F)

	PWR Fuel		BWR FUEL	
Temperature (°F)	Planar	Axial	Planar	Axial
200	0.257	0.753	0.282	0.897
450	0.406	0.833	0.425	0.988
700	0.604	0.934	0.606	1.104

Table 4.4.3

[deleted]

Table 4.4.4

[deleted]

Table 4.4.5

MATRIX OF HI-STORM SYSTEM THERMAL EVALUATIONS

Scenario	Description	Ultimate Heat Sink	Analysis Type	Principal Input Parameters	Results in FSAR Subsection
1	Long Term Normal	Ambient	SS	N_T, Q_D, ST, SC, I_O	4.4.4
2	Off-Normal Environment	Ambient	SS(B)	O_T, Q_D, ST, SC, I_O	4.6.1
3	Extreme Environment	Ambient	SS(B)	E_T, Q_D, ST, SC, I_O	4.6.2
4	Partial Ducts Blockage	Ambient	SS(B)	N_T, Q_D, ST, SC, $I_{1/2}$	4.6.1
5	All Inlets Ducts Blocked	Overpack	TA	N_T, Q_D, ST, SC, I_C	4.6.2
6	Fire Accident	Overpack	TA	Q_D, F	4.6.2
7	Burial Under Debris	Overpack	AH	Q_D	4.6.2

Legend:

N_T - Maximum Annual Average (Normal) Temperature (80°F)
O_T - Off-Normal Temperature (100°F)
E_T - Extreme Hot Temperature (125°F)
Q_D - Design Basis Maximum Heat Load
SS - Steady State
SS(B) - Bounding Steady State
TA - Transient Analysis
AH - Adiabatic Heating

I_O - All Inlet Ducts Open
$I_{1/2}$ - Half of Inlet Ducts Open
I_C - All Inlet Ducts Closed

ST - Insolation Heating (Top)
SC - Insolation Heating (Curved)
F - Fire Heating (1475°F)

Table 4.4.6

MAXIMUM MPC TEMPERATURES FOR LONG-TERM NORMAL STORAGE CONDITION[2]

Component	Temperature, °F	
	MPC-32	MPC-68
Fuel Cladding	**711**	697
MPC Basket	**708**	692
Basket Periphery	**604**	566
MPC Shell	**469**	452

Table 4.4.7

BOUNDING HI-STORM OVERPACK TEMPERATURES FOR LONG-TERM NORMAL STORAGE[3]

Component	Local Section Temperature[4], °F
Inner shell	322
Outer shell	174
Lid bottom plate	302
Lid top plate	190
Overpack Body Concrete	248
Overpack Lid Concrete	246
Area Averaged Air outlet[5]	235

2 The temperatures reported in this table for the bounding fuel storage configuration (regionalized storage at X = 0.5) are below the design temperatures specified in Chapter 2, Table 2.2.3. Results of the bounding canister (MPC-32) are highlighted in bold.

3 The temperatures reported in this table (all for MPC-32 at X = 0.5) are below the design temperatures specified in Chapter 2, Table 2.2.3.

4 Section temperature is defined as the through-thickness average temperature.

5 Reported herein for the option of temperature measurement surveillance of outlet ducts air temperature as set forth in the Technical Specifications.

Table 4.4.8

SUMMARY OF MPC FREE VOLUME CALCULATIONS

Item	Volume (MPC-24) [ft^3]	Volume (MPC-24E) [ft^3]	Volume (MPC-32) [ft^3]	Volume (MPC-68) [ft^3]
Cavity Volume	367.9	367.9	367.9	367.3
Basket Metal Volume	44.3	51.4	24.9	34.8
Bounding Fuel Assemblies Volume	78.8	78.8	105.0	93.0
Basket Supports and Fuel Spacers Volume	6.1	6.1	9.0	11.3
Net Free Volume*	238.7 (6,759 liters)	231.6 (6,558 liters)	229 (6,484 liters)	228.2 (6,462 liters)

* Net free volumes are obtained by subtracting basket, fuel, supports and spacers metal volume from cavity volume. The free volumes used for MPC internal pressure calculations are conservatively understated.

Table 4.4.9

SUMMARY OF MPC INTERNAL PRESSURES UNDER LONG-TERM STORAGE*

Condition	MPC-24*** (psig)	MPC-24E*** (psig)	MPC-32 (psig)	MPC-68 (psig)
Initial backfill** (at 70°F)	48.5	48.5	48.5	48.5
Normal:				
intact rods	99.0	99.0	99.0	96.8
1% rods rupture	100.0	99.7	99.7	97.2
Off-Normal (10% rods rupture)	106.0	106.2	108.7	101.2
Accident (100% rods rupture)	169.3	171.5	196.4	141.1

* Per NUREG-1536, pressure analyses with ruptured fuel rods (including BPRA rods for PWR fuel) is performed with release of 100% of the ruptured fuel rod fill gas and 30% of the significant radioactive gaseous fission products.

** Conservatively assumed at the Tech. Spec. maximum value (See Table 4.4.12).

*** Pressure calculations use the bounding MPC-32 temperature field.

Table 4.4.10

SUMMARY OF HI-STORM DIFFERENTIAL THERMAL EXPANSIONS

Gap Description	Cold Gap U (in)	Differential Expansion V (in)	Is Free Expansion Criterion Satisfied (i.e., U > V)
Fuel Basket-to-MPC Radial Gap	0.1875	0.095	Yes
Fuel Basket-to-MPC Axial Gap	1.25	0.487	Yes
MPC-to-Overpack Radial Gap	0.5	0.139	Yes
MPC-to-Overpack Minimum Axial Gap	1.0	0.771	Yes

Table 4.4.11

THEORETICAL LIMITS* OF MPC HELIUM BACKFILL PRESSURE**

MPC	Minimum Backfill Pressure (psig)	Maximum Backfill Pressure (psig)
MPC-32/24/24E	44.1	49.1
MPC-68	45.2	50.3
* The helium backfill pressures are set forth in the Technical Specifications with a margin (See Table 4.4.12). ** The pressures tabulated herein are at a reference gas temperature of 70°F.		

Table 4.4.12

MPC HELIUM BACKFILL PRESSURE SPECIFICATIONS

Item	Specification
Minimum Pressure	45.5 psig @ 70°F Reference Temperature
Maximum Pressure	48.5 psig @ 70°F Reference Temperature

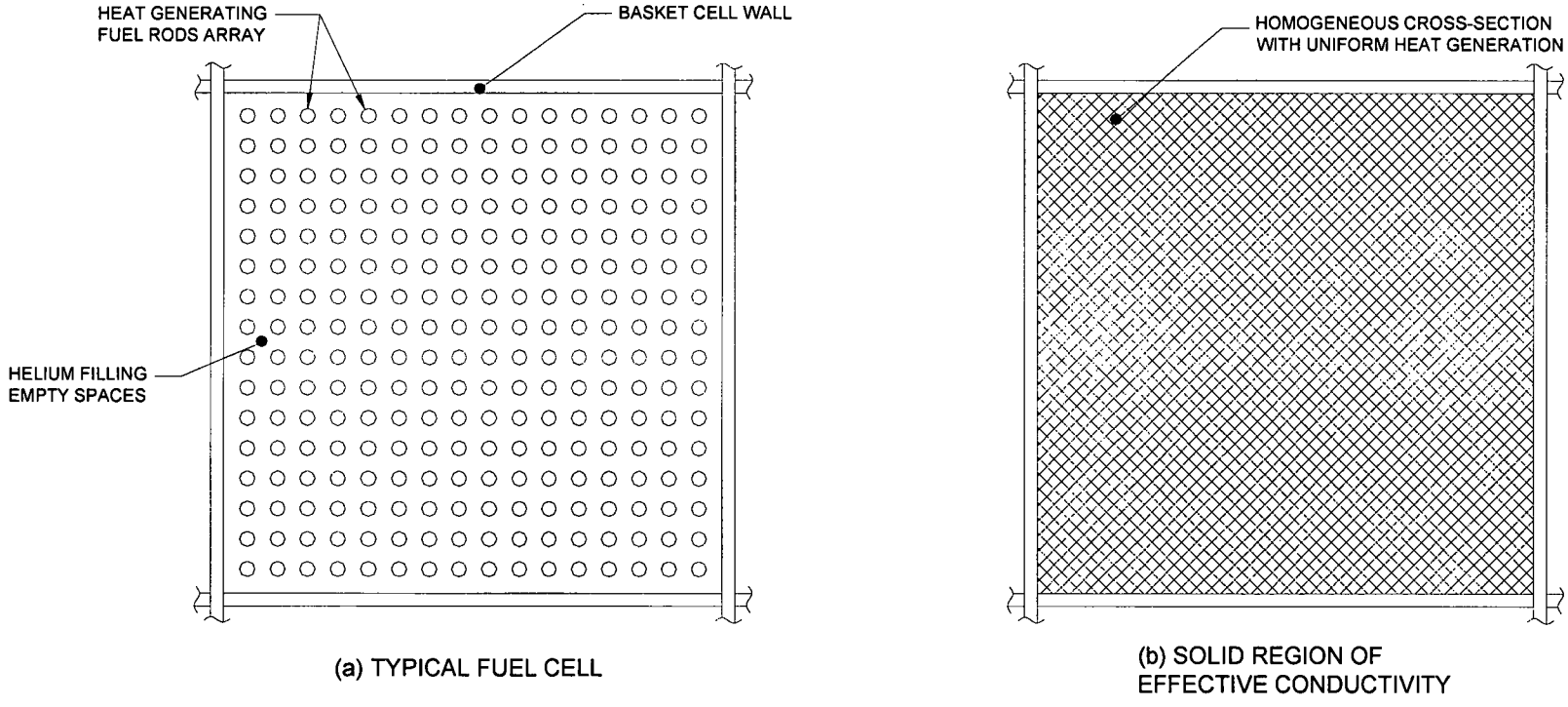

FIGURE 4.4.1: HOMOGENIZATION OF THE STORAGE CELL CROSS-SECTION

FIGURE 4.4.2

[Intentionally Deleted]

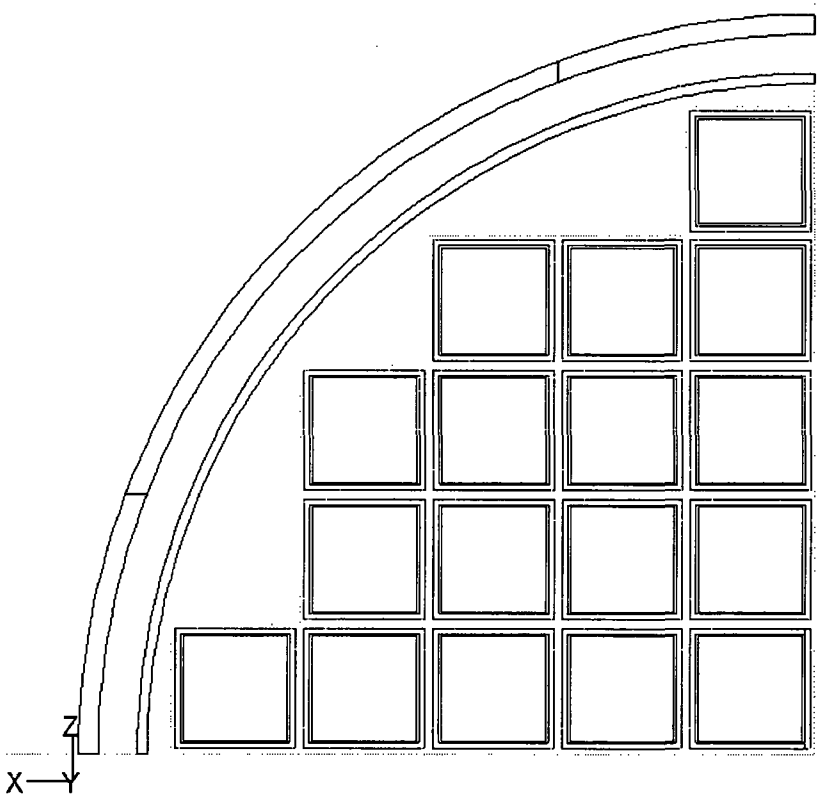

Grid

Dec 23, 2004
FLUENT 6.1 (3d, dp, segregated, ske)

FIGURE 4.4.3: PLANAR VIEW OF HI-STORM MPC-68 QUARTER SYMMETRIC 3-D MODEL

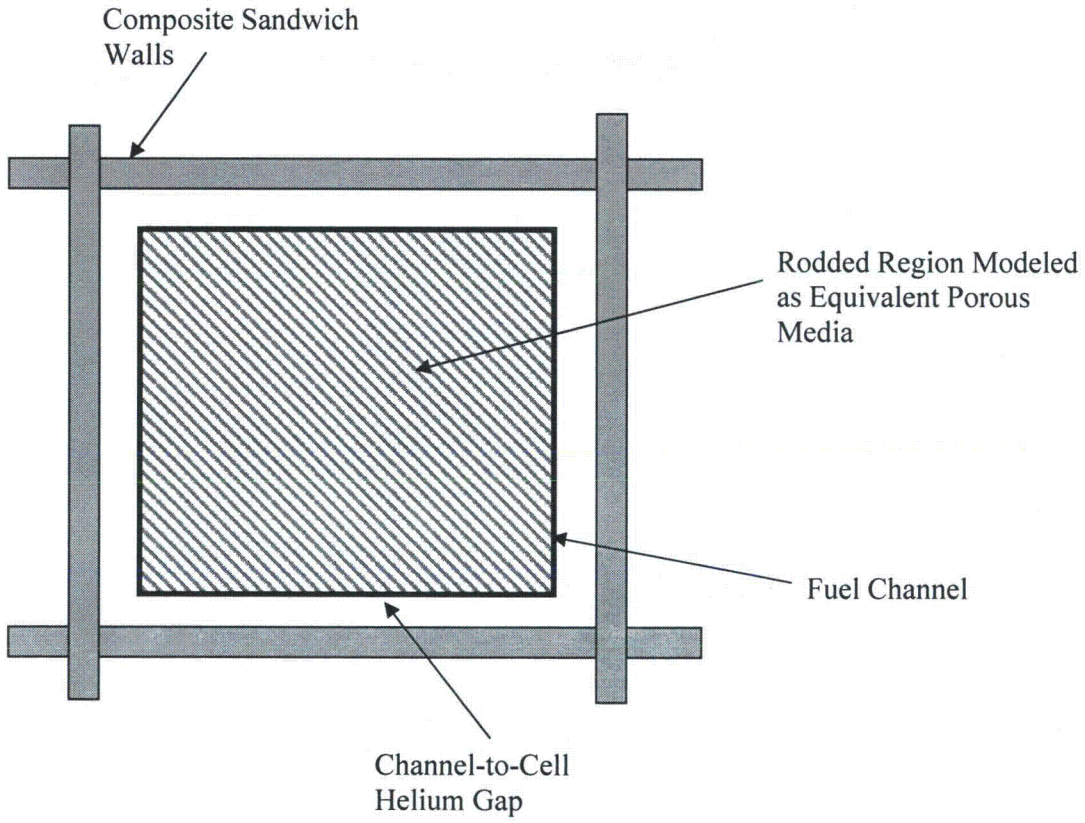

FIGURE 4.4.4: CLOSEUP VIEW OF THE MPC-68 CHANNELED FUEL CELL SPACES

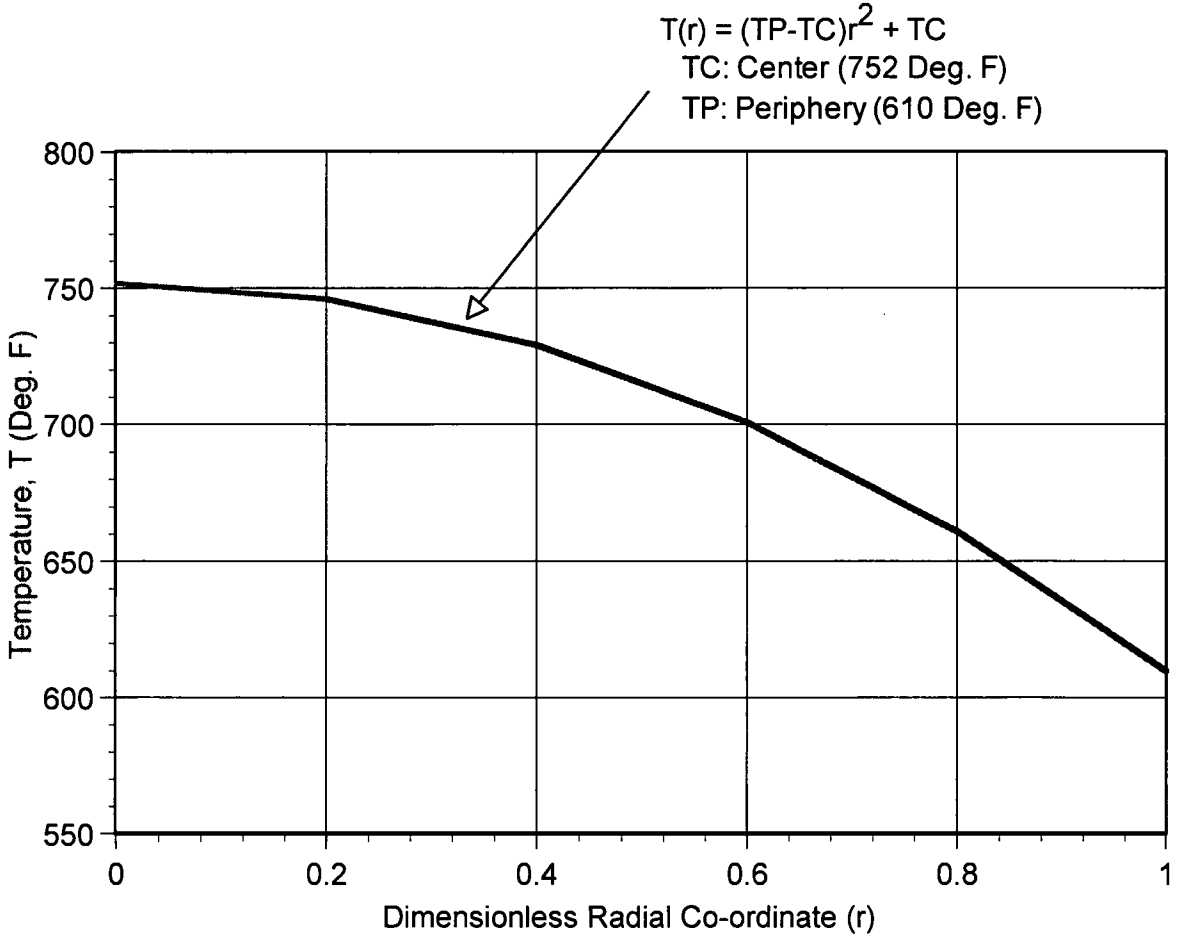

FIGURE 4.4.5: BOUNDING BASKET TEMPERATURE PROFILE FOR DIFFERENTIAL EXPANSION

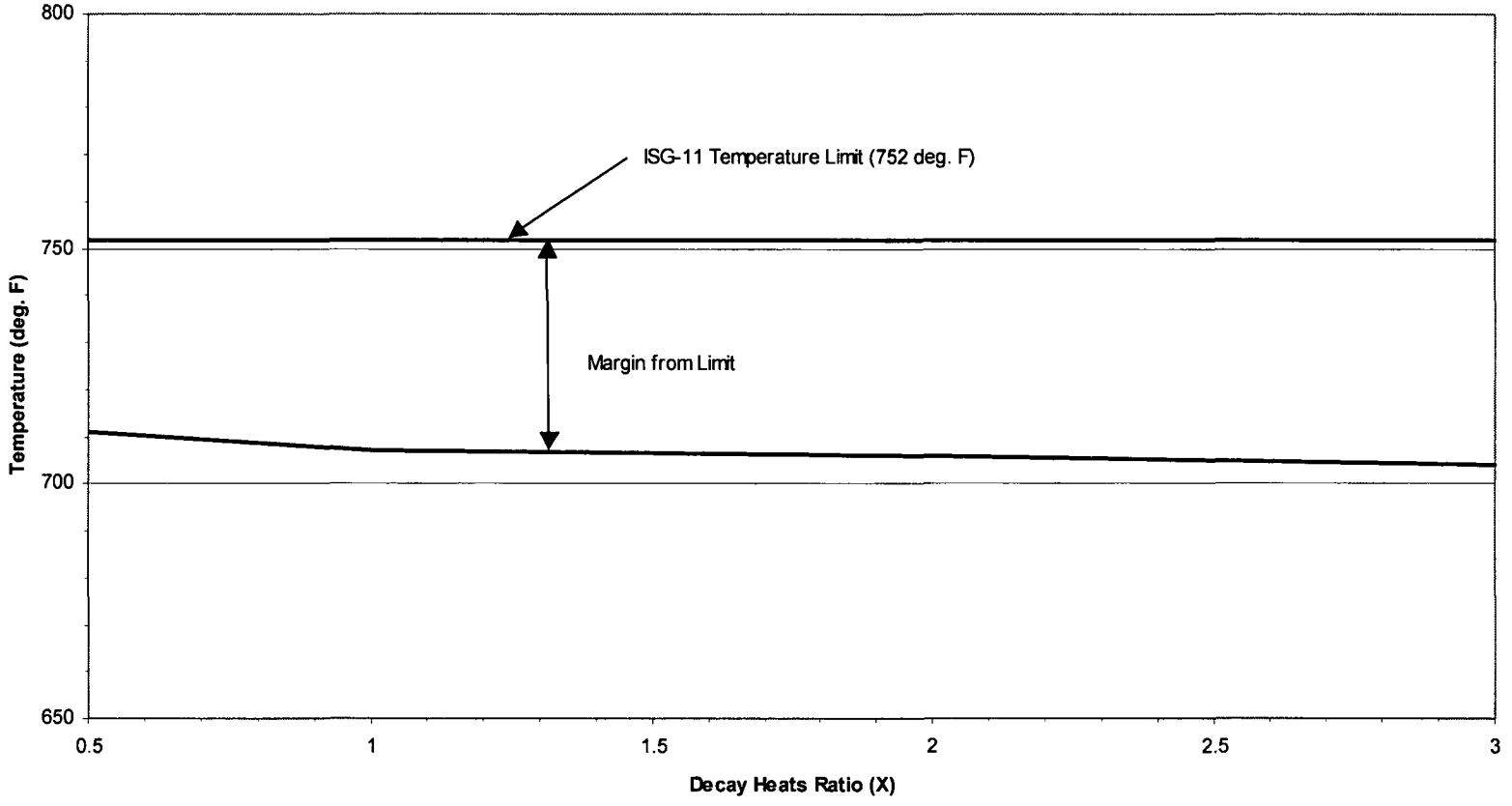

FIGURE 4.4.6: PEAK CLADDING TEMPERATURE VARIATION IN REGIONALIZED STORAGE (MPC 32)

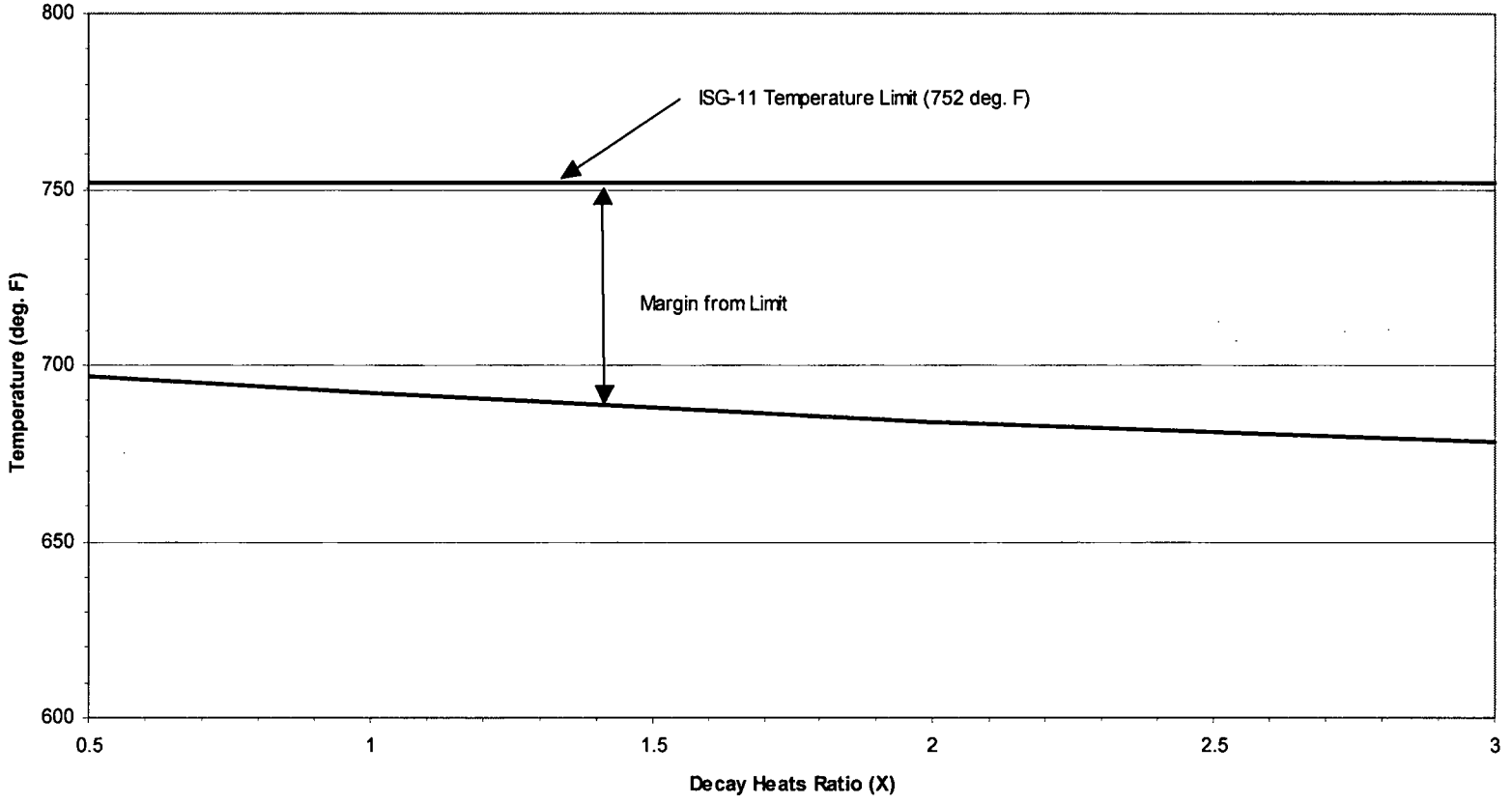

FIGURE 4.4.7: PEAK CLADDING TEMPERATURE VARIATION IN REGIONALIZED STORAGE (MPC-68)

4.5 THERMAL EVALUATION OF SHORT TERM OPERATIONS

Prior to placement in a HI-STORM overpack, an MPC must be loaded with fuel, outfitted with closures, dewatered, dried, backfilled with helium and transported to the HI-STORM module. In the unlikely event that the fuel needs to be returned to the spent fuel pool, these steps must be performed in reverse. Finally, if required, transfer of a loaded MPC between HI-STORM overpacks or between a HI-STAR transport overpack and a HI-STORM storage overpack must be carried out in an assuredly safe manner. All of the above operations, henceforth referred to as "short term operations", are short duration events that would likely occur no more than once or twice for an individual MPC.

The device central to all of the above operations is the HI-TRAC transfer cask that, as stated in Chapter 1, is available in two anatomically similar weight ratings (100- and 125-ton). Two different versions of the 100 ton and the 125 ton HI-TRAC, the classical version and the version D, are available for use during fuel transfer operations. The HI-TRAC transfer cask is a short-term host for the MPC; therefore it is necessary to establish that, during all thermally challenging operation events involving either the 100-ton or 125-ton versions of the HI-TRAC, the permissible temperature limits presented in Section 4.3 are not exceeded. The following discrete thermal scenarios, all of short duration, involving the HI-TRAC transfer cask, have been identified as warranting thermal analysis.

i. Post-Loading Wet Transfer Operations
ii. MPC Cavity Vacuum Drying
iii. Normal Onsite Transport in a Vertical Orientation
iv. MPC Cooldown and Reflood for Unloading Operations

Onsite transport of the MPC occurs with the HI-TRAC in the vertical orientation, which preserves the thermosiphon action within the MPC. To avoid excessive temperatures, transport with the HI-TRAC in the horizontal condition is generally not permitted. However, it is recognized that an occasional downending of a HI-TRAC may become necessary to clear an obstruction such as a low egress bay door opening. In such a case the operational imperative for HI-TRAC downending must be ascertained and the permissible duration of horizontal configuration must be established on a site-specific basis and compliance with the thermal limits of ISG-11 [4.1.4] must be demonstrated as a part of the site-specific safety evaluation.

The fuel handling operations listed above place a certain level of constraint on the dissipation of heat from the MPC relative to the normal storage condition. Consequently, for some scenarios, it is necessary to provide additional cooling when decay heat loads are such that short-term cladding temperature limits would be exceeded. For such situations, the Supplemental Cooling System (SCS) is required to provide additional cooling during short term operations. The SCS is required by the CoC for any MPC when the MPC heat load is such that short-term cladding temperature limits would be exceeded. The specific design of an SCS must accord with site-specific needs and resources, including the availability of plant utilities. However, a set of specifications to ensure that the performance objectives of the SCS are satisfied by plant-specific designs are set forth in Appendix 2.C.

4.5.1 HI-TRAC Thermal Model

The HI-TRAC transfer cask is used to load and unload the HI-STORM concrete storage overpack, including onsite transport of the MPCs from the loading facility to an ISFSI pad. Section views of the HI-TRAC have been presented in Chapter 1. Within a loaded HI-TRAC, heat generated in the MPC is transported from the contained fuel assemblies to the MPC in the manner described in Section 4.4. From the outer surface of the MPC to the ambient air, heat is transported by a combination of conduction, thermal radiation and natural convection. For evaluation of the thermal state of a loaded canister during all short-term operations, the three dimensional (3D) thermal model of the MPC described in Section 4.4 is utilized.

All FLUENT thermal analyses to establish margins of safety are carried out for the MPC model that yields the highest peak cladding temperature and MPC cavity pressure under the long term storage condition as discussed in Section 4.4. The above criterion identifies MPC-32 under regionalized fuel loading with X = 0.5 and X=3 as the governing cases.

Two HI-TRAC transfer cask designs, namely, the 125-ton and the 100-ton versions, are developed for onsite handling and transport, as discussed in Chapter 1. The two designs are principally different in terms of lead thickness and the thickness and number of the heat dissipating ribs (radial connectors) in the water jacket region. The aggregate heat dissipation by the ribs is defined by the product of the number of radial ribs, N and thickness, t_r. The numerical model developed for HI-TRAC thermal characterization conservatively accounts for these differences by applying the higher lead thickness and constructing the water jacket region having the lowest product of N and t_r. In this manner, the HI-TRAC thru-wall resistance to heat transfer is overestimated, yielding higher MPC internal and fuel cladding temperatures.

Transport of heat within HI-TRAC occurs through multiple concentric layers of air, steel and shielding materials. A small gap exists between the outer surface of the MPC and the inner surface of the HI-TRAC overpack. Heat is transported across this gap by the parallel mechanisms of natural convection, conduction and thermal radiation. Assuming that the MPC is centered and does not contact the transfer cask walls conservatively minimizes heat transport across this gap. Heat is transported through the cylindrical wall of the HI-TRAC transfer cask by conduction through successive layers of steel, lead, and steel. A water jacket, which provides neutron shielding for the HI-TRAC transfer cask, surrounds the cylindrical steel wall. The water jacket is essentially an array of carbon steel radial ribs with welded, connecting enclosure plates. Heat is dissipated by conduction and natural convection in the water cavities and by conduction in the radial ribs. Heat is passively rejected to the ambient from the outer surface of the HI-TRAC transfer cask by natural convection and thermal radiation.

The HI-TRAC transfer cask thermal analysis is based on a 3D FLUENT model that incorporates several conservative features, namely:

i. A constant solar flux is assumed with maximum permissible heat load and asymptotic steady state conditions to yield the most adverse temperature field in the cask. A theoretically bounding solar absorbtivity of 1.0 is applied to all exposed surfaces.

ii. Air motion in the HI-TRAC annulus is explicitly modeled. The MPC is assumed to be concentrically aligned with the cask cavity and the annulus is filled with air.

iii. Although the HI-TRAC transfer cask baseplate is in contact with supporting surfaces, for conservatism, an insulated boundary condition is applied to the HI-TRAC baseplate.

iv. The HI-TRAC transfer cask fluid columns in the water jacket and the open air volume above the MPC are conservatively assumed to remain in the laminar flow regime.

v. The annular gap between the HI-TRAC transfer cask and MPC shrinks under heat up to operating temperatures. The enhancement of heat transfer due to the gap reduction is conservatively neglected.

vi. Buoyancy driven motion of air above the MPC is included in the thermal model.

vii. Radiation heat transfer is simulated by the more robust Discrete Ordinates (DO) model deployed in the HI-STAR 180 (Docket 71-9325) and HI-STORM FW (72-1032) in lieu of the DTRM model.

viii. The rodded zone, which contains the spent fuel assemblies, is modeled as a homogeneous porous media using the flow resistance properties based on extensive CFD simulations [4.4.2] performed in the HI-STORM 100 docket and used in subsequent safety evaluations in both HI-STORM 100(Docket 72-1014) and HI-STORM FW dockets (Docket 72-1032). A recent experimental work by the Sandia National Laboratory (SNL), however, indicates that the axial flow resistance in the PWR fuel may be somewhat greater [4.5.1]. Although the SNL experimental data is not yet published by the NRC as of this writing (March, 2014), in the interest of conservatism, the higher flow resistance, $1x10^6$ m^{-2} for all three zones of fuel assembly, indicated by their work has been used in all of the thermal simulations for HI-TRAC [4.5.1].

ix. The HI-TRAC external surfaces are modeled as surfaces with convection, radiative heat exchange with air and a constant maximum incident solar heat flux load. Insolation on cylindrical surfaces is conservatively based on 12-hour levels prescribed in 10CFR71 averaged on a 24-hour basis. It is considered appropriate to use the 24-hour averaged insolation level due to the large thermal inertia of HI-TRAC which precludes it from reaching a steady-state thermal condition during a twelve-hour period.

The computational fluid dynamics model of the HI-TRAC transfer cask captures all essential details of the cask body including the radial ribs, lead, steel shells and the water jacket. Figures 4.5.1 show the discretization of the cask and its enclosed MPC for FLUENT implementation.

4.5.2 Time-to-Boil for a Water-Filled MPC

Fuel loading operations are conducted with the HI-TRAC transfer cask and its contents submerged in pool water. Under these conditions, the HI-TRAC transfer cask is essentially at the pool water temperature. When the HI-TRAC transfer cask and the loaded MPC under water-flooded conditions is removed from the pool and staged in an ambient air environment, the water, MPC, and HI-TRAC transfer cask metal absorb the decay heat emitted by the fuel assemblies. This results in a slow temperature rise of the HI-TRAC transfer cask with time, starting from an initial pool water temperature. The rate of temperature rise is limited by the thermal inertia of the HI-TRAC transfer cask.

The available time before the water in the MPC would reach boiling is computed under a conservative set of assumptions summarized below:

i. Heat loss by natural convection and radiation from the exposed HI-TRAC surfaces to ambient air is neglected (i.e., an adiabatic heat-up calculation is performed).

ii. The smaller of the two (i.e., 100-ton and 125-ton) HI-TRAC transfer cask metal mass is credited in the analysis. The 100-ton design has a significantly smaller quantity of metal mass, which will result in a higher rate of temperature rise.

iii. The water mass in the MPC cavity is understated.

Table 4.5.2 summarizes the lower bound weights and thermal inertias of the constituent components in the loaded HI-TRAC transfer cask. The rate of temperature rise of the HI-TRAC transfer cask and contents during an adiabatic heat-up is given by the ratio Q/C where:

Q = Coincident fuel decay heat in the canister
C = Thermal inertia of a loaded HI-TRAC (Btu/°F) (See Table 4.5.2)

Therefore, the time-to-boil, τ is given by the simple algebraic formula $\tau = C(212-T)/Q$ where 212°F has been set as the boiling temperature and T represents the temperature of the pool water under fuel loading operations. The time-to-boil clock starts when the HI-TRAC is no longer submerged in the pool water. Table 4.5.3 provides a summary of τ at several representative heat loads and initial pool water temperatures. The calculation of time-to-boil for a loaded canister shall be made using the above formula.

As set forth in the HI-STORM operating procedures, in the unlikely event that the maximum allowable time provided in Table 4.5.3 is found to be insufficient to complete wet transfer operations, a forced water circulation shall be initiated and maintained to remove the decay heat from the MPC cavity. In this case, relatively cooler water will enter via the MPC lid drain port connection and heated water will exit from the vent port. The minimum water flow rate required

to maintain the MPC cavity water temperature below boiling with an adequate subcooling margin is determined as follows:

$$M_W = \frac{Q}{C_{pW}(T_{max} - T_{in})}$$

where:

M_W = minimum water flow rate (lb/hr)
C_{pw} = water heat capacity (Btu/lb-°F)
T_{max} = maximum MPC cavity water mass temperature (must be less than 212°F)
T_{in} = MPC water inlet temperature

For example, the MPC cavity water temperature limited to 150°F, MPC water inlet temperature at 125°F and design basis maximum heat load (36.9 kW), the water flow rate computes as 5038 lb/hr (10.1 gpm).

4.5.3 MPC Temperatures During Moisture Removal Operations

4.5.3.1 Vacuum Drying Operation

The initial loading of SNF in the MPC requires that the water within the MPC be drained, fuel dried and the water replaced with helium. Vacuum drying of fuel is conducted by evacuating the MPC after completion of MPC draining operation. For MPCs containing Moderate Burnup Fuel (MBF) assemblies only, this operation may be carried out using the vacuum drying method up to the threshold heat loads defined in Table 4.5.1. In this Table threshold heat loads Q1 and Q2 are defined wherein Q1 is the threshold heat load for vacuum drying operations without time limits and Q2 is the threshold heat load for time-limited vacuum drying. The requirements and limits for moisture removal are provided in LCO 3.1.1 of the HI-STORM 100 CoC and are specific to the amendment to which the HI-STORM 100 System is being loaded. To minimize fuel temperatures during vacuum drying operations the HI-TRAC annulus must be water filled.

Vacuum drying of MPCs containing High Burnup Fuel (HBF) is not permitted. High burnup fuel drying must be conducted by using forced helium drying (FHD) process as discussed in Section 4.5.3.2.

A 3-D FLUENT thermal model of the MPC is constructed in the same manner as described in Section 4.4. The principal input to this model is the effective conductivity of fuel under vacuum drying operations. To reasonably bound vacuum drying operations the effective conductivity of fuel is computed assuming the MPC is filled with water vapor at a very low pressure (1 torr) for the entire duration of vacuum drying[2]. The methodology for computing the effective conductivity is given in

[2] This is conservative as the MPC pressure is progressively lowered below ambient pressure to facilitate moisture removal. Near the end of the vacuum drying operation the pressure is substantially lowered to approximately 1 torr to facilitate the 30-minute 3-torr vacuum rebound test followed by backfilling of the MPC with helium.

Section 4.4.1. To ensure a conservative evaluation the thermal model is incorporated with the following assumptions:

i. Threshold heat load Q1, defined in Table 4.5.1, is assumed and steady-state condition reached under Q1 results in vacuum drying without time limits.
ii. Threshold heat load Q2, defined in Table 4.5.1, is assumed and a transient calculation is performed to determine the permissible vacuum drying time under Q2. The transient calculation is started assuming the MPC has reached 212°F boiling temperature in the operational step preceding vacuum drying (i.e. water blow down operations). The vacuum drying clock starts when the MPC is drained.
iii. The external surface of the MPC shell is postulated to vary linearly from 100°C (212°F) normal boiling temperature of water at the top to 111°C (231°F) elevated pressure boiling temperature at the bottom to account for the hydrostatic head.
iv. The bottom surface of the MPC is insulated.
v. MPC internal convection heat transfer is suppressed.
vi. Top surface of the MPC is in communicative contact with air. Natural convection and radiation cooling from the MPC top is included in the thermal model.

The principle objective of the vacuum drying analysis is to ensure that fuel temperatures are below ISG-11, Rev. 3 temperature limits (See Table 4.3.1). Under threshold heat load Q1 the results and margins are tabulated in Table 4.5.5. Under the time limited threshold heat load Q2 the peak cladding temperature plot is shown in Figure 4.5.2. The results under the scenarios Q1 and Q2 (with appropriate time limit) show that ISG-11, Rev. 3 limits are met with ample margins.

4.5.3.2 Forced Helium Dehydration

To dry the MPC cavity using a Forced Helium Dehydration (FHD) system, a conventional, closed loop dehumidification system consisting of a condenser, a demoisturizer, a compressor, and a pre-heater is utilized to extract moisture from the MPC cavity through repeated displacement of its contained helium, accompanied by vigorous flow turbulation. A vapor pressure of 3 torr or less is assured by verifying that the helium temperature exiting the demoisturizer is maintained at or below the psychrometric threshold of 21°F for a minimum of 30 minutes. See Appendix 2.B for detailed discussion of the design criteria and operation of the FHD system.

The FHD system provides concurrent fuel cooling during the moisture removal process through forced convective heat transfer. The attendant forced convection-aided heat transfer occurring during operation of the FHD system ensures that the fuel cladding temperature will remain below the applicable peak cladding temperature limit for normal conditions of storage, which is well below the high burnup cladding temperature limit 752°F (400°C) for all combinations of SNF type, burnup, decay heat, and cooling time. Because the FHD operation induces a state of forced convection heat transfer in the MPC, (in contrast to the quiescent mode of natural convection in long term storage), it is readily concluded that the peak fuel cladding temperature under the latter condition will be greater than that during the FHD operation phase. In the event that the FHD system malfunctions, the forced convection state will degenerate to natural convection, which corresponds to the conditions of

normal onsite transport. As a result, the peak fuel cladding temperatures will approximate the values reached during normal onsite transport as described elsewhere in this chapter.

4.5.4 Cask Cooldown and Reflood Analysis During Fuel Unloading Operation

NUREG-1536 requires an evaluation of cask cooldown and reflood procedures to support fuel unloading from a dry condition. Two options are available for cask cooldown: Direct Water Quenching and Helium Cooldown followed by Direct Water Quenching. It is not mandatory to perform helium cooldown prior to quenching but some users may choose to perform helium cooldown for high heat load MPCs.

4.5.4.1 Option 1: Direct Water Quenching

Past industry experience generally supports cooldown of cask internals and fuel from hot storage conditions by direct water quenching. Direct MPC cooldown is effectuated by introducing water through the lid drain line. From the drain line, water enters the MPC cavity near the MPC baseplate. Steam produced during the direct quenching process will be vented from the MPC cavity through the lid vent port. To maximize venting capacity, both vent port RVOA connections must remain open for the duration of the fuel unloading operations. As direct water quenching of hot fuel results in steam generation, it is necessary to limit the rate of water addition to avoid MPC overpressurization. For example, steam flow calculations using bounding assumptions (100% steam production and MPC at design pressure) show that the MPC is adequately protected upto a reflood rate of 3715 lb/hr. Limiting the water reflood rate to this amount or less would prevent exceeding the MPC design pressure.

During direct reflood operations the fuel cladding is subject to high temperature gradients and concomitant thermal stresses. The integrity of fuel under direct quenching is evaluated in a generic manner in the HI-STORM FW SAR (Docket No. 72-1032, Ref. [4.5.2]). To define a bounding scenario at time t = 0 sec, a uniformly bounding temperature throughout the entire fuel rod is set at 752°F (400°C), which is the temperature limit of fuel cladding. At time t = 0.1 sec, a reasonably bounding 80°F quench water temperature is assigned to the lower half of the fuel rod to simulate a thermal shock with a large step change in the cladding temperature. The resulting transient stress and strain distributions in the fuel rod are evaluated with finite element ANSYS models. The results show that the maximum stress and strain values remain within the elastic range and remain well within failure strain limit (a factor of 6 against failure strain). This safety analysis documented in Section 3.4.4.1.11 of the HI-STORM FW FSAR provides the assurance that the MPC reflood event will not cause a breach of fuel cladding.

4.5.4.2 Option 2: Helium Cooldown followed by Direct Water Quenching

Under a closed-loop forced helium circulation condition, the helium gas is cooled, via an external chiller. The chilled helium is then introduced into the MPC cavity from connections at the top of the MPC lid. The helium gas enters the MPC basket and moves through the fuel basket cells, removing heat from the fuel assemblies and MPC internals. The heated helium gas exits the MPC from the lid

connection to the helium recirculation and cooling system. Because of the turbulation and mixing of the helium contents in the MPC cavity by the forced circulation, the MPC exiting temperature is a reliable measure of the thermal condition inside the MPC cavity. The objective of the cooldown system is to lower the bulk helium temperature in the MPC cavity to below the normal boiling temperature of water (212°F). For this purpose, the rate of helium circulation shall be sufficient to ensure that the helium exit gas temperature is below this threshold limit with a margin.

An example calculation for the required helium circulation rate is provided below to limit the helium temperature to 200°F. The calculation assumes no heat loss from the MPC boundaries and a conservatively bounding heat load (38 kW (1.3×10^5 Btu/hr)). Under these assumptions, the MPC helium is heated adiabatically by the MPC decay heat from a given inlet temperature (T_1) to a temperature (T_2). The required circulation rate to limit T_2 to 200°F is computed as follows:

$$m = \frac{Q_d}{C_p(T_2 - T_1)}$$

where:

Q_d = Design maximum decay heat load (Btu/hr)
m = Minimum helium circulation rate (lb/hr)
Cp = Heat capacity of helium (1.24 Btu/lb-°F (Table 4.2.5))
T_1 = Helium supply temperature (assumed 15°F in this example)

Substituting the values for the parameters in the equation above, m is computed as 567 lb/hr.

4.5.5 Maximum Temperatures under Onsite Transport Conditions

4.5.5.1 HI-TRAC Transport outside a Building

The requirements of utilizing SCS system in the onsite transfer operation are listed in Table 4.5.4. Condition 3 of Table 4.5.4 mandates the use of SCS for an MPC containing one or more HBF above the threshold heat load. This will assure that cladding temperature limits are met for HBF at heat loads higher than threshold heat load. See Appendix 2.C for the SCS requirements.

A 3-D FLUENT thermal model of an MPC inside a HI-TRAC transfer cask was constructed as described in Subsection 4.5.1 to evaluate temperature distributions under onsite transport. In the normal onsite transport mode, the annular region between the canister and the cask has air and the cask is subject to heat input from insolation. The ambient temperature when HI-TRAC is placed in the outdoor environment corresponds to the maximum outdoor ambient temperature specified in Table 2.2.2 under short term operations. Even though the duration of onsite transport is typically short enough to preclude the MPC and HI-TRAC from reaching steady-state, a steady-state thermal analysis is conservatively performed. The results summarized herein are when steady state conditions have been reached.

The safety analysis of the onsite transport scenario requires the computation of the margins of safety with respect to the peak fuel cladding temperature of moderate and high burnup fuel[3], MPC internal pressure, fuel basket metal temperature, hydraulic pressure in the water jacket and the temperature of the HI-TRAC body parts.

The water in the water jacket surrounding the HI-TRAC transfer cask body provides necessary neutron shielding. During normal handling and onsite transport operations this shielding water is contained within the water jacket at an elevated pressure. The water jacket is equipped with two pressure relief devices to prevent overpressure.

The steady state analyses are first performed for the design basis heat load under the two extreme allowable regionalized storage scenarios (Q = 36.9 kW, X = 0.5 and Q = 30.17 kW, X = 3 in MPC-32), which are the maximum permissible heat load allowed to be stored in HI-STORM system defined in Subsection 2.1.9.1. The computed fuel temperatures in this scenario remain below the cladding temperature limit of moderate burnup fuel, but exceed the temperature limit of high burnup fuel (Table 4.3.1). For both regionalized storage scenarios, the MPC internal pressure, fuel basket and the HI-TRAC parts temperatures are presented in Table 4.5.6, and their corresponding allowable limits show positive margins of safety. As these are bounding steady state temperatures, the results support onsite transport of fuel in the HI-TRAC without the aid of any supplemental cooling for MPC containing only moderate fuel burnup and cooling times up to the maximum design basis heat load of the HI-STORM System.

The steady state analyses are then performed for the threshold heat load which requires SCS for MPC containing HBF, which is defined in Table 4.5.4. In this scenario, the heat generation rate in the MPC is reduced to 90% of maximum design basis rate. Under the two extreme allowable regionalized storage scenarios (Q = 33.21 kW, X = 0.5 and Q = 27.15 kW, X = 3 in MPC-32), the computed fuel temperatures remain below the cladding temperature limits of high and moderate burnup fuel (Table 4.3.1). The MPC components, fuel basket and the HI-TRAC parts temperatures are presented in Table 4.5.7, and their corresponding allowable limits show positive margins of safety. Therefore, the results support onsite transport of fuel in the HI-TRAC without the aid of any supplemental cooling for any fuel burnup and cooling times up to 90% of maximum design basis heat load† of the HI-STORM System.

4.5.5.2 Evaluation of HI-TRAC inside a Building

When HI-TRAC is located inside the fuel loading building, the ambient air temperature inside a building may be higher than the outdoor environment evaluated in Subsection 4.5.5.1. Since ambient air temperature may be higher inside the building, a maximum indoor air temperature specified in Table 2.2.2 under short term operations is used in the analysis. Since the cask is inside a building, no solar insolation is applied to the cask. A steady state analysis is performed for the 90% of design basis heat load under the regionalized storage scenario (Q = 27.15 kW, X = 3 in MPC-32), which

[3] The cladding temperature limit for the high burn up fuel is more restrictive (See Table 4.3.1).
† The individual storage cell heat loads are also restricted to 90% of their design maximum heat loads.

results in the lowest PCT safety margin for high burnup fuel. The peak cladding, fuel basket and the HI-TRAC parts temperatures are presented in Table 4.5.8. The predicted component temperatures are below their corresponding temperatures for outdoor environment presented in Table 4.5.7. Therefore, the normal on-site transfer of a HI-TRAC outside the building and with solar insolation as evaluated in Subsection 4.5.5.1 is the limiting thermal condition.

4.5.5.3 Evaluation of SCS Failure

Table 4.5.4 mandates the use of the SCS for MPC containing one or more HBF above the threshold heat load to ensure fuel remains below the short-term operation temperature limits mandated by ISG-11, Rev. 3. If the SCS fails during operation, an accident condition defined in Section 11.2, the thermal state of the fuel would asymptotically approach steady state maximum conditions corresponding to the coincident thermal payload in the HI-TRAC transfer cask. The results of steady state analysis are provided in Table 4.5.6 for the design basis heat load. It is shown that the fuel remains well below its accident limit (Table 4.3.1).

4.5.5.4 Evaluation of SCS for Lower Backfill Pressure Limit

As stated in Table 1.2.2, MPC is allowed to be backfilled with a lower pressure limit than that specified in Table 4.4.12, if the MPC heat load meets the threshold heat load requirement in Table 1.2.2. The analyses that support the threshold heat load scenario and lower helium backfill pressure limits are reported in the Revision 6 of HI-STORM 100 FSAR. To evaluate the requirement of SCS system (Table 4.5.4) for the threshold heat load with lower backfill pressure limit, a steady state analysis is performed for the bounding heat load scenario, i.e. MPC-32 with heat load of uniform 28.74 kW under an ambient environment outside the building. The computed fuel temperatures in this scenario remain below the cladding temperature limit of moderate burnup fuel, but exceed the temperature limit of high burnup fuel (Table 4.3.1). The fuel basket and the HI-TRAC parts temperatures are presented in Table 4.5.9, and their corresponding allowable limits show positive margins of safety. As these are bounding steady state temperatures, the results support onsite transport of fuel in the HI-TRAC without the aid of any supplemental cooling for MPC containing only moderate fuel burnup and cooling times up to the threshold heat load in Table 1.2.2.

The steady state analyses are then performed for 90% of threshold heat load†, i.e. Q = 25.86 kW uniform in MPC-32, the computed fuel temperatures remain below the cladding temperature limits of high and moderate burnup fuel (Table 4.3.1). The MPC components, fuel basket and the HI-TRAC parts temperatures are presented in Table 4.5.9, and their corresponding allowable limits show positive margins of safety. Therefore, the results support onsite transport of high burnup fuel in the HI-TRAC without the aid of any supplemental cooling up to the 90% of threshold heat load† in Table 1.2.2.

† The individual storage cell heat loads are also restricted to 90% of their threshold maximum heat loads.

4.5.5.5 Environmental Temperature Requirements

Short term operations involving the HI-TRAC transfer cask can be carried out on the basis of the safety evaluation herein if the reference ambient temperature (three day average around the cask) is below the "Threshold Temperature" defined in Table 2.2.2 as 110 deg. F for operations inside the part 50 structural boundary and 90 deg. F outside of it. The determination of the Threshold Temperature compliance shall be made based on the best available thermal data for the site.

If the reference ambient temperature exceeds the corresponding Threshold Temperature then a site specific analysis using the methodology set down in Section 4.5 shall be performed using the actual heat load and reference ambient temperature equal to the three day average to ensure that the steady state peak fuel cladding temperature will remain below the Table 2.2.3 limit. If the peak fuel cladding temperature exceeds Table 2.2.3 limit then the use of a Supplemental Cooling System (SCS) is mandatory.

4.5.6 Maximum Internal Pressure

After fuel loading and vacuum drying, but prior to installing the MPC closure ring, the MPC is initially filled with helium. During handling and on-site transfer operations in the HI-TRAC transfer cask, the gas temperature within the MPC rises to its maximum operating temperature as determined by on the thermal analysis methodology described previously. In Table 4.5.6, the MPC internal pressure co-incident with the MPC temperature is reported and compared with the short term (off-normal) pressure limit specified in Table 2.2.1 to show compliance with design limit. The MPC gas pressure listed in Table 4.5.6 is below the MPC design internal pressure listed in Table 2.2.1.

Table 4.5.1

THRESHOLD HEAT LOADS FOR MOISTURE REMOVAL OPERATIONS

Drying Method	Fuel Burnup	Threshold Heat Load[Note 1]	Time Limits
Vacuum Drying	MBF	Q1	None
Vacuum Drying	MBF	MPC Heat Load > Q1 and ≤ Q2	Yes (40 hrs)
FHD	MBF and/or HBF	36.9 kW	None
Note 1: Threshold heat loads are defined below: Q1 = 26 kW (Uniform) Q2 = 30 kW (Uniform)			

Table 4.5.2

HI-TRAC TRANSFER CASK LOWERBOUND
WEIGHTS AND THERMAL INERTIAS

Component	**Weight (lbs)**	**Heat Capacity (Btu/lb-°F)**	**Thermal Inertia (Btu/°F)**
Water Jacket	7,000	1.0	7,000
Lead	52,000	0.031	1,612
Carbon Steel	40,000	0.1	4,000
Alloy-X MPC (empty)	39,000	0.12	4,680
Fuel	40,000	0.056	2,240
MPC Cavity Water*	6,500	1.0	6,500
			26,032 (Total)
* Conservative lower bound water mass.			

Table 4.5.3

TIME-TO-BOIL FOR WATER IN THE MPC CAVITY

Initial Temperature (°F)	Time (hrs) @ Q = 36.9 kw	Time (hrs) @ Q = 30 kw	Time (hrs) @ Q = 25 kw	Time (hrs) @ Q = 20 kw
80	27.3	33.6	40.3	50.4
90	25.2	31.0	37.2	46.5
100	23.2	28.5	34.2	42.7
110	21.1	25.9	31.1	38.9
120	19.0	23.4	28.1	35.1
125	18.0	22.1	26.5	33.2

Table 4.5.4

THRESHOLD HEAT LOADS FOR SUPPLEMENT COOLING SYSTEM REQUIREMENT

Condition*	Fuel in MPC	Heat Load Reduction Factor *	SCS Required
1	All MBF	100%	NO
2	One or More HBF	≤ 90%	NO
3	One or More HBF	> 90%	YES
* The threshold heat load is obtained by multiplying the design basis heat load per storage cell defined in Subsection 2.1.9.1 by the reduction factor listed in this table.			

Table 4.5.5

MAXIMUM FUEL TEMPERATURES UNDER VACUUM DRYING OPERATIONS

Threshold Heat Load[Note 1]	Time Limit	Temperature (°F)	Temperature Limit[Note 2]	Margin (°F)
Q1	None	1046	1058	12
Q2	40 hrs	1035	1058	23

Notes:
1) Threshold heat loads defined in Table 4.5.1.
2) Temperature limit of moderate burnup fuel shown. Vacuum drying of high burn-up fuel is not permitted (See Subsection 4.5.3).

Table 4.5.6

HI-TRAC ONSITE TRANSFER- TEMPERATURE AND PRESSURE FOR DESIGN BASIS HEAT LOAD

Component	Maximum Temperatures (°F)	
	X=0.5	X=3
Fuel Cladding	748	784
MPC Basket	745	779
Basket Peripheral Panels	612	567
MPC Shell	473	459
HI-TRAC Inner Shell	282	268
Radial Lead	279	266
HI-TRAC Water Jacket Shell	250	232
Axial Neutron Shield[Note1]	280	279
Water Jacket Bulk Water	244	225
Pressure (psig) [Note 2]		
Normal Condition	103.0	96.6

Note 1: Maximum section average temperature.
Note 2: The MPC pressure is computed under the maximum backfill pressure specified in Table 4.4.12.

Table 4.5.7

HI-TRAC ONSITE TRANSFER- TEMPERATURE
FOR 90% OF DESIGN BASIS HEAT LOAD

Component	Maximum Temperatures (°F)	
	X=0.5	X=3
Fuel Cladding	702	734
MPC Basket	698	729
Basket Peripheral Panels	577	534
MPC Shell	446	437
HI-TRAC Inner Shell	268	257
Radial Lead	266	253
HI-TRAC Water Jacket Shell	239	223
Axial Neutron Shield[Note1]	279	266
Water Jacket Bulk Water	234	217
Note 1: Maximum section average temperature.		

Table 4.5.8

HI-TRAC ONSITE TRANSFER- TEMPERATURE
FOR 110°F AMBIENT TEMPERATURE AND WITHOUT INSOLATION [Note 1]

Component	Maximum Temperatures (°F)
Fuel Cladding	730
MPC Basket	723
Basket Peripheral Panels	532
MPC Shell	430
HI-TRAC Inner Shell	246
Radial Lead	244
HI-TRAC Water Jacket Shell	216
Axial Neutron Shield[Note2]	262
Water Jacket Bulk Water	210
Note 1: The results presented in this table are for 90% of design basis heat load with X=3. Note 2: Maximum section average temperature.	

Table 4.5.9

HI-TRAC ONSITE TRANSFER- TEMPERATURE
FOR THRESHOLD HEAT LOAD AND LOWER BACKFILL PRESSURE IN TABLE 1.2.2

Component	Maximum Temperatures (°F)	
	Threshold Heat Load	90% Threshold Heat Load
Fuel Cladding	774	721
MPC Basket	768	716
Basket Peripheral Panels	558	527
MPC Shell	426	401
HI-TRAC Inner Shell	257	246
Radial Lead	253	244
HI-TRAC Water Jacket Shell	228	219
Axial Neutron Shield[Note1]	255	250
Water Jacket Bulk Water	223	214
Note 1: Maximum section average temperature.		

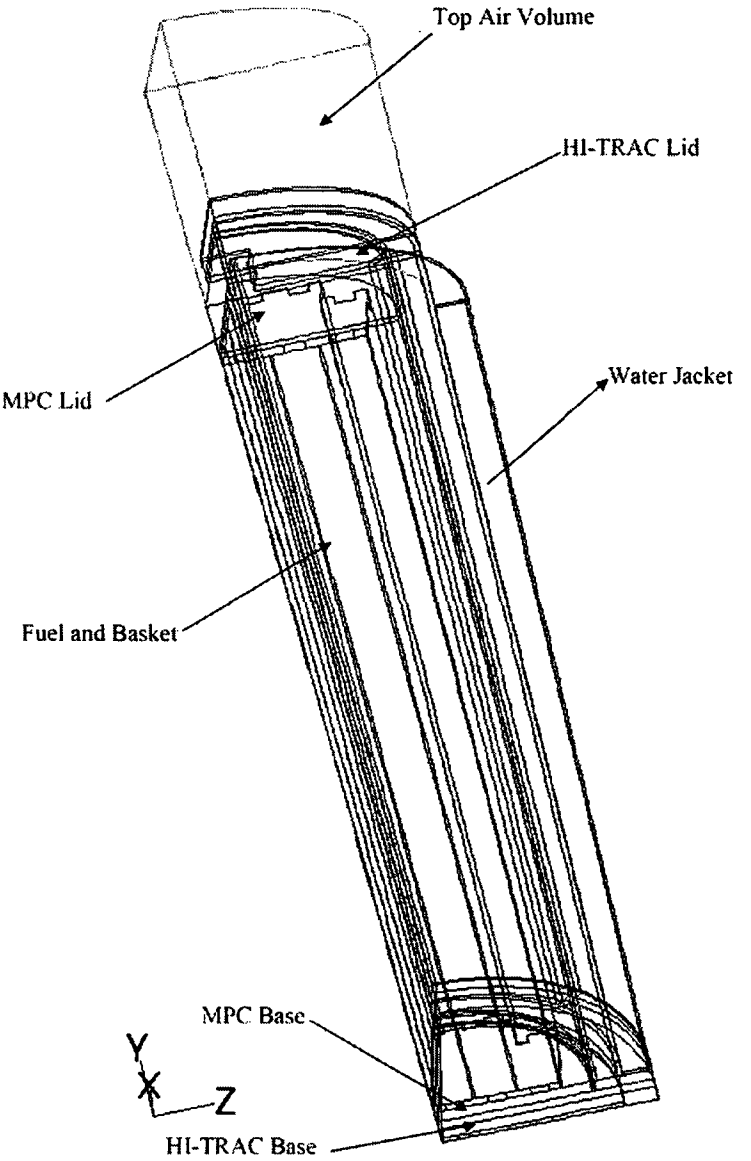

Figure 4.5.1: 3D QUARTER SYMMETRIC THERMAL MODEL OF THE HI-TRAC TRANSFER CASK

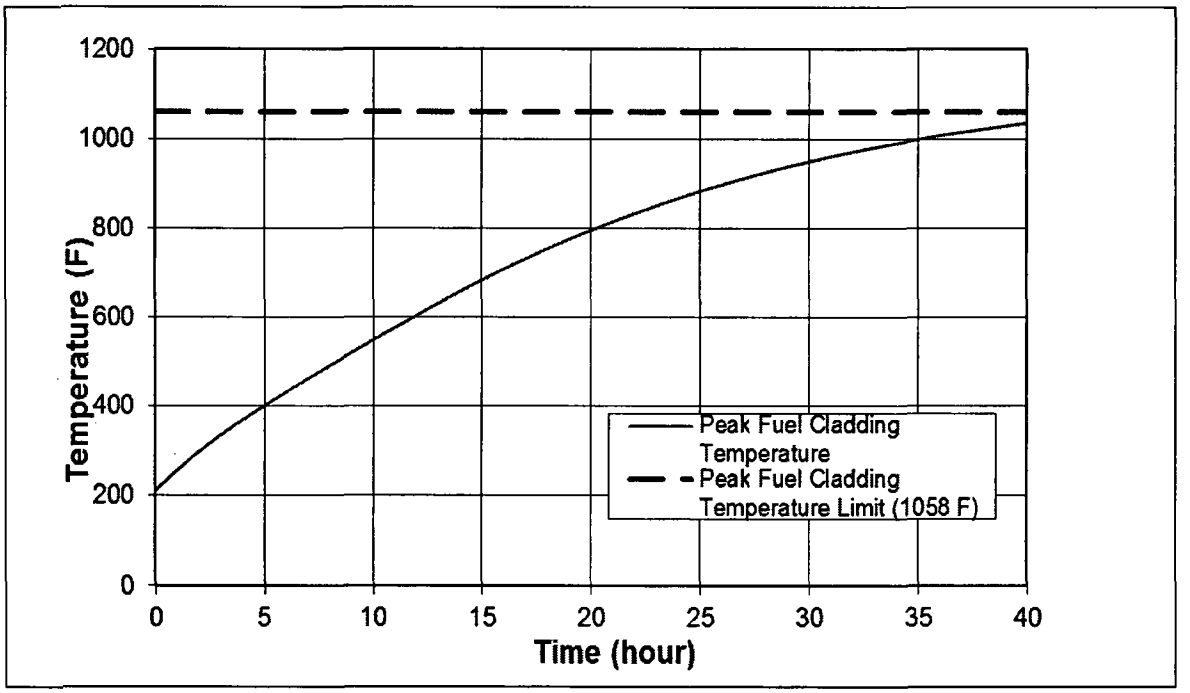

Figure 4.5.2: PEAK CLADDING TEMPERATURE CURVE UNDER VACUUM DRYING OPERATIONS AT THRESHOLD HEAT LOAD Q2

4.6 OFF-NORMAL AND ACCIDENT EVENTS[1]

In accordance with NUREG 1536 the HI-STORM 100 System is evaluated for the effects of off-normal and accident events. The design basis off-normal and accident events are defined in Chapter 2. For each event, the cause of the event, means of detection, consequences, and corrective actions are discussed and evaluated in Chapter 11. To support the Chapter 11 evaluations, thermal analyses of limiting off-normal and accident events are provided in the following.

To ensure a bounding evaluation for the array of fuel storage configurations permitted in Section 2.1, a limiting storage condition is evaluated in this section. The limiting storage condition is previously determined in the Section 4.5 and adopted herein for all off-normal and accident evaluations.

4.6.1 Off-Normal Events

4.6.1.1 Off-Normal Pressure

This event is defined as a combination of (a) maximum helium backfill pressure (Table 4.4.12), (b) 10% fuel rods rupture, and (c) limiting fuel storage configuration. The principal objective of the analysis is to demonstrate that the MPC off-normal design pressure (Table 2.2.1) is not exceeded. The MPC off-normal pressures are reported in Table 4.4.9. The result[2] is confirmed to be below the off-normal design pressure (Table 2.2.1).

4.6.1.2 Off-Normal Environmental Temperature

This event is defined by a time averaged ambient temperature of 100°F for a 3-day period (Table 2.2.2). The results of this event (maximum temperatures and pressures) are provided in Table 4.6.1 and 4.6.2. The results are below the off-normal condition temperature and pressure limits (Tables 2.2.1 and 2.2.3).

4.6.1.3 Partial Blockage of Air Inlets

The HI-STORM 100 System is designed with debris screens installed on the inlet and outlet openings. These screens ensure the air passages are protected from entry and blockage by foreign objects. As required by the design criteria presented in Chapter 2, it is postulated that the HI-STORM air inlet vents are 50% blocked . The resulting decrease in flow area increases the flow resistance of the inlet ducts. The effect of the increased flow resistance on fuel temperature is analyzed for the normal ambient temperature (Table 2.2.2) and a limiting fuel storage configuration. The computed temperatures are reported in Table 4.6.1 and the corresponding MPC internal pressure in Table 4.6.2.

---

1 A new standalone Section 4.6 is added in CoC Amendment 3 to address thermal analysis of off-normal and accident events. The results are evaluated in Chapter 11.

2 Pressures relative to 1 atm absolute pressure (i.e. gauge pressures) are reported throughout this section.

The results are confirmed to be below the temperature limits (Table 2.2.3) and pressure limit (Table 2.2.1) for off-normal conditions.

4.6.2 Accident Events

4.6.2.1 Fire Accidents

Although the probability of a fire accident affecting a HI-STORM 100 System during storage operations is low due to the lack of combustible materials at an ISFSI, a conservative fire event has been assumed and analyzed. The only credible concern is a fire from an on-site transport vehicle fuel tank. Under a postulated fuel tank fire, the outer layers of HI-TRAC or HI-STORM overpacks are heated for the duration of fire by the incident thermal radiation and forced convection heat fluxes. The amount of fuel in the on-site transporter is limited to a volume of 50 gallons.

(a) HI-STORM Fire

The fuel tank fire is conservatively assumed to surround the HI-STORM Overpack. Accordingly, all exposed overpack surfaces are heated by radiation and convection heat transfer from the fire. Based on NUREG-1536 and 10 CFR 71 guidelines [4.6.1], the following fire parameters are assumed:

1. The average emissivity coefficient must be at least 0.9. During the entire duration of the fire, the painted outer surfaces of the overpack are assumed to remain intact, with an emissivity of 0.85. It is conservative to assume that the flame emissivity is 1.0, the limiting maximum value corresponding to a perfect blackbody emitter. With a flame emissivity conservatively assumed to be 1.0 and a painted surface emissivity of 0.85, the effective emissivity coefficient is 0.85. Because the minimum required value of 0.9 is greater than the actual value of 0.85, use of an average emissivity coefficient of 0.9 is conservative.

2. The average flame temperature must be at least 1475°F (800°C). Open pool fires typically involve the entrainment of large amounts of air, resulting in lower average flame temperatures. Additionally, the same temperature is applied to all exposed cask surfaces, which is very conservative considering the size of the HI-STORM cask. It is therefore conservative to use the 1475°F (800°C) temperature.

3. The fuel source must extend horizontally at least 1 m (40 in), but may not extend more than 3 m (10 ft), beyond the external surface of the cask. Use of the minimum ring width of 1 meter yields a deeper pool for a fixed quantity of combustible fuel, thereby conservatively maximizing the fire duration.

4. The convection coefficient must be that value which may be demonstrated to exist if the cask were exposed to the fire specified. Based upon results of large pool fire thermal measurements [4.6.2], a conservative forced convection heat transfer coefficient of 4.5 Btu/(hr×ft^2×°F) is applied to exposed overpack surfaces during the short-duration fire.

Based on the 50 gallon fuel volume, the overpack outer diameter and the 1 m fuel ring width [4.6.1], the fuel ring surrounding the overpack covers 147.6 ft^2 and has a depth of 0.54 in. From this depth and a constant fuel consumption rate of 0.15 in/min, the fire duration is calculated to be 3.62 minutes. The fuel consumption rate of 0.15 in/min is a lowerbound value from a Sandia National Laboratories report [4.6.2]. Use of a lowerbound fuel consumption rate conservatively maximizes the duration of the fire.

To evaluate the impact of fire heating of the HI-STORM overpack, a thermal model of the overpack cylinder was constructed using the ANSYS computer code. The initial temperature of the overpack was conservatively assumed to be the maximum temperature field during storage (Table 4.4.7).. In this model the outer surface and top surface of the overpack were subjected for the duration of fire (3.62 minutes) to the fire conditions defined in this subsection. In the post-fire phase, the ambient conditions preceding the fire were restored. The transient study was conducted for a period of 5 hours, which is sufficient to allow temperatures in the overpack to reach their maximum values and begin to recede.

Due to the severity of the fire condition radiative heat flux, heat flux from incident solar radiation is negligible and is not included. Furthermore, the smoke plume from the fire would block most of the solar radiation. It is recognized that the ventilation air in contact with the inner surface of the HI-STORM Overpack with design-basis decay heat and normal ambient temperature conditions varies between 80°F at the bottom and 220°F at the top of the overpack. It is further recognized that the inlet and outlet ducts occupy a miniscule fraction of area of the cylindrical surface of the massive HI-STORM Overpack. Due to the short duration of the fire event and the relative isolation of the ventilation passages from the outside environment, the ventilation air is expected to experience little intrusion of the fire combustion products. As a result of these considerations, it is conservative to assume that the air in the HI-STORM Overpack ventilation passages is held constant at a substantially elevated temperature (300°F) during the entire duration of the fire event.

The thermal transient response of the storage overpack is determined using the ANSYS finite element program. Time-histories for points in the storage overpack are monitored for the duration of the fire and the subsequent post-fire equilibrium phase.

Heat input to the HI-STORM Overpack while it is subjected to the fire is from a combination of an incident radiation and convective heat fluxes to all external surfaces. This can be expressed by the following equation:

$$q_F = h_{fc}(T_A - T_S) + \sigma\varepsilon[(T_A + C)^4 - (T_S + C)^4]$$

where:

q_F =Surface Heat Input Flux (Btu/ft^2-hr)
h_{fc} = Forced Convection Heat Transfer Coefficient (4.5 Btu/ft^2-hr-°F)
σ = Stefan-Boltzmann Constant
T_A = Fire Temperature (1475°F)

C= Conversion Constant (460 (°F to °R))
T_S = Surface Temperature (°F)
ε = Average Emissivity (0.90 per 10 CFR 71.73)

The forced convection heat transfer coefficient is based on the results of large pool fire thermal measurements [4.6.2].

After the fire event, the ambient temperature is restored and the storage overpack cools down (post-fire temperature relaxation). Heat loss from the outer surfaces of the storage overpack is determined by the following equation:

$$q_S = h_S (T_S - T_A) + \sigma\varepsilon [(T_S + C)^4 - (T_A + C)^4]$$

where:

q_S =Surface Heat Loss Flux (W/m^2 (Btu/ft^2-hr))
h_S = Natural Convection Heat Transfer Coefficient (Btu/ft^2-hr-°F)
T_S = Surface Temperature (°F))
T_A = Ambient Temperature (°F)
σ = Stefan-Boltzmann Constant
ε = Surface Emissivity
C= Conversion Constant (460 (°F to °R))

In the post-fire temperature relaxation phase, h_s is obtained using literature correlations for natural convection heat transfer from heated surfaces [4.2.9].

During the fire the overpack external shell temperatures are substantially elevated (~550°F) and an outer layer of concrete approximately 1 inch thick reaches temperatures in excess of short term temperature limit. This condition is addressed specifically in NUREG-1536 (4.0,V,5.b), which states that:

> "The NRC accepts that concrete temperatures may exceed the temperature criteria of ACI 349 for accidents if the temperatures result from a fire."

These results demonstrate that the fire accident event analyzed in a most conservative manner is determined to have a minor affect on the HI-STORM Overpack. Localized regions of concrete are exposed to temperatures in excess of accident temperature limit. The bulk of concrete remains below the short term temperature limit. The temperatures of steel structures are within the allowable temperature limits.

Having evaluated the effects of the fire on the overpack, we now evaluate the effects on the MPC and contained fuel assemblies. Guidance for the evaluation of the MPC and its internals during a fire event is provided by NUREG-1536 (4.0,V,5.b), which states:

"For a fire of very short duration (i.e., less than 10 percent of the thermal time constant of the cask body), the NRC finds it acceptable to calculate the fuel temperature increase by assuming that the cask inner wall is adiabatic. The fuel temperature increase should then be determined by dividing the decay energy released during the fire by the thermal capacity of the basket-fuel assembly combination."

The time constant of the cask body (i.e., the overpack) can be determined using the formula:

$$\tau = \frac{c_p \times \rho \times L_c^2}{k}$$

where:

c_p = Overpack Specific Heat Capacity (Btu/lb-°F)
ρ = Overpack Density (lb/ft^3)
L_c = Overpack Characteristic Length (ft)
k = Overpack Thermal Conductivity (Btu/ft-hr-°F)

The concrete contributes the majority of the overpack mass and volume, so we will use the specific heat capacity (0.156 Btu/lb-°F), density (142 lb/ft^3) and thermal conductivity (1.05 Btu/ft-hr-°F) of concrete for the time constant calculation. The characteristic length of a hollow cylinder is its wall thickness. The characteristic length for the HI-STORM Overpack is therefore 29.5 in, or approximately 2.46 ft. Substituting into the equation, the overpack time constant is determined as:

$$\tau = \frac{0.156 \times 142 \times 2.46^2}{1.05} = 128\,hrs$$

One-tenth of this time constant is approximately 12.8 hours (768 minutes), substantially longer than the fire duration of 3.62 minutes, so the MPC is evaluated by considering the MPC canister as an adiabatic boundary. The fuel temperature rise is computed next.

Table 4.5.2 lists lower-bound thermal inertia values for the MPC and the contained fuel assemblies. Applying a conservative upperbound decay heat load (38 kW (1.3x10^5 Btu/hr)) and adiabatic heating for the 3.62 minutes fire, the fuel temperature rise computes as:

$$\Delta T_{fuel} = \frac{\text{Decay heat} \times \text{Time duration}}{\text{(MPC + Fuel) heat capacities}} = \frac{1.3 \times 10^5 \text{ Btu/hr} \times (3.62/60)hr}{(2240 + 4680) \text{ Btu/°}F} = 1.1°F$$

This is a very small increase in fuel temperature. Consequently, the impact on the MPC internal helium pressure will be quite small. Based on a conservative analysis of the HI-STORM 100 System response to a hypothetical fire event, it is concluded that the fire event does not adversely affect the temperature of the MPC or contained fuel. We conclude that the ability of the HI-STORM 100

System to cool the spent nuclear fuel within design temperature limits during and after fire is not compromised.

(b) HI-TRAC Fire

During the handling of the HI-TRAC transfer cask, the transporter fuel tank capacity must be limited to a 50 gallons. The duration of the 50-gallon fire under the conservatively postulated spill defined in the HI-STORM fire evaluation computes as 4.775 minutes. To demonstrate the fuel cladding and MPC pressure boundary integrity under exposure to this fire duration event during a fire accident analysis of the loaded 100-ton HI-TRAC is performed. In this analysis, the contents of the HI-TRAC are conservatively postulated to undergo a transient heat-up as a lumped mass from the decay heat input and heat input from the short duration fire. This analysis, because of the lower mass of the 100-ton HI-TRAC, bounds the effects for the 125-ton HI-TRAC. Using understated thermal inertia of the HI-TRAC and design maximum heat load (36.9 kW) the temperature rise rate computes as 5.553°F/min. Therefore, the temperature rise computed as the product of this rate and the fire duration reported above is 26.5°F. In this manner the maximum cladding temperature obtained by adding the temperature rise to the initial condition (See Table 4.5.6 for design basis heat load with X=3) computes as 811°F. The maximum fire temperature computed in the conservative manner above remains below the 1058°F accident temperature limit (Table 4.3.1) by substantial margins.

The elevated temperatures as a result of the fire accident will cause the pressure in the water jacket to increase and the overpressure relief valves to vent steam to the atmosphere. Based on the fire heat input to the water jacket, 11% of the water in the water jacket is boiled off. However, it is conservatively assumed, for dose calculations, that all the water in the water jacket is lost. In the 125-ton HI-TRAC, which uses Holtite in the lids for neutron shielding, the elevated fire temperatures would cause the Holtite to exceed its design accident temperature limits. This condition is conservatively addressed by ignoring neutron shield in the accident dose calculations.

Due to the increased temperatures of the MPC during fire accident the internal MPC pressure increases. The fire accident pressure is computed assuming the MPC cavity temperature rises by the fire accident temperature rise computed in this section. The result is tabulated in Table 4.6.2. The fire accident MPC pressure is substantially below the accident pressure limit (Table 2.2.1).

4.6.2.2 Jacket Water Loss

In this subsection, the fuel cladding and MPC boundary integrity is evaluated for a postulated loss of water from the HI-TRAC water jacket. The HI-TRAC is equipped with an array of water compartments filled with water. For a bounding analysis, all water compartments are assumed to lose their water and be replaced with air. Heat dissipation by natural convection and radiation in the air space is included in the thermal model. The HI-TRAC is assumed to have the maximum thermal payload (design heat load) and assumed to have reached steady state (maximum) temperatures. Under these assumed set of adverse conditions, the maximum temperatures are computed using the 3D HI-TRAC thermal model constructed in Section 4.5 with the water in water jacket spaces

replaced with air. The computed results are tabulated in Table 4.6.3 for the design basis heat load. The results of jacket water loss evaluation confirm that the cladding, MPC and HI-TRAC component temperatures are below the limits prescribed in Chapter 2 (Table 2.2.3). The co-incident MPC pressure is also computed and compared with the MPC accident design pressure (Table 2.2.1). The result (Table 4.6.2) is confirmed to be below the limit.

4.6.2.3 Extreme Environmental Temperatures

To evaluate the effect of extreme weather conditions, an extreme ambient temperature (Table 2.2.2) is postulated to persist for a 3-day period. For a conservatively bounding evaluation the extreme temperature is assumed to last for a sufficient duration to allow the HI-STORM 100 System to reach steady state conditions. Because of the large mass of the HI-STORM 100 System, with its corresponding large thermal inertia and the limited duration for the extreme temperature, this assumption is conservative. Starting from a baseline condition evaluated in Section 4.4 (normal ambient temperature and limiting fuel storage configuration) the temperatures of the HI-STORM 100 System are conservatively assumed to rise by the difference between the extreme and normal ambient temperatures (45°F). The HI-STORM extreme ambient temperatures computed in this manner are reported in Table 4.6.4. The co-incident MPC pressure is also computed (Table 4.6.2) and compared with the accident design pressure (Table 2.2.1). The result is confirmed to be below the accident limit.

4.6.2.4 100% Blockage of Air Inlets

This event is defined as a complete blockage of all four bottom inlets. The immediate consequence of a complete blockage of the air inlets is that the normal circulation of air for cooling the MPC is stopped. An amount of heat will continue to be removed by localized air circulation patterns in the overpack annulus and outlet ducts, and the MPC will continue to radiate heat to the relatively cooler storage overpack. As the temperatures of the MPC and its contents rise, the rate of heat rejection will increase correspondingly. Under this condition, the temperatures of the overpack, the MPC and the stored fuel assemblies will rise as a function of time.

As a result of the considerable inertia of the storage overpack, a significant temperature rise is possible if the inlets are substantially blocked for extended durations. This accident condition is, however, a short duration event that is identified and corrected through scheduled periodic surveillance. Nevertheless, this event is conservatively analyzed assuming a substantial duration of blockage. The event is analyzed using the FLUENT CFD code. For MPC heat load up to the full design basis, the HI-STORM thermal model is the same 3-Dimensional model constructed for normal storage conditions (see Section 4.4) except for the bottom inlet ducts, which are assumed to be impervious to air. Using this model, a transient thermal solution of the HI-STORM 100 System starting from normal storage conditions is obtained. The results of the blocked ducts transient analysis are presented in Table 4.6.5 and confirmed to be below the accident temperature limits (Table 2.2.3). The co-incident MPC pressure is also computed and compared with the accident design pressure (Table 2.2.1). The result (Table 4.6.2) is confirmed to be below the limit.

For MPC heat loads which meet the values in Table 4.5.7 or 4.5.8, the results of the transient analysis that support the required action completion times for clearing the inlets are presented in Table 4.6.7 and confirm all temperatures are below the accident temperature limits (Table 2.2.3).

4.6.2.5 Burial Under Debris

Burial of the HI-STORM 100 System under debris is not a credible accident. During storage at the ISFSI there are no structures over the casks. Minimum regulatory distances from the ISFSI to the nearest ISFSI security fence precludes the close proximity of substantial amount of vegetation. There is no credible mechanism for the HI-STORM 100 System to become completely buried under debris. However, for conservatism, complete burial under debris is considered.

To demonstrate the inherent safety of the HI-STORM 100 System, a bounding analysis that considers the debris to act as a perfect insulator is considered. Under this scenario, the contents of the HI-STORM 100 System will undergo a transient heat up under adiabatic conditions. The minimum available time ($\Delta\tau$) for the fuel cladding to reach the accident limit depends on the following: (i) thermal inertia of the cask, (ii) the cask initial conditions, (iii) the spent nuclear fuel decay heat generation and (iv) the margin between the initial cladding temperature and the accident temperature limit. To obtain a lowerbound on $\Delta\tau$, the HI-STORM 100 Overpack thermal inertia (item i) is understated, the cask initial temperature (item ii) is maximized, decay heat overstated (item iii) and the cladding temperature margin (item iv) is understated. A set of conservatively postulated input parameters for items (i) through (iv) are summarized in Table 4.6.6. Using these parameters $\Delta\tau$ is computed as follows:

$$\Delta\tau = \frac{m \times c_p \times \Delta T}{Q}$$

where:

$\Delta\tau$ = Allowable burial time (hr)
m = Mass of HI-STORM System (lb)
c_p = Specific heat capacity (Btu/lb-°F)
ΔT = Permissible temperature rise (°F)
Q = Decay heat load (Btu/hr)

Substituting the parameters in Table 4.6.6, a substantial burial time (34.6 hrs) is obtained. The co-incident MPC pressure is also computed and compared with the accident design pressure (Table 2.2.1). The result (Table 4.6.2) is confirmed to be below the limit.

Table 4.6.1
OFF-NORMAL CONDITION MAXIMUM
HI-STORM TEMPERATURES[3]

Location[4]	Off-Normal Ambient Temperature[5] (°F)	Partial Inlet Ducts Blockage (°F)
Fuel Cladding	731	725
MPC Basket	728	721
MPC Shell	489	478
Overpack Inner Shell	342	339
Lid Concrete Bottom Plate	322	321
Lid Concrete Section Temperature	266	260

[3] The temperatures reported in this table are below the off-normal temperature limits specified in Chapter 2, Table 2.2.3.
[4] Temperatures of limiting components reported.
[5] Obtained by adding the off-normal-to-normal ambient temperature difference of 20°F (11.1°C) to normal condition HI-STORM temperatures reported in Section 4.4.

Table 4.6.2

OFF-NORMAL AND ACCIDENT CONDITION MAXIMUM MPC PRESSURES FOR DESIGN BASIS HEAT LOAD

Condition	Pressure (psig)
Off-Normal Conditions	
Off-Normal Ambient	101.4
Partial Blockage of Inlet Ducts	100.4
Accident Conditions	
Extreme Ambient Temperature	104.4
100% Blockage of Air Inlets	118.1
Burial Under Debris	134.8
HI-TRAC Fire Accident	106.2
HI-TRAC Jacket Water Loss	108.6

Table 4.6.3
HI-TRAC JACKET WATER LOSS ACCIDENT MAXIMUM
TEMPERATURES FOR DESIGN BASIS HEAT LOAD

Component	Temperature (°F)	
	X = 0.5	X =3
Fuel Cladding	811	837
MPC Basket	808	829
MPC Shell	514	496
HI-TRAC Inner Shell	365	342
HI-TRAC Radial Lead Gamma Shield	363	342
HI-TRAC Water Jacket Shell	289	271
HI-TRAC Lid Neutron Shield Section Average	304	309

Table 4.6.4
EXTREME ENVIRONMENTAL CONDITION MAXIMUM
HI-STORM TEMPERATURES

Component	Temperature[6] (°F)
Fuel Cladding	756
MPC Basket	753
MPC Shell	514
Overpack Inner Shell	367
Lid Concrete Bottom Plate	347
Lid Concrete Section Temperature	291

6 Obtained by adding the extreme ambient to normal temperature difference (45°F) to normal condition temperatures reported in Section 4.4.

Table 4.6.5

32-HOURS BLOCKED INLET DUCTS MAXIMUM HI-STORM TEMPERATURES FOR DESIGN BASIS HEAT LOAD

Component	Temperatures@32 hrs (°F)
Fuel Cladding	890
MPC Basket	884
MPC Shell	583
Overpack Inner Shell	480
Lid Concrete Bottom Plate	433
Lid Concrete Section Temperature	328

Table 4.6.6

SUMMARY OF INPUTS FOR BURIAL UNDER DEBRIS ANALYSIS

Thermal Inertia Inputs: M (Lowerbound HI-STORM 100 Weight) Cp (Carbon steel heat capacity)[7]	 150000 lb 0.1 Btu/lb-°F
Cask initial temperature[8]	728°F
Q (Decay heat)	1.3×10^5 Btu/hr
ΔT (clad temperature margin)[9]	300°F

[7] Carbon steel has the lowest heat capacity among the principal materials employed in MPC and overpack construction (carbon steel, stainless steel and concrete).

[8] Conservatively overstated.

[9] The clad temperature margin is conservatively understated in this table.

Table 4.6.7
SUMMARY OF BLOCKED AIR INLET DUCT EVALUATION RESULTS FOR MPC HEAT LOAD UP TO 28.74 kW

	Max. Initial Steady-State Temp. [†] **(°F)**	**Temperature Rise (°F)**		**Transient Temperature (°F)**	
		at 33 hrs	at 72 hrs	at 33 hrs	at 72 hrs
Fuel Cladding	740	101	160	841	900
MPC Shell	351	184	250	535	601
Overpack Inner Shell #1[††]	199	113	174	312	373
Overpack Inner Shell #2[†††]	155	193	286	348	441
Overpack Outer Shell	145	14	40	159	185
Concrete Section Average	172	79	141	251	313

[†] Conservatively bounding temperatures reported includes a hypothetical rupture of 10% of the fuel rods.

[††] Coincident with location of initial maximum temperature.

[†††] Coincident with active fuel axial mid-height.

4.7 REGULATORY COMPLIANCE

4.7.1 Normal Conditions of Storage

NUREG-1536 [4.4.1] and ISG-11 [4.1.4] define several thermal acceptance criteria that must be applied to evaluations of normal conditions of storage. These items are addressed in Sections 4.1 through 4.4. Each of the pertinent criteria and the conclusion of the evaluations are summarized here.

As required by ISG-11 [4.1.4], the fuel cladding temperature at the beginning of dry cask storage is maintained below the anticipated damage-threshold temperatures for normal conditions for the licensed life of the HI-STORM System. Maximum clad temperatures for long-term storage conditions are reported in Section 4.4.

As required by NUREG-1536 (4.0,IV,3), the maximum internal pressure of the cask remains within its design pressure for normal, off-normal, and accident conditions, assuming rupture of 1 percent, 10 percent, and 100 percent of the fuel rods, respectively. Assumptions for pressure calculations include release of 100 percent of the fill gas and 30 percent of the significant radioactive gases in the fuel rods. Maximum internal pressures are reported in Sections 4.4, 4.5 and 4.6 for normal, short term operations, and off-normal & accident conditions. Design pressures are summarized in Table 2.2.1.

As required by NUREG-1536 (4.0,IV,4), all cask and fuel materials are maintained within their minimum and maximum temperature for normal and off-normal conditions in order to enable components to perform their intended safety functions. Maximum and minimum temperatures for long-term storage conditions are reported in Section 4.4. Design temperature limits are summarized in Table 2.2.3. HI-STORM System components defined as important to safety are listed in Table 2.2.6.

As required by NUREG-1536 (4.0,IV,5), the cask system ensures a very low probability of cladding breach during long-term storage. For long-term normal conditions, the maximum CSF cladding temperature is below the ISG-11 [4.1.4] limit of 400°C (752°F).

As required by NUREG-1536 (4.0,IV,7), the cask system is passively cooled. All heat rejection mechanisms described in this chapter, including conduction, natural convection, and thermal radiation, are completely passive.

As required by NUREG-1536 (4.0,IV,8), the thermal performance of the cask is within the allowable design criteria specified in FSAR Chapters 2 and 3 for normal conditions. All thermal results reported in Section 4.4 are within the design criteria allowable ranges for all normal conditions of storage.

4.7.2 Short Term Operations

Evaluation of short term operations is presented in Section 4.5. This section establishes complete compliance with the provisions of ISG-11 [4.1.4]. In particular, the ISG-11 requirement to ensure that maximum cladding temperatures under all fuel loading and short term operations be below 400°C (752°F) for high burnup fuel and below 570°C (1058°F) for moderate burnup fuel is demonstrated as stated below.

Specifically as required by ISG-11, the fuel cladding temperature is maintained below the applicable limits for HBF and MBF (Table 4.3.1) during short term operations.

As required by NUREG-1536 (4.0,IV,3), the maximum internal pressure of the cask remains within its design pressure for normal and off-normal conditions, assuming rupture of 1 percent and 10 percent of the fuel rods, respectively. Assumptions for pressure calculations include release of 100 percent of the fill gas and 30 percent of the significant radioactive gases in the fuel rods.

As required by NUREG-1536 (4.0,IV, 4), all cask and fuel materials are maintained within their minimum and maximum temperature for all short term operations in order to enable components to perform their intended safety functions.

As required by NUREG-1536 (4.0,IV,8), the thermal performance of the cask is within the allowable design criteria specified in FSAR Chapters 2 and 3 for all short term operations.

4.8 REFERENCES

[4.1.1] ANSYS Finite Element Modeling Package, Swanson Analysis Systems, Inc., Houston, PA, 1993.

[4.1.2] FLUENT Computational Fluid Dynamics Software, Fluent, Inc., Centerra Resource Park, 10 Cavendish Court, Lebanon, NH 03766.

[4.1.3] "The TN-24P PWR Spent-Fuel Storage Cask: Testing and Analyses," EPRI NP-5128, (April 1987).

[4.1.4] "Cladding Considerations for the Transportation and Storage of Spent Fuel," Interim Staff Guidance – 11, Revision 3, USNRC, Washington, DC.

[4.1.5] "Topical Report on the HI-STAR/HI-STORM Thermal Model and its Benchmarking with Full-Size Cask Test Data," Holtec Report HI-992252, Revision 1, Holtec International, Marlton, NJ, 08053.

[4.1.6] "Identifying the Appropriate Convection Correlation in FLUENT for Ventilation Air Flow in the HI-STORM System", Holtec Report HI-2043258, Holtec International, Marlton, NJ, 08053.

[4.1.7] "Performance Testing and Analyses of the VSC-17 Ventilated Concrete Cask", EPRI TR-100305, (May 1992).

[4.2.1] Baumeister, T., Avallone, E.A. and Baumeister III, T., "Marks' Standard Handbook for Mechanical Engineers," 8th Edition, McGraw Hill Book Company, (1978).

[4.2.2] Rohsenow, W.M. and Hartnett, J.P., "Handbook of Heat Transfer," McGraw Hill Book Company, New York, (1973).

[4.2.3] Creer et al., "The TN-24P Spent Fuel Storage Cask: Testing and Analyses," EPRI NP-5128, PNL-6054, UC-85, (April 1987).

[4.2.4] Rust, J.H., "Nuclear Power Plant Engineering," Haralson Publishing Company, (1979).

[4.2.5] Kern, D.Q., "Process Heat Transfer," McGraw Hill Kogakusha, (1950).

[4.2.6] "A Handbook of Materials Properties for Use in the Analysis of Light Water Reactor Fuel Rod Behavior," NUREG/CR-0497, (August 1981).

[4.2.7] "Spent Nuclear Fuel Effective Thermal Conductivity Report," US DOE Report BBA000000-01717-5705-00010 REV 0, (July 11, 1996).

[4.2.8] ASME Boiler and Pressure Vessel Code, Section II, Part D, (1995).

[4.2.9] Jakob, M. and Hawkins, G.A., "Elements of Heat Transfer," John Wiley & Sons, New York, (1957).

[4.2.10] ASME Steam Tables, 3rd Edition (1977).

[4.2.11] "Nuclear Systems Materials Handbook, Vol. 1, Design Data", ORNL TID 26666.

[4.2.12] "Scoping Design Analyses for Optimized Shipping Casks Containing 1-, 2-, 3-, 5-, 7-, or 10-Year-Old PWR Spent Fuel", ORNL/CSD/TM-149 TTC-0316, (1983).

[4.2.13] "Holtite A: Development History and Thermal Performance Data", Holtec Report HI-2002396, Rev. 3., Holtec International, Marlton, NJ, 08053.

[4.2.14] "Qualification of METAMIC for Spent-Fuel Storage Application", EPRI Report 1003137, (October 2001), EPRI, Palo Alto, CA.

[4.2.15] "Sourcebook for METAMIC Performance Assessment", Holtec Report HI-2043215, Holtec International, Marlton, NJ, 08053.

[4.2.16] USNRC Docket no 72-1027, TN-68 FSAR & Docket no 72-1021 TN-32 FSAR.

[4.2.17] Hagrman, Reymann and Mason, "MATPRO-Version 11 (Revision 2) A Handbook of Materials Properties for Use in the Analysis of Light Water Reactor Fuel Rod Behavior," NUREG/CR-0497, Tree 1280, Rev. 2, EG&G Idaho, August 1981.

[4.2.18] "Effective Thermal Conductivity and Edge Conductance Model for a Spent-Fuel Assembly," R. D. Manteufel & N. E. Todreas, Nuclear Technology, 105, 421- 440, (March 1994).

[4.3.1] Lanning and Beyer, "Estimated Maximum Cladding Stresses for Bounding PWR Fuel Rode During Short Term Operations for Dry Cask Storage," PNNL White Paper, (January 2004).

[4.4.1] NUREG-1536, "Standard Review Plan for Dry Cask Storage Systems," USNRC, (January 1997).

[4.4.2] "Pressure Loss Charactersistics for In-Cell Flow of Helium in PWR and BWR Storage Cells", Holtec Report HI-2043285, Holtec International, Marlton, NJ, 08053.

[4.5.1] "HI-STORM THERMAL-HYDRAULIC ANALYSES SUPPORTING UP TO 36.9 KW HIGH HEAT LOAD AMENDMENT", Holtec Report HI-2043317, Revsion 18.

[4.5.2] HI-STORM FW FSAR, Holtec Report HI-2084239, Rev. 1, Section 3.4.4.1.11, Docket No. 72-1032.

[4.6.1] United States Code of Federal Regulations, Title 10, Part 71.

[4.6.2] Gregory, J.J. et. al., "Thermal Measurements in a Series of Large Pool Fires", SAND85-1096, Sandia National Laboratories, (August 1987).

APPENDIX 4.A:

INTENTIONALLY DELETED

APPENDIX 4.B

[Intentionally Deleted]

SUPPLEMENT 4.I[1]

THERMAL EVALUATION OF THE HI-STORM 100U SYSTEM

4.I.0 OVERVIEW

The HI-STORM 100U is an underground vertical ventilated module (VVM) with openings for air ingress and egress and internal passages for ventilation cooling of loaded MPCs. The HI-STORM 100U construction is described in Supplement 1.I and illustrated in Figures 1.I.1 through 1.I.4. The HI-STORM 100U utilize the same MPCs used in the aboveground systems. The HI-STORM 100U inlets and outlets are 360° (axisymmetric) openings provided in the lid. The overall ventilation airflow path from inlet to outlet is illustrated in Figure 1.I.4. The licensing drawing package for the HI-STORM 100U VVM is provided in Section 1.I.5. This supplement provides a thermal evaluation of the HI-STORM 100U for normal, off-normal and accident conditions. The evaluations described herein parallel those of the aboveground HI-STORM cask contained in the main body of Chapter 4 of this FSAR. To ensure readability, the section in the main body of the chapter to which each section in this supplement corresponds is clearly identified. All tables in this supplement are labeled sequentially.

4.I.1 INTRODUCTION

The information presented in this supplement is intended to serve as a complement to the information provided in the main body of Chapter 4. Thus, information in Chapter 4 that remains applicable to the HI-STORM 100U is not repeated herein. Specifically, the following information in the main body of Chapter 4 is not repeated:

1. The thermal properties of materials in Section 4.2 applicable to the HI-STORM 100U System.

2. The specifications for components in Section 4.3 applicable to the HI-STORM 100U System.

3. The descriptions of the thermal modeling of the MPC and its internals, including fuel assemblies, in Section 4.4 which are applicable in their entirety to the HI-STORM 100U.

4. The descriptions of the short-term loading operations, carried out using the HI-TRAC transfer cask, in Section 4.5 which remain applicable in their entirety to the HI-STORM 100U.

As confirmed by appropriate supporting analyses, the heat rejection capability of the HI-STORM 100U System is essentially equivalent to its aboveground counterparts for quiescent conditions (strictly speaking, slightly better, because of the larger intake and outlet passages located in the

[1] For ease of supplement review the sections are numbered in parallel with the main Chapter 4.

VVM lid). Further, its underground configuration renders its resistance to accident events such as fire greater than that of aboveground casks.

4.I.2 THERMAL PROPERTIES OF MATERIALS[1]

The material properties compiled in Section 4.2 of the FSAR provide the required information, except for the material properties of thermal insulation and soil surrounding the HI-STORM 100U VVM, which is not present in the aboveground designs. The functional performance of insulation (applied on the cylindrical surface of the divider shell) is ensured by specifying a minimum thermal resistance. The thermal resistance is defined in conventional US units as the insulation temperature gradient (^{o}F) per unit rate of heat loss (Btu/ft^2-hr). To compute insulation resistance the insulation thickness is divided by the insulation thermal conductivity. The maximum acceptable conductivity of insulating material is obtained by dividing the insulation thickness by the specified thermal resistance. For use in transient evaluations, the density and specific heat capacity of the insulation are conservatively assumed to be the same as that of air. Property data on insulation and soil is provided in Table 4.I.1.

4.I.3 SPECIFICATIONS FOR COMPONENTS[2]

All applicable material temperature limits in Section 4.3 of the FSAR continue to apply to the HI-STORM 100U. Temperature limits for insulation (used only in the HI-STORM 100U VVM) are specified in Table 2.I.8.

4.I.4 THERMAL EVALUATION FOR NORMAL CONDITIONS OF STORAGE[3]

4.I.4.1 HI-STORM 100U Thermal Model

The HI-STORM 100U underground cask, like the aboveground overpack, is a vertical storage system designed to dissipate heat by ventilation cooling. The principal cask components - container shell, closure lid, support foundation and MPC - are shown in Figure 1.I.1. Internal cask details relevant to cask operation are shown in Figure 1.I.2. The cooling passages in the HI-STORM 100U cask is shown in Figure 1.I.4. As shown in this figure the cask lid is engineered with 360^{o} air inlet and outlet openings. During storage, air enters the inlet opening and flows downwards in the outer annulus gap between the cask container shell and the divider shell. The divider shell is insulated to avoid heating of this incoming air. Near the bottom of the cask cavity, the air U-turns and flow upwards in the inner annulus gap between the MPC and divider shell. During its upward travel, the air extracts heat from the heat generating MPC cylinder. A concomitant effect of heat removal is the monotonic heating of air in the inner annulus. Near the top of the MPC the air enters the internal flow passages in the closure lid. Heated air exits from the vents openings in the top of the closure lid. To model the ventilation cooling engineered in

[1] This section supplements Section 4.2.
[2] This section supplements Section 4.3.
[3] This section supplements Section 4.4.

the underground cask, a 3-D thermal model of the HI-STORM 100U VVM is constructed as described next.

In this Supplement the HI-STORM 100U System consisting of the HI-STORM100U VVM and a loaded MPC is evaluated under normal, off-normal and accident conditions and during short-term operations. The thermal evaluations use the same aboveground MPC 3-D thermal models of the bounding PWR and BWR canisters (MPC-32 and MPC-68) situated in an underground 100U VVM. These models use the same 3-Zone porous media model used in the thermal analysis for the aboveground Overpack (HI-STORM 100S[1]) to represent the flow resistance of bounding BWR (GE-10x10) and PWR (W-17x17) fuel assemblies (See Chapter 4, Subsection 4.4.1.2).

The key attributes of MPC thermal model are as follows:

1. The MPC is modeled as a geometrically accurate 3D array of square shaped cells inside a cylindrical shell with bottom and top closures. The fuel basket bottom and top mouseholes are explicitly modeled as rectangular openings with understated flow area. The MPC model is identical to that described in the main body of Chapter 4.

2. The helium flow within the MPC is modeled as laminar. This is the same modeling approach used in the aboveground cask analyses.

3. The hydraulic resistance of the fuel assemblies stored within the MPC is represented in the 3D model by 3-Zone porous media flow resistances. This is the same as used in the HI-STORM aboveground modeling (See Chapter 4, Subsection 4.4.1.2).

Consistent with the aboveground HI-STORM 100S Overpack modeling a geometrically accurate 3D model of the HI-STORM 100U VVM is constructed for thermal analysis of the belowground casks. The VVM lid with its inlet and outlet vents and internal flow passages, the inner and outer annulus, the U-turn and the gas plenum above the MPC are explicitly modeled. Access to ambient air is artificially restricted in the model by erecting a vertical cylinder above the VVM. The cylinder is open at the top to allow air ingress and exit. In this manner lateral access to air is blocked and the potential for hot air mixing above the VVM is maximized.

The airflow through the cooling passages of the VVM is modeled as turbulent, using the k-ω model with transitional option as recommended in the Holtec-proprietary benchmarking report [4.1.6]. This is the same modeling approach as used in the aboveground cask analyses. The underside of the VVM foundation pad (see Figure 1.I.1) is assumed to be supported on a subgrade at 77°F. This is the same boundary condition applied to the bottom of the ISFSI pad for the aboveground cask modeling in Section 4.4. For conservatism heat dissipation from the vertical surfaces of the VVM is suppressed by the assumption of zero heat flux model

[1] The aboveground HI-STORM System includes a classical overpack design (HI-STORM 100) and a shortened version (HI-STORM 100S). The limiting design (HI-STORM 100S) is used in the aboveground thermal analysis.

boundaries. The VVM thermal models are constructed using the same modeling platform used for aboveground analysis (FLUENT version 6.2).

4.I.4.2 Thermal Analysis

The HI-STORM 100U System design has been designed with the objective of ensuring that it meets all temperature and pressure limits set forth in Chapter 2 and Supplement 2.I. In this supplement the HI-STORM 100U System is evaluated to demonstrate compliance with these limits.

The 100U is evaluated under an array of uniform and regionalized heat loads defined in Chapter 2 as a function of regionalization parameter X. To determine the most limiting heat load configuration an array of analyses are performed for the principal storage condition – long-term normal storage and fuel temperatures computed. The results of the analysis for the bounding PWR and BWR canisters (MPC-32 and MPC-68) are summarized in Table 4.I.2. The results show the following:

i) The fuel temperatures in the underground VVM are essentially the same as or slightly better than fuel temperatures in the aboveground storage overpack (See Table 4.4.6).
ii) The highest fuel temperatures are reached under regionalized storage at X = 0.5 (same as in the case of the aboveground (HI-STORM 100S) overpack).
iii) Higher fuel temperatures are reached in MPC-32 (same as in the case of the aboveground (HI-STORM 100S) Overpack).
iv) Fuel storage in the MPC-32 under regionalized fuel storage at X=0.5 is the limiting scenario for 100U System. This scenario is co-incident with the maximum permissible MPC heat load and therefore temperatures of other sub-systems (such as fuel basket, MPC and VVM) also reach their highest values. This result is also in keeping with the HI-STORM 100S solution presented in Section 4.4 in the main body of Chapter 4. Accordingly, this condition is adopted for evaluation of normal, off-normal and accident events and short-term operations.

Table 4.I.3 presents the HI-STORM 100U maximum temperatures and pressures for the limiting fuel storage scenario defined above. The results are below the Chapter 2 and Supplement 2.I temperature and pressure limits for normal storage.

4.I.4.3 Effect of Elevation

An evaluation of the effects of elevation on thermal performance is performed for the HI-STORM 100U. The methodology described in Subsection 4.4.4.3 is applied for the HI-STORM 100U evaluation. The peak cladding temperatures are calculated for a bounding configuration (non-uniform storage at X = 0.5) assuming no reduction of ambient temperature with elevation and compared to the sea level conditions. The results are given in the Table 4.I.4. The results show that the PCT, including the effects of site elevation, continues to be well below the regulatory cladding temperature limit of 752°F for quiescent conditions. In light of the above

evaluation, it is not necessary to place any ISFSI elevation constraints for HI-STORM deployment at elevations up to 1500 feet that have quiescent conditions. If, however, an ISFSI is sited at an elevation greater than sea level with non-quiescent conditions, the effect of altitude on the PCT shall be quantified as part of the 10 CFR 72.212 evaluation for the site using the site ambient and wind conditions.

4.I.4.4 Wind Conditions

Non-quiescent ambient conditions defined as a horizontal wind on an isolated HI-STORM 100U module is evaluated. These evaluations conservatively assume a unidirectional wind of sufficient duration for the HI-STORM 100U System to reach the asymptotic maximum (steady-state) temperatures. This event is evaluated using the 3D thermal model mentioned in the foregoing (in Section 4.I.4.1). To properly model wind effects, a half-symmetric model is constructed and non-quiescent ambient conditions modeled as a horizontal wind blowing into the HI-STORM 100U inlet and outlet openings from one direction. Because the 100U ventilation openings are axisymmetric the maximum cladding temperature from a wind of a certain velocity is the same regardless of direction. However, under a wind condition, the fuel rod subject to the maximum cladding temperature migrates downstream from the canister's axis of symmetry. Thus, even though the spatial peak cladding temperature remains the same as the wind velocity vector is rotated, the location of the peak changes. Thus, for steady state conditions to be reached, the wind velocity vector (magnitude and direction, and sense of action) must remain constant for a long enough time to enable steady state conditions to be reached. The wind model is used to compute fuel temperatures at several wind speeds and results are tabulated in Table 4.I.7 for the case of X=3, which corresponds to 30.17 kW. The results show that, depending on magnitude of the wind velocity vector, the peak cladding temperature may be above or below the temperature corresponding to the quiescent condition. In particular, the 5 mph wind is identified as being in the narrow range where the peak cladding temperature plateaus to its maximum value.

In recognition of the new design embodiment of HI-STORM 100U, the design basis heat load for the system is based on the assumption that the 5 mph horizontal wind velocity vector prevails for a sufficiently long time. Further, the inlet air temperature into the plenum is assumed to be elevated by 7°K (or 12.6°F) due to intermixing from the presence of other modules in the ISFSI array. This assumption has the effect of raising the design basis inlet air temperature to 92.6°F (from the quiescent condition reference value of 80°F).

Furthermore, an inspection of the thermal results for the quiescent condition cases in Table 4.I.2 indicates that the case of X = 0.5 produces the largest peak cladding temperature (6°F more than other values of X). Therefore X = 0.5 case is used for the thermal analysis. Finally, because the MPC-32 case yields maximum value of the peak cladding temperature (see Table 4.I.2), MPC-32 is selected for computing the allowable heat load. Thus, the thermal problem posed herein assumes that:

i. A 5 mph horizontal wind (constant speed and direction) is blowing.

ii. The inlet air is at 92.6°F (not 80°F as assumed in the aboveground HI-STORM simulations), to factor the effect of limited mixing of the feed air with heated exhaust air streams.

iii. The VVM contains a loaded MPC-32 with the most adverse regionalized storage condition (i.e., X = 0.5).

iv. For the aboveground system, using Paragraph 2.I.9.1, the aggregate heat load and specific heat loads in Regions 1 and 2 are computed as follows:

Q_d = 36.9 kW
q_1 = 0.709 kW
q_2 = 1.419 kW

Therefore, the thermal problem for the constant adverse wind velocity vector case is posed as follows:

Determine the penalty factor α on Q_d such that the computed peak cladding temperature is bounded by 400°C.

The penalty factor α is computed under the most punitive fuel loading scenario corresponding to X = 0.5 wherein the highest peak cladding temperature is reached as discussed in subsection 4.I.4.2. It therefore follows by physical reasoning that α computed in this manner is bounding under fuel loading scenarios X = 1, 2 and 3 defined in Chapter 2, Paragraph 2.1.9.1. As described later in this section α is conservatively adopted to penalize the maximum permissible heat loads under X = 1, 2 and 3.

The following peak cladding temperatures were calculated for the above problem for the two different heat loads:

Q_d (kW)	Maximum Cladding Temperature, °C
36.9	423.7
35.05	408.8

By examining the trend of the two cladding temperatures for Q, an approximately 1 kW additional penalty is taken to reduce the maximum allowable heat load to 33kW, which results in a temperature of approximately 390°C considering the trend in temperature change. This examination of temperature trend, including the 10 degree margin below 400°C, affirms the requirements for cladding integrity are satisfied for this design. Therefore, the penalty factor α = 33/36.9 = 0.894.

The design basis heat load for the range of uniform and regionalized fuel storage scenarios defined in Chapter 2 Paragraph 2.1.9.1 are reduced as shown below:

X	Penalized Heat Load ($Qr=\alpha \cdot Q$) (kW)
0.5	$\alpha \cdot 36.9$ kW = 33.0 kW
1	$\alpha \cdot 34$ kW = 30.4 kW
2	$\alpha \cdot 31.48$ kW = 28.1 kW
3	$\alpha \cdot 30.17$ kW = 27.0 kW

This reduced heat load Q_r satisfies the requirement that the peak cladding temperature meet the 400°C under the constant adverse wind velocity vector case. This reduced value of the design basis heat load is conservatively adopted in the system Technical Specification for the "100U' model only.

4.I.5 THERMAL EVALUATION OF SHORT TERM OPERATIONS

The short-term evaluations presented in Section 4.5 are applicable in their entirety for the underground VVM.

4.I.6 THERMAL EVALUATION OF OFF-NORMAL AND ACCIDENT CONDITIONS[1]

4.I.6.1 Off-Normal Conditions

(a) Elevated Ambient Air Temperature

The elevated ambient air temperature off-normal condition is defined in Table 2.I.1 as an ambient temperature of 100°F. This is 20°F higher than the normal condition ambient temperature of 80°F, also defined in Table 2.I.1 and used in the analyses described in Section 4.I.4.2 above. This condition is conservatively evaluated by adding 20°F to the calculated normal condition fuel cladding and component temperatures in Table 4.I.3. Results for this off-normal condition are presented in Table 4.I.5. The results are well below the permissible short-term temperature limits for fuel cladding, concrete, and structural steels.

(b) Partial Blockage of Air Inlets

In contrast to HI-STORM 100S, which features four inlet and four outlet vents, HI-STORM 100U has 360° (radially symmetric) vents making duct blockage in HI-STORM 100U more unlikely. Nevertheless, the case of 50% blockage of the HI-STORM 100U inlet vents is postulated. The partial air inlets blockage event is defined in Table 2.I.1 as the blockage of 50% of the air inlet flow area. This event is conservatively evaluated as a blockage of sufficient duration to reach the asymptotic maximum (steady-state) temperature field. Results for this off-

[1] This section supplements Section 4.6.

normal condition are presented in Table 4.I.6. The results show large margins of safety with respect to the permissible short-term temperature limits for fuel cladding, concrete, and structural steels.

4.I.6.2 Accident Conditions

(a) Fire

The fire accident is defined in Table 2.I.1 as a 1475°F fire lasting 217 seconds. This is the same intensity and duration as the fire accident evaluated in Section 4.6 of this FSAR for the aboveground overpack. The existing fire evaluation therein bounds the HI-STORM 100U fire event, for the following reasons:

1. Because the fire evaluated in Section 4.6 is an engulfing fire, the cask area exposed to the fire heat flux is maximized. The underground surfaces of the HI-STORM 100U VVM are not directly exposed to the fire heat flux, which significantly reduces the fire heat input to the VVM as compared to an aboveground overpack. The total heat input to the VVM during the fire event is therefore much lower than is evaluated in Section 4.6.

2. The openings of the inlet ducts and outlet ducts are both located near the top of the VVM. Because heated gases rise, a downward flow of combustion gases into the module cavity is not credible. The internal surfaces of the VVM cannot, therefore, be subjected to any significant temperature elevation due to fire.

The above considerations lead to the conclusion that the fire evaluation for the aboveground overpack bounds the HI-STORM 100U fire accident.

(b) Flood

The flood accident is defined in Table 2.I.1 as a deep submergence. The worst flood from a thermal perspective is a "smart flood" that just prevents all airflow with *no* MPC cooling by water. Although the HI-STORM 100U includes design features to prevent "smart flood" occurrence such a hypothetical condition is bounded by the 100% inlet ducts blocked accident evaluated in 4.I.6.2(d). As shown in the HI-STORM 100U licensing drawings, the bottom of the MPC is situated several inches below the top of the airflow cutouts in the bottom of the divider shell. Thus, even if the bottom cutouts are substantially covered by flood water the MPC baseplate heat dissipation ensures adequate cooling of the MPC and its stored fuel. This effect is significant, because the thermosiphon convective flow within the MPC is an efficient means of heat rejection to the thermal sink (wetted baseplate).

(c) Burial Under Debris

The burial under debris accident is defined in Table 2.I.1 as an adiabatic heat-up at the maximum decay heat load. The existing burial under debris evaluation in Section 4.6 bounds the HI-

STORM 100U burial under debris event because the HI-STORM 100U System thermal inertia is greater than that of the aboveground systems. This results from the higher aggregate mass of the VVM as compared to the aboveground overpack. As such the existing burial under debris evaluation for the aboveground overpack bounds the HI-STORM 100U burial under debris accident.

(d) 100% Blockage of Air Ducts

The 100% air ducts blockage accident is defined in Table 2.I.1 as the blockage of 100% of the air inlet duct flow area. This event is evaluated by blocking the entire inlet opening for a considerable duration (24 hours) and performing a transient calculation of VVM, MPC and cladding temperatures. The only difference between this evaluation and the evaluation described in Section 4.I.4.2 for normal storage is the blockage of the inlet vents and the inclusion of transient effects in the 3D HI-STORM 100U model. Numerical results for this accident are presented in Table 4.I.9. The results demonstrate that all fuel cladding and component temperatures remain below their respective short-term limits.

It should be noted that the increase in temperature would increase the MPC internal pressure. The calculation performed for this accident recognizes an increase in thermosiphon cooling within the MPC that would accompany from pressure increase in a conservative manner.

(e) Extreme Environmental Temperature

The extreme environmental temperature accident condition is defined in Table 2.I.1 as an ambient temperature of 125°F. This is 45°F higher than the normal condition ambient temperature of 80°F, also defined in Table 2.I.1 and used in the analyses described in Section 4.I.4.2 above. This condition is conservatively evaluated by adding 45°F to the calculated normal condition fuel cladding and component temperatures in Table 4.I.3. Results for this off-normal condition are presented in Table 4.I.8. The results are confirmed to be less than accident temperature limits for fuel cladding, concrete, and ASME Code materials.

It should be noted that an increase in temperature is followed by a concomitant increase in MPC helium pressure. The bounding calculation performed for this accident does not credit the increase in thermosiphon cooling within the MPC that would accompany the pressure increase. As an increase in thermosiphon cooling would limit the temperature rise resulting from an elevated ambient temperature, the calculated temperatures and pressures are conservatively bounding for this event.

4.I.7 REGULATORY COMPLIANCE

As required by ISG-11, the fuel cladding temperature at the beginning of dry cask storage is maintained below the anticipated damage-threshold temperatures for normal conditions for the licensed life of the HI-STORM System.

As required by NUREG-1536 (4.0,IV,3), the maximum internal pressure of the cask remains within its design pressure for normal, off-normal, and accident conditions. Design pressures are summarized in Table 2.2.1.

As required by NUREG-1536 (4.0,IV,4), all cask materials and fuel cladding are maintained within their temperature limits for normal, off-normal and accident conditions in order to enable components to perform their intended safety functions. Material temperature limits are summarized in Tables 2.2.3 and 2.I.7. HI-STORM 100U System components defined as important to safety are listed in Tables 2.2.6 and 2.I.7.

As required by NUREG-1536 (4.0,IV,5), the cask system ensures a very low probability of cladding breach during long-term storage. For long-term normal conditions, the maximum CSF cladding temperature is below the ISG-11 limit of 400°C (752°F).

As required by NUREG-1536 (4.0,IV,7), the cask system is passively cooled. All heat rejection mechanisms described in this supplement, including conduction, natural convection, and thermal radiation, are passive.

As required by NUREG-1536 (4.0,IV,8), the thermal performance of the cask is within the allowable design criteria specified in Chapters 2 and 3 for normal conditions. All thermal results are within the allowable limits for all normal conditions of storage.

Table 4.I.1

Thermal Properties for HI-STORM 100U

Insulation	
Thermal Property	Specified Minimum Values
Divider Shell Insulation Thermal Resistance	4 ($^{o}F \times ft^2 \times hr$)/Btu
Density[1]	0.075 lb/ft^3
Specific Heat Capacity[1]	0.24 Btu/(lb×°F)
Emissivity	0.5
Soil	
Conductivity[2]	0.3 Btu/ft×hr×°F

Table 4.I.2

100U Long-Term Normal Storage Maximum Fuel Temperatures (Quiescent Condition)

X[3]	Q (kW)	MPC-32 (°F)	MPC-68 (°F)
0.5	36.9	**711**[4]	658
1	34.0	705	656
2	31.48	705	652
3	30.17	705	648

[1] Conservatively assumed to be that of air.

[2] "Fundamentals of Heat and Mass Transfer", Table A.3, 4th Edition, by F. Incropera and D. Dewitt, John Wiley and Sons.

[3] X is defined as the ratio of maximum permissible assembly decay heat generation rates in the inner and outer regions.

[4] Highest fuel cladding temperature is highlighted in bold. The co-incident storage scenario, MPC-32 under regionalized fuel storage at X = 0.5, is the limiting scenario for thermal evaluation.

Table 4.I.3

Maximum Normal Temperatures and Pressures Under the Limiting Fuel Storage Scenario (Quiescent Condition)

Component	Temperature (°F)	Permissible Limit (°F) (from Tables 2.2.3, 2.I.8 and 2.2.1)	Thermal Margin (°F)
Fuel Cladding	711	752	41
Fuel Basket	707	725	18
Fuel Basket Periphery	607	725	118
MPC Shell	476	500	24
MPC Lid	519	550	31
VVM Container Shell	122	800	678
VVM Lid Bottom Plate	308	800	492
Lid Concrete	270	300	30
Area Averaged Air Outlet Temperature	165	NA	NA
Divider Shell Insulation[1]	356	800	444
Pressure (psig)			
MPC	99.5	100	0.5

[1] To support thermal expansion evaluation in Section 3.I.4.4, the axially averaged divider shell temperature, 272°F, is reported in this footnote.

Table 4.I.4

Effect of Site Elevation on Peak Cladding Temperature (Quiescent Condition)

MPC Design	PCT at Sea Level (°F)	PCT at 1500 feet (°F)
MPC-68 (BWR)	658	667
MPC-32 (PWR)	711	731

Table 4.I.5

Maximum Temperatures Under Off-Normal Ambient Temperature (Quiescent Condition)

Component	Temperature (°F)	Permissible Limit (°F) (from Tables 2.2.3, 2.I.8 and 2.2.1)	Thermal Margin (°F)
Fuel Cladding	731	1058	327
Fuel Basket	727	1000	273
Fuel Basket Periphery	627	1000	373
MPC Shell	496	775	279
MPC Lid	539	775	236
VVM Container Shell	142	800	658
VVM Lid Bottom Plate	328	800	472
Lid Concrete	290	350	60
Divider Shell Insulation	376	800	424
Pressure (psig)			
MPC	101.9	110	8.1

Table 4.I.6

Maximum Temperatures Under Partial Blockage of Air Inlets (Quiescent Condition)

Component	Max. Temperature (°F)	Permissible Limit (°F) (from Tables 2.2.3, 2.I.8 and 2.2.1)	Thermal Margin (°F)
Fuel Cladding	744	1058	314
Fuel Basket	741	1000	259
Fuel Basket Periphery	631	1000	369
MPC Shell	494	775	281
MPC Lid	546	775	229
VVM Container Shell	130	800	670
VVM Lid Bottom Plate	338	800	462
Lid Concrete	276	350	74
Divider Shell Insulation	379	800	421
Pressure (psig)			
MPC	102.4	110	7.6

Table 4.I.7

Effect of Wind on Peak Cladding Temperatures (X=3)

Wind Speed (mph)	Peak Clad Temperature (°F)
5	749
10	713
15	676

Table 4.I.8

Results Under Extreme Environmental Temperature Accident (Quiescent Condition)

Component	Max. Temperature (°F)	Permissible Limit (°F) (from Tables 2.2.3, 2.I.8 and 2.2.1)	Thermal Margin (°F)
Fuel Cladding	756	1058	302
Fuel Basket	752	950	198
Fuel Basket Periphery	652	1000	348
MPC Shell	521	775	254
MPC Lid	564	775	211
VVM Container Shell	167	800	633
VVM Lid Bottom Plate	353	800	447
Lid Concrete	315	350	35
Divider Shell Insulation	401	800	399
Pressure (psig)			
MPC	104.9	200	95.1

Table 4.I.9

Results Under 24-Hour 100% Air Inlets Blockage Accident (Quiescent Condition)

Component	Max. Temperature (°F)	Permissible Limit (°F) (from Tables 2.2.3, 2.I.8 and 2.2.1)	Thermal Margin (°F)
Fuel Cladding	942	1058	116
Fuel Basket	938	950	12
Fuel Basket Periphery	805	1000	195
MPC Shell	681	775	94
MPC Lid	627	775	148
VVM Container Shell	254	800	546
VVM Lid Bottom Plate	475	800	325
Lid Concrete	322	350	28
Divider Shell Insulation	632	800	168
Pressure (psig)			
MPC	129.5	200	70.5

SUPPLEMENT 4.III[1]

THERMAL EVALUATION OF THE MPC-68M

4.III.0 OVERVIEW

The MPC-68M is a 68 cell BWR canister engineered with a high B^{10} containing Metamic-HT basket for enhanced criticality control. The MPC-68M is evaluated for storage in the aboveground family of HI-STORM overpacks. For a bounding evaluation an MPC-68M emplaced in the most flow resistive HI-STORM 100S Version B overpack[2] is analyzed under normal, off-normal and accident conditions. The evaluations described herein parallel those of the aboveground HI-STORM cask contained in the main body of Chapter 4 of this FSAR. To ensure readability, the section in the main body of the chapter to which each section in this supplement corresponds is clearly identified. All tables in this supplement are labeled sequentially.

4.III.1 INTRODUCTION

The information presented in this supplement is intended to serve as a complement to the information provided in the main body of Chapter 4. Except for the fuel basket and basket support materials, the information in Chapter 4 that remains applicable to the MPC-68M analysis is not repeated herein. Specifically the following information in the main body of Chapter 4 is not repeated:

1. The thermal properties of materials in Section 4.2 applicable to the MPC-68M.

2. The specifications for components in Section 4.3 applicable to the MPC-68M.

3. The descriptions of the thermal modeling of the MPC and its internals, including fuel assemblies, in Section 4.4 which are applicable in their entirety to the MPC-68M.

4. The descriptions of the short-term loading operations, carried out using the HI-TRAC transfer cask, in Section 4.5 applicable to the MPC-68M.

As confirmed by appropriate supporting analyses, the heat rejection capacity of the MPC-68M[3] is equal to or better than its counterparts (strictly speaking, much better because of the highly conducting Metamic-HT fuel basket). This renders its resistance to accident events such as fire with greater margins of safety.

---

[1] For ease of supplement review the sections are numbered in parallel with the main Chapter 4.

[2] This approach is identical to the HI-STORM thermal analysis in Section 4.4.

[3] Heat rejection capacity is defined as the amount of heat the storage system containing an MPC loaded with CSF stored in uniform storage will reject with the ambient environment at the normal temperature and the peak fuel cladding temperature at 400°C.

4.III.2 THERMAL PROPERTIES OF MATERIALS[1]

The material properties compiled in Section 4.2 of the FSAR provide the required information, except for the material properties of Metamic-HT fuel basket and aluminum basket shims. The Metamic-HT and shims thermo-physical properties data is provided in Table 4.III.1.

4.III.3 SPECIFICATIONS FOR COMPONENTS[2]

All applicable material temperature limits in Section 4.3 of the FSAR continue to apply to the MPC-68M. Temperature limits of MPC-68M fuel basket and basket shim materials is specified in Table 4.III.2.

4.III.4 THERMAL EVALUATION FOR NORMAL CONDITIONS OF STORAGE[3]

4.III.4.1 Thermal Model

The MPC-68M thermal design is same as that of the currently licensed MPC-68. It features a 68 cells capacity fuel basket for storing BWR fuel. The basket is engineered with a bottom plenum by providing flow holes, a top open plenum by providing an engineered clearance and a peripheral downcomer to facilitate heat dissipation by thermosiphon action. The MPC-68M is helium pressurized to same backfill specifications defined in Chapter 4, Table 4.4.12. The principal differences are in the basket material of construction (Metamic-HT), the installation of aluminum basket shims in the basket peripheral spaces and replacement of the cell walls sandwich construction by monolithic (i.e. gaps free) basket panels. The design characteristics of the basket are as follows:

i. The fuel basket is assembled from a rectilinear gridwork of thick plates having precision machined slots for facilitating snug-fit assembly and ensuring uninterrupted lateral dissipation of heat.

ii. Aluminum basket shims conforming to the shapes of the fuel basket and MPC shell are installed in the peripheral spaces between the outside walls of the fuel basket and the inside walls of the Enclosure Vessel. The axial holes in the basket shims serve as the passageway for the downward flow of the helium gas under the thermosiphon action, which is intrinsic to the thermal design of all MPCs in the HI-STORM 100 system.

iii. The fuel basket consists of adjacent square openings (cells) separated by one monolithic wall of the Metamic-HT neutron absorber.

---

[1] This section supplements Section 4.2.
[2] This section supplements Section 4.3.
[3] This section supplements Section 4.4.

In this supplement the MPC-68M placed in an above ground HI-STORM 100 System is evaluated under normal, off-normal and accident conditions and during short-term operations. The thermal evaluations use *the same aboveground MPC 3-D thermal modeling methodology* and the *same 3-Zone porous media model* used in the thermal analysis of the aboveground overpack (HI-STORM 100S[1]) to represent the flow resistance of bounding BWR (GE-10x10) fuel assemblies (See Chapter 4, Subsection 4.4.1.2).

The key attributes of MPC-68M thermal model are as follows:

1. The MPC-68M is modeled as a geometrically accurate 3D array of square shaped cells inside a cylindrical shell with bottom and top closures. The fuel basket bottom flow holes with understated flow area and top plenum are explicitly modeled.

2. The helium flow within the MPC is modeled as laminar. This is the same modeling approach used in the HI-STORM 100 cask analyses.

3. The hydraulic resistance of the fuel assemblies stored within the MPC is represented in the 3D model by 3-Zone porous media flow resistances. This is the same as used in the HI-STORM 100 modeling (See Chapter 4, Subsection 4.4.1.2).

Consistent with the HI-STORM 100 cask analyses a geometrically accurate 3D model of the HI-STORM 100 overpack is constructed for thermal analysis. The inlet and outlet vents and internal flow passages are explicitly modeled. The airflow through the cooling passages of the HI-STORM 100 overpack is modeled as turbulent, using the k-ω model with transitional option as recommended in the Holtec-proprietary benchmarking report [4.1.6]. This is the same modeling approach used in the HI-STORM 100 cask analyses. The underside of the HI-STORM 100 concrete pad is assumed to be supported on a subgrade at 77°F. This is the same boundary condition applied to the bottom of the ISFSI pad for the HI-STORM 100 modeling in Section 4.4.

4.III.4.2 Thermal Analysis

The MPC-68M has been designed to permit storage under the array of uniform and regionalized heat loads defined in Chapter 2 as a function of the regionalization parameter X. As shown in Chapter 4 the highest cladding temperatures are reached under regionalized storage at X = 0.5. This scenario is co-incident with the maximum permissible MPC heat load and therefore temperatures of other sub-systems (such as fuel basket, MPC shell and overpack) also reach their highest values. This scenario is adopted for demonstration of compliance with the temperature and pressure limits set forth in this Supplement and Chapter 2. The limiting scenario is analyzed and maximum temperatures and pressures under normal storage tabulated in Tables 4.III.3 and 4.III.4. The results are below the Chapter 2 and Supplement 4.III normal temperature and

[1] The aboveground HI-STORM System includes a classical overpack design (HI-STORM 100) and a shortened version (HI-STORM 100S). The limiting design (HI-STORM 100S) is used in the aboveground thermal analysis.

pressure limits. In accordance with NUREG-1536 MPC-68M pressures are computed assuming 1% (normal), 10% (off-normal) and 100% (accident) rod ruptures with 100% rods fill gases and fission gases release in accordance with NUREG-1536 release fractions. The pressures are computed and tabulated in Table 4III.4. The 100% rods rupture pressure is below the accident design pressure (Table 2.2.1).

4.III.4.3 Engineered Clearances to Eliminate Thermal Interferences

To minimize thermal stresses in load bearing members, the MPC-68M is engineered with adequate gaps to permit free thermal expansion of the fuel basket and MPC in axial and radial directions. In this subsection, differential thermal expansions are evaluated to ensure the adequacy of engineered gaps. The following gaps are evaluated:

a. Fuel Basket-to-MPC Radial Gap
b. Fuel Basket-to-MPC Axial Gap
c. MPC-to-Overpack Radial Gap
d. MPC-to-Overpack Axial Gap

The FLUENT thermal model articulated above provides the temperature field in the HI-STORM overpack and MPC-68M from which the changes in the above gaps are directly computed. The initial minimum gaps and their corresponding value under normal storage conditions is tabulated in Table 4.III.8. The calculations show significant margins against restraint to free-end expansion are available in the design.

4.III.4.4 Evaluation of Fuel Debris Storage

Fuel debris is permitted for storage in up to eight peripheral cells under the uniform loading heat load limits specified in Section 2.4 of the Technical Specifications. Although fuel debris is not required to meet cladding temperature limits, its effect on fuel stored in the interior cells must be assessed. Fuel debris in the canister is thermally conservatively evaluated assuming a bounding debris configuration and design heat load in all storage cells. The following assumptions are adopted to maximize the computed cladding temperatures:

1. The fuel debris is assumed to be completely pulverized and compacted into a square prismatic bar enclosed by the damaged fuel canister (DFC) with open helium space above it. In this manner the height of the prismatic bar emitting heat is minimized resulting in the maximization of lineal thermal loading (kw/ft) of the DFC and co-incident local heating of the fuel basket and neighboring storage cells.
2. Fuel debris assumed to be completely composed of UO_2. As UO_2 has a lower conductivity relative to cladding, heat dissipation is understated.
3. The fuel debris is assumed to block through flow of helium inside the DFC.
4. All 16 peripheral storage locations (not just the 8 permitted by CoC) are assumed to contain fuel debris emitting maximum heat permitted by Technical Specifications

(CoC Appendix B, Section 2.4, Table 2.4-1) and all interior cells are emitting design heat under the uniform loading storage scenario.

5. The MPC operating pressure is understated to minimize internal convection heat transfer

The results of the analysis are tabulated in Table 4.III.11. The results support the following conclusions:

- Cladding temperature is substantially below the ISG-11, Rev. 3 limit.
- MPC basket is below the design limit (Table 4.III.2) by large margin.
- MPC shell and Overpack metal temperatures are below design limits (Table 2.2.3).
- Overpack body and lid concrete are well below design limits (Table 4.3.1).

4.III.5 THERMAL EVALUATION OF SHORT TERM OPERATIONS

4.III.5.1 HI-TRAC Thermal Model

The HI-TRAC thermal model presented in Section 4.5 is adopted for the evaluation of MPC-68M under short term operations.

4.III.5.2 Maximum Time Limit During Wet Transfer Operations

As the MPC thermal inertia credited in the time-to-boil calculations is bounded by the MPC-68M thermal inertia the evaluation of wet transfer operations in Section 4.5 remains applicable to the MPC-68M.

4.III.5.3 MPC Temperature During Moisture Removal Operations

4.III.5.3.1 Vacuum Drying

Prior to helium backfill the MPC-68M must be drained of water and demoisturized. At the start of draining operation, both the HI-TRAC annulus and the MPC are full of water. The presence of water in the MPC ensures that the fuel cladding temperatures are lower than design basis limits by large margins. As the heat generating region is uncovered during the draining operation, the fuel and basket mass will undergo a monotonic heat up from the initially cold conditions when the heated surfaces were submerged under water. To limit fuel temperatures demoisturization of the MPC-68M by the vacuum drying method is permitted provided the HI-TRAC annulus remains water filled during vacuum drying operations. To support vacuum drying operations two limiting scenarios are defined below:

Scenario A: The MPC-68M is loaded with Moderate Burnup Fuel assemblies generating heat at the maximum permissible rate defined in Chapter 2 under the bounding regionalized storage scenario X = 0.5.

Scenario B: The MPC-68M is loaded with one or more High Burnup Fuel assemblies and the MPC-68M decay heat is less than a conservatively defined threshold heat load Q = 29 kW[1].

To evaluate the above scenarios the vacuum drying analysis methodology presented in Section 4.5 is adopted and an MPC-68M specific thermal model constructed. The principal features of the thermal model are as follows:

i. A bounding steady-state analysis is performed under the heat loads defined in the scenarios above.
ii. The water in the HI-TRAC annulus is conservatively assumed to be boiling under the hydrostatic head of water at the annulus bottom (232°F).
iii. The bottom surface of the MPC is insulated.

The thermal model articulated above is used to compute the maximum cladding temperature under the vacuum drying scenarios defined above. The results tabulated in Table 4.III.5 are in compliance with the ISG-11 temperature limits of Moderate Burnup Fuel (Scenario A) and High Burnup Fuel (Scenario B).

4.III.5.3.2 Forced Helium Dehydration

Evaluation of Forced Helium Dehydration in Section 4.5 is applicable to MPC-68M.

4.III.5.4 Cask Cooldown and Reflood During Fuel Unloading Operations

Evaluation of cask cooldown and reflood operation in Section 4.5 is applicable to MPC-68M.

4.III.5.5 HI-TRAC Onsite Transfer Operation

A 3D FLUENT thermal model of an MPC-68M emplaced in a HI-TRAC transfer cask is constructed to evaluate the thermal state of fuel under onsite transport in the vertical orientation[2]. A bounding analysis is performed under the following conditions:

(i) Steady state maximum temperatures have reached.
(ii) The MPC-68M is loaded with fuel generating heat at the maximum permissible level under the limiting regionalized storage scenario X = 0.5.
(iii) The HI-TRAC annulus is air filled.

The scenario defined above represents upper bound temperatures reached in the HI-TRAC without the aid of any auxiliary cooling such as the Supplemental Cooling System (SCS) defined

[1] Threshold heat load is defined as the product of maximum loaded assembly heat load r_{max} and the number of fuel storage cells (n=68). Under this stipulation r_{max} must not exceed 0.426 kW.
[2] In accordance with Section 4.5 onsite transfer in the horizontal orientation is not permitted.

in Section 4.5. The maximum cladding temperatures computed using the thermal model articulated above are tabulated in Table 4.III.6. As the cladding temperatures are below the limiting High Burnup Fuel temperature limits mandated by ISG-11 [4.1.4] SCS cooling is not necessary for ensuring cladding safety under onsite transfer operations involving the MPC-68M. Accordingly SCS cooling is not mandated in the MPC-68M Technical Specifications.

4.III.6 THERMAL EVALUATION OF OFF-NORMAL AND ACCIDENT CONDITIONS[1]

4.III.6.1 Off-Normal Conditions

(a) Elevated Ambient Air Temperature

The principal effect of elevated ambient temperature is a rise of the HI-STORM 100 temperatures from the baseline normal storage temperatures by the difference between elevated ambient and normal ambient temperatures. As the normal storage temperatures under MPC-68M storage in the HI-STORM 100 overpack are bounded by the HI-STORM 100 System temperatures reported in Section 4.4, the temperatures under this event are likewise bounded by the off-normal ambient evaluation in Section 4.6.

(b) Partial Blockage of Air Inlets

The principal effect of partial inlets blockage is a rise in the HI-STORM 100 annulus temperature from the baseline normal storage temperatures and to leading order a similar rise in the MPC temperatures. As the normal storage temperatures under MPC-68M storage in the HI-STORM 100 overpack are bounded by the HI-STORM 100 System temperatures reported in Section 4.4, the temperatures under this event are likewise bounded by the partial ducts blockage evaluation in Section 4.6.

(c) Off-Normal Pressure

This event is defined as a combination of (a) maximum helium backfill pressure (Table 4.4.12), (b) 10% fuel rods rupture, and (c) limiting fuel storage configuration. The principal objective of the analysis is to demonstrate that the MPC off-normal design pressure (Table 2.2.1) is not exceeded. The MPC-68M off-normal pressure is reported in Table 4.III.4. The result[2] is below the off-normal design pressure (Table 2.2.1).

[1] This section supplements Section 4.6.
[2] Pressures relative to 1 atm absolute pressure (i.e. gauge pressures) are reported throughout this section.

4.III.6.2 Accident Conditions

(a) Fire

Although the probability of a fire accident affecting a HI-STORM 100 System during storage operations is low due to the lack of combustible materials at an ISFSI, a conservative fire event has been assumed and analyzed. The only credible concern is a fire from an on-site transport vehicle fuel tank. Under a postulated fuel tank fire, the outer layers of HI-TRAC or HI-STORM overpacks are heated for the duration of fire by the incident thermal radiation and forced convection heat fluxes. The amount of fuel in the on-site transporter is limited to a volume of 50 gallons.

(i) HI-STORM Fire[1]

The fuel tank fire is conservatively assumed to surround the HI-STORM Overpack. Accordingly, all exposed overpack surfaces are heated by radiation and convection heat transfer from the fire. Based on NUREG-1536 and 10 CFR 71 guidelines [4.III.2], the following fire parameters are assumed:

1. The average emissivity coefficient must be at least 0.9. During the entire duration of the fire, the painted outer surfaces of the overpack are assumed to remain intact, with an emissivity of 0.85. It is conservative to assume that the flame emissivity is 1.0, the limiting maximum value corresponding to a perfect blackbody emitter. With a flame emissivity conservatively assumed to be 1.0 and a painted surface emissivity of 0.85, the effective emissivity coefficient is 0.85. Because the minimum required value of 0.9 is greater than the actual value of 0.85, use of an average emissivity coefficient of 0.9 is conservative.

2. The average flame temperature must be at least 1475°F (800°C). Open pool fires typically involve the entrainment of large amounts of air, resulting in lower average flame temperatures. Additionally, the same temperature is applied to all exposed cask surfaces, which is very conservative considering the size of the HI-STORM cask. It is therefore conservative to use the 1475°F (800°C) temperature.

3. The fuel source must extend horizontally at least 1 m (40 in), but may not extend more than 3 m (10 ft), beyond the external surface of the cask. Use of the minimum ring width of 1 meter yields a deeper pool for a fixed quantity of combustible fuel, thereby conservatively maximizing the fire duration.

4. The convection coefficient must be that value which may be demonstrated to exist if the cask were exposed to the fire specified. Based upon results of large pool fire thermal

[1] The HI-STORM fire accident methodology is same as the generic methodology in Section 4.6 of the HI-STORM 100 FSAR.

measurements [4.III.3], a conservative forced convection heat transfer coefficient of 4.5 Btu/(hr×ft^2×°F) is applied to exposed overpack surfaces during the short-duration fire.

Based on the 50 gallon fuel volume, the overpack outer diameter and the 1 m fuel ring width [4.III.2], the fuel ring surrounding the overpack covers 147.6 ft^2 and has a depth of 0.54 in. From this depth and fuel consumption rate of 0.15 in/min, the fire duration is calculated to be 3.62 minutes. The fuel consumption rate of 0.15 in/min is a lowerbound value from a Sandia National Laboratories report [4.III.3]. Use of a lowerbound fuel consumption rate conservatively maximizes the duration of the fire.

To evaluate the impact of fire heating of the HI-STORM overpack, a thermal model of the overpack cylinder was constructed and evaluated in Section 4.6 of the HI-STORM FSAR with overstated inputs. As justified below this overpack fire analysis remains conservative. It is recognized that the ventilation air in contact with the inner surface of the HI-STORM Overpack under design-basis decay heat varies between 80°F at the bottom and 275°F at the top of the overpack. It is further recognized that the inlet and outlet ducts occupy a miniscule fraction of area of the cylindrical surface of the massive HI-STORM Overpack. Due to the short duration of the fire event and the relative isolation of the ventilation passages from the outside environment, the ventilation air is expected to experience little intrusion of the fire combustion products. However, as a conservative measure the air in the HI-STORM Overpack ventilation passages was held constant at a substantially elevated temperature (300°F) during the entire duration of the fire event.

During the fire the overpack external shell temperatures are substantially elevated (~550°F) and an outer layer of concrete approximately 1 inch thick reaches temperatures in excess of short term temperature limit. This condition is addressed specifically in NUREG-1536 (4.0,V,5.b), which states that:

> "The NRC accepts that concrete temperatures may exceed the temperature criteria of ACI 349 for accidents if the temperatures result from a fire."

These results demonstrate that the fire accident event analyzed in a most conservative manner is determined to have a minor affect on the HI-STORM Overpack. Localized regions of concrete are exposed to temperatures in excess of accident temperature limit. The bulk concrete temperature away from the localized regions remains below the accident limit. The temperatures of steel structures are within allowable limits.

Having evaluated the effects of the fire on the overpack, we now evaluate the effects on the MPC-68M and contained fuel assemblies. Guidance for the evaluation of the MPC and its internals during a fire event is provided by NUREG-1536 (4.0,V,5.b), which states:

> "For a fire of very short duration (i.e., less than 10 percent of the thermal time constant of the cask body), the NRC finds it acceptable to calculate the fuel temperature increase by assuming that the cask inner wall is adiabatic. The fuel

temperature increase should then be determined by dividing the decay energy released during the fire by the thermal capacity of the basket-fuel assembly combination."

The time constant of the cask body (i.e., the overpack) can be determined using the formula:

$$\tau = \frac{c_p \times \rho \times L_c^2}{k}$$

where:

c_p = Overpack Specific Heat Capacity (Btu/lb-°F)
ρ = Overpack Density (lb/ft^3)
L_c = Overpack Characteristic Length (ft)
k = Overpack Thermal Conductivity (Btu/ft-hr-°F)

The concrete contributes the majority of the overpack mass and volume, so we will use the specific heat capacity (0.156 Btu/lb-°F), density (140 lb/ft^3) and thermal conductivity (1.05 Btu/ft-hr-°F) of concrete for the time constant calculation. The characteristic length of a hollow cylinder is its wall thickness. The characteristic length for the HI-STORM Overpack is therefore 29.5 in, or approximately 2.46 ft. Substituting into the equation, the overpack time constant is determined as:

$$\tau = \frac{0.156 \times 140 \times 2.46^2}{1.05} = 126\,hrs$$

One-tenth of this time constant is approximately 12.6 hours (756 minutes), substantially longer than the fire duration of 3.62 minutes, so the MPC is evaluated by considering the MPC canister as an adiabatic boundary. The fuel temperature rise is computed next.

Table 4.III.10 lists lower-bound thermal inertia values for the MPC-68M and the contained fuel assemblies. Applying design heat load (36.9 kW (1.26×10^5 Btu/hr)) and adiabatic heating for the 3.62 minutes fire, the fuel temperature rise computes as:

$$\Delta T_{fuel} = \frac{\text{Decay heat} \times \text{Time duration}}{(\text{MPC} + \text{Basket \& Shims} + \text{Fuel})\text{ heat capacities}} = \frac{1.26 \times 10^5\ \text{Btu/hr} \times (3.62/60)hr}{(2400 + 2339 + 2780)\ \text{Btu/}°F} = 1.0°F$$

This is a very small increase in fuel temperature. Consequently, the impact on the MPC internal helium pressure will be quite small. Based on a conservative analysis of the HI-STORM 100 System response to a hypothetical fire event, it is concluded that the fire event does not adversely affect the temperature of the MPC or contained fuel. We conclude that the ability of the HI-STORM 100 System to cool the spent nuclear fuel within design temperature limits during and after fire is not compromised.

(ii) HI-TRAC Fire[1]

To demonstrate the fuel cladding and MPC pressure boundary integrity under an exposure to a hypothetical short duration fire event during on-site handling operations, a fire accident analysis of the loaded 100-ton HI-TRAC is performed. This analysis, because of the lower mass of the 100-ton HI-TRAC, bounds the effects for the 125-ton HI-TRAC. In this analysis, the contents of the HI-TRAC are conservatively postulated to undergo a transient heat-up as a lumped mass from the decay heat input and heat input from the short duration fire. The rate of temperature rise of the HI-TRAC depends on the thermal inertia of the cask, the cask initial conditions, the spent nuclear fuel decay heat generation, and the fire heat flux. Using conservatively bounding inputs – lowerbound thermal inertia, steady state maximum cask temperatures (Table 4.III.6) and design heat load (36.9 kW) - a bounding cask temperature rise of 5.178°F per minute is computed from the combined radiant and forced convection fire and decay heat inputs to the cask. During the handling of the HI-TRAC transfer cask, the transporter is limited to a maximum of 50 gallons. The duration of the 50-gallon fire using the methodology articulated above for HI-STORM fire is 4.775 minutes. Therefore, the temperature rise computed as the product of the rate of temperature rise and the fire duration is 24.7°F, and the co-incident fuel cladding temperature (664.7°F)[2] is below the 1058°F accident limit.

The elevated temperatures as a result of the fire accident will cause the pressure in the water jacket to increase and cause the overpressure relief valves to vent steam to the atmosphere. Based on the fire heat input to the water jacket, less than 11% of the water in the water jacket can be boiled off. However, it is conservatively assumed, for dose calculations, that all the water in the water jacket is lost. In the 125-ton HI-TRAC, which uses Holtite in the lids for neutron shielding, the elevated fire temperatures would cause the Holtite to exceed its design accident temperature limits. It is conservatively assumed, for dose calculations, that all the Holtite in the 125-ton HI-TRAC is lost.

Due to the increased temperatures the MPC experiences as a result of the fire accident in the HI-TRAC transfer cask, the MPC internal pressure increases. The pressure rise is computed using the Ideal Gas Law and upperbound helium backfill pressure defined in Chapter 4, Table 4.4.12 and results tabulated in Table 4.III.9. The computed MPC accident pressure is substantially below the accident design pressure (Table 2.2.1).

(b) Flood

The flood accident is defined in Chapter 2 as a deep submergence event. The worst flood from a thermal perspective is a "smart flood" that just rises to the top of the inlets to prevent airflow without the benefit of MPC cooling by water. This effect is bounded by the 100% inlets ducts blockage accident evaluated herein in Section 4.III.6.2(d).

---

[1] The HI-TRAC fire accident methodology is same as the generic methodology in Section 4.6 of the HI-STORM 100 FSAR.

[2] Computed by adding the fire temperature rise to initial fuel temperature (Table 4.III.6).

(c) Burial Under Debris

The burial under debris evaluation in Section 4.6 is bounding because of the following:

(i) The MPC thermal inertia is neglected.
(ii) The initial storage temperatures under MPC-68M storage are less than the HI-STORM 100 System temperatures.

(d) 100% Blockage of Air Ducts

This accident is defined in Section 4.6 as 100% blockage of the air inlet ducts for 32 hours. This event is evaluated by blocking the air inlets in the FLUENT thermal model and computing the 32-hour temperature rise of the MPC and stored fuel. The results of this analysis are tabulated in Table 4.III.7. The results show that fuel cladding and component temperatures remain below their respective accident limits specified in Chapter 2 and Supplement 4.III. The increase in temperature results in a concomitant rise of the MPC pressure. The maximum accident pressure tabulated in Table 4.III.7 is below the design limit specified in Chapter 2.

(e) Extreme Environmental Temperature

The principal effect of elevated ambient temperature is a rise of the HI-STORM 100 temperatures from the baseline normal storage temperatures by the difference between elevated ambient and normal ambient temperatures. As the normal storage temperatures under MPC-68M storage in the HI-STORM 100 overpack are bounded by the HI-STORM 100 System temperatures reported in Section 4.4, the temperatures under this event are likewise bounded by the extreme ambient evaluation in Section 4.6.

(f) 100% Rods Rupture Accident

In accordance with NUREG-1536 a 100% rods rupture accident is evaluated assuming 100% of the rods fill gases and fission gases release in accordance with NUREG-1536 release fractions. The MPC-68M pressure under this postulated accident is computed and tabulated in Table 4III.4. The pressure is below the accident design pressure (Table 2.2.1).

(g) Jacket Water Loss

The principal effect of jacket water loss accident is a temperature increment in the stored fuel and MPC from the baseline conditions under in a HI-TRAC. As the MPC-68M temperatures in the HI-TRAC are bounded by MPC-68 temperatures the jacket water loss temperatures are likewise bounded by the HI-TRAC jacket water loss evaluation in Section 4.6.

4.III.7 REGULATORY COMPLIANCE

As required by ISG-11, the fuel cladding temperature at the beginning of dry cask storage is maintained below the anticipated damage-threshold temperatures for normal conditions for the licensed life of the HI-STORM System.

As required by NUREG-1536 (4.0,IV,3), the maximum internal pressure of the cask remains within its design pressure for normal, off-normal, and accident conditions. Design pressures are specified in Table 2.2.1.

As required by NUREG-1536 (4.0,IV,4), all cask materials and fuel cladding are maintained within their temperature limits under normal, off-normal and accident conditions to enable them to perform their intended safety functions. Material temperature limits are specified in Tables 2.2.3 and 4.III.2.

As required by NUREG-1536 (4.0,IV,5), the cask system ensures a very low probability of cladding breach during long-term storage. For long-term normal conditions, the maximum CSF cladding temperature is below the ISG-11 limit of 400°C (752°F).

As required by NUREG-1536 (4.0,IV,7), the cask system is passively cooled. All heat rejection mechanisms described in this supplement, including conduction, natural convection, and thermal radiation, are passive.

As required by NUREG-1536 (4.0,IV,8), the thermal performance of the cask is within the normal storage design criteria specified in Chapters 2 and 4. All thermal results are within the limits under normal conditions of storage.

4.III.8 REFERENCES

[4.III.1] Aluminum Alloy 2219 Material Data Sheet, ASM Aerospace Specification Metals, Inc., Pompano Beach, FL.

[4.III.2] United States Code of Federal Regulations, Title 10, Part 71.

[4.III.3] Gregory, J.J. et. al., "Thermal Measurements in a Series of Large Pool Fires", SAND85-1096, Sandia National Laboratories, (August 1987).

[4.III.4] Jakob, M. and Hawkins, G.A., "Elements of Heat Transfer," John Wiley & Sons, New York, (1957).

Table 4.III.1: Thermal Properties of Fuel Basket and Basket Shim Materials

Property	Minimum Value	Reference
Metamic-HT (fuel basket)		
Conductivity	104 Btu/ft-hr-°F	Appendix 1.III.A
Emissivity	Note 1	Appendix 1.III.A
Density	168.7 lb/ft^3	Appendix 1.III.A
Heat Capacity	0.21 Btu/lb-°F	Appendix 1.III.A
Aluminum Alloy 2219 (basket shims)		
Conductivity	69.3 Btu/ft-hr-°F	[4.III.1]
Emissivity	Note 1	Appendix 1.III.A
Density	177.3 lb/ft^3	[4.III.1]
Heat Capacity	0.207 Btu/lb-°F	[4.III.1]
Note 1: Fuel basket and basket shims are hard anodized to yield high emissivities. Lowerbound surface emissivity of hard anodized surfaces is defined in Appendix 1.III.A.		

Table 4.III.2: Temperature Limits of Fuel Basket and Basket Shim Materials

Metamic-HT (Note 1)	
Normal storage	752°F
Short term operations, Off-Normal and Accident conditions	932°F
Aluminum Alloy 2219 Shims (Note 2)	
Normal storage	752°F
Short term operations, Off-normal and Accident conditions	932°F

Notes:

1. The B_4C component in Metamic-HT is a refractory material that is unaffected by these temperatures and the aluminum component is solid at temperatures in excess of 1000°F.
2. To preclude melting the temperature limits are set well below the melting temperature of Aluminum Alloys.

Table 4.III.3: Maximum Temperatures Under Normal Long-Term Storage

Component	Temperature (^{0}F)
Fuel Cladding	598
Basket	585
Basket Shims	500
MPC Shell	443
Overpack Inner Shell	309
Overpack Body Concrete	234
Overpack Lid Concrete	228
Overpack Outer Shell	169
Area Averaged Air Outlet[1]	220

[1] Reported herein for the option of outlet ducts air temperature surveillance set forth in the Technical Specifications.

Table 4.III.4: Maximum Pressures Under Normal Long Term Storage

Condition	Pressure (psig)
Initial backfill* (at 70°F)	48.5
Normal: intact rods 1% rods rupture**	 95.5 96
Off-Normal (10% rods rupture)	100.5
Accident (100% rods rupture)	145.8
* Conservatively assumed at the Tech. Spec. maximum value (see Table 4.4.12). ** Per NUREG-1536, pressure analyses with ruptured fuel rods (including BPRA rods for PWR fuel) is performed with release of 100% of the ruptured fuel rod fill gas and 30% of the significant radioactive gaseous fission products.	

Table 4.III.5: Maximum MPC-68M Temperatures Under Vacuum Drying Scenarios

Component	Scenario A (°F)	Scenario B (°F)
Cladding	754	732
Fuel Basket	729	698
Basket Shims	522	482
MPC Shell	325	307
Notes: (1) The cladding temperatures are below the ISG 11 temperature limits of Moderate Burnup Fuel (Scenario A) and High Burnup Fuel (Scenario B). (2) The component temperatures are below the Chapter 2 and Supplement III temperature limits.		

Table 4.III.6: Maximum HI-TRAC Temperatures and Pressures Under On-site Transfer Operations

Component	Temperature [°F]
Fuel Cladding	640[1]
MPC Basket	626
Basket Periphery	567
MPC Outer Shell Surface	442
Aluminum Shims	528
HI-TRAC Inner Shell Inner Surface	331
Water Jacket Inner Surface	264
Enclosure Shell Outer Surface	261
Water Jacket Bulk Water	250
Top Lid Neutron Shield (Holtite)[2]	296
Pressure (psig)	
Initial Backfill	48.5
Operating Pressure	101.6
With 1% rods rupture	102.1
With 10% rods rupture	106.9

[1] The calculated value is below the permissible limit for high-burnup fuel. Therefore auxiliary cooling of the HI-TRAC is not necessary to ensure cladding safety under onsite transfer operations involving the MPC-68M. Accordingly SCS cooling is not mandated in the MPC-68M Technical Specifications

[2] Local neutron shield section temperature.

Table 4.III.7: Maximum Temperatures and Pressures Under
32-Hour 100% Air Inlets Blockage Accident

Component	Temperature (^{0}F)
Fuel Cladding	722
Fuel Basket	709
Basket Shims	626
MPC Shell	571
MPC Lid	543
Overpack Inner Shell	462
Body Concrete	304
Lid Concrete	295
Pressure (psig)	
MPC	111.6

Table 4.III.8: Differential Thermal Expansion

Gap Description	Cold Gap U mm (in)	Differential Expansion δ_i mm (in)	Is Free Expansion Criterion Satisfied (i.e., $U > \delta_i$)
Fuel Basket-to-MPC Radial Gap	3.175 (0.125)	2.55 (0.101)	Yes
Fuel Basket-to-MPC Axial Gap	63.5 (2.5)	9.69 (0.382)	Yes
MPC-to-Overpack Radial Gap	7.9375 (0.3125)	3.07 (0.121)	Yes
MPC-to-Overpack Minimum Axial Gap	182.5625 (7.1875)	13.16 (0.52)	Yes

Table 4.III.9: MPC-68M Pressure Under HI-TRAC Fire Accident

Initial Operating Pressure	101.6 psig
Fire Pressure Rise	2.9 psig
Fire Accident Pressure	104.5 psig

Table 4.III.10: MPC-68M Thermal Inertia

Fuel	2780 Btu/°F
Basket and Aluminum Shims	2339 Btu/°F
Pressure Boundary (lid, baseplate and shell)	2400 Btu/°F

Table 4.III.11: HI-STORM Temperatures Under Fuel Debris Storage

Component	**Temperature**
Cladding	583°F[Note 1]
Basket	561°F
Aluminum Shims	451°F
MPC Shell	406°F
Overpack Inner Shell	268°F
Overpack Outer Shell	162°F
Overpack Body Concrete	194°F
Overpack Lid Concrete	210°F
Average Air Outlet	208°F

Note 1: It is recognized that the assumption of all 16 DFC locations having fuel debris instead of permitted 8 cells has the effect of slightly understating the MPC heat load because of the lower per assembly heat permitted in DFC cells. However, because the effect is small (32.288 kW with all 16 cells versus 33.144 kW with permitted 8 cells) and the margins from limits are substantial, this has no adverse effect on the reported temperatures or conclusions. Moreover, the DFC is stored in the basket periphery cells. The effect of a slight change in the heat load in the periphery cells will have a second order effect on the peak cladding temperature which occurs in the inner cell locations.